THE USE OF HYDROGEN AS A FUEL FOR COMPRESSION IGNITION ENGINES

Thesis by

Jorge M.G. Antunes

In Partial Fulfilment of the Requirements

for the Degree of

Doctor of Philosophy

Date of Submission

September 2010

Keywords: diesel engine, compression ignition, hydrogen, injection, simulation, pulsed injection, emissions, HCCI, Miller cycle,

Abstract

The objective of this research was to investigate the applicability of hydrogen as a fuel for compression ignition engines. The research indicates that hydrogen is a suitable fuel for "compression ignition" (CI) engines, "fumigated diesel" (FD), "homogeneous charge compression ignition" (HCCI) and "direct injection of hydrogen" (DIH_2).

Peculiarities of the various modes of operation with hydrogen were investigated using a high speed commercial direct injection diesel engine, Deutz 1FL 511 with a compression ratio of 17:1, as well as a simulation model to assist with on the understanding of certain phenomena that were impossible to reproduce due to the engine and transducers physical limitations.

Instrumentation with high-speed data acquisition was designed and installed to measure crankshaft speed and position, airflow rate, inlet air pressure and temperature, fuel consumption, brake power, cylinder combustion pressure, and exhaust gas temperature. The design, construction and characterization of a pulse controlled hydrogen injection system for HCCI and DIH_2 was carried out and discussed.

In this research, special attention was paid to characterize and identify the operating parameters that control the hydrogen combustion in a CI engine. High rates of engine cylinder pressure rise were found when using hydrogen and some form of control solution is required. Simulation and engine tests were carried out to characterize and identify new design approaches to control such high rates of pressure rise, culminating in the proposal of a pulsed injection methodology, and also the use of the Miller cycle to mitigate the observed high rates of pressure rise. A number of possible

innovative solutions and measures, making the hydrogen engine operation reliable and safe are also presented.

Acknowledgments

This research work was carried out at the *TecnoVeritas - Services of Engineering and Systems Technology Ltd.* laboratory, without which it would not be possible.

Profound thanks are due to my family for their unconditional support, and love given throughout my student life, most in particular during the present research work, for bearing my bad mood when research work looked like being impossible, and the discouragement was beating hard.

During the development of this research at the School of Marine Science and Technology, I received a valuable help, advice and financial support from my friend and supervisor Professor A. P. Roskilly.

I wish to thank, Mr. João Reis, for the Saturdays and nights spent with me around the engine and Dr Yao Dong Wang for his patience and support.

Thank you GOD! There is more to come! I will be counting on you!

To: Margarida, Joana, Anucha, Gabi, Mia e Jaime.

List of papers

Antunes J. and Roskilly A., (2004). **"The use of H_2 on compression ignition engines",**
3rd European Congress on economics and management of energy in industry, Lisbon.

Antunes J. and Roskilly A., (2006). **"Opportunities & advantages of the use of hydrogen on board ships – new concepts",**
X International Naval Engineering Conference, Lisbon.

Antunes J. and Roskilly A. R.Mikalsen, (2008). **"An investigation of hydrogen-fuelled HCCI engine performance and operation",**
Published by the International Journal of Hydrogen Energy.

Antunes J. and Roskilly A. R.Mikalsen, (2008). **"An experimental study of a direct injection compression ignition hydrogen engine",**
Published by International Journal of Hydrogen Energy.

Antunes J. and Roskilly A. R.Mikalsen, (2009). **"The hydrogen-fuelled HCCI engine performance and operation",**
Paper presented at the Conference HYPOTHESIS VIII Hydrogen Power Theoretical and Engineering Solutions - International Symposium April 2009.

Antunes J. and Roskilly A. R.Mikalsen (2009) "**Conversion of large-bore diesel engines for heavy fuel oil and natural gas dual fuel operation**".
Paper submitted in 2009, waiting for publication by CIMAC.

Contents

List of Figures:

List of Tables:

Nomenclature

A	Area [m^2]
A	Orifice area [m^2]
A	Area of throat at valve seat [m^2]
A_0	Supply orifice area [m^2]
A_p	Actuator piston area [m^2]
A_{SACK}	Lateral area of the cone inside the sack volume [m^3]
ATDC	After Top Dead Centre
B	Cylinder Bore [m]
BDC	Bottom Dead Centre
BTDC	Before Top Dead Centre
CAD	Crank angle degrees [°]
Cd	Valve Discharge coefficient [1]
c_d	Coefficient of discharge [1]
C_p	Specific heat constant pressure [kJ/kg K]
C_v	Specific heat constant volume [kJ/kg K]
COV	Coefficient of variation
d_{MD}	Diameter at Mach disc [m]
EGR	Exhaust Gas Recirculation
ER	Equivalence ratio [1]
g	Length of air gap [m]
H	Magnetic field intensity [A/m]
h	Heat transfer coefficient [W/m^2K]

I	Solenoid current [A]
IMEP	Indicated mean effective pressure [Pa]
k	Spring elastic constant [N/m]
k_0	Flow coefficient [1]
k_{rw}	Flow coefficient [1]
ks	Spring constant [N/m]
k_{sp}	Spring constant [N/m]
L	Stroke length [m]
L_{BARREL}	Barrel length [m]
L_{exh}	Exhaust valve lift [m]
L_{inlet}	Work inlet valve [m]
L_{steel}	Magnetic circuit length in steel [m]
LHV	Lower Calorific Value [kJ/kg]
M	Mass [kg]
M	Mach number [1]
MMF	Magnetic motive force [N]
M_p	Net actuator mass [kg]
m	Mass [kg]
$\dot{m}$	Mass flow rate [kg/s]
m_t	mass of the needle actuator group [kg]
N	Number of turns
N_e	Engine speed [rpm]
P	Pressure [Pa]
P_0	Pressure of the sack volume [m^3]

P_0*	Pressure at nozzle exit [Pa]
P_1	H_2 upstream pressure [Pa]
P_2	In cylinder pressure [Pa]
P_a	Atmospheric pressure [Pa]
P_a	Pressure at Mach disc [Pa]
P_c	Critical pressure [Pa]
P_{comp}	Compression Pressure [Pa]
P_{cp}	Combustion chamber pressure [Pa]
p_{cr}	Gas pressure at crevice [Pa]
P_e	Pressure at sack volume [Pa]
P_{exp}	Expansion Pressure (36°ATDC) [Pa]
P_{H2}	Hydrogen supply pressure [Pa]
P_{hyd}	Hydraulic pressure of brake [Pa]
P_{HYD}	Hydraulic oil pressure [Pa]
P_{max}	Maximum combustion pressure [Pa]
p_{mot}	Motored pressure [Pa]
p_r	Reference pressure [Pa]
P_s	Supply pressure [Pa]
P_t	Pressure at throat [Pa]
PWM	Pulse Width Modulation
Q	Heat flow [W]
Q_{static}	Static mass flow rate [kg/s]
q_{net}	flow that makes the actuator to move upwords [kg/s]
R	Actuator radius [m]

R	Coil resistance [Ω]
R	Nozzle radius [m]
R_e	Reynolds number [1]
RPR	Rate of Pressure Rise [bar/°], [Pa/ms]
r	Actuator stem radius [m]
r	Critical pressure ratio [1]
S	Stroke [m]
$\overline{S_p}$	Average piston speed [m/s]
T	Torque [Nm]
T	Temperature [°C]
T	Upstream H_2 temperature [K]
T*	Temperature at nozzle exit [K]
T_0	Temperature of hydrogen in the sack volume [K]
T_a	Ambient temperature [°C]
$T_{air\ inlet}$	Air inlet temperature [°C]
$T_{chamber}$	Gas temperature at the combustion chamber [K]
T_{cr}	Gas temperatures at the crevices [K]
T_{exh}	Exhaust gas temperature [°C]
T_{ign}	Ignition temperature [°C]
T_{MD}	Temperature at Mach disc
T_r	Reference temperature [k]
t	Time [s]
U*	Speed at nozzle exit [m/s]
U_0	Velocity of hydrogen in the sack volume [m/s]
U_{MD}	Hydrogen speed at Mach disc [m/s]

u	Velocity [m/s]
V	Volume [m^3]
v	Linear speed [m/s]
v	Velocity of the needle actuator [m/s]
V_d	Displaced volume [m^3]
V_r	Reference volume [m^3]
V_{sol}	Solenoid Voltage [V]
V_t	Velocity at throat [m/s]
X	Position [m]
X	Armature position [m]
X	Ball travel [m]
x'	Displacement [m]
X_p	Actuator piston position [m]
α	Angle [rad]
β	Bulk modulus of the oil [Pa]
γ	Specific heat ratio C_p/C_v [1]
Δ	Difference
δ	Difference
θ	Crank angle [rad]
θ	Penetration cone angle[rad]
λ	Air fuel ratio [1]
λ	Excess air factor [$\lambda=1/\varphi$]
μ	Magnetic permeability [H/m]
μ_0	Magnetic permeability of air [H/m]
ρ	Density [kg/m^3]

ρ^*	Density at nozzle exit [kg/m^3]
ρ_0	Density of Hydrogen in the sack volume [kg/m^3]
ρ_{MD}	Density at Mach disc [kg/m^3]
φ	Magnetic flux [Wb]
φ	Equivalence ratio [1]
φ	Half angle of the injector needle tip cone [rad]
Φ d_{MD}	Mach disc diameter [m]
ω	Angular velocity [rad/s]

Chapter 1
Introduction

«*A problem is a chance for you to do your best!* »

Duke of Ellington

Compression ignition (CI) internal combustion engines have been on the market for more than one hundred years, being and having been the "work horse" of the power generation and transport industries. These engines are known for their ability to burn a wide variety of fuels, from gasified biomass to heavy fuel oils, and even pulverized coal. Despite a great deal of effort on the development of other concepts of prime movers in recent years, industry is still very much dependent on CI engines. The reasons for this are concerned with fuel efficiency, reliability and running costs, in which CI engines often provide superior performance. Despite much research on alternative technologies, it is generally accepted that the internal combustion engine will play a critical role in power generation for years to come.

Governments, scientific communities, industry and the general public have become increasingly aware of environmental effects resulting from the extensive use of hydrocarbon fuels as a source of energy. Use of hydrocarbon fuels, whether derived from the crude oil or from vegetable oils, for land and sea based transport and power generation results in the emission to the atmosphere of significant quantities of carbon dioxide and other pollutants. Therefore, the development of more efficient plants and the use of non carbon based sources of energy are two fronts of development of new environmentally friendly power generation. Much of this research work is

driven by the need for engines to comply with ever-tightening environmental legislation imposed by governments worldwide, requiring drastic reductions in emissions which pose health risks to humans, such as carbon monoxide, nitrous oxides, volatile organic compounds and particulates.

The research work presented in this thesis was conducted to improve the understanding of the practical options and respective design features which should be considered if a CI engine is to be operated using hydrogen as the fuel.

1.1 Alternative power generating systems

To comply with current and future environmental regulations, there is currently an increasing interest into technologies that were developed in the past and were abandoned because they were not economically attractive, and new or unconventional technologies that make use of alternative fuels.

1.1.1 Stationary power generation

The majority production of electric power worldwide is based on fossil fuels. For example, in the UK more than two thirds of electric power generation is provided by gas or coal fired power stations [ref1]. In such plants a considerable part of the energy supplied cannot be used, since it is rejected as low temperature heat and transport to the final consumer centres is not feasible. Much research is therefore being undertaken in the areas of decentralised production of combined heat and power to reduce overall losses. The production of heat and power closer of the consumers allows more flexibility of the generating plant as well as direct use of the thermal power available, therefore resulting in a increased total efficiency. However, decentralised power production is not sufficient to achieve the required

reductions in carbon dioxide emissions set out in the Kyoto Protocol and the Climate Change Bill 2007. Such drastic reductions can probably only be obtained by increasing the use of renewable fuels.

1.1.2 Propulsion systems

The automotive industry is presently offering a number of technologies that are claimed to provide near zero emissions. Both hybrid electric and fully electric power trains are presently being offered. However, some other technologies are under development, most prominently the use of hydrogen as an energy carrier for use in fuel cells and internal combustion engines. Since hydrogen can be produces from renewable sources, this has a high potential to become classified as a zero carbon emission technology. The adoption of hydrogen as a fuel by the car industry has been politically supported through governmental funding of research into hydrogen technologies, but many challenges still exist. The use of hydrogen as an automotive fuel continues to be under intense research and development in many countries, in particular Germany and the United States. It is widely agreed that if the problems related to cost-effective hydrogen production, safe and compact on-board hydrogen storage, fuel cell reliability and operational safety can be resolved, then this technology has substantial potential.

The use of hydrogen on board marine vessels is another interesting application, as large amounts of low temperature heat can be recovered and potentially used to produce hydrogen. Hydrogen can then be stored and used as a combustion improver or even as a main fuel for power production in diesel engines, either at sea or, particularly, in port where exhaust emissions regulations are stricter. The concept of on board production and use of hydrogen as a fuel can be seamlessly integrated with the all-electric ship concept.

1.2 Internal combustion engines

The principle design of today's internal combustion engines have a similar form to that we know since the mid-19th century. Although significant improvements in engine performance have been achieved, those are mainly due to developments in materials, manufacturing and control engineering. Despite the fact that the first principles remain the same as 100 years ago, new design challenges driven by the need for improved thermal efficiencies and lower exhaust emissions are now being studied using refined computational models for each engine system, such as engine control, fuel injection, knocking control, supercharging, etc.

1.2.1 The use of hydrogen in CI engines

There are various methods of using hydrogen as a fuel in CI engines and the ones addressed in this research are:

a) Fumigation of hydrogen. This method is the easiest way of using hydrogen in a CI engine and can be divided into two categories:

- fumigation of hydrogen in the inlet air manifold at a pressure slightly above atmospheric pressure (typically about 300 mbar), with ignition controlled by diesel fuel injection, and inlet port injection during the time interval corresponding to the induction stroke, while the inlet valve is open and the exhaust valve is closed; the cylinder charge ignition being controlled by diesel fuel injection.

The main difference between these two methods is that the second one makes better use of the hydrogen charge, since hydrogen is injected only during the engine induction stroke and while the exhaust valve is already closed. As a result, there is a reduction in the concentration of hydrogen in the exhaust gases, since no hydrogen can pass through the cylinder during the valve overlap period.

These two forms of hydrogen use in CI engines have similar characteristics, are relatively simple to implement, and make use of modest hydrogen pressures. Nevertheless, there are problems associated with risk of inlet manifold explosions, engine power de-rating due to the displacement of intake air when injecting hydrogen and the potential for hydrogen slip into the exhaust gases.

b) Homogeneous Charge Compression Ignition (HCCI).

Hydrogen HCCI can be achieved using a high compression ratio diesel engine, typically above 20:1 is required. With such a high compression ratio, the final temperature of compression will be sufficiently high to ignite the cylinder charge. This method typically uses timed injection of hydrogen at a low pressure in the engine inlet manifold. Hydrogen is injected only during the engine induction stroke, while the exhaust valve is already closed. This method has interesting characteristics, including a potential for high engine thermal efficiency and extremely low exhaust gas emissions. There are, however, some important problems which need to be solved, such as engine load and speed control, mechanical component loading, and also the possibility of air manifold explosions.

c) Direct injection.

The direct injection of hydrogen constitutes possibly the most promising method of hydrogen use in CI engines.

The method can be divided into two slightly different concepts: one that makes use of moderate hydrogen pressures and a second that makes use of high hydrogen pressures. In both methods, the injection takes place only when the cylinder valves are closed. In the first mode, the fuel is injected at low pressure early in the compression process and ignition takes place only when the final temperature of compression is reached, making the ignition angle slightly erratic and difficult to control. With the high pressure direct injection

method, hydrogen is injected only when the final compression temperature is above the self-ignition temperature of the hydrogen charge. (Similarly as in a standard diesel engine.)

The main advantages of the high pressure direct injection are:

- There is no power reduction due to displacement of intake air, hence a direct injection hydrogen engine will have a higher maximum power output compared with pre-mixed operation. The exhaust gas emissions are well controlled, since the engine can be operated very lean, in this way controlling in particular the NO_x production. Because hydrogen is injected only with the cylinder closed, no short-circuiting or air manifold explosions are possible, providing safer engine operation.
- Since hydrogen direct injection makes it possible to control the heat input per cycle accurately, good engine load control is achievable.
- Control of the ignition timing is achieved through controlling the start of injection, and an optimized injection pattern can be used for each engine load.

As will be shown later, there are difficulties essentially related with the limitation of the rate of pressure rise, which must be limited to acceptable levels to avoid mechanical damage.

1.3 Contribution to existing research

The amount of research reports describing the use of hydrogen as a fuel for CI engines is very low compared to the vast amount of research on conventional fuels. However, several authors have presented studies of the performance of hydrogen as a fuel for spark ignition engines, and some reports exist presenting results from compression ignition test chambers, though not resulting in the establishment of general rules or concepts.

This thesis presents contributions to the existing state of the art in the form of detailed investigation into the performance and operational characteristics of Homogeneous Charge Compression Ignition (HCCI) and Direct Injection Hydrogen (DIH_2) engines.

The research work included the simulation and development of hydrogen injection systems for HCCI and DIH_2 operation. A single cylinder test engine for hydrogen fuelled operation was developed, and extensive test results are presented. A direct comparison of each mode of hydrogen operation, as well as conventional diesel-fuelled operation, is presented, allowing an evaluation of the potential advantages of hydrogen engine operation. Computational simulation models have been used to investigate the general operational characteristics more widely, including injection timing, knocking and thermal efficiency for both modes of operation studied.

The HCCI and DIH_2 operation modes of CI engines were evaluated in relation to the need for future engine technology to allow efficient operation with hydrogen as an alternative fuel for near zero carbon emissions power generation. The thesis has the following structure:

- Chapter 2 presents a detailed background study, thoroughly evaluating the particular features of the use of hydrogen as a fuel for reciprocating engines. Also, a review of reported hydrogen CI engines application and their performance is presented.
- Based on Chapter 2, Chapter 3 describes how the experiments were designed. The various components of the experimentation test rigs that were developed are presented, as well as the justification for the chosen designs and some of the challenges encountered.
- Chapter 4 presents the results of the tests carried out to set up the hydrogen injection systems and the HCCI and DIH_2 operation modes respectively. In-cylinder process characterization of the two modes of

operation was carried out using a comprehensive data acquisition system to gather the test data.

- Chapter 5 presents full cycle simulation models for HCCI and DIH_2 modes of operation. A model of the hydrogen direct injection system is also presented.
- Chapter 6 addresses engine control and thermodynamic performance of both modes of hydrogen engine operation using the developed simulation framework. Thermodynamic performance and control considerations resulting from variations in the input variables are presented, and control strategies are investigated.
- Finally in Chapter 7, the results of the research are summarised and evaluated, and further work is suggested.

Chapter 2

Hydrogen engine research review

«None of us are as smart as all of us.»

(Japanese proverb)

This introductory chapter presents an overview of previous research into hydrogen fuelled internal combustion engines. The characteristics of hydrogen as an engine fuel is described and the main features of the HCCI and DIH_2 modes of engine operation are presented, establishing the terminology for the rest of the thesis. Reported advantages and disadvantages of both modes of operation are reviewed and analysed. The hydrogen injection technology required and its relationship with the hydrogen combustion characteristics and engine performance and control are also introduced.

2.1 Hydrogen utilisation as an engine fuel

In the 17th century, Robert Boyle reported that "combustible air" was obtained when iron was dissolved in sulphuric acid and hydrochloric acid. Later, Henry Cavendish recognised the nature of the detonation of this gas and was able to isolate hydrogen (TUV Suddeutschland, 2003). The designation of the gas originates from the terms "hydrogène" or "hydrogenium" which were coined by Lavoisier in the 18th century **(**Colin, 2001).

The use of hydrogen to produce mechanical work has been attempted by numerous researchers and inventors. In 1820, the vicar and scientist William Cecil had developed the first model of a hydrogen internal spark ignition (SI) combustion engine, and described in a paper how this engine could be built (Cecil, 1820). In the 1920s, a German engineer, Rudolf Erren,

developed a hydrogen gas detonation engine (SI) based on a two stroke cycle process. This engine was patented in Germany in 1929 and later also in the United Kingdom (Erren, 1932). Oemichen (1942) reported engine efficiencies around 50%, converting more than 1000 SI engines to use hydrogen fuel.

Table 2.1: Comparison of hydrogen and methane physical properties (Karim, 2003).

Property	**Hydrogen**	**Methane**
Density (0.1 MPa, 300 K) [kg/m^3]	0.082	0.717
Stoichiometric composition in air [% by volume]	29.53	9.48
Stoichiometric fuel/air ratio (mass basis) [1]	0.029	0.058
Higher heating value [MJ/kg]	141.7	52.68
Lower heating value [MJ/kg]	119.7	46.72
Higher heating value [MJ/m^3]//$^{3)}$	12.10	37.71
Lower heating value [MJ/m^3]	10.22	33.95
Combustion energy (stoich. mixture) [MJ/kg]	3.37	2.56
Kinematic viscosity (300 K) [mm/s^2]	110	17.2
Diffusion coefficient into air (NPT) [cm^2/s]	0.61	0.189
Flammability limits [% by volume]	4-75	5.3-15.0
Minimum ignition energy [mJ]	0.02	0.28
Laminar flame speed (NTP) [m/s]	1.90	0.38
Adiabatic flame temperature [K]	2318	2190
Autoignition temperature [K]	858	813
Quenching gap (NTP) [mm]	0.64	2.03

In Table 2.1, some of the key properties of hydrogen that are relevant to its use as an engine fuel are compared with the corresponding properties of methane (the main component of natural gas). It is evident that hydrogen is lighter than methane and requires less air by volume stoichiometric combustion, while it requires a higher relative mass of air. Its heating value on mass basis is higher than methane but on volume basis it is much lower. There is a significant difference between its higher and lower heating values, since the product of combustion in air is only water. However, its energy release during combustion per unit mass of stoichiometric mixture is one of the highest among all the fuels. Hydrogen has a high diffusion coefficient, benefiting fuel-air mixing and the combustion process. Further characteristics which influence the behaviour of hydrogen as a fuel for reciprocating engines include its wide flammable range when mixed with

air, permitting extremely lean as well as rich combustion. The amount of energy required to ignite hydrogen is very low when compared with methane. This, together with its fast flame speed, results in a fast development of the combustion, despite of the fact that the self ignition temperatures are similar. The thermodynamic and heat transfer characteristics of hydrogen allow high compression temperatures, resulting in a better engine efficiency and lean mixture operation. The chemical kinetics of hydrogen combustion are simple and well understood whereas the chemical kinetics of hydrocarbon fuel oxidation, in particular complex hydrocarbons, involve slower endothermic reactions that are associated with fuel breakdown.

However, there are some disadvantages associated with the use of hydrogen as a fuel in internal combustion engines. Hydrogen compressed at 200 bar pressure and room temperature only has approximately one third of the energy density of methane under the same conditions. The mass flow of intake air is reduced for any engine size because of the relatively high stoichiometric hydrogen to air ratio. The high combustion rates of hydrogen produce high peak pressures and temperatures in engines when operating with near-stoichiometric mixtures. Further, the material used to construct the engine must be selected carefully, as some materials can react with hydrogen. Heat transfer losses can be high, unless special attention is paid to engine heat transfer design.

2.2 Spark ignition hydrogen engine operation

Much of the information reported in the open literature about hydrogen engines refer to spark ignited engines, and tend to highlight the positive features of the hydrogen fuelled engines while de-emphasizing or even ignoring the many limitations associated with such fields of application. There is a need to focus equally well on these negative hydrogen features that may need some research effort. Karim,(2003), has dedicated a great deal of attention to the use of hydrogen as a fuel for reciprocating engines, in his paper “Hydrogen as a spark ignition engine fuel” presented a realistic

survey of positive and negative features of the hydrogen spark ignited engines, their characterization and the need for further research. A great deal of research has been directed towards the use of hydrogen as a combustion improver of natural gas fuelled spark ignited engines, but no agreement has been obtained in terms of a generalised value for mixture percentages to use, Yi H. et al., (2000), Karim et al., (1999), , Verhelst et al., (2001). Aspects of combustion duration, performance and emissions of hydrogen fuelled SI engines is well explained by Yamin J. et al.,(2000), that concluded that one of the main parameters affecting engine performance and emissions is the combustion duration which is controlled by adequate timing. On this paper it is discussed how the combustion duration is affected by engine operating parameters such as compression ratio, equivalence ratio, spark plug location, spark timing and engine speed, therefore being a reference work on hydrogen SI engines. Finally another important area of research of hydrogen fuelled SI engines is dedicated to the discussions around the most appropriate heat loss model and the respective heat transfer coefficients, T.Shudo et al., (2002); Assanis D. et al. (2004); however a consensus is far to be obtained, except on the non adherence to the conventional heat transfer models, as there is almost no radiation due to the absence of carbon, and therefore the heat transfer during the hydrogen combustion needs to be adequately modelled.

2.3 Improvement of CI engines performance: bi-fuel experience

Bi-fuel operation was and is still a way of using hydrogen in CI engines, although the hydrogen usually burns via flame propagation in such engines. Hydrogen was designated as such an “auxiliary fuel” by many authors for quite a long time and well known as an improver of CI engine performance. Auxiliary fuels were all the fuels that being induced or introduced into the engine cylinder contributed positively for the improvement of the engine performance. The simplest way of achieving this was by means of “fumigation” of such a fuel into the engine inlet air manifolds. From this

single point architecture, other architectures were derived, for example mechanical and electronic auxiliary fuel port injection systems. Ignition of the auxiliary fuel was obtained by the in-cylinder direct injection of, for example, diesel fuel.

During the compression stroke the auxiliary fuel has ample time to become dispersed throughout the cylinder volume. On the basis of the work reported by various investigators on pre-combustion reactions, it is speculated that this fuel undergoes pre-flame oxidation but not ignition when properly proportioned with the air charge. A favourable cylinder environment is thus created which serves as a homogeneous propagation environment for the flame when this is triggered by the diesel charge ignition.

2.3.1 Early work on bi-fuel CI engine operation

The motivation that first led to fumigation operation of diesel engines was to maintain the diesel engine fuel efficiency while keeping the smoke within acceptable limits and to allow the used of fuels with poor ignition quality. Alperstein et al. (1958) reported manifold introduction of fuel into a compression ignition engine as early as 1941 at Pennsylvania State University. Vaporisation and carburetting were used for introducing auxiliary fuels such as hexane, heptane, different diesel oils, white gasoline, hydrogen peroxide, benzoyl peroxide, methyl alcohol, benzene, cetane, and diethyl ether. Cetane, hexane and low boiling point diesel fuels were found to be most effective, whereas acetone, benzene and ethyl alcohol were the least effective when introduced into the intake manifold.

McLaughlin (1956) and others used manifold introduction of fuels, mostly gasoline and liquid petroleum gas, to kill smoke and/or boost power. In most cases, the main fuel was injected into the cylinder in the conventional manner and a small amount of auxiliary fuel was introduced into the intake manifold as an aid to combustion. Also tested was carburetted alcohol as a main fuel injected and a small quantity of diesel fuel fumigated into the air intake manifold to ignite the compressed air-

alcohol vapour mixture. Using this technique it was possible to burn alcohol that otherwise could not be ignited and used as a main fuel of a compression ignition engine.

Derry et al. (1953) reported that by fumigating an auxiliary fuel into the air inlet manifold it is possible to reach a power increase in the order of 20% above the maximum rated load, without producing more smoke than when the engine is operated at full load under normal conditions.

Alperstein et al. (1958) introduced a portion of the fuel charge as a fine mist into the manifold of a compression ignition engine of open and swirl chamber types reporting smoke reductions in the order of 80%, an increase in smoke limited power output of up to 18.5%, and a decrease in specific fuel consumption of up to 9.8%. Further, shorter ignition lag, lower maximum rate of pressure rise and smoother operation were found. Alperstein reported that a diesel engine could operate satisfactorily on substandard fuels down to a cetane number of zero when fumigation was employed.

Arnold et al. (1957) carried out a systematic study of the types of fumigation fuels and their impact on the engine under residual fuel operation. They concluded that the benefits of bi-fuel operation are not the same for all types of engines but found some favourable results in tests using medium and high speed diesel engines. Fumigation allowed low-quality fuels to be effectively burned under conventional engine operating conditions and with an acceptable exhaust gas smoke level. A reduction in wear and deposits was found, to a level considerably below that generally obtained with low quality fuels. Bi-fuel operation allowed smoke limited power output of an engine to be increased, as well as allowing operation on fuels normally not considered feasible for use in conventional diesel engines.

2.3.2 Bi-fuel operation with hydrogen induction

Varde et al. (1983) studied fumigation of hydrogen into the air inlet manifold of a diesel engine. The focus of this investigation was the

reduction of particulates levels in the exhaust by fumigation of small quantities of gaseous hydrogen. Hydrogen flow rates equivalent to 10% of the fuelling rate (on an energy basis) reduced the smoke emissions at part load, however at full load the particulate reductions were more modest most probably due to the reduced amounts of excess air available in the cylinder. It was also found that very low hydrogen flow rates had adverse effects on the engine thermal efficiency but that notable improvements in efficiency were achieved by increasing the percentage of hydrogen supplied to the engine. Figure 2.1 shows the effect of hydrogen addition on the engine brake thermal efficiency for a fixed diesel fuel injection timing and different hydrogen flow rates. A clear positive effect on the brake thermal efficiency for certain hydrogen injection rates can be seen.

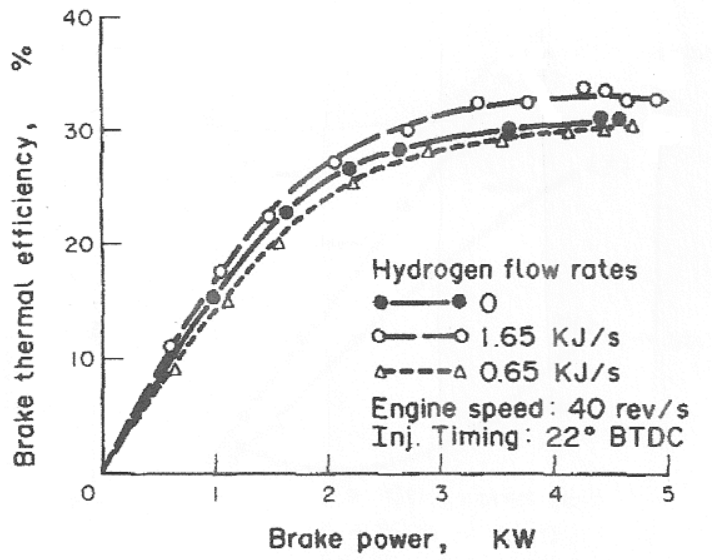

Figure 2.1: Engine brake thermal efficiency as a function of brake power for different hydrogen flow rates (Varde et al., 1983).

Figure 2.2 shows the effect of hydrogen addition on the smoke levels in the diesel engine exhaust. A clear trend of allowing the engine to run at higher power without being limited by smoke emissions is seen.

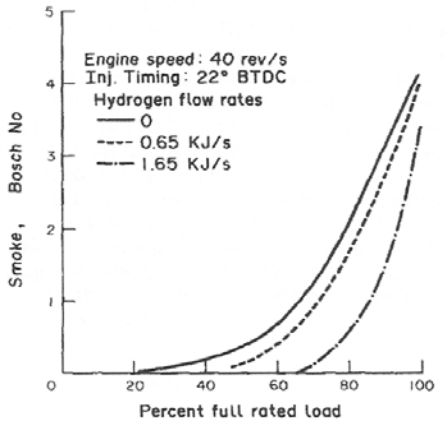

Figure 2.2: Exhaust gas smoke levels as a function of engine load for varying hydrogen injection rates (Varde et al., 1983).

A more recent study on bi-fuel operation of diesel engines with hydrogen as a way to burn low quality residual fuels was carried out by Geisler et al. (1993). This group performed a number of tests using a medium speed engine to evaluate the possibilities of using hydrogen and natural gas as fuels on LH_2 carriers from Canada to Europe. In this study, the gaseous fuels (hydrogen and natural gas) were introduced into the engine cylinder using a pre-injection injector and a pilot injector. The quantity of hydrogen was varied from 0% to 100% of the gaseous fuel mixture, allowing a smooth transfer from natural gas to hydrogen, with the pilot fuel amounting to a maximum of 7% of the engine heat input rate at full load. It was found that pre-injection of gaseous fuels significantly reduces the ignition delay, the cylinder pressure rise rate and the combustion noise, in particular under part load operation. Also, it was concluded by the authors that using hydrogen together with low quality fuels with poor ignition quality could be employed in medium speed diesel engines with pre-injection systems to decrease the smoke levels. It was identified by the authors that further increase in the hydrogen fuelling rate will result in too high maximum combustion pressures and thereby excessive mechanical and thermal loads.
Herbert et al. (1993) carried out work on the same test plant as Geisler et al., but with port injection solenoid valves. The research aimed at the use of gaseous hydrogen in a dual fuel stationary engine to minimise CO_2 emissions. A number of other findings were presented regarding the

beneficial effects of hydrogen use as a fuel for four stroke medium speed diesel engines, namely in what concerns the thermal efficiency and reduced emissions of CO_2, NO_x, CO and unburnt hydrocarbons. The authors tested experimentally the limits of engine operation with hydrogen by successively increase of hydrogen content by varying the gas mixture through the variation of the turbocharger power (an electrically driven centrifugal compressor). The limit of minimum excess air (or rich mixture) was identified by excessive exhaust gas temperatures whereas the maximum excess air (or lean mixture) limit was identified through ignition failures with corresponding emissions and erratic operation. Values of excess air of $\lambda > 2.4$ were reached whereas for natural gas excess air ratios varied between $1.7 < \lambda < 1.8$. It was concluded that concentration in the fuel gas mixture of 60% (vol.) was achievable at full load, reducing the CO_2 emissions down to 30%. A further increase of hydrogen concentration results in a reduction of power of about 30% for pure hydrogen operation. To counteract the engine power de-rating, compression ratio control should be adopted in such a way that for higher engine loads the compression ratio is decreased, allowing the combustion of a larger hydrogen quantity without excessive combustion pressures and heavy knocking. Some hydrogen slip into the exhaust gas was experienced in this research, influenced by the timing of the port hydrogen injection, leading to direct passage of hydrogen into the exhaust channel before the cylinder is closed. This research work also suggested that the use of hydrogen direct injection into the cylinder should be adopted to avoid flash-back and pre-ignition.

2.4 Compression ignition hydrogen engines

As discussed previously, the use of hydrogen as a fuel in spark ignition engines was first investigated around 1820, however hydrogen use in compression ignition engines was not seriously investigated until the 1990s. The information available on direct injection of hydrogen (DIH_2), is limited to a few academic research reports. One project, carried out by the technical university of Munich in cooperation with among others MAN under the WE-NET Phase II programme, aimed at the development of a hydrogen-

fuelled single cylinder CI engine of 100 kW power output and with a thermal efficiency above 40%.

The amount of research on the use hydrogen in homogeneous charge compression ignition (HCCI) engines is also scarce; however, a number of engine research groups around the world have recognised the potential advantages of this mode of operation in terms of thermal efficiency and emissions. The main difficulty with HCCI operation is the engine controllability, and until now no commercial HCCI engine has been offered on the market.

Figure 2.3 Illustrates the conceptual difference between port injected systems, in which hydrogen gas is injected close to the intake port but external to the cylinder, and direct injection, where hydrogen is injected directly into the closed cylinder.

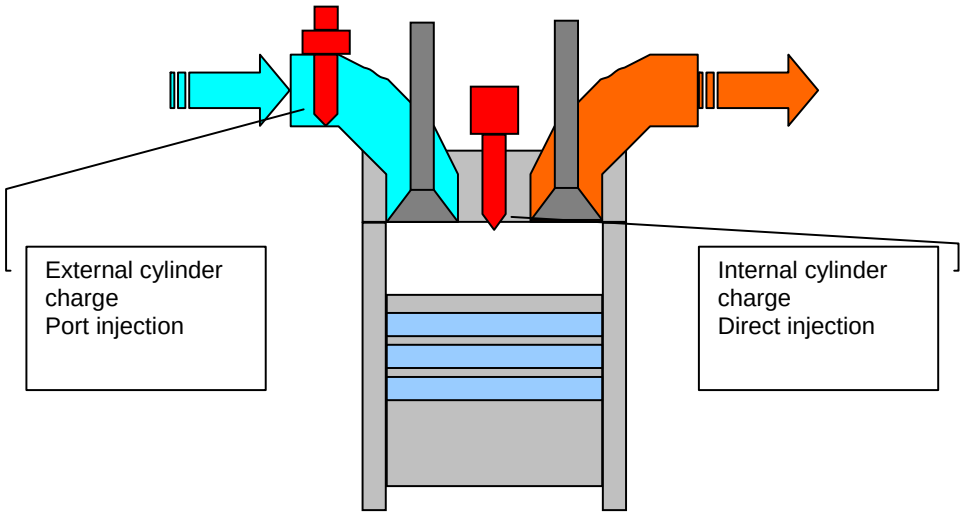

Figure 2.3 Internal and external cylinder charge formation.

2.4.1 The DIH_2 engine

The stratified charge compression ignition engine is characterised by the direct or indirect injection of the hydrogen fuel into the cylinder during the compression stroke and after the closure of both exhaust and intake valves. The thermal energy required for the ignition of the injected fuel is provided by the compression of the air contained inside the cylinder.

The temperature of the cylinder charge depends on a number of operational variables, in particular on the air inlet temperature, engine load, speed and residual fuel temperature. Despite this, it is possible to ensure that the temperature of the charge at the time of fuel injection is above the ignition temperature or very close. In this way the angle of ignition can be controlled by the angle of injection. Direct injection engines are further characterised by:

- acceptable controllability, in particular when load variations are present during operation;
- high thermal efficiencies;
- very lean combustion possible; and
- low emissions, in particular NO_x.

Among the most recent research on diesel engines fuelled with hydrogen are the reports by Fukuma et al. (1986) and Welch et al. (1990). Fukuma studied hydrogen direct injection where cylinder charge ignition was achieved by using a glow plug as a hot surface and one injector nozzle with only one hole. The conclusions from this research work was later revisited as engine performance deterioration due to a slow flame propagation through the heterogeneous mixture was identified, and better performance was achieved with an eight-hole nozzle. The use of a hot surface to assist ignition in a direct injection hydrogen engine was followed by Welch. This group concluded that the hydrogen fuelled diesel engine with glow plug ignition develops more power with lower emissions than the same engine operated with diesel fuel. Indicated thermal efficiencies for lower brake loads were above 50%. Welch et al. also identified an exponential dependence between the rate of pressure rise and the engine load. This increase can be explained by an increased thermal load of the cylinder and a higher temperature at the end of compression due to a larger mass of hot residual gases.

The work reported by Rottengruber et al. (2004) is considered a reference work for a commercial CI engine because of the methodology and

consistency of results. The test engine used in this research was a MAN type 1L24/30 single cylinder engine with a bore of 240 mm and a stroke of 300 mm. The original diesel fuel injection system was kept in place and a hydraulically actuated hydrogen injection system with electronic control was installed, allowing control of the start and duration of the hydrogen injection. Figure 2.4 illustrates the test rig, showing the separate fuel systems and the injector hydraulic system. The engine was not turbocharged; instead an air fan driven by an electric motor was used. An air heater was installed to assist during starting and to study the effects of the inlet air temperature on engine operation.

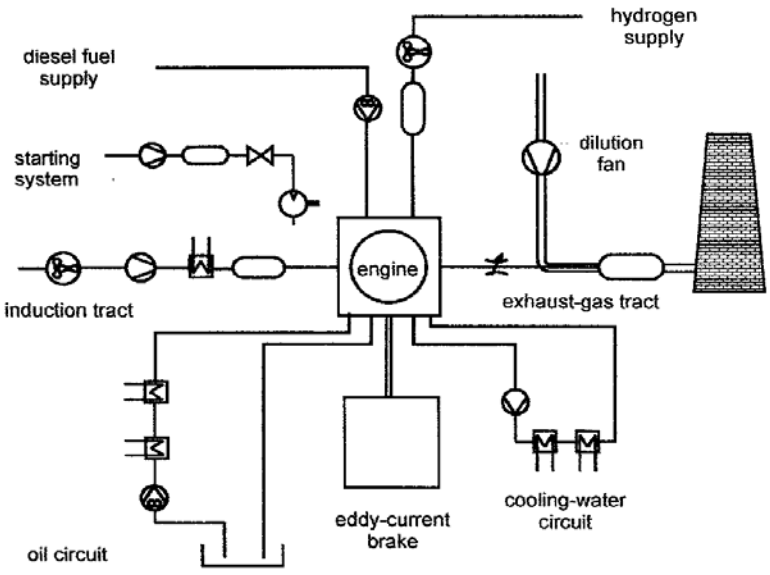

Figure 2.4: Hydrogen engine and sub-systems experimental setup (Rottengruber et al., 2004).

Using a dynamic pressure transducer to measure the in-cylinder pressure development it was identified that the DIH_2 combustion is of very short duration, commencing at the initiation of the injection and terminating with the end of the injection. Figure 2.5 shows among other things the measured pressure trace and calculated rate of heat release as a function

of the crank angle for a start of injection at 350º, injection duration 47º and an engine load corresponding to bmep = 18.17 bar. Also, it is evident from the heat release plot in Figure 2.5 that the start of combustion and its end are almost coincident with the injector needle lift. This suggests that the ignition delay is small and that good engine control can be achieved through control of the hydrogen injection timing.

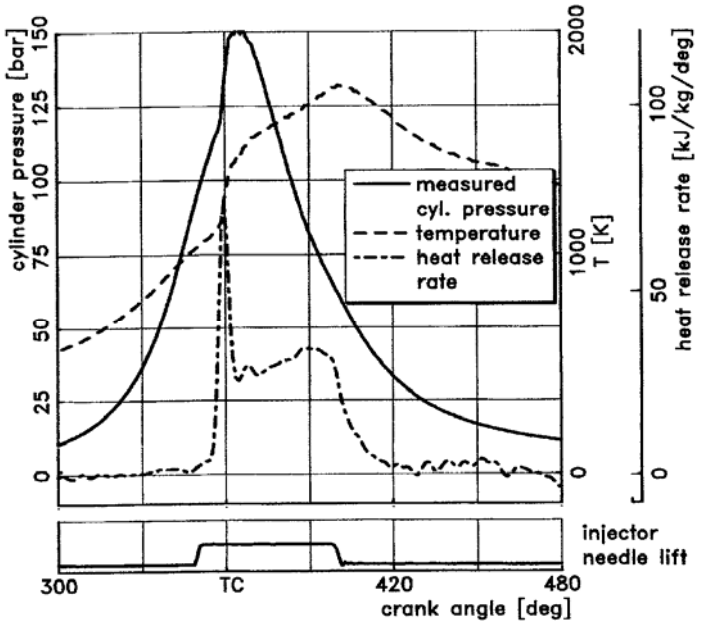

Figure 2.5: Engine performance under direct injection hydrogen operation (Rottengruber et al., 2004).

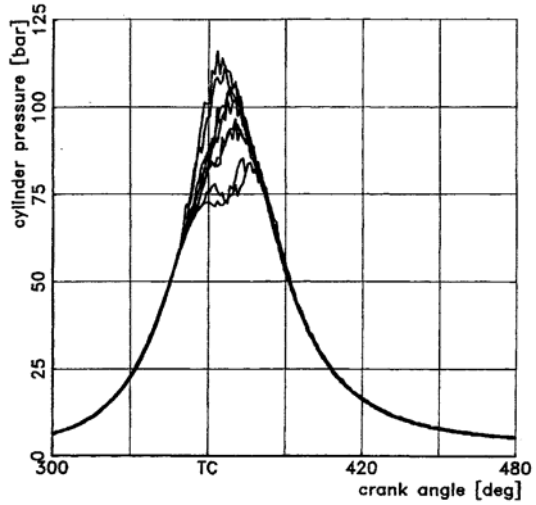

Figure 2.6: Cycle-to-cycle variations in cylinder pressure under DIH_2 operation (Rottengruber et al., 2004).

Rottengruber et al. also analysed the cycle-to-cycle variations in cylinder pressure as shown in Figure 2.6. It was concluded that variations in the pressure trace tended to be less for higher engine loads and more pronounced for medium to light loads. It was also reported that the nozzle geometry has little influence on the indicated thermal efficiency for engine loads varying between indicated mean effective pressures from 8 to 12 bar. Under these conditions, the indicated efficiency stayed around 50%, as illustrated in Figure 2.7.

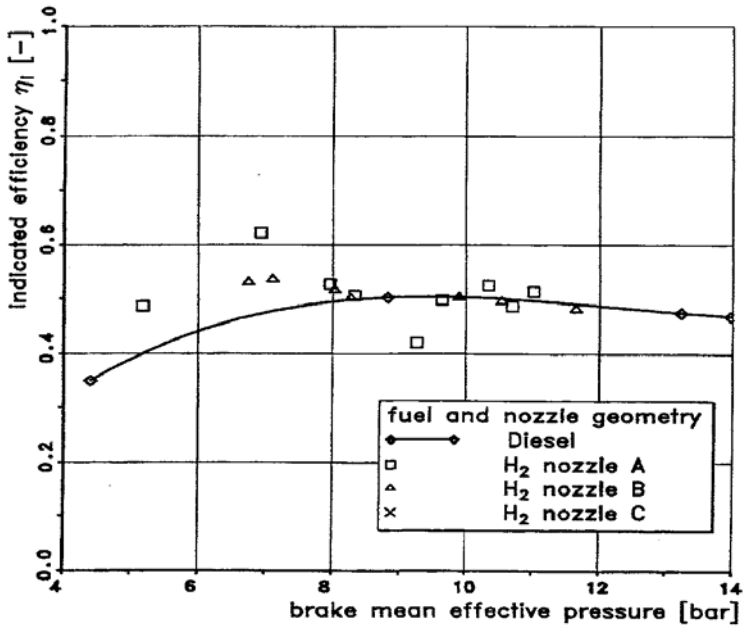

Figure 2.7: Indicated thermal efficiency as a function of brake mean effective pressure for different injector nozzle designs (Rottengruber et al., 2004).

In summary, Rottengruber et al. found that the use of hydrogen as a fuel in CI engines has the following advantages in comparison to hydrogen fuelled spark ignition engines: good engine control; no danger of combustion in the intake manifolds; absence of knocking; increased power output; and increased thermal efficiency.

Research work carried out by Naber et al. (1998) focussed on the characterization of the combustion of hydrogen in a CI engine and considered the variation of parameters such as injection pressure and temperature, nozzle orifice diameter, and ambient gas pressure and temperature. Results from the tests are illustrated in Figures 2.8-2.13. From Figure 2.8 it can be seen that hydrogen ignition delay is dependent on the temperature of the cylinder charge. The same type of dependency can be seen in Figure 2.9 for the effect of cylinder charge density. It was concluded that the ignition delay of hydrogen under direct injection operation varies exponentially with temperature; the influence of other parameters was not significant. Ignition delays of approximately 1.0 ms were observed for injection at TDC.

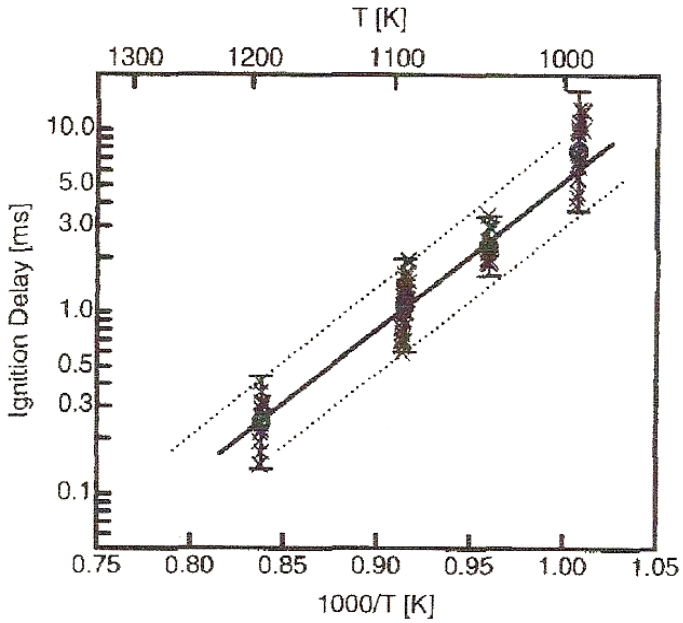

Figure 2.8: Effect of ambient gas temperature on hydrogen ignition delay (Naber et al., 1998).

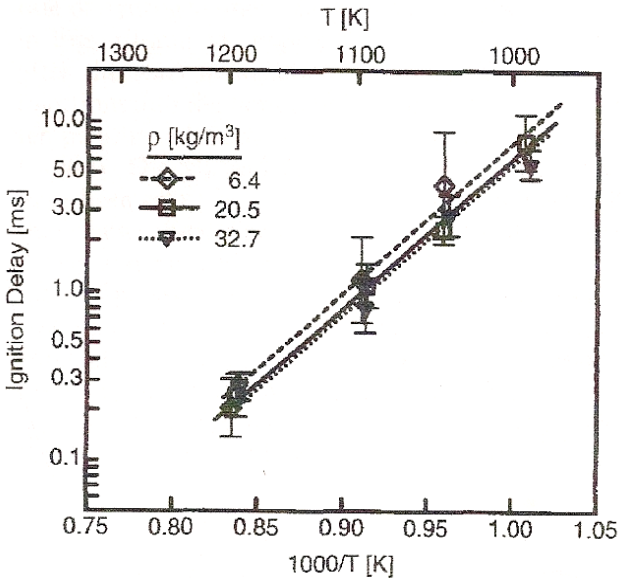

Figure 2.9: Effect of the ambient gas density (ρ) on hydrogen ignition delay (Naber et al., 1998).

The effect of oxygen concentration on the ignition delay was also studied and ignition of the cylinder charge with concentration of oxygen as low as 5% (by volume) was achieved. This suggests that the rates of combustion are insensitive to reduced oxygen concentrations and that there are good burning characteristics in tight volumes of the cylinder, such as crevices, where oxygen concentrations are usually low. In turn this means that there is a potential for a reduction in emissions.

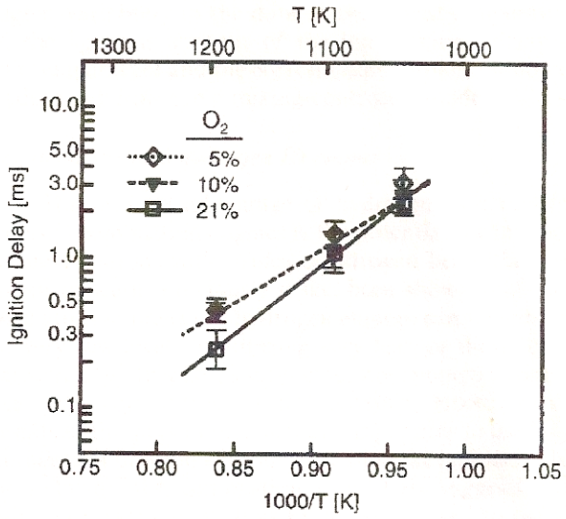

Figure 2.10: Effect of O_2 concentration on ignition delay (Naber et al., 1998).

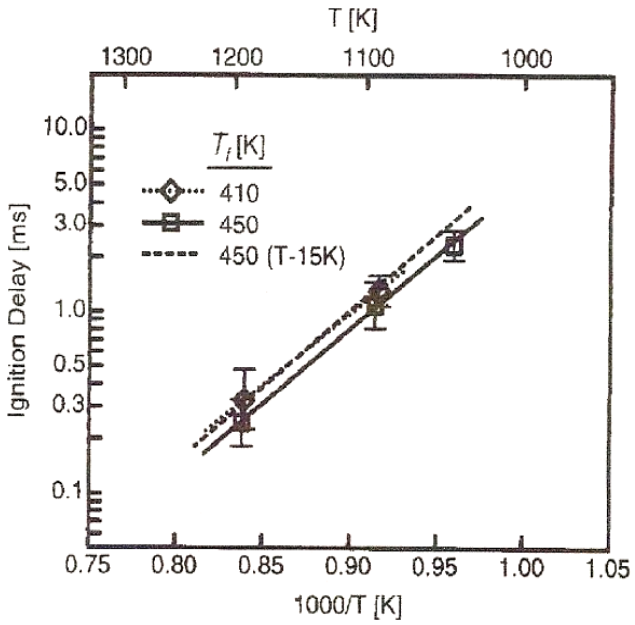

Figure 2.11: Effect of fuel temperature on ignition delay (Naber et al., 1998).

As illustrated in Figure 2.11, the ignition delay is also dependent on hydrogen temperature at injection. This is comparable with the dependence of ignition delay on cylinder charge temperature, underlining the strong effect of the charge temperature on that parameter. The effect of cylinder charge oxygen concentration on the pressure rise is illustrated in Figure 2.12, showing that for all concentrations of oxygen the rate of pressure rise is the same.

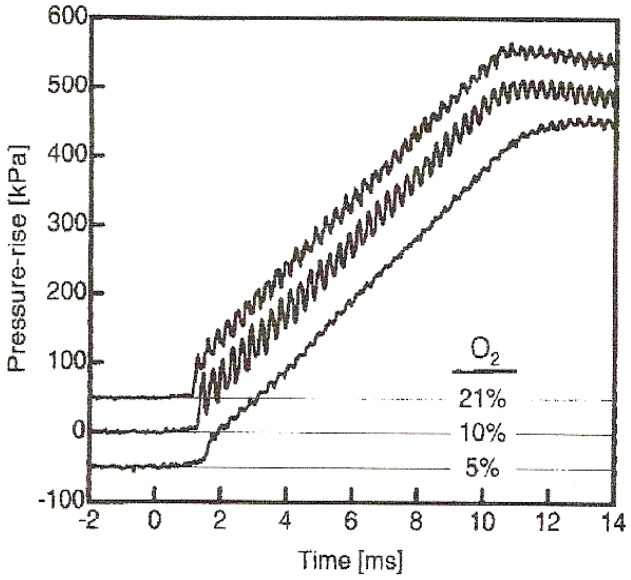

Figure 2.12: Effect of ambient gas O_2 concentration on H_2 combustion and pressure rise with ambient temperature 1000 K (Naber et al., 1998).

The effect of temperature on the rate of heat release is illustrated in Figure 2.13, indicating that the oxygen concentration and temperature of the cylinder charge has an negligible effect on the rate of combustion and heat release.

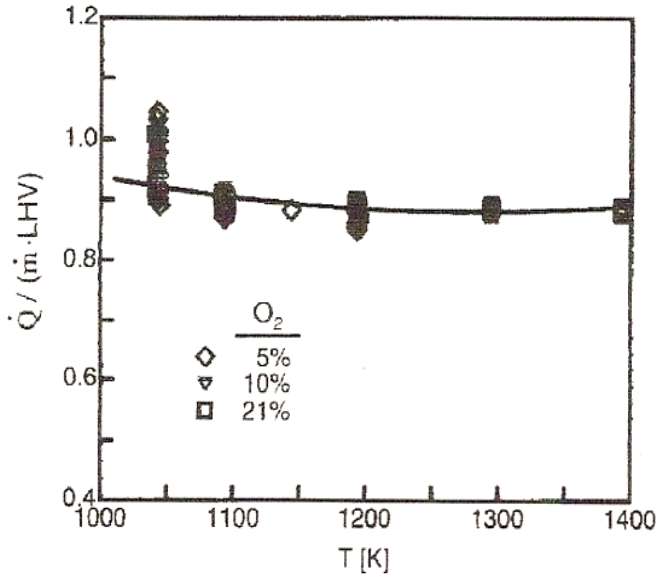

Figure 2.13: Effect of ambient air temperature and O_2 concentration on the rate of heat release (Naber et al., 1998).

These findings are in agreement with those of Rottengruber, further indicating that compression ignition of hydrogen is possible in a diesel engine.

2.4.2 DIH_2 engine specific problems

Due to its working principle, the DIH_2 compression ignition engine can provide good speed and load control, however control of the in-cylinder gas pressure and pressure rise rates, and the consequent mechanical stress on the piston rings and piston crank mechanism, needs to be addressed to ensure reliable engine operation (Rotengrubber et al., 2004, Naber et al., 1998). The DIH_2 engine should therefore be equipped with an electronic hydrogen injection system, to allow accurate control of the quantity of hydrogen being injected as well as the manner of injection. This can be achieved through pulsed injection, as described in Chapter 4 below; this gives rise to a certain amount of recirculation of the combustion products which is an effective way of controlling the rate of pressure rise.

In summary, the feasibility of the DIH_2 engine concept has been demonstrated, and it is currently at a stage where it is ready to undergo operational tests that will give better insight into engine performance and operational characteristics.

2.4.3 The HCCI hydrogen engine

A hydrogen homogeneous charge compression ignition engine is characterised by the induction or injection of hydrogen during the air intake stroke, after the exhaust valve closure. As is the case for the stratified charge compression ignition engine, the thermal energy required for the ignition of the cylinder charge is provided by the compression of the trapped volume of air contained inside the cylinder, provided by the crankshaft/connecting rod mechanism. Unlike the stratified charge compression ignition engine, the ignition of the cylinder charge will take

place at the crank angle at which the ignition temperature is reached. This means that the angle of ignition can be somewhat erratic as the temperature of the charge can vary between cycles, depending on a number of operational variables, in particular the air inlet temperature, engine load, speed and residual gas temperature. The quantity of hydrogen that can be used per cycle is limited by the volume air displaced, resulting in a power limitation compared with direct injection operation. Hydrogen HCCI engines are also characterised by:

- reduced controllability, in particular when load variations are present during operation;
- high thermal efficiencies due to fast combustion; and
- homogeneous and very lean combustion possible, giving reduced emissions, in particular NO_x.

Pursuing the objective of achieving extremely low exhaust emissions and high thermal efficiencies, researchers early identified the HCCI engine as a strong candidate. A detailed study of four stroke HCCI natural gas fuelled engines was carried by Fiveland et al. (2000), in which indicated thermal efficiencies in the range of 55% were reported. This work further demonstrated that a prediction of heat transfer losses in HCCI engines using the Woschni method differs substantially from the observed heat transfer rates. The main reason for this is due to the database from which the Woschni coefficients are derived, and also due to the ignition angle shift which can be as big as 10ºCA. Fiveland et al. conducted a number of tests varying the compression ratio through active control of the inlet valve and natural gas injection pressure, concluding that the lowest compression ratio and the highest injection pressure resulted into the highest thermal efficiency and power output. The most favourable value for the compression ratio and gas injection pressure was found to be respectively 17:1 and the 3.0 bar.

HCCI hydrogen fuelled engines were also investigated by Stenlaas et al. (2004). This research work focussed on the characterization of HCCI hydrogen engines in terms of efficiency, combustion phasing and emissions

using a single cylinder engine modified to allow variation of the air fuel ratio, speed, compression ratio and air intake temperature. Stenlaas reported that engine operation with very lean air to fuel ratios, up to 6, was possible. The hydrogen temperature was used to control the angle of ignition but it was found that this was not ideal as control was very limited, in particular for richer cylinder charges. It was also identified that the power developed by the HCCI hydrogen engine was about half the power developed by the same engine when fuelled with other fuels. The NO_x emissions decreased with the increase of the air fuel ratio, as expected.

2.4.4 HCCI hydrogen engine specific problems

As stated in the literature, the HCCI engine concept presents a great potential for reduced emissions and high thermal efficiencies, but a number of problems remain to be solved. This includes engine load and speed control, operational stability and also the reduction in power output compared with using direct injection. These problems become more difficult to solve when using hydrogen fuel because the combustion is faster and the quantity of hydrogen introduced in the cylinder per cycle is limited by its specific volume. A number of methods have been proposed to control the angle of ignition, for example the use of a secondary fuel with a well-established ignition angle (Derry et al., 1953), or the use of a spark plug (Rottengruber et al., 2004). However, the first method would not be easy to achieve in practice and the second method would mean that the engine would be a spark ignition engine.

There is, however, not much doubt that HCCI and DIH_2 hydrogen fuelled engines will be a valid option in the future for automotive applications, as stated by Rottengruber et al. (2004). Despite the fact that the research was carried out using a spark plug to initiate ignition, the authors maintain that the DIH_2 (with spark ignition) concept has the potential to achieve better performance than conventional gasoline fuelled engines. It was estimated that the maximum engine power output can be increased by more than 20% with an indicated thermal efficiency above 33% and that for lower loads an

external mixture formation (port injection) can be used to give thermal efficiencies of more than 40%. Rottengruber et al.2004, therefore recommended that an engine control strategy contemplating both modes of hydrogen fuelled engine operation should be implemented.

2.5 Fundamental hydrogen engine specific properties

Comprehensive research results on hydrogen engine combustion have been presented by Professor Tushio Shoudo from Hokkaido University, and some of the main findings will be introduced here as they constitute the state of the art in the area.

Shudo et al., (1999) recognised that reciprocating engines designed for conventional hydrocarbon fuels have different heat balances when they are operated with hydrogen. To understand the reasons for such differences, a number of experiments were carried out using the same engine and identical operation conditions with hydrogen and methane fuel. Although the engine used for the experiments was of a spark ignited type, many of the conclusions will be extendible to CI engines. Based on the relationship between indicated thermal efficiency, η_i , and the cylinder cooling losses, Shudo et al. (1999) defined the following characterisation of the heat balance:

$$\eta_i = \eta_{th}\eta_{glh}\eta_u\left(1-\varphi_w\right) \qquad (2.1)$$

where η_{th} is theoretical thermal efficiency, η_{glh} is the degree of constant volume combustion, η_u is combustion efficiency and φ_w is a cooling loss ratio given as $\varphi_w = Q_C / Q_B$, where Q_c and Q_B are the cylinder heat loss and the actual heat release calculated from the indicator diagram, respectively.

The cooling loss ratio and the combustion efficiency, η_u , were estimated using the pressure data and respective heat release in a cycle, Q, as well as the heating value of the fuel supplied in the cycle, Q_{fuel} , as follows:

$$\frac{Q}{Q_{fuel}} = \frac{(Q_B - Q_C)}{Q_{fuel}} = \frac{(Q_B - Q_C)\times \eta_u}{Q_B} = \eta_u (1-\varphi_w) \qquad (2.2)$$

Therefore, Q/Q_{fuel} corresponds to a function of combustion efficiency η_u and cooling loss ratio φ_w that can be evaluated with indicator diagrams for quasi-constant combustion efficiency η_u .

2.5.1 Comparison of hydrogen versus methane combustion

Using the above defined variables and theoretical approach, it was possible to compare in what respects the hydrogen and methane combustion processes differ. Figure 2.14 shows the effect of ignition timing on in-cylinder pressure, rate of heat release (ROHR), cumulative heat release, in-cylinder gas temperature and cylinder wall temperature (under constant engine operating conditions).

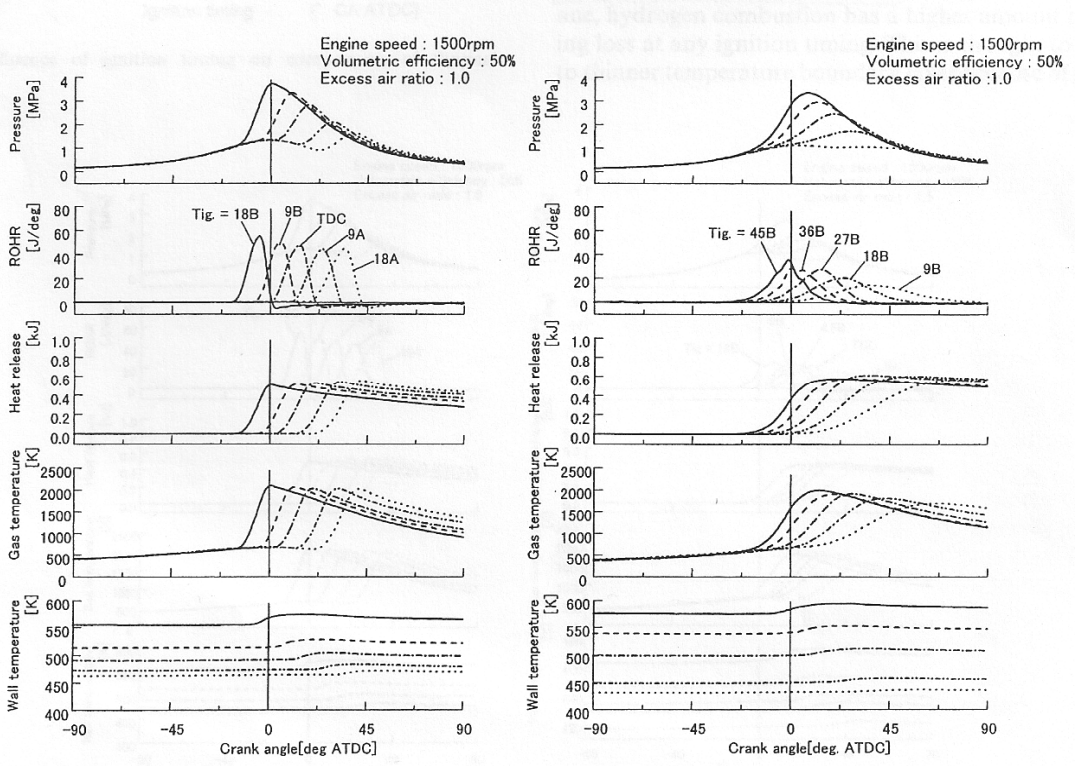

(a) Hydrogen (b) Methane

Figure 2.14: Influence of ignition timing on hydrogen and methane combustion (Shudo et al., 1999).

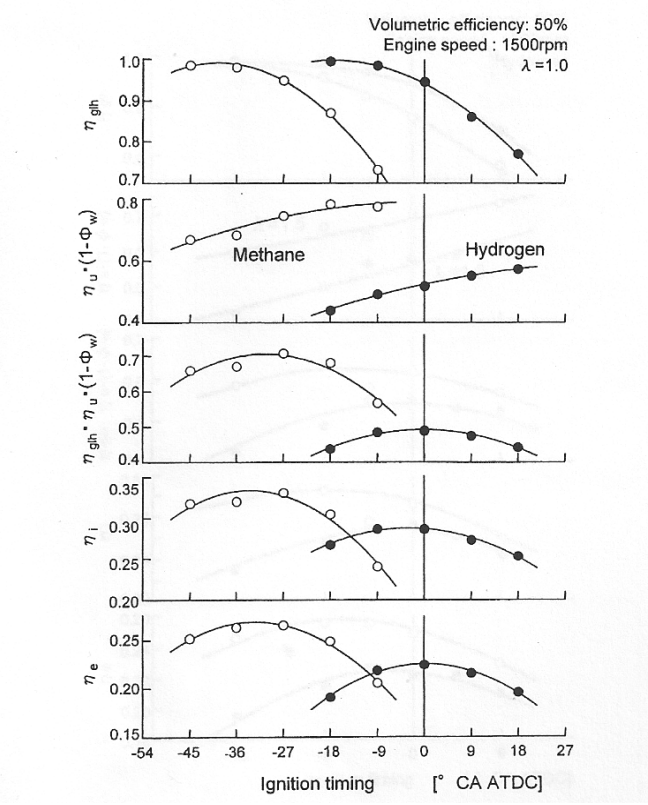

Figure 2.15: Influence of ignition timing on components of thermal efficiency (Shudo et al., 1999).

Figure 2.15 summarises graphically the effect of ignition timing on the various components of thermal efficiency. From Figure 2.15 it can be concluded that the degree of constant volume combustion, η_{glh} , and cooling loss to the combustion chamber walls control the thermal efficiency in hydrogen stoichiometric combustion, and that compared with methane combustion, hydrogen has a higher amount of cooling losses for any ignition timing. This is though to be due to a thinner temperature boundary layer because of the shorter quenching distance of hydrogen, but also increased forced convection due to higher combustion velocity may promote the heat transfer to the combustion chamber walls. However, in particular for rich mixtures and high pressures, the influence of the higher values of specific heats for hydrogen (at 200 C and 1 bar, hydrogen specific heats are: C_p = 14.32 kJ/kgK and C_v = 10.16 kJ/kgK, whereas those for methane are: C_p = 2.22 kJ/kgK and C_v = 1.70 kJ/kgK) compared with those of methane should

be the main reason of the differences in cooling losses between these two gases.

Figure 2.16 shows a comparison between stoichiometric and lean combustion with an excess air ratio of $\lambda = 1.5$. The results show slower combustion due to decreased combustion velocity, therefore decreasing the gas temperature. Also, the combustion chamber wall temperatures are decreased and the reduction in thermal losses increase the engine thermal efficiency. As a result, the cooling loss, defined as $\eta_u(1-\varphi_w)$, decreases with the increase in excess air ratio therefore being a possible and plausible reason for the high thermal efficiencies of the hydrogen fuelled engines.

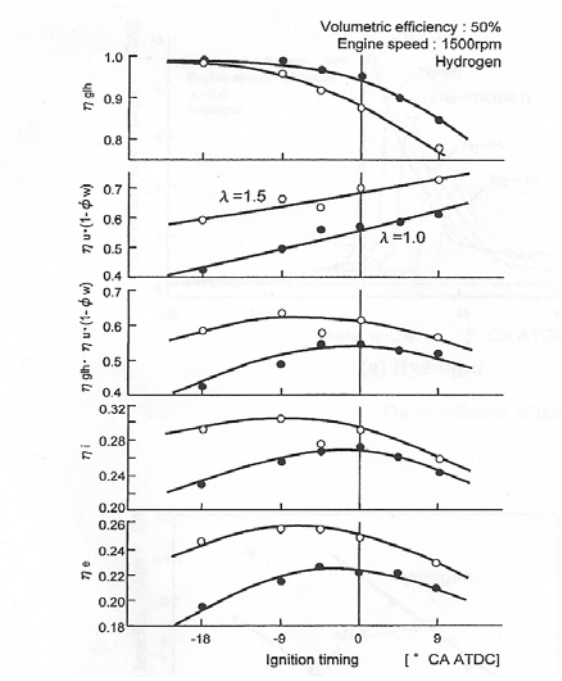

Figure 2.16: Influence of excess air ratio on the components of thermal efficiency (Shudo et al., 1999).

Based on this research work, Shudo et al. concluded that the increase of excess air is an effective way of increasing the engine thermal efficiency by decreasing the heat losses, and that hydrogen has a higher amount of cooling losses than methane. Also, it was found that there is a relationship between the degree of constant volume combustion and thermal losses, the two factors that dominate the thermal efficiency.

2.5.2 Heat transfer in hydrogen fuelled engines

As a consequence of the identified heat loss characteristics of hydrogen fuelled engines, Shudo et al., (2002) concluded that current heat transfer models developed for hydrocarbon fuel operated engines do not apply directly to hydrogen fuelled engines. Comparing the heat losses predicted using a number of existing models applicable to hydrocarbon fuelled engines with the measured heat losses from an experimental engine, Shudo et al. concluded that those models underestimate heat transfer losses, and that the use of correction coefficients doesn't accurately define the actual heat transfer rate. A new heat transfer model for hydrogen fuelled engines had to be derived to better predict the real process. According to the authors, the existing models, based on turbulent heat transfer in tubes and correlating mean cylinder gas temperatures and mean in-cylinder pressure to determine average heat transfer coefficients, give rise to errors in the determination of heat losses in the order of 4 compared with experimental data. As a consequence, the following equation for the calculation of heat transfer to the combustion chamber wall as a function of crank angle was proposed:

$$\frac{dQ_w}{d\theta} = S\alpha\left(T_g - T_w\right)\frac{1}{6\mathrm{n}} \qquad (2.3)$$

Here, S is the total surface area of the combustion chamber (m^2), n is the engine speed (rpm), α is the heat transfer coefficient ($W/m^2/K$) and T_g and T_w are the mean in-cylinder gas temperature and the mean combustion chamber wall temperature, respectively.

The authors used standard techniques when calculating the rate of apparent heat release from the test data. However, an important finding was the variation in the cylinder charge specific heat has high influence in hydrogen engines. For hydrocarbon combustion, the change in specific heat ratio γ over the cycle is relatively small and can therefore be neglected, this cannot be done for hydrogen engines. When subjected to in-cylinder pressures and temperatures, a hydrogen-air mixture experiences high variations of C_p and C_v, therefore also giving large variations of the

specific heat ratio γ. For richer cylinder charge, this effect becomes increasingly important.

Hydrogen heat losses depend on the amount of constant pressure combustion in the cycle and can analysed using the methodology outlined by Shudo et al. (1999). Shudo et al., (2002) used two fuels, methane and hydrogen, to establish a comparison for the same engine under identical operating conditions, and the differences are presented in Figure 2.17.

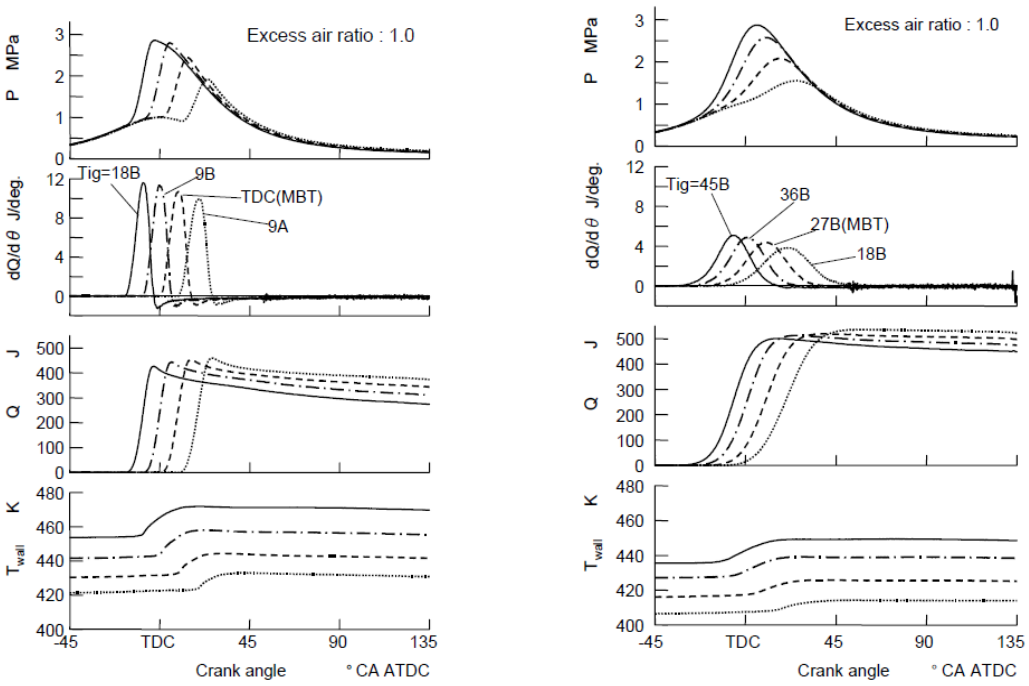

Figure 2.17: Comparison of hydrogen and methane combustion.

Figure 2.17 shows a comparison of stoichiometric combustion of hydrogen and methane under various ignition timing conditions. It was found that the heat release of hydrogen combustion is completed in a shorter period of time than that of methane combustion because of the higher burning velocity. A negative apparent heat release after the end of combustion is significant in hydrogen combustion. Changes in the temperature of the combustion chamber wall during the combustion period are also significant. These results suggest higher heat transfer losses in hydrogen combustion. Having demonstrated the limitations of existing heat transfer models, including well-established models such as those of Van Tyen, Nusselt, Eichelberg, Woschni and Briling, Shudo et al., (2002) presented a new heat

transfer equation applicable to hydrogen fuelled engines, taking into account factors such as the higher flame speed of hydrogen and the differences in combustion chamber heat transfer when compared with hydrocarbon fuels. It was suggested that the heat transfer coefficient, α, should be calculated as:

$$\alpha = C_1 D^{-0.2} P^{0.8} T_g^{-0.53} w^{0.8} \qquad (2.4)$$

$$w = C_m + C_2 \frac{dQ}{dt} \frac{T_r}{(P_r V_r)} \qquad (2.5)$$

C_m is the mean piston speed and dQ/dt is evaluated as defined above. The coefficients C_1 and C_2 in the new heat transfer equation for hydrogen combustion with different ignition timings and excess air ratios are shown in Figure 2.18. It can be seen by inspection of the figure that the influence of the excess air ratio on the coefficients is larger than that of the ignition timing. Both coefficients increase with a decrease in the excess air ratio, hence for high excess air ratios the heat losses through the combustion chamber walls is decreased. In future research, expressing the coefficients C_1 and C_2 as a function of the various wide operation conditions and fuel properties could increase the universality of the proposed heat transfer equations.

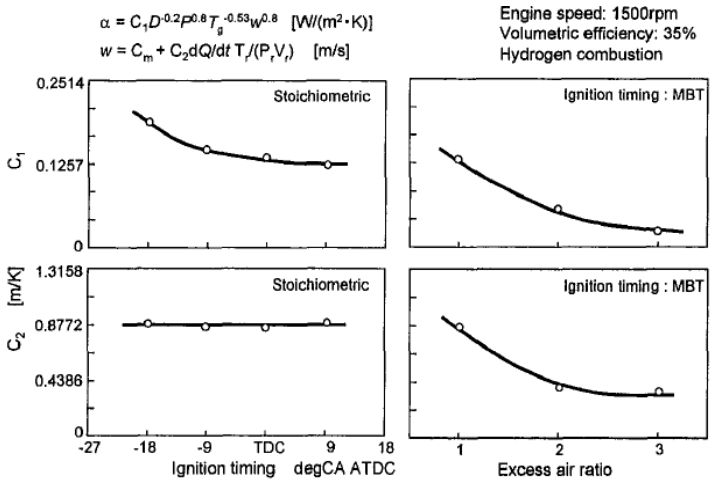

Figure 2.18: Coefficients in the new proposed heat transfer equations for different operating conditions (Shudo et al., 2002).

2.5.3 Exhaust heat losses in hydrogen fuelled engines

Following their line of research on hydrogen fuelled engines and the associated heat losses, Shudo et al., (2007) carried out a number of tests with direct injection of hydrogen, i.e. stratified charge, in order to reduce heat losses and improve engine efficiency. A reduction in cooling losses does not always translate directly into an improvement in indicated thermal efficiency, however it can do so if simultaneous exhaust losses do not increase as well.

Based on the previously presented cooling loss ratio theory, the indicated thermal efficiency can be defined as

$$\eta_i = \eta_{th}\eta_{glh}\eta_u\left(1-\varphi_w\right) \qquad (2.6)$$

By defining the cooling loss fraction φ_w as the fraction of the cumulative cooling loss heat Q_C to the cumulative real heat release Q_B, the apparent heat release fraction Q/Q_{fuel} corresponds to a function of the combustion efficiency and the cooling loss fraction $\eta_u\left(1-\varphi_w\right)$ (Shudo et al., 1999). Therefore:

$$Q/Q_{fuel} = \eta_u\left(1-\varphi_u\right) \qquad (2.7)$$

This can be used to express the cooling losses as a function of the heat supplied and the combustion efficiency:

$$\varphi_w = 1-Q/\left(\eta_u Q_{fuel}\right) \qquad (2.8)$$

Similarly, the exhaust gas loss ratio can be defined as follows: Exhaust heat loss Q_{ex}, is the heat carried away by the exhaust gases per cycle, which can be defined as a function of the heat supplied per cycle and the indicated work W_i produced per cycle as:

$$Q_{ex} = Q - W_i \qquad (2.9)$$

where Q is the cumulative apparent heat release calculated from the measured pressure data and the amount of heat supplied per cycle, Q_{fuel}. The cumulative heat release is

$$Q = \eta_u\left(1-\varphi_w\right)Q_{fuel} \qquad (2.10)$$

From the definition of indicated thermal efficiency, the indicated work can be defined as

$$W_i = \eta_{th}\eta_{glh}\eta_u(1-\varphi_w)Q_{fuel} = \eta_{th}\eta_{glh}Q \qquad (2.11)$$

Therefore the exhaust heat loss, Q_{ex} , can be described as

$$Q_{ex} = (1-\eta_{th}\eta_{glh})\eta_u(1-\varphi_w)Q_{fuel} \qquad (2.12)$$

Combining these, an exhaust loss fraction φ_{ex} , i.e. the fraction of exhaust gas heat Q_{ex} to the supplied fuel heat Q_{fuel} , can be defined as follows:

$$\varphi_{ex} = Q_{ex} / Q_{fuel} \qquad (2.13)$$

The exhaust loss fraction can then be expressed as a function of the heat loss fraction as follows:

$$\varphi_{ex} = (1-\eta_{th}\eta_{glh})\eta_u(1-\varphi_w) \qquad (2.14)$$

From the above equations it is expected that there will be an optimum point of operation, at which the losses of heat through the exhaust gases and the heat losses to the combustion chamber walls give the highest possible engine efficiency. According to Shudo et al., (2007), this depends on the degree of constant volume combustion η_{glh} , therefore a method that doesn't reduce η_{glh} can be the stratified direct injection of hydrogen. When the degree of constant volume combustion is lower than a critical value (depending on the actual engine characteristics), the exhaust loss fraction increases and leads to a decrease in the theoretical thermal efficiency. Therefore, engines with lower compression ratios require higher degrees of constant volume combustion to improve the thermal efficiency, due to the cooling loss reduction. The increase in the apparent heat release fraction effectively leads to improvements in thermal efficiency, because the stratified charge reduces the cooling loss without lowering the degree of constant volume combustion. The authors reported that for one engine with a compression ratio of 14 and a degree of constant volume combustion of 0.95, a 15 % cooling loss fraction achieves a very high value of indicated thermal efficiency, over 50%. Therefore, according to the authors, direct injection stratified charge is an effective technique to improve the thermal efficiency of hydrogen combustion engines.

2.6 Hydrogen engine safety

Hydrogen fuelled engines require particular safety measures in the design of the engine, auxiliary equipment and operating environment. These safety measures can be grouped into three main groups:

1. Prevention of explosive atmosphere.
2. Removal of ignition sources outside the combustion chamber.
3. Protection against explosion in engine components.

The measures required for hydrogen fuelled engine operation can typically include:

- installation of a hydrogen leakage sensor on the supply lines;
- sufficient ventilation of the engine room (at least 20 air volume renewals per hour);
- monitoring of the engine room atmosphere for hydrogen leakage;
- crank case ventilation with fresh air, or connection to the engine air inlet;
- glow plugs fitted at the exhaust pipe flange to ensure that any hydrogen is combusted at the engine outlet; and
- dilution of the exhaust gas on the stack by installing a forced draft ventilator to ensure that LEL (Lower Explosion Limit) concentrations are never reached.

Avoidance of ignition outside the combustion chamber is achieved by using equipment designed for explosive atmospheres, for example with ATEX certification. Protection against explosion is achieved by installing rupture discs in the exhaust system, to ensure that the pressure in the exhaust system does not rise above its design limit. Safety measures for hydrogen engine operation will be discussed in more detail in Chapter 3.

2.7 Conclusions

From the limited research work available on HCCI and DIH_2 engines, the large potential of these modes of operation is clear, in particular when a comparison of thermal efficiencies with other fuels and modes of operation is made. However, significant research and development efforts in a number of areas related to engine operation, safety and fuel supply and storage are required before hydrogen fuelled engines will present a realistic commercial alternative to conventional engines.

An important conclusion that can be drawn from this research review is that the very distinct physical properties of hydrogen make the use of existing modelling approaches developed for hydrocarbon fuel combustion questionable, and care should be taken if such models are used. Possibly, new approaches need to be developed, tested and validated, in particular for compression ignition hydrogen engines. Improving the understanding of hydrogen engine combustion and operation is fundamental for achieving high thermal efficiencies.

The design of HCCI or DIH_2 engines can in principle be derived from existing commercial models, however development work in the control of the rate of pressure rise for both modes of operation and on the control of the ignition timing for the HCCI mode will be required. One option to develop this technology and allow it to mature before the use of hydrogen as fuel is to operate such engines with natural gas, which has more favourable properties with respect to storage, availability and safety.

High performance HCCI and DIH_2 hydrogen engines will be suitable for use in a range of applications. In addition to automotive engines, which much of the recent research focuses on, such engines should be suitable for marine and rail propulsion, as well as stationary power generation such as combined heat and power systems. Considering the challenges associated

with storage and transport of hydrogen, stationary systems are perhaps the most realistic application for hydrogen engines in the near future.

Chapter 3

Engine performance analysis through experimentation

« There is no such thing as a failed experiment, only experiments with unexpected outcomes. »

Buckminster Fuller

This chapter presents the engine and monitoring system which was designed and constructed to conduct experiments on HCCI and DIH_2 hydrogen fuelled operation. Both hydrogen injection system designs and their characterization, control and engine monitoring are discussed.

3.1 Engine experimental setup

The compression ignition engine test rig was designed to allow the experimentation of various modes of operation covered by this research, namely, homogeneous charge compression ignition and direct injection of hydrogen operating with a compression ignition engine.

3.1.1 Compression ignition engine

With the objective of adhering as much as possible to an implementation of the most common industrial type of engine, the main experimental part of the research work was carried out using a production four stroke, single cylinder, direct injection, naturally aspirated, air cooled compression ignition engine. The engine is illustrated in Figure 3.1.

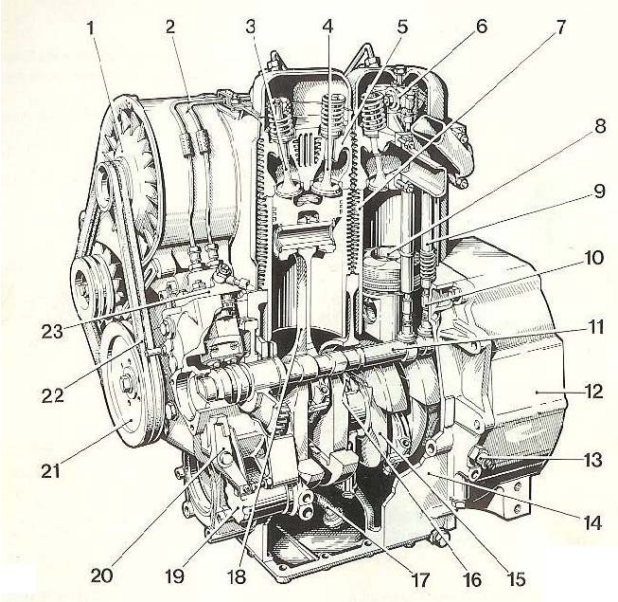

Figure 3.1: Cross section of the test diesel engine. (In this case the two-cylinder version of the Deutz F1L 511).

Engine components illustrated in Figure 3.1 include:

1: Air cooling fan

2: Fuel injector pipes

3: Inlet valve

4: Exhaust valve

5: Cylinder head

6: Rocker arm

7: Finned cylinder liners

8: Piston

10: Push rod

11: Camshaft

12: Flywheel cover

13: Oil level plug

14: Crankcase

15: Crank

16: Counterweight

17: Lub oil suction pipe

18: Connecting rod

19: Lub oil pump

20:Rack lever

21: Main distribution pulley

22: Driving belts

23: Fuel injection pump

The specification of the engine used for experimentation was:

Manufacturer:	Deutz
Model:	F1L511
Bore	100 mm
Stroke	105 mm
Swept volume	825 cm^3
Compression ratio	17:1
Maximum engine speed	3000 rpm
Intake air valve opens	32º BTDC
Intake air valve closes	59º ATDC
Intake air valve open duration	91º
Intake air valve closed duration	269º
Exhaust valve opens	71º BTDC
Exhaust valve closes	32º ATDC
Injection angle (diesel oil)	24º BTDC
Exhaust valve open duration	103º
Exhaust valve closed duration	257º
Valve overlap duration	27º

The engine was directly coupled to a constant displacement hydraulic pump via two flexible couplings. The engine load using the hydraulic pump was changed through a restriction valve, by varying the discharge pressure. The hydraulic system arrangement of the test rig allowed a stable load to be applied under all the engine operating conditions. The hydraulic pump compression line was instrumented with a pressure sensor which, in conjunction with the speed signal from an encoder fitted to the engine camshaft end, allowed the calculation of the engine shaft power. This calculation was performed based on the pump displacement, hydraulic pressure and pump efficiency. The hydraulic pump efficiency was

considered over the entire operating range and incorporated into the power calculation.

Figure 3.2 shows the engine test rig and the hydraulic brake specification is given in Table 3.1.

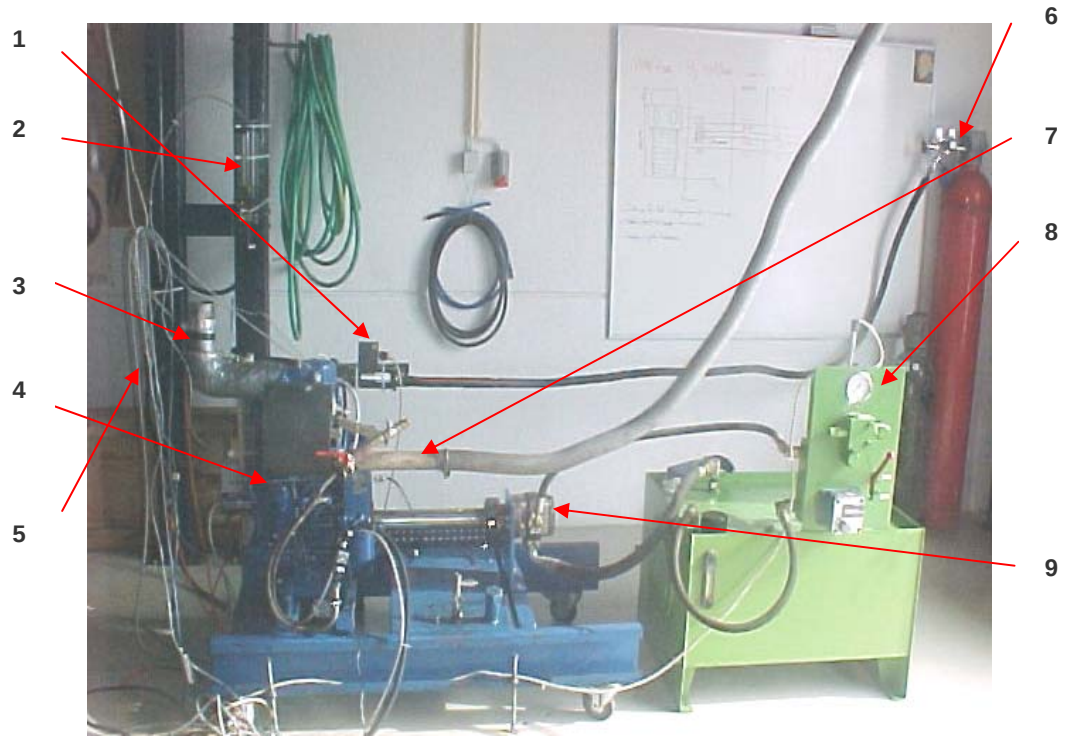

1 - H_2 flow meter; 2 - diesel fuel burette; 3 - Air inlet manifold; 4 – Engine; 5 - Data acquisition system cables; 6 - 200 bar H_2 cylinder; 7 - Exhaust pipe; 8 - Hydraulic oil tank, brake control panel and pressure transmitter; 9 - Hydraulic brake pump

Figure 3.2: Engine test rig.

Table 3.1: Specification of the hydraulic engine pump.

Hydraulic pump characteristics:	
Hydraulic pump maker:	Voith
Hydraulic pump model:	IPH 3-10
Pump displacement:	5.2cm^3/turn
Maximum speed:	3000 RPM
Maximum discharge pressure:	300 bar
Efficiency (100 – 200 bar range):	0.85 – 0.90
Hydraulic tank capacity:	200 dm^3

3.1.2 Air supply system modifications

The engine air supply system, as shown in Figure 3.3, was modified to accommodate a 3.5 kW air heater, capable of raising the air inlet temperature up to approximately 120ºC, with an ambient temperature of 10ºC. Also, an air mass flow meter was installed in the air inlet manifold and the air filter was removed, in order to reduce the pressure loss across supply system.

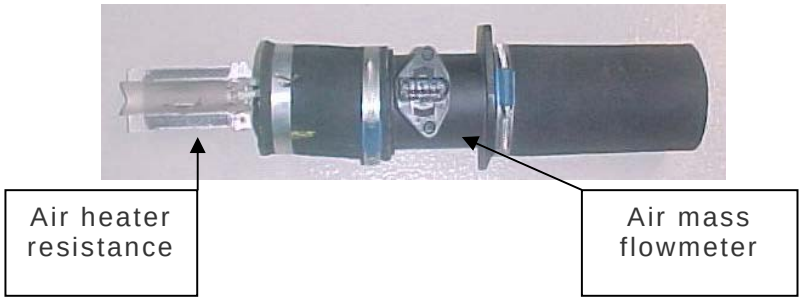

Figure 3.3: Inlet manifold heater and mass flow meter.

3.1.3 Fuel system

The diesel fuel system, as shown in Figure 3.4, allowed diesel consumption measurement through an electric pulse type flow meter installed in the diesel fuel pipe. This signal was acquired by a data acquisition system. As an additional measurement of the fuel flow rate, a 1.5 dm^3 graduated

burette, placed 1.5 m above the injection pump was used and consumption measured manually.

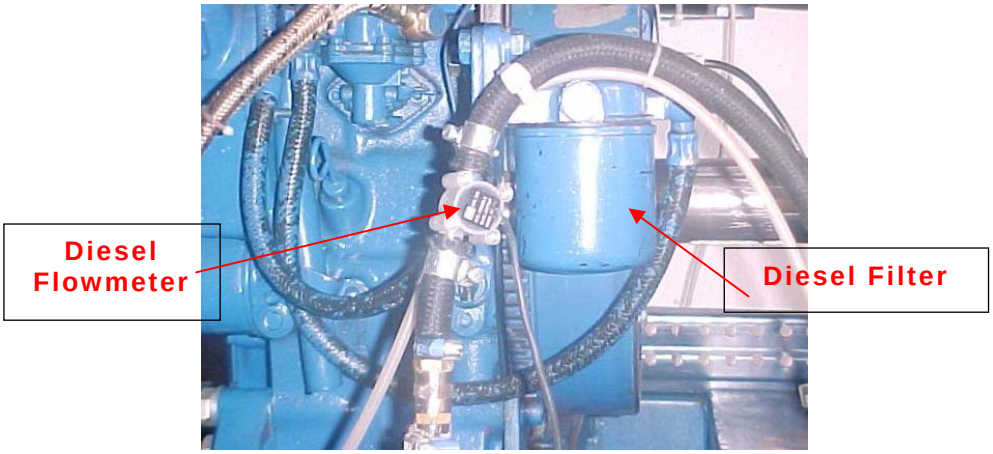

Figure 3.4: Diesel oil flow meter.

Hydrogen was supplied to the engine, from an 80 dm^3 hydrogen cylinder at 200 bar. The engine hydrogen fuel system comprised two different arrangements, depending on the injection pressure in use. For hydrogen low pressure injection (< 8 bar) the system was operated with two pressure regulators, one that reduced the pressure from 200 bar to 15 bar, in series with a second regulator with a fine regulating adjustment valve and respective pressure indicator allowing a constant pressure regulation between 15 bar to 0.3 bar. For hydrogen high pressure injection (>120 bar) the system was operated with only one pressure regulator, capable of supply constant pressure between 45 bar and 200 bar. A needle isolating valve and a flame trap were placed before the hydraulic injector in both supply systems.

3.1.4 Exhaust gas system

In order to allow the engine exhaust gas to be analysed, a ball valve was fitted after the silencer, to allow the exhaust gas analyser probe to be inserted inside the exhaust pipe.

3.1.5 Test rig instrumentation and data acquisition system

To collect the data from engine test rig, a high speed data acquisition system was developed based on National Instruments hardware. Software was also developed to control the engine using a purpose developed injector controller. The instrumentation used on the engine test rig, for DIH_2 and HCCI operation is presented in Figures 3.5 and 3.6. All the sensors shown were interfaced with the data acquisition system described below.

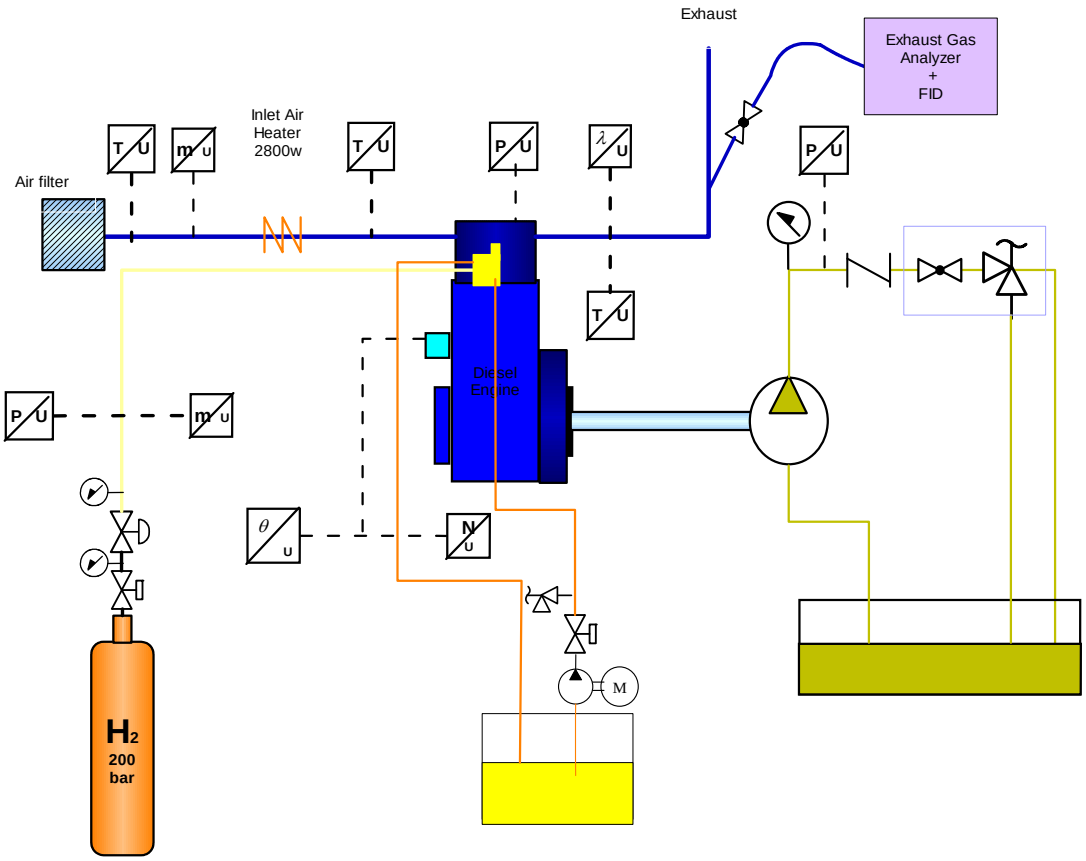

Figure 3.5: Hydrogen direct injection engine test rig schematic diagram.

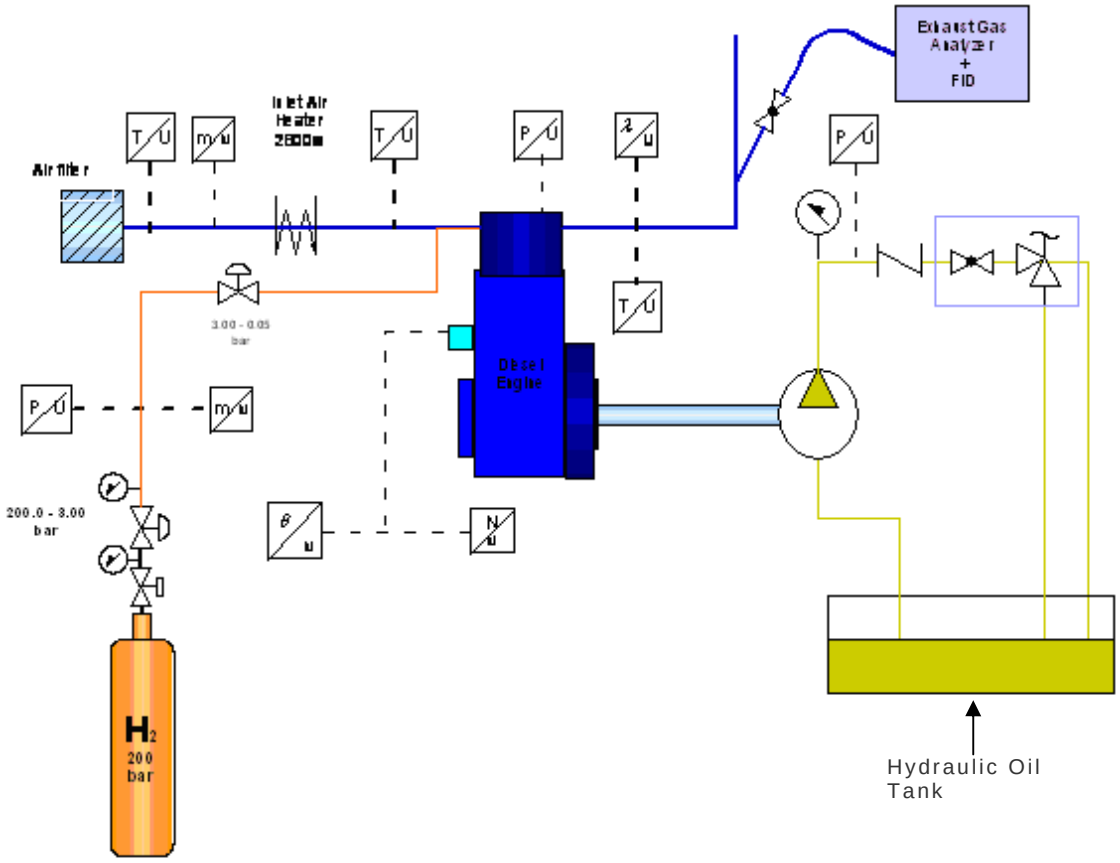

Figure 3.6: Hydrogen Homogenous Charge Compression Ignition engine test rig schematic diagram.

3.1.6 Data acquisition system hardware

A real time data acquisition system, based on LabView software and National Instruments hardware was developed for data logging and monitoring. The engine speed and crank angle was measured using an absolute encoder directly fitted on the engine camshaft, allowing the cylinder pressure data to be referenced to the piston top dead centre (TDC). The sampling speed and resolution of the system was 100 kHz and 16-bit respectively.

The data acquisition system was made up of five National Instruments boards and its block diagram is presented in Figure 3.7. One NI PCI-7830R (a communication board using the digital input output (DIO) connection with 40 I/O digital lines); two cRIO-9423, which has 8 input voltage channels up to 30 volt, one cRIO-9211 (four thermocouple analogue input board); CB68-

LP (a terminal block board which allowed four analogue inputs, four digital outputs and sixteen additional high speed digital lines TTL) and the expansion chassis RIO NI cRIO-9151, into which all the boards were inserted. The system shared the engine crank angle and speed signal from the encoder.

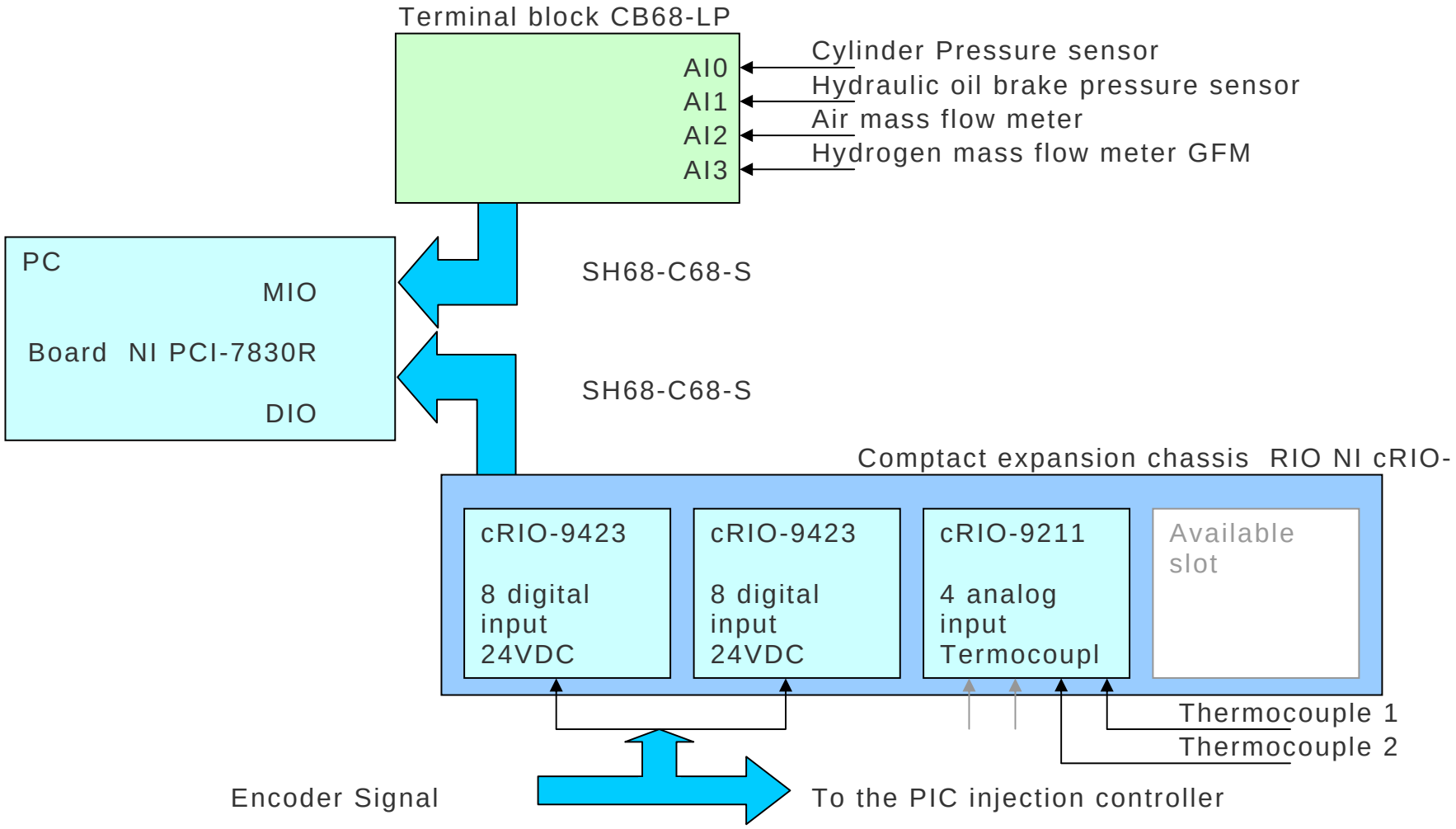

Figure 3.7 Data acquisition block diagram

3.1.7 Data acquisition system software

A high speed data acquisition program was developed to allow the engine variables acquired, monitored and analysed on and off line. This software was developed using LabView, and was designed to have four interface displays: Visualization, Analysis, Configuration and Diagnosis.

The *Visualization Display* (Figure 3.8) was designed to allow the simultaneous acquisition and monitoring of the following variables: engine power (kW); in cylinder pressure (bar); hydraulic load pressure (bar); hydrogen flow rate (l/min and kg/h); diesel fuel oil flow rate (kg/h); air mass flow rate (kg/h); equivalence ratio; air intake temperature (ºC); exhaust gas temperature (ºC); crank angle (º); engine speed (rpm); and engine thermal efficiency (%).

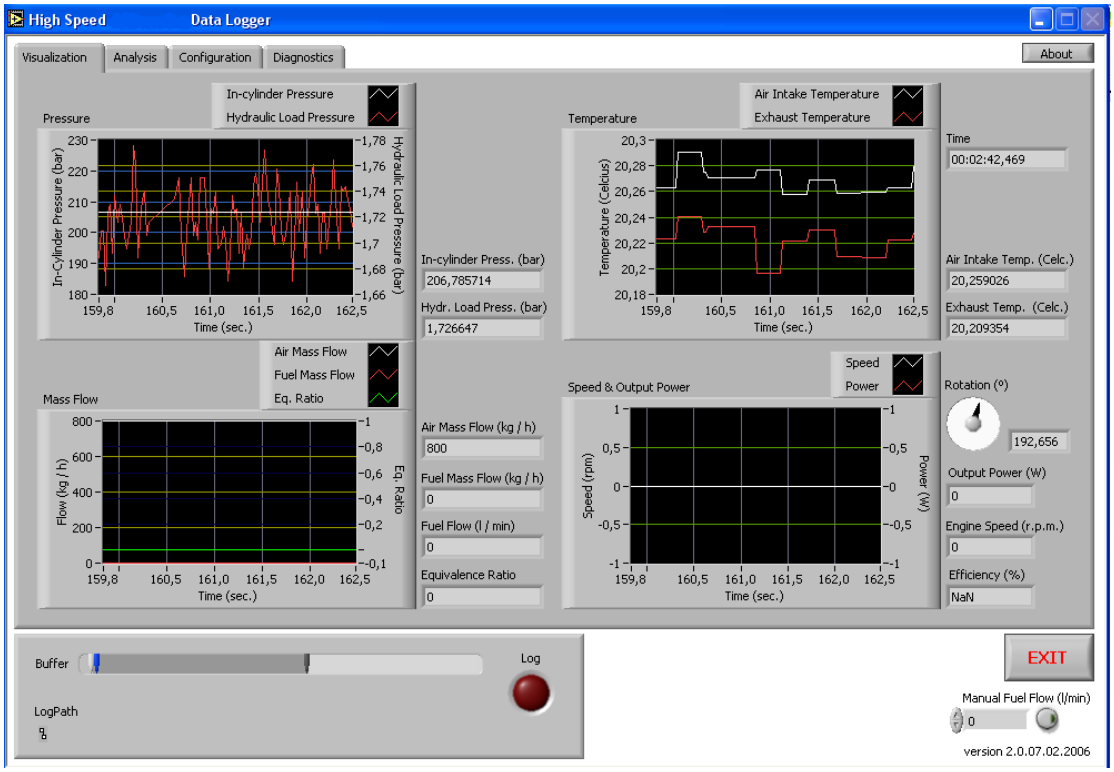

Figure 3.8: Visualization Display menu.

The *Analysis display* menu is shown in Figure 3.9 and was designed to allow the simultaneous analysis of selected variables and provided a series of analysis tools, such as:

- Plots with zoom and graph scaling functions, indicating the variable magnitude against crank angle or time.
- Derivatives in the time domain or crank angle domain. This analysis tool can be used to analyse the signals, for example rate of change in the cylinder pressure and the determination of ignition angle.
- Fast Fourier Transform (FFT) of any signal. FFT analysis can be used to determine the existence of resonance phenomena during the measurement of the in-cylinder pressure.
- Forward 720º and rewind 720º to analyse cycle by cycle graphically.
- Averaging of cycles: the average from a number of cycles can be derived. This is a basic parameter to overcome the noise effect present in the signals.
- Median filter. As the derivative tends to amplify the signals noise, a median filter was included to mitigate such effect.

The *Analysis display* menu allowed the selection of any of the available variables and also the export and import of data in ”CSV”, “DAT” and “BMP” formats.

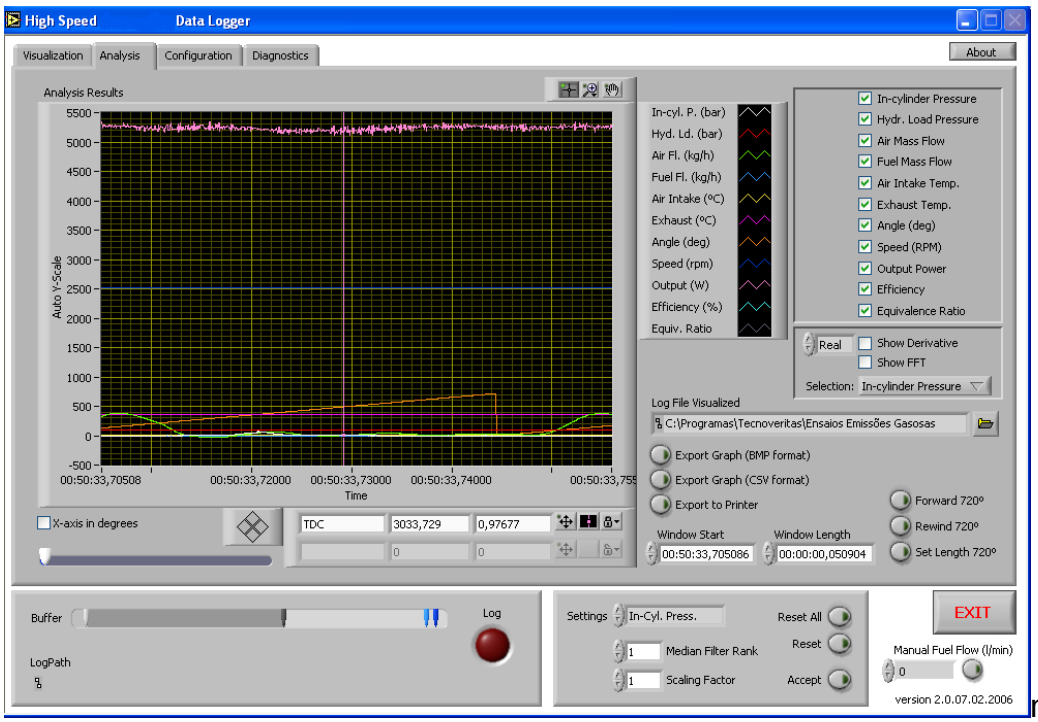

Figure 3.9: Analysis Display menu.

Figure 3.10 shows an example of a cylinder pressure diagram (against crank angle) produced by selecting the in-cylinder pressure option in the software.

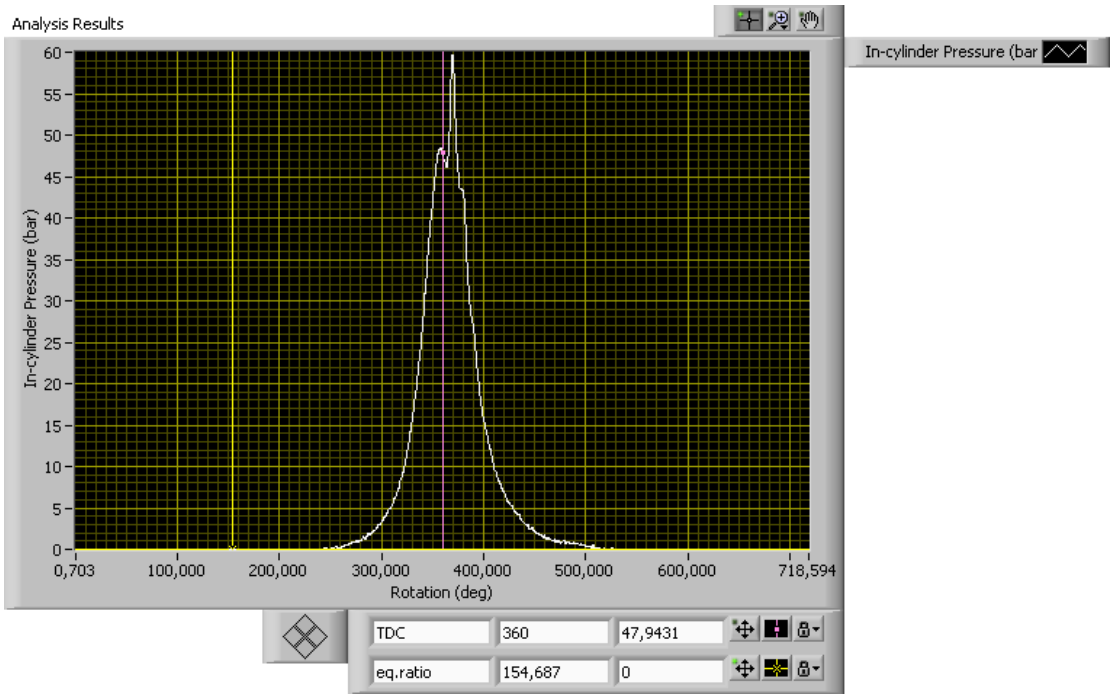

Figure 3.10: Cylinder pressure against crank angle analysis display.

The *Configuration display* menu is shown in Figure 3.11 and was designed to allow calibration of the various interfaced transducers and also the introduction of all the constants required for the program algorithm calculations.

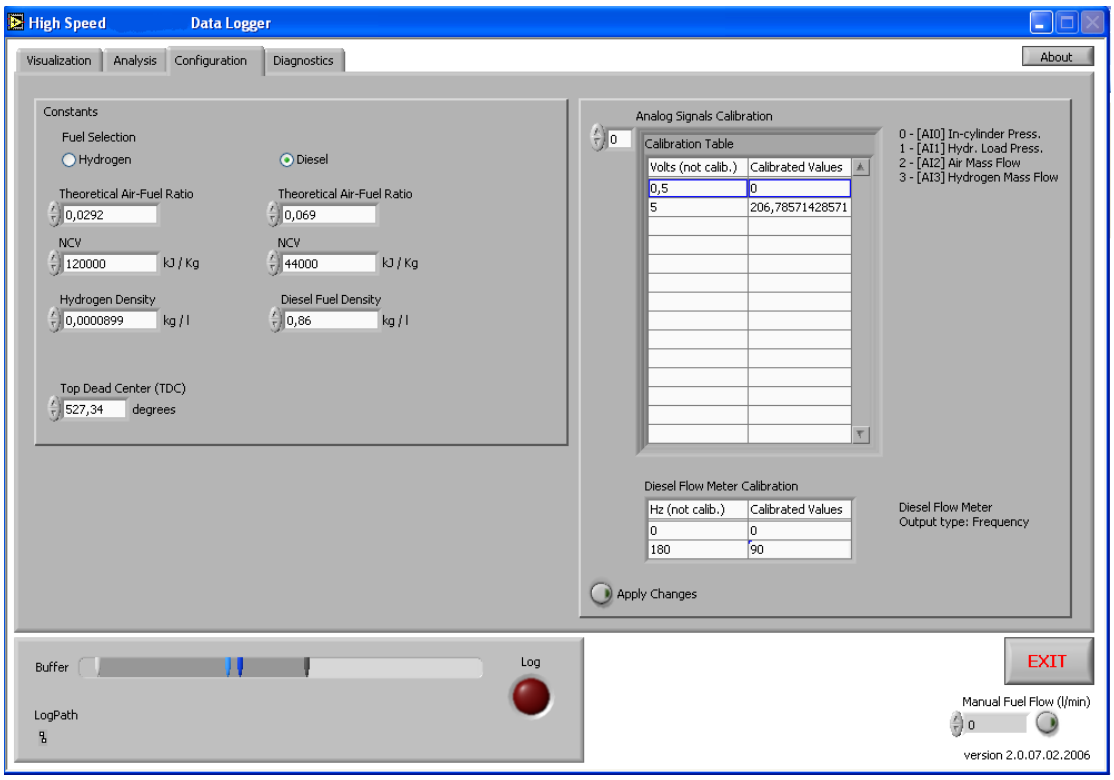

Figure 3.11: Configuration display menu.

The *Diagnosis display* menu is shown in Figure 3.12 and was designed to allow the setting of sampling rate to be used, memory space management, and monitoring of the channels data.

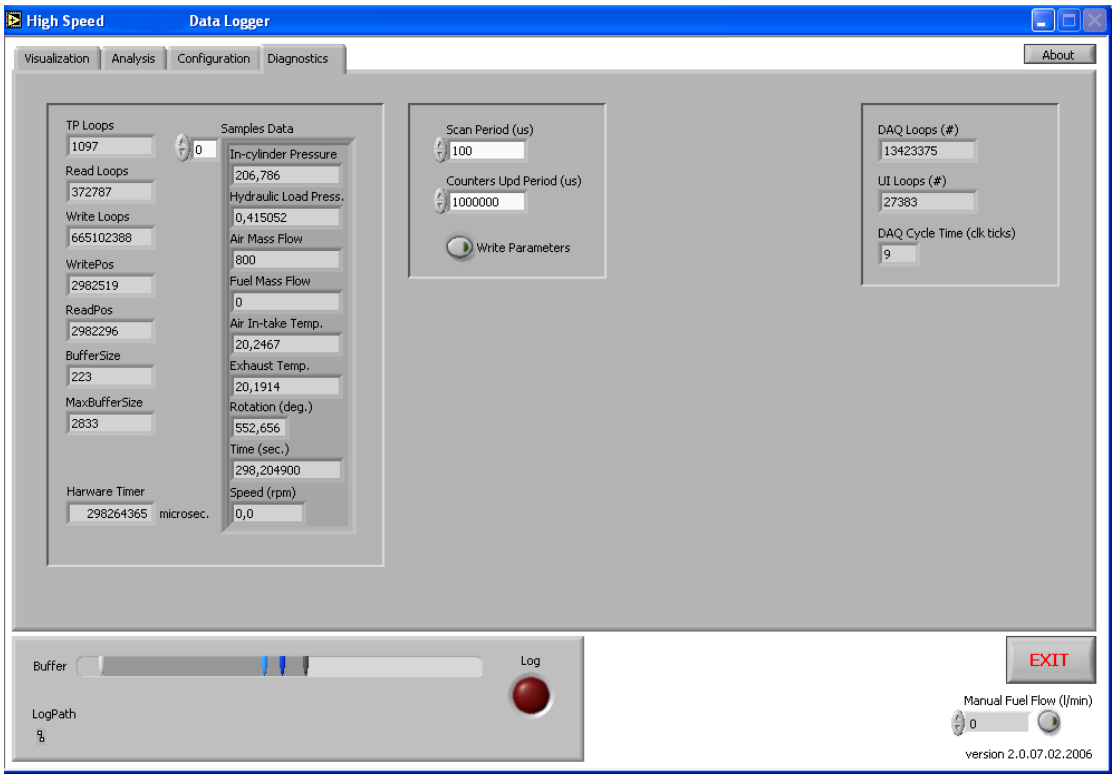

Figure 3.12: Diagnosis display menu.

3.1.8 Engine speed and crank angle measurement

The engine speed and crank angle measurements were made using an absolute encoder fitted at the engine camshaft end, as shown in Figure 3.13. This encoder fed its signal to the injection control system and the high speed data acquisition system through a specially made junction box.

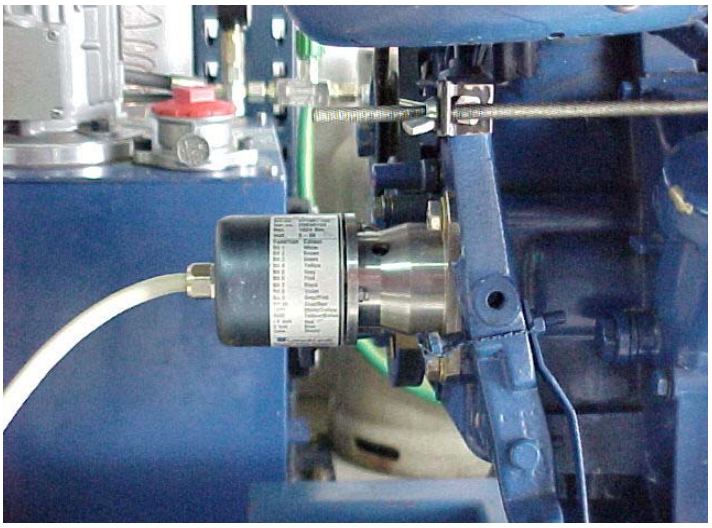

Figure 3.13: Absolute encoder fitted at the camshaft end of the test engine.

3.1.9 Cylinder pressure transducer

A autoPSI-S cylinder pressure transducer was utilised to measure in-cylinder pressure variation over the engine cycle. The accuracy of this transducer is within ± 1.0 % (linearity and hysteresis combined). Special care was taken in the selection of the sensor in respect of its resonance frequency, since masking of cylinder pressure transients could occur if the sensor resonance frequency coincides with the pressure transient frequency.

3.1.10 Air mass flow transducer and measurement

Air mass flow to the engine was measured using a special hot film mass flow meter (Bosch HFM5), shown in Figure 3.14. By processing the sensor data it was possible to detect when return flow takes place during air flow pulsation. The air mass flow was compensated in terms of density and temperature and had an extensive measuring range.

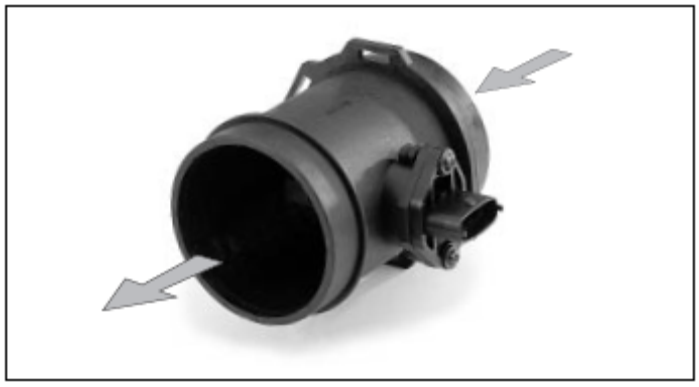

Figure 3.14: Air mass flow meter Bosch HFM5.

The transducer had a measuring range of 8 to 800 kg/h, accuracy better than ±3 %, a fast response of 15 ms, and was able to withstand vibration accelerations up to 150 m/s^2.

3.1.11 Hydrogen mass flow measurement

Hydrogen mass flow was measured using a Dwyer GFM-1107 mass flow meter with a totalizer. It was based on a straight tube sensor with a restrictor flow element to provide high accuracy (±1.5% of full scale) and repeatability (± 0.5% of full scale).

3.1.12 Lambda oxygen transducer and measurement

A lambda oxygen sensor (Bosch LSM 11) was installed just after the exhaust port, to monitor λ, the O_2 concentration in the exhaust gas from the engine.

The response time for lean mixtures was approximately 2 s and the relative sensitivity $\Delta U_s / \Delta\lambda$ at a λ-value of 1.3 was 0.65 mV / 0.01, where the ΔU_s is the sensor supply voltage.

3.2 Hydrogen fuel injection systems

As described above, hydrogen injection systems for both HCCI and DIH_2 operation was developed for this project. This section describes design considerations and the solutions chosen in this work.

3.2.1 Material considerations when using hydrogen

A difficult problem with the use of hydrogen is associated with a form of corrosion caused by the depletion of oxygen from protective metal oxide coatings. Without the protecting oxide film most metals are highly reactive and corrosion results. Electrons pass through the metal to areas where oxygen availability is greatest and this leaves metal ions in the exposed area free to enter into solution if an electrolyte is present. The electrolyte may be formed by a film of water that is acidic due to dissolved hydrogen.
Damage to stainless steel in strained areas where sufficient oxygen is available is characterised by the following stress corrosion process. The

reaction provides hydrogen ions to make the water electrolytic and to enter the metal lattice:

$$4Fe^{++} + O_2 + 10H_2O \rightarrow 4Fe(OH)_3 + 8H^+$$

Stainless steel sealing surfaces are often designed to be deformed by mechanical stress until a line of contact produces the desired sealing effect. Near the line of contact capillaries are formed which trap moisture. As a result of this mechanism stainless steel seals near the line of contact and under gaskets experience deterioration in their physical properties. Discolouration and pitting may result from depletion of the protective chromium oxide coatings. Dark red, brown, or black stains reveal the migration of iron from the sealing surfaces where the chromium oxide is depleted or damaged and cannot be repaired because of oxygen deficiency. Exposure to air during inspection causes these iron ions to rapidly oxidise. Leaks develop because corrosive movement of metal ions leaves pathways through seal surfaces through which hydrogen can pass. G.Santhana et al 1988.

Rapid embrittlement of steel and other metals, such as nickel and copper nickel alloys, will occur at ambient temperatures when exposed to hydrogen gas at high pressure. The embrittlement is produced by the effects of solution and diffusion of hydrogen on the crystal structures of these metals. At temperatures above approximately 300ºC, in addition to embrittlement, hydrogen attack occurs where it reacts with the carbon in the steel to produce gaseous methane:

$$Fe_3C + 4H \rightarrow CH4 + 3Fe$$

Methane molecules are much larger than hydrogen and carbon in solid solution and produces internal pressure. Accumulation of methane molecules greatly increases internal stress. The disappearance of the carbides and the formation of methane can seriously weaken the alloy in question. However, alloy steels containing such elements as chromium, tungsten, titanium, and vanadium, which form chemically stable intermetallic carbides with the carbon within the steel, are resistant to

high-temperature hydrogen attack and allow them to retain their strength up to about 400ºC. G.Santhana et al 1988.

3.2.2 Hydrogen HCCI injection system

To operate the engine in HCCI mode, hydrogen is injected in the proximity of the air intake manifold, through a fast injection solenoid valve controlled by a microprocessor. The frequency of injection was set by the engine speed, whilst injection duration was determined by a pulse width modulation signal (PWM) control. Figure 3.15 shows the injection valve fitted on the engine air inlet manifold.

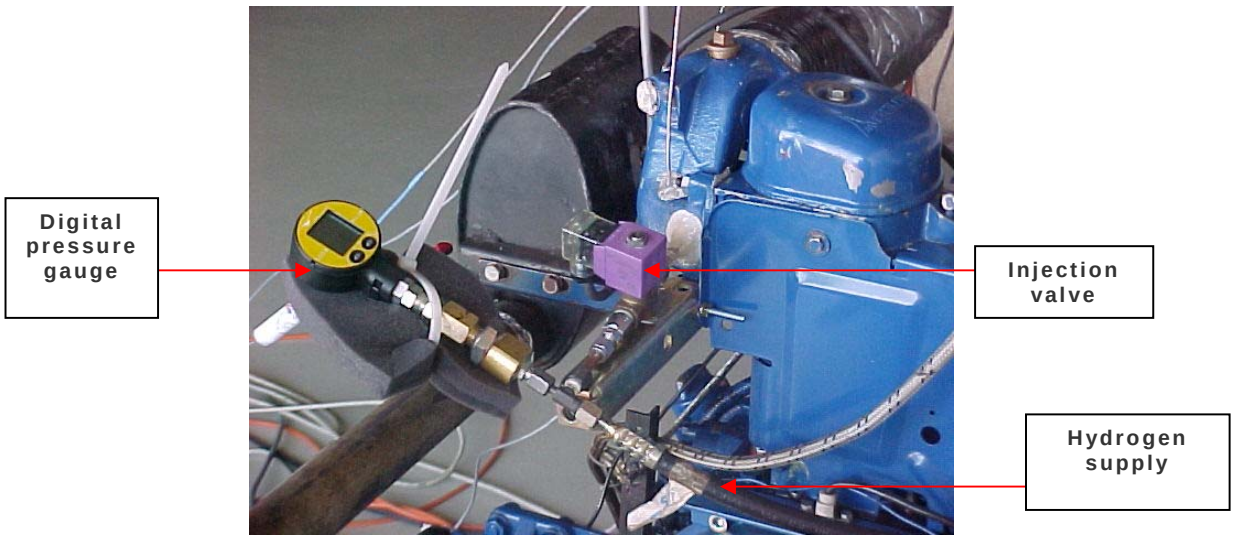

Figure 3.15: Fast-acting solenoid injection valve and hydrogen pressure gauge, fitted on the engine

The injector system for the HCCI mode of operation was relatively simple as the pressure and temperature of operation was low and the time available for injection was over a relatively large crank angle. A pulse width modulated (PWM), two way, normally closed solenoid activated ball valve injector was used in this mode of operation. The valve is shown in Figure 3.16 and a simplified cross section is presented in Figure 3.17. Designed with hydrogen embrittlement resistant materials, this was used to inject hydrogen directly into the engine intake air manifold in a controlled

manner. For adequate control of hydrogen flow rate, the pulse width modulation was used to meter fuel quantity at injection frequencies up to 200Hz and with timing precision of ± 25 microseconds. Under these conditions, sonic flow across the valve inlet occurs when fully open and mass flow is approximately proportional to the supply pressure (Barkhimer et al., 1995).

Figure 3.16: HCCI Hydrogen injection solenoid activated ball valve.

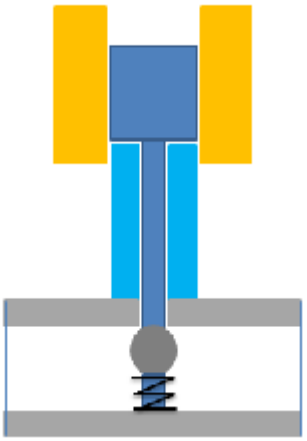

Figure 3.17: Simplified diagram of the HCCI hydrogen injection solenoid activated ball valve.

With the solenoid de-energised, the supply pressure, assisted by a spring, forces the solenoid ball poppet on its seat, barring gas flow. When the solenoid is energised, the ball poppet is lifted off the seat and held against the stop. Gas then passes through the valve seat and outlet port of the injector. The solenoid has a low impedance coil designed for fast response. It is typically actuated by a current of 4 amperes, which is reduced and held at 1 ampere to conserve energy for the duration of the energised time (pulse width) (Barkhimer et al., 1995).

3.2.3 Hydrogen direct injection system

There are no hydrogen injectors available on the market, therefore it was necessary to design, construct and calibrate a DIH_2 injector operating at

high pressure. Flow, dynamic response and leak tests were performed to characterise the injector.

The DIH_2 fuel system comprised a high pressure hydrogen cylinder (200 bar), a regulator to reduce the hydrogen pressure before the hydraulic injector (from 200 bar to 90 bar), a flame trap valve, and a solenoid valve controlled hydraulic injector controller. (See Figure 3.5 for a schematic diagram of the setup.) The frequency of injection was set by the engine speed whilst the injection duration was determined by the engine load. The hydraulic actuation oil supply was provided by a hydraulic pack which was continuously flushed with nitrogen to avoid an explosive atmosphere inside the hydraulic oil tank in case any hydrogen leakage occurred.

The design of the DIH_2 injector was carried out using Solid Works, and the injector cross section is shown in Figure 3.18. Figure 3.19 shows the manufactured solenoid controlled DIH_2 injector and Figure 3.20 the installation of the injector in the engine.

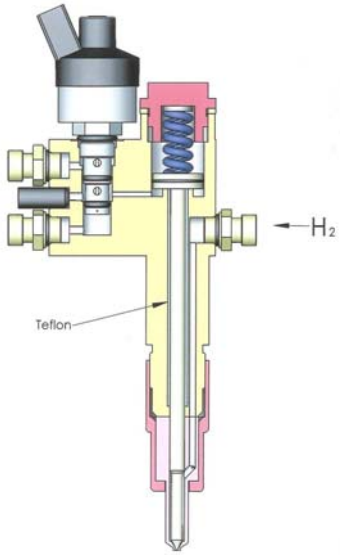

Figure 3.18: Solenoid controlled hydraulic DIH_2 cross section.

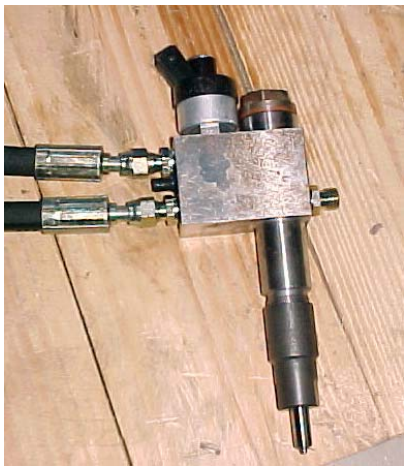

Figure 3.19: Solenoid controlled hydraulic DIH2 injector.

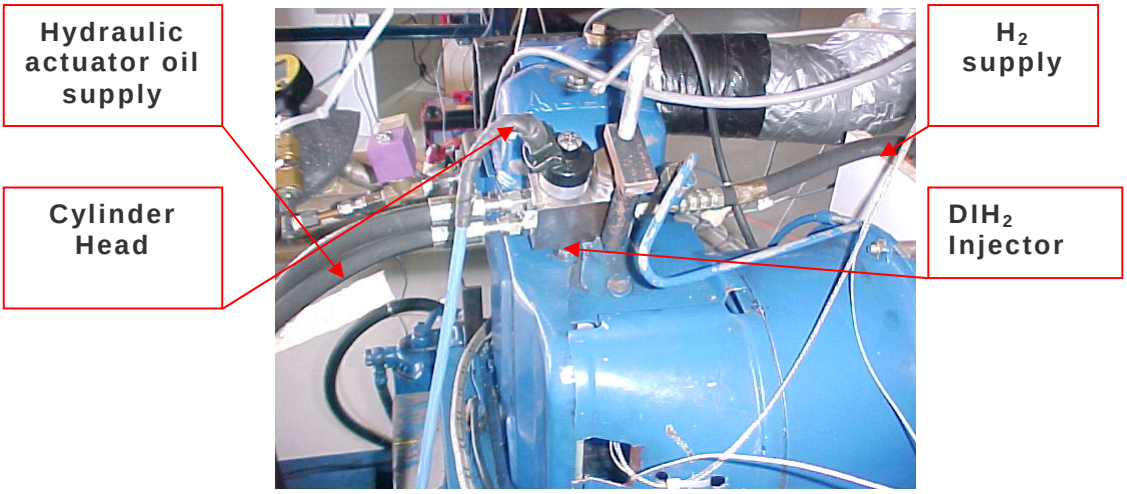

Figure 3.20: Solenoid controlled hydraulic DIH_2 injector installation.

Important design considerations for the hydrogen injector include clearances and tolerances, weight, rubbing and lubrication of the moving parts, and material selection for resistance to hydrogen embrittlement. Clearances are critical to eliminate hydrogen leakage into the hydraulic actuation oil system or the atmosphere. The injector developed and used in the experimental work exhibited a considerable amount of leakage of hydrogen into the hydraulic actuation system, caused by excessive clearances found between the needle valve and the injector body. The clearance was due to inappropriate tolerances in the machining process, and this needs to be rectified in case of a non-experimental injector production.

The injector body was manufactured from steel, and the needle valve and nozzle were manufactured from highly tempered steel. Since hydrogen has a "washing effect" over the lubricating oil, lowering the oil viscosity and therefore the oil adherence to the moving parts, the injector was designed with a Teflon liner to accommodate the actuator rod, which is solidly attached to the needle valve. Hydrogen embrittlement was observed mainly on the needle valve tip, since it operates at around 300ºC and the hydrogen flow speed is high. Nitrile® O-rings were used to seal injector components as shown in Figure 3.18. No detrimental effects of using

hydrogen was found, however it is known that cracking can occur when in contact with certain rubber materials. Therefore, the use of special O-ring materials such as Viton® may need to be considered.

The dynamic performance of the injector was determined by the mass of the moving parts, the pre-load of the needle valve spring, and the hydraulic actuation pressure. The spring stiffness and hydraulic pressure could be adjusted to optimise the dynamic response. Lighter materials can also be employed to reduce the inertia of the moving parts and therefore providing a better injector dynamic response. For example, Titanium could be used for the actuator and needle valve which were found not to experience embrittlement problems.

3.2.4 Injector hydraulic power pack

The DIH_2 injector was designed to be hydraulically actuated and electronically controlled using a solenoid valve. Therefore, a hydraulic power pack was used to generate the hydraulic power required by the injector actuator. Figures 3.21 and 3.22 show a picture of the hydraulic power pack and injector and a schematic diagram of the system respectively. The hydraulic power pack has the capability of regulating the actuation delivery pressure and also the flow rate through the injector. The power pack system consists of an electro-hydraulic pump, a pressure safety valve, a pressure control valve, a flow control valve, a thermo-static valve and a plate heat exchanger.

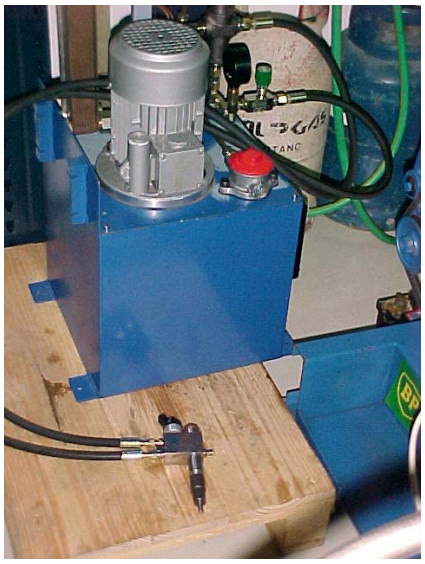

Figure 3.21: Hydraulic power pack and DIH_2 injector.

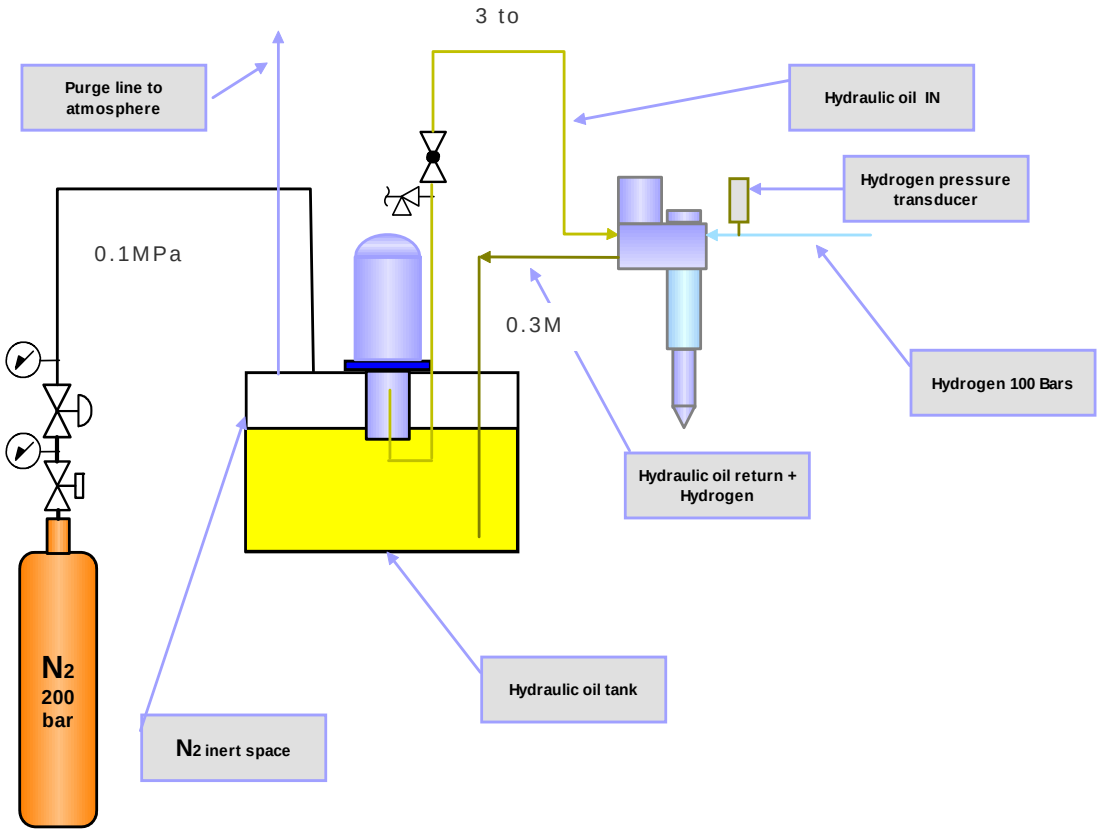

Figure 3.22: DIH_2 hydraulic actuating and inert gas (nitrogen) purging systems

A fast actuating hydraulic three way valve was incorporated to control the direction and duration of the hydraulic oil pulses, based on a PWM signal from the injection controller. Once the solenoid valve allows high pressure

oil to enter the actuator lower chamber, an upward force is exerted on the injector needle valve, causing the injector to open and allowing hydrogen to flow into the engine cylinder. With the removal of the PWM signal pulse, the oil in the lower chamber is forced back through the control valve into the hydraulic oil tank. This forces the piston and needle valve downwards, closing the injector again.

3.2.5 Alternative DIH_2 injector design

A second injection system was designed and developed, but not implemented as it was not sufficiently flexible for experimental purposes. The injection system, illustrated in Figures 3.23 and 3.24, provides rapid hydrogen injection without requiring any electronic control system. The system utilises the camshaft actuated diesel fuel injection pump to pressurise the working fluid, a blend of 50% diesel oil and 50% lubricating oil (10W-30). It therefore eliminates the complexity associated with the external hydraulic actuation system. The stroke of the injection pump would set the duration of injection, and the timing of the injection would be set by steel shims placed under the injection pump body after the cam rise. At the end of the injection pump stroke, the compressed spring would provide the energy required to force the injector needle on to its seat, as the working fluid flows through the bleed valve.

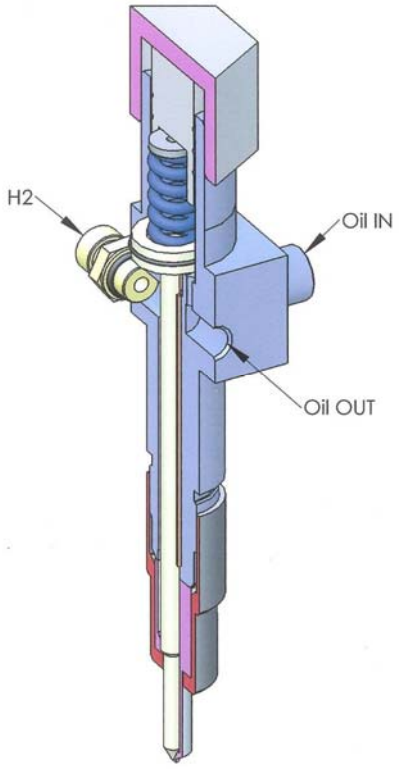

Figure 3.23: Hydraulically controlled and actuated hydrogen injector.

The duration of hydrogen injection would be determined by the rack setting of the injection pump, which is controlled by the existing engine governor. By adjusting the bleed valve, the ideal compromise between the opening and closing response time can be achieved.

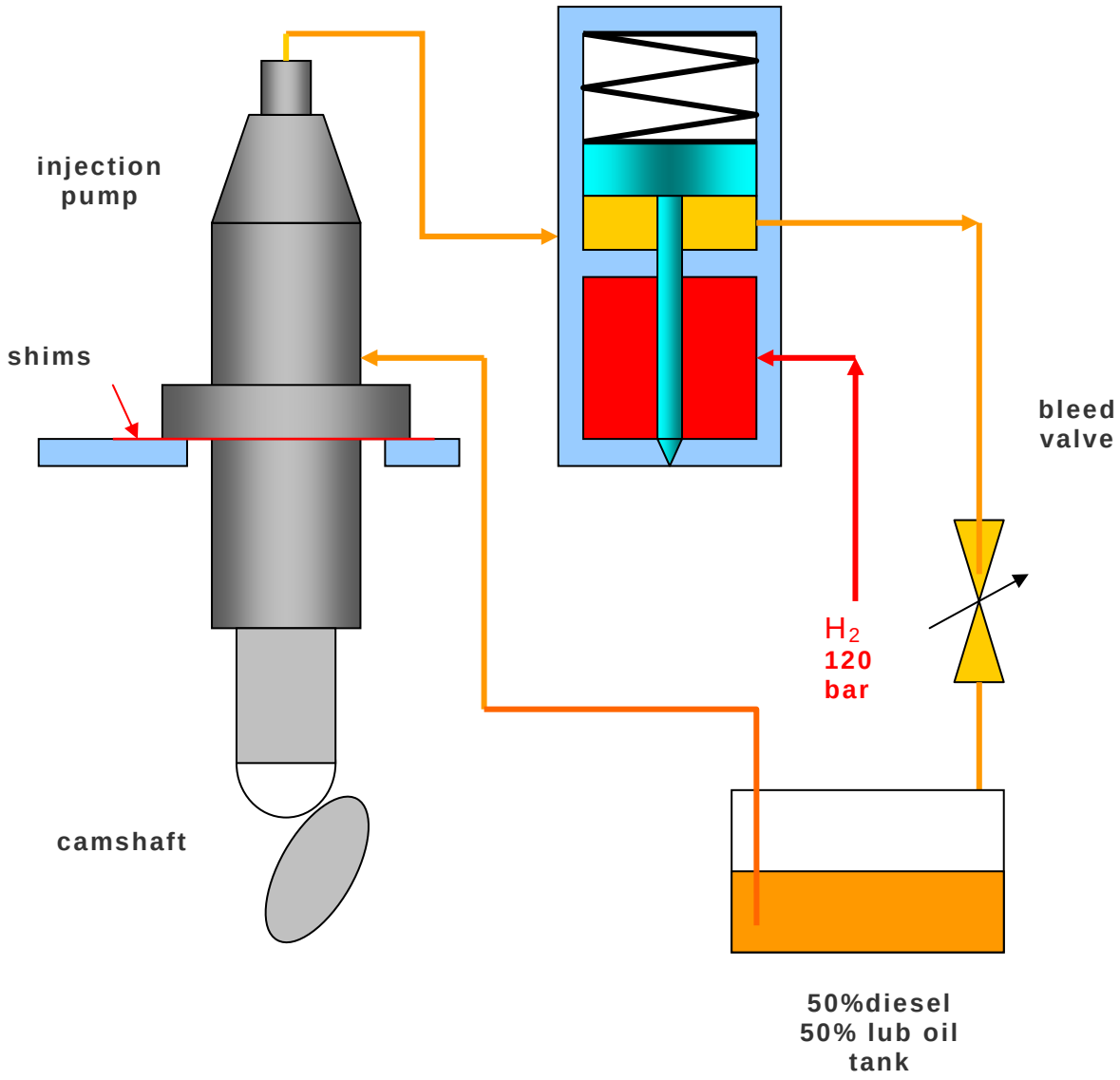

Figure 3.24: Schematic diagram of the hydraulically controlled and actuated injection system

As mentioned this injector system was built but not fully implemented for hydrogen injection on the engine. Although this system is simple and functional, the control of the start of injection (an important engine control parameter) was not possible as it was set by the shims height. Therefore a solenoid controlled injector was developed to overcome this problem. Therefore the solenoid controlled injector with external hydraulic actuation, which allowed the use of electronic controller circuit to change the start of injection and duration as a function of engine load, was used

for the experiments. For a commercial engine, an injection system such as this may however be investigated further.

3.3 Hydrogen injector test rig

It was necessary to characterise the hydrogen injection system with respect to its flow rate and the PWM control settings, so that the correct amount of fuel is injected per engine cycle. Therefore, a test rig was designed and built to carry out the static and dynamic characterisation process for both the HCCI and DIH_2 injectors.

3.3.1 Pressure vessel for injector testing

Due to the hydrogen pressures involved, it was decided to construct a pressure vessel to test the injectors, shown in Figures 3.25 and 3.26.

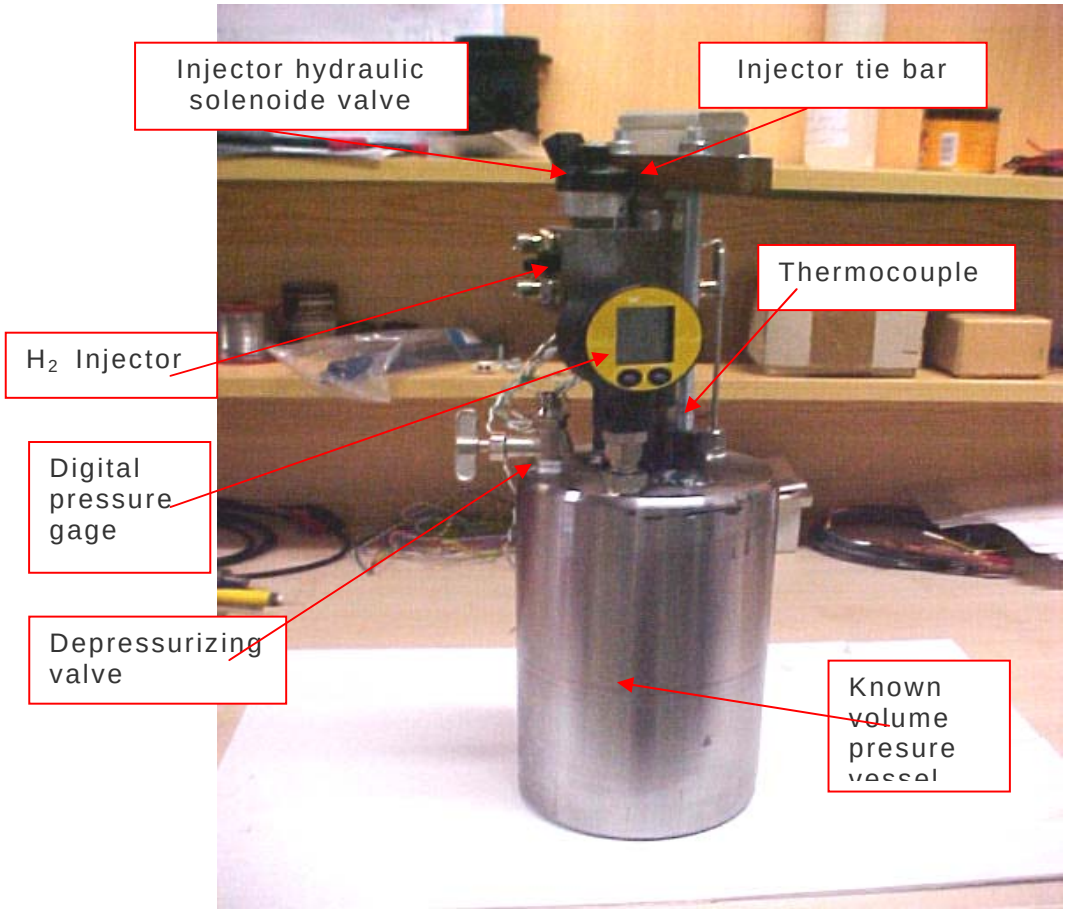

Figure 3.25: Injector test vessel.

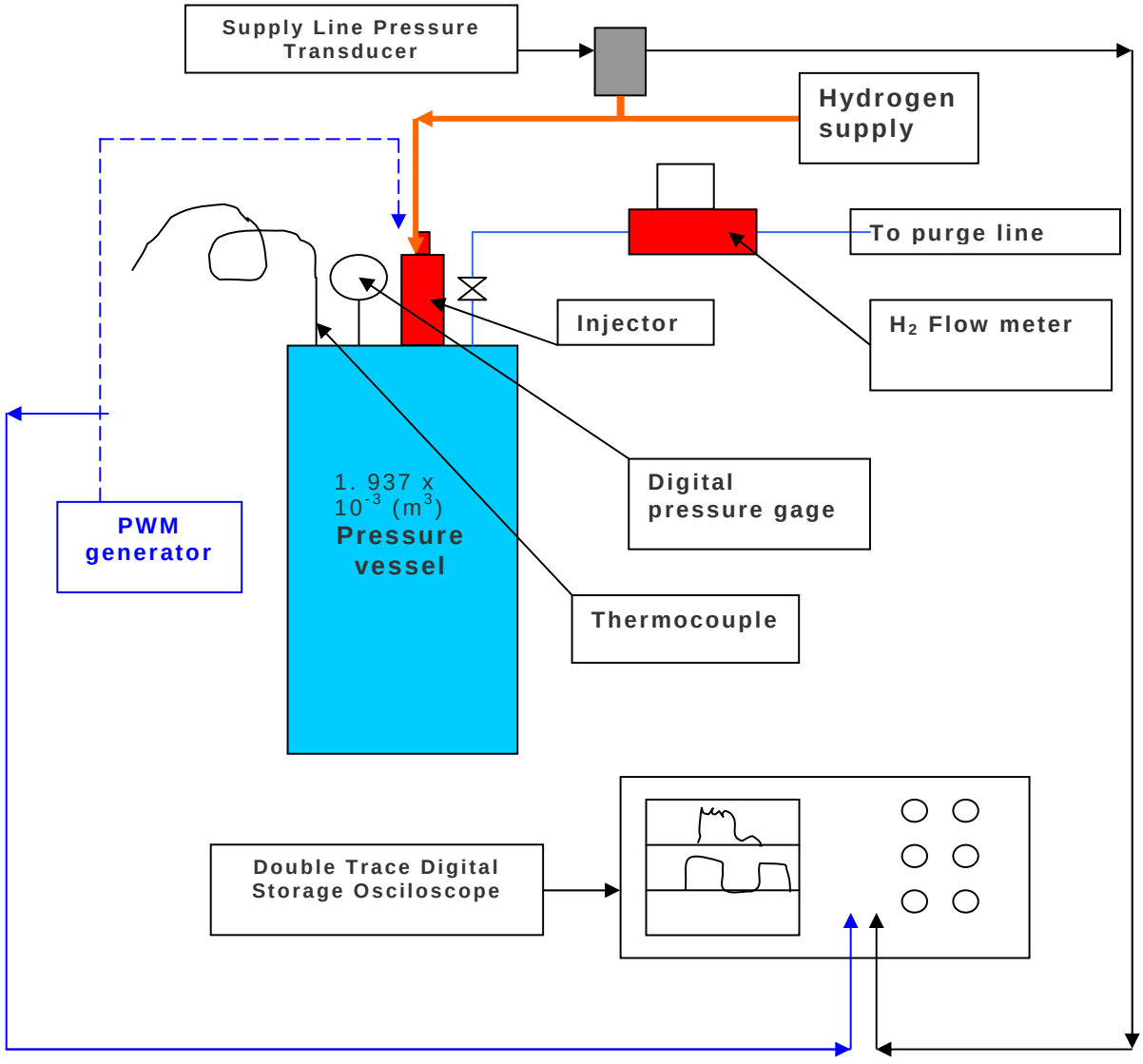

Figure 3.26: Injector testing rig.

The injector test vessel was designed to be capable of supporting a gas pressure up to 90 bar, and equipped with a temperature measuring system (a K type thermocouple), a digital pressure gauge, an injector pocket and a needle valve. According with the perfect gas law, the mass of hydrogen contained within a volume is given by the following expression:

$$m = \frac{p \times v}{R \times T} \quad , \qquad (3.1)$$

Therefore, knowing the pressure and the temperature inside the vessel, it was possible to determine the mass of hydrogen injected into the vessel during testing. Knowing the frequency of injection, pulse width, and the time of observation, it is possible to determine the quantity of hydrogen injected per injection at constant injection frequency and pulse width.

Great care was required to make sure all measurements were taken at a stabilised temperature, with the added difficulty of reducing the heat losses through the vessel walls as close as possible to zero.

In addition to this method, the hydrogen injected and contained inside the vessel was released through a hydrogen flow meter, which produced another reading of the hydrogen quantity contained in the vessel. In this way two independent methods of measuring the mass of injected hydrogen were used to characterise the injector being tested. Figure 3.27 shows the hydraulic injector testing apparatus; the oscilloscope was used to set the frequency of injection and the power supply was used to feed the PWM electronic circuit.

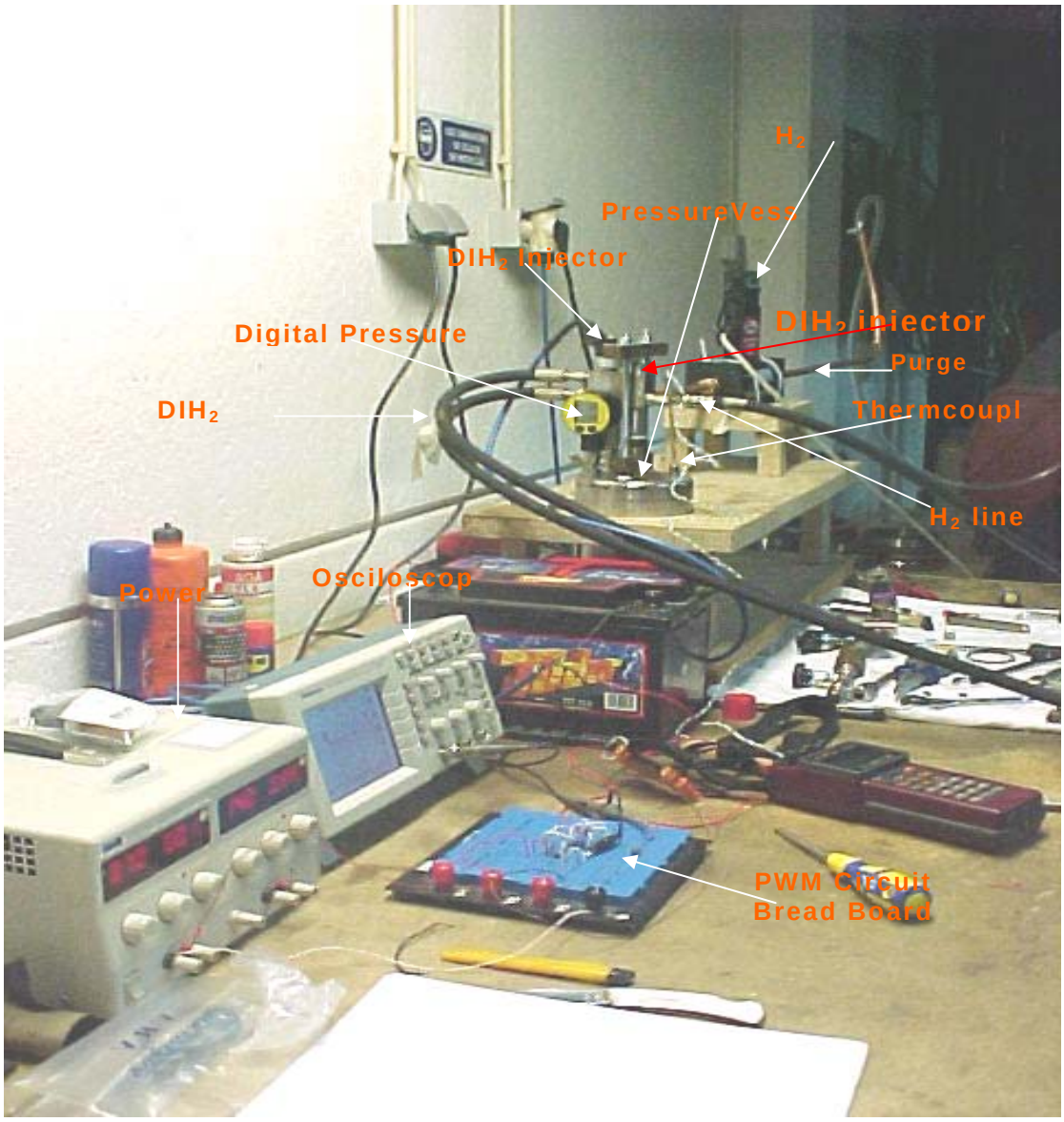

Figure 3.27: Photograph of the DIH_2 injector under test.

3.3.2 Pulse width modulation control circuit

To generate a pulse width modulated signal to control the injector solenoid valve, a circuit was developed based on the oscillator LM 555 and the comparator LM 393. The control circuit interfaced with the power circuit (12 V battery, 55 Ah) through a Zener diode and an opto-isolated Silicon

Controlled Rectifier (SCR). The Zener diode was used to limit and therefore to protect the circuit from a current surge developed by the 2 ohm impedance coil of the solenoid valve when it is activated.

The circuit, shown in Figure 3.28, operates at a frequency determined by R1, R2 and C1 and has a pulse width range of 0 to 100 percent.

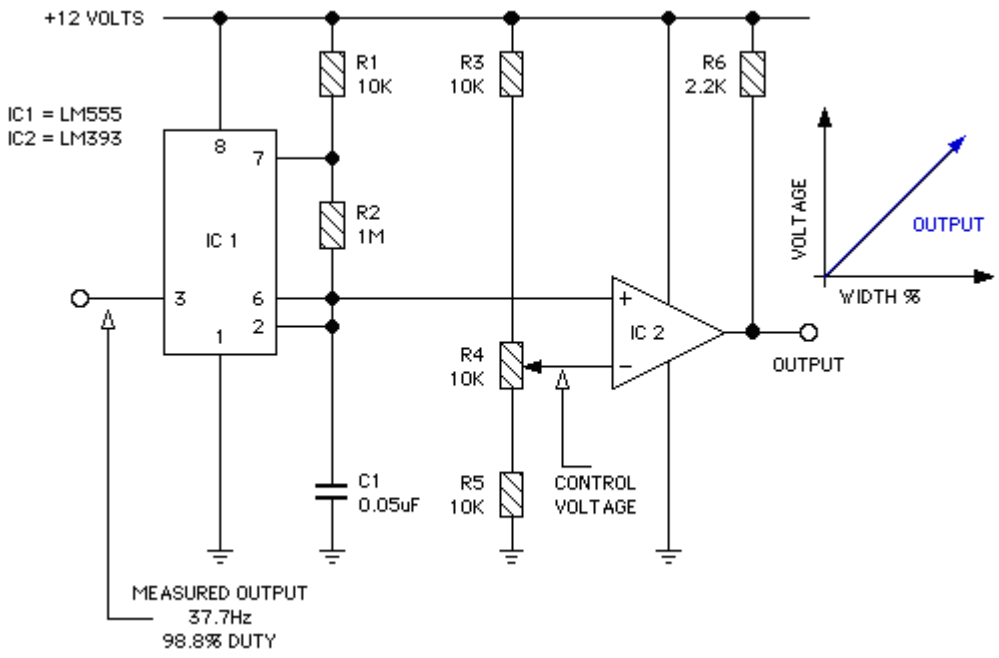

Figure 3.28: Pulse width modulation control circuit.

Figure 3.29 shows the pulse width modulation output of the basic circuit for a given control voltage input. All measurements were made with a calibrated multimeter. Figure 3.30 shows a modified circuit which uses a second LM 555 oscillator timer to provide a power output stage for the basic PWM circuit. The PWM circuit was constructed using a “bread board” as shown in Figure 3.31.

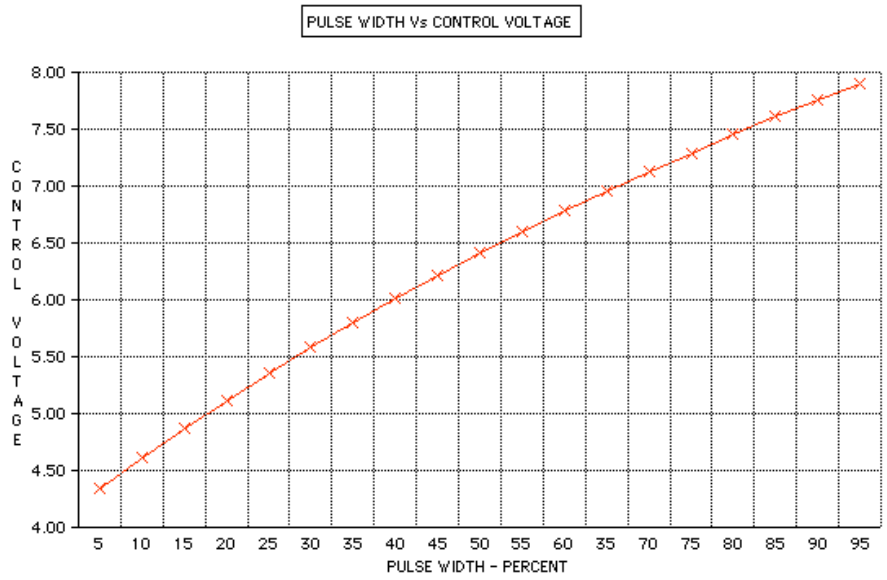

Figure 3.29: Basic pulse width modulation control circuit characteristic curve.

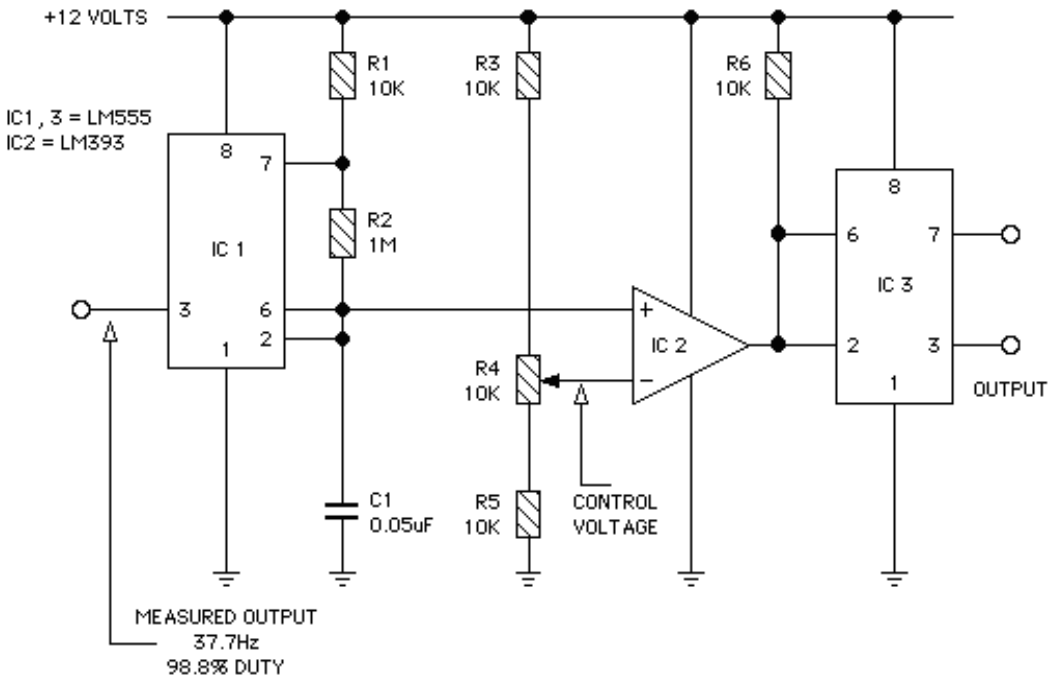

Figure 3.30: Variable pulse width modulation control circuit.

Figure 3.31: Variable pulse width modulation control circuit bread board.

3.3.3 Static and dynamic characterisation of HCCI and DIH_2 injectors

The injectors are used to inject the right quantity of hydrogen at the right time. To perform these tasks, the injectors need to be characterised in terms of their static and dynamic performance, which depend on variables such as supply pressure, back pressure, frequency, and injection frequency.

The static performance test objective was to determine the injector full open flow rate. The high speed at which the injector operates, and the small flow rate for each opening, meant that it was impossible to measure the flow rate per injection directly. Therefore, to determine the mass flow rate of hydrogen per injection the following experimentation procedure was implemented.

Once the injector was installed in the pressure vessel, sealed with copper washers, and hydrogen, hydraulic oil, and electric connections done, a PWM injection frequency equal to 16.66 Hz (corresponding to an engine speed of 2000 RPM) and a series of duty cycles from 6.67% to 26.71% were set on the PWM generator.

After a time interval of injection into the closed pressure vessel, the hydrogen was slowly released and measured using the calibrated flow meter. In parallel, using the thermocouple and pressure gage readings, a calculation of the hydrogen injected into the cylinder was carried out using the ideal gas law. However, this gave results which deviated when the pressure inside the vessel was above 20 bar and therefore it could not be used to check the DIH_2 injector. This deviation was observed using thermal isolation of the pressure vessel, as the vessel increased its temperature during injection and decreased its temperature during expansion. Another factor contributing to this deviation was the ambient temperature of 11ºC at the time of the tests. Even though this calculation of the injected flow produced inaccurate results at higher pressures, it was valuable to check the calibration of the flow meter for low pressures. Also, it was possible to conclude that the use of the ideal gas law it is not sufficiently accurate when temperature can not be maintained constant.

The hydrogen injection test procedure was repeated four times for each selected pulse width for both injectors (DIH_2 and HCCI injectors).

3.3.3.1 Static performance test results for the HCCI injector

The static performance test results for the HCCI injector using the test rig are presented in Tables 3.2 to 3.5. These results are plotted in Figure 3.32 and show the hydrogen flow rate as a function of pressure and pulse width. Knowing the test duration and the set injection frequency, the number of injections was determined. The total mass flow rate measured was divided by the number of injections to obtain the mass of hydrogen per injection.

Table 3.2: HCCI Injector flow rate (mg/injection) data for an average supply pressure of 2.47 bar.

Pulse width (ms)	Test 1	Test 2	Test 3	Test 4	AVG Q	ST Dev.
4	1.56	1.55	1.54	1.54	1.55	0.0094
6	2.21	2.21	2.20	2.20	2.21	0.0031
8	2.79	2.79	2.78	2.79	2.79	0.0058
10	3.36	3.37	3.36	3.37	3.37	0.0084
12	4.01	4.01	4.02	4.01	4.01	0.0083
14	4.62	4.63	4.63	4.63	4.62	0.0061
16	5.24	5.25	5.26	5.26	5.25	0.0080

Table 3.3: HCCI Injector flow rate (mg/injection) data for an average supply pressure of 7.58 bar.

Pulse width (ms)	Test 1	Test 2	Test 3	Test 4	AVG Q	ST Dev.
4	2.91	2.91	2.89	2.88	2.90	0.0152
6	3.50	3.52	3.53	3.51	3.52	0.0100
8	4.68	4.66	4.68	4.67	4.67	0.0076
10	5.77	5.78	5.78	5.78	5.78	0.0041
12	6.85	6.86	6.86	6.86	6.86	0.0041
14	7.95	7.99	7.99	7.99	7.98	0.0227
16	9.12	9.12	9.14	9.14	9.13	0.0127

Table 3.4: HCCI Injector flow rate (mg/injection) data for an average supply pressure of 10.96 bar.

Pulse width (ms)	Test 1	Test 2	Test 3	Test 4	AVG Q	ST Dev.
4	3.46	3.45	3.46	3.48	3.46	0.0137
6	4.69	4.70	4.76	4.70	4.71	0.0314
8	6.20	6.23	6.26	6.26	6.24	0.0248
10	7.81	7.83	7.84	7.84	7.83	0.0157
12	9.47	9.54	9.53	9.53	9.51	0.0396
14	11.02	11.06	11.09	11.07	11.06	0.0296
16	12.78	12.79	12.81	12.83	12.80	0.0216

Table 3.5: HCCI Injector flow rate (mg/injection) data for an average supply pressure of 14.5 bar.

Pulse width (ms)	Test 1	Test 2	Test 3	Test 4	AVG Q	ST Dev.
4	4.49	4.45	4.44	4.48	4.46	0.0247
6	5.88	5.83	5.79	5.83	5.83	0.0383
8	7.74	7.76	7.76	7.75	7.75	0.0094
10	9.88	9.87	9.89	9.87	9.88	0.0120
12	12.14	12.13	12.16	12.13	12.14	0.0145
14	14.33	14.34	14.36	14.34	14.34	0.0127
16	16.46	16.47	16.44	16.46	16.46	0.0108

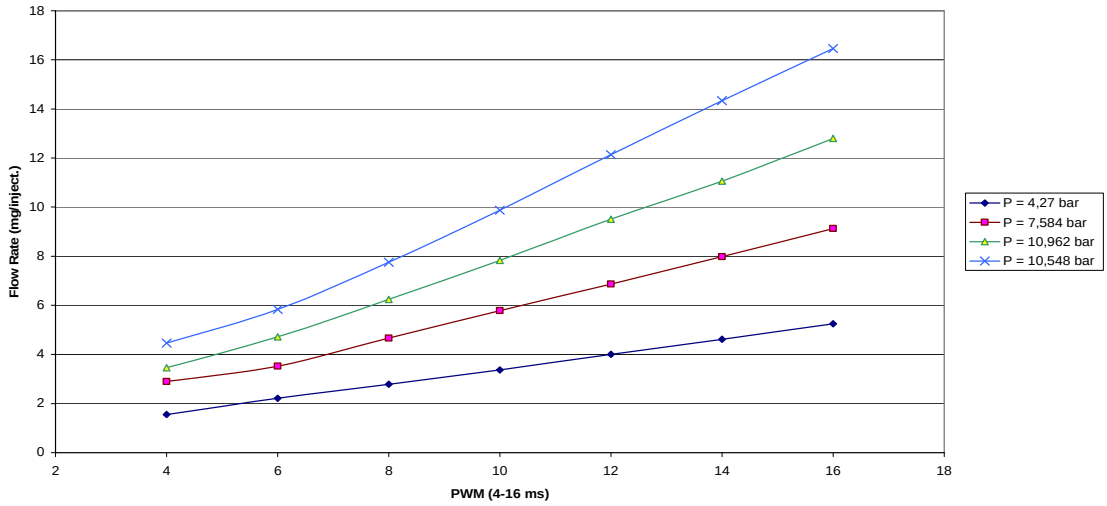

Figure 3.32: Flow rate (mg/injection) as a function of the PWM and supply pressure for the HCCI injector.

As can be seen from Figure 3.32, above an 8 ms pulse the flow rate with respect to PWM is approximately linear. Below an 8 ms pulse, the control characteristic of the valve flow becomes non-linear. The results presented in Figure 3.32 provide the characterisation of the HCCI injector and allowed the initial setting up of the injection system on the engine to be carried out. The small standard deviation observed for each pulse width sets of tests was indicative of a good metering behaviour of the injector, therefore allowing a precise control of the fuel quantity injected per cycle. It was possible to conclude that the injector dynamics is playing an important role in terms of its response for smaller pulse widths, therefore limiting the engine operation at very low loads.

3.3.3.2 Static performance tests of the DIH_2 injector

The static performance test results for the DIH_2 injector using the test rig are presented in Tables 3.6 to 3.8. These results are plotted in Figure 3.33 and show the hydrogen flow rate as a function of average supply pressure and pulse width.

Table 3.6: DIH_2 injector flow rate data for an average supply pressure of 60 bar.

Pulse width (ms)	test 1	Test 2	Test 3	Test 4	AVG Q	ST Dev.
4	3,99	3,97	3,97	3,94	3,97	0,0233
6	5,07	5,03	5,03	5,03	5,04	0,0189
8	6,81	6,8	6,8	6,79	6,8	0,0098
10	8,44	8,44	8,44	8,42	8,42	0,0066
12	10,2	10,21	10,21	10,19	10,2	0,0089
14	12,15	12,2	12,19	12,22	12,19	0,0288
16	13,82	13,9	13,93	13,96	13,9	0,0606

Table 3.7: DIH_2 injection flow rate data for an average supply pressure of 70 bar.

Pulse width (ms)	Test 1	Test 2	Test 3	Test 4	AVG Q	ST Dev,
4	4,1	4,04	3,99	3,98	4,02	0,0549
6	5,75	5,78	5,77	5,77	5,77	0,0138
8	7,5	7,44	7,42	7,42	7,45	0,0366
10	9,41	9,41	9,4	9,38	9,4	0,0129
12	11,72	11,72	11,71	11,71	11,71	0,0054
14	13,8	13,79	13,76	13,77	13,78	0,0197
16	15,77	15,68	15,55	15,96	15,74	0,1748

Table 3.8: DIH_2 injection flow rate data for an average supply pressure of 80 bar.

Pulse width (ms)	Test 1	Test 2	Test 3	Test 4	AVG Q	ST Dev,
4	4,28	4,31	4,32	4,34	4,31	0,0219
6	5,9	5,91	5,89	5,88	5,89	0,0092
8	8,26	8,28	8,28	8,22	8,26	0,027
10	10,35	10,34	10,39	10,35	10,36	0,0202
12	12,99	12,97	12,96	12,93	12,96	0,0224
14	15,31	15,28	15,23	15,23	15,27	0,0396
16	17,6	17,62	17,61	17,61	17,61	0,0104

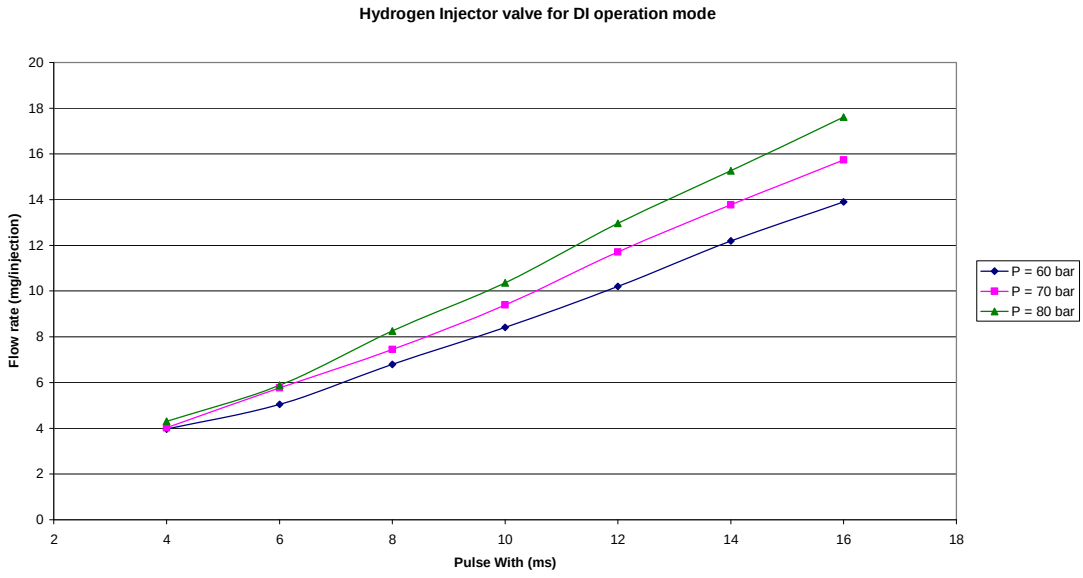

Figure 3.33: Flow rate (mg/injection) as a function of the PWM and average supply pressure for the DIH_2 injection.

As can be seen from Figure 3.33, for the DIH_2 injector above a 10 ms pulse the flow rate with respect to PWM is approximately linear. Below a 10 ms pulse, the control characteristic of the valve flow becomes non-linear.

It was noticed that the DIH_2 injector had substantial hydrogen leakage into the hydraulic oil return pipe. However, since the flow meter was used to

measure the amount of hydrogen injected into the vessel and then allowed to flow out, this corresponded to the actual injected mass flow of hydrogen which would be injected into the engine cylinder. Also, the injector preload, the hydraulic pressure and PWM setting determine the injector performance. It was possible to conclude that the injector dynamics is playing an important role in terms of its response for smaller pulse widths, therefore limiting the engine operation at very low loads.

3.3.3.3 HCCI dynamic injector response

For the HCCI injector, the time delay between the injector receiving the opening signal and commencing fuel injection is mainly a function of the solenoid time response and this introduced a 3.0 ms delay when opening and a 2.0 ms delay when closing. It was assumed that all other factors contributing to the dynamic response of the HCCI injector were lumped together and taken in consideration on the considered delays, therefore no additional dynamic testing was performed.

3.3.3.4 DIH_2 dynamic injector response

The speed of response is an extremely important parameter for the DIH_2 injector and the operation delay must be included in the programming of the injection controller. As DIH_2 engines control is dependent on the injection timing, and hydrogen ignition delay is short, the ignition angle and combustion control require an accurate injection. If the delays are not taken into account in the controlled operation then a long delay in opening time would lead to late injection, and hydrogen being wasted if the injector closing has a large delay. The ideal injector should have a fast dynamic response giving the smallest possible time delay to open and close. This inherent delay must be compensated for in the controller.

It was found using a dynamic simulation model of the injector that opening and closing times were not significantly determined by the inertia of its moving parts but dominated by the hydraulic and injector spring preload

forces. Therefore, the injector dynamic response was predominately found to be a function of the actuating piston effective area, hydraulic pressure, and the spring elastic constant and preload. An additional factor which adversely affected the injector dynamic response was the frictional force introduced by the O-rings used to seal the piston within the hydraulic actuator cylinder. The effect of this and the other variables mentioned which determine the injector dynamic performance was studied in more detail using dynamic simulation and this is presented in Chapter 5. The dynamic model was used to simulate the engine test conditions contributing to know in advance the values of hydraulic oil pressure and piston pre load, but also to understand the effect of increasing the frequency of injection and the respective duty cycle over the pattern of injection. To determine the injector time delay in opening and closing experimentally, a pressure transducer (dynamic response type) was installed on the hydrogen supply line. The hydrogen pressure signal was fed into a dual beam oscilloscope, together with the PWM signal. In this way, the time difference between the edge of each PWM signal and the distinct change in hydrogen pressure was used to determine the opening and closing time delay. Both these time delay values were used in the injection controller to ensure correct injection timing. The time delay test results from the oscilloscope are presented in Figure 3.34 and show that there was a 21 ms delay in opening and a 16 ms delay in closing for the DIH_2 injector.

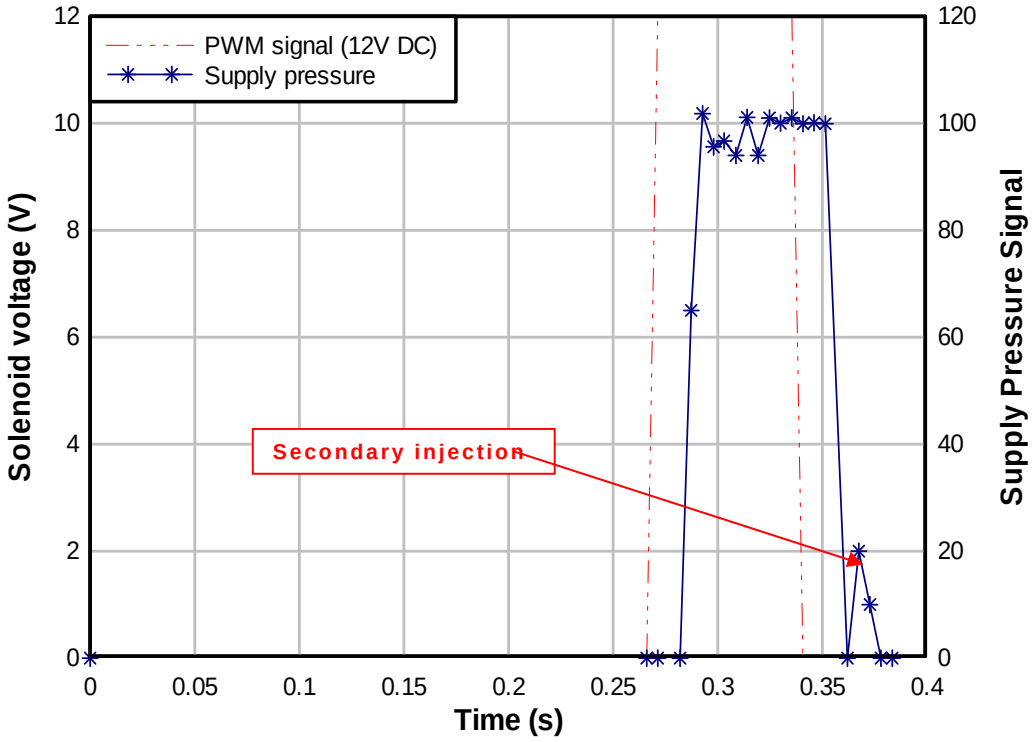

Figure 3.34: Oscilloscope traces showing time delay measurements for the DIH2 injector. Supply pressure signal (0-100%).

(Delay: 21 ms to open 16 ms to close)

3.4 Hydrogen injection engine control system

The hydrogen injection engine control system was designed to operate with a high and low level control loop. The low level hydrogen injection control system was used to monitor the crank angle of the engine via the camshaft encoder and provide the control signal to actuate either the HCCI or the DIH_2 fuel injector.

The high level control loop consisted of software which ran on a PC communicating with the low level control loop via the PC serial port. The high level control loop provided a user interface to program parameters such as the desired start of injection and its duration.

3.4.1 Low level hydrogen injection control loop

The main component of the low level hydrogen injection control loop was a Microchip PIC16F677A 8-bit microcontroller which has a built-in serial port and analogue to digital converter. A custom-designed printed circuit board for this microcontroller and supporting components is shown Figure 3.35. This circuit board was mounted in a rugged plastic enclosure to provide the low level hydrogen injection control loop hardware shown in Figure 3.36.

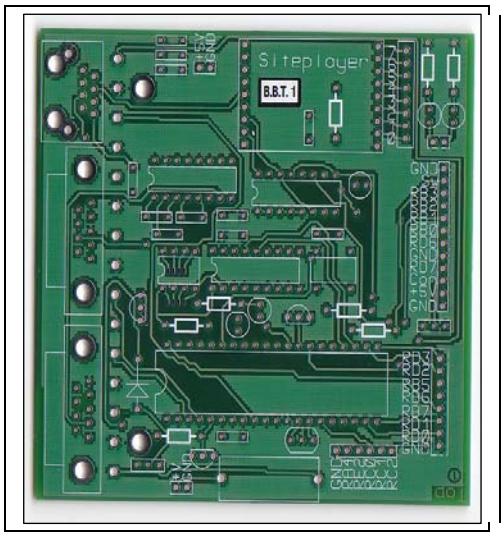

Figure 3.35: Low level hydrogen control loop circuit board.

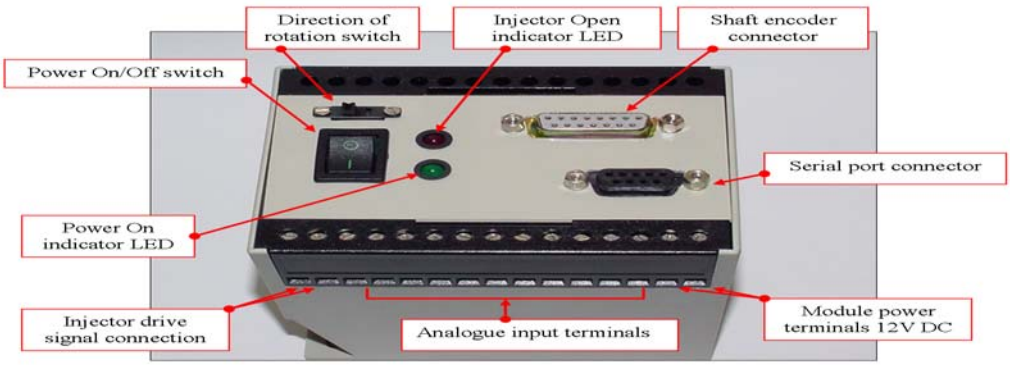

Figure 3.36: Low level hydrogen injector control system hardware.

The microcontroller firmware was largely interrupt-driven, and the main programming loop monitored the camshaft encoder output and activated the injector control signal at the appropriate time. The activation of the injector started a timer and the injector was closed once the timer expired.

All communication between the low level hydrogen injection control loop hardware and the PC was via a microcontroller USART module, set up as an asynchronous bi-directional serial port with a baud rate of 19.2 kbps. A MAX232CPE RS232 voltage level converter device was used to convert the signal voltage from the 5V used by the microcontroller to the ±12V required by the host PC.

The main microcontroller program structure is shown in Figure 3.37. The programme was designed to run in a loop, continually checking the value of the camshaft encoder and comparing it with the encoder value at the start of injection. When a match has been detected, the "Trigger Injector" subroutine is called and the duration of injection period is programmed into the TMR1 timer. The timer is then activated and the processor returns to the main program structure, running the "Check Encoder" loop. The TMR1 timer runs in parallel with the main program structure and triggers an interrupt when it reaches zero.

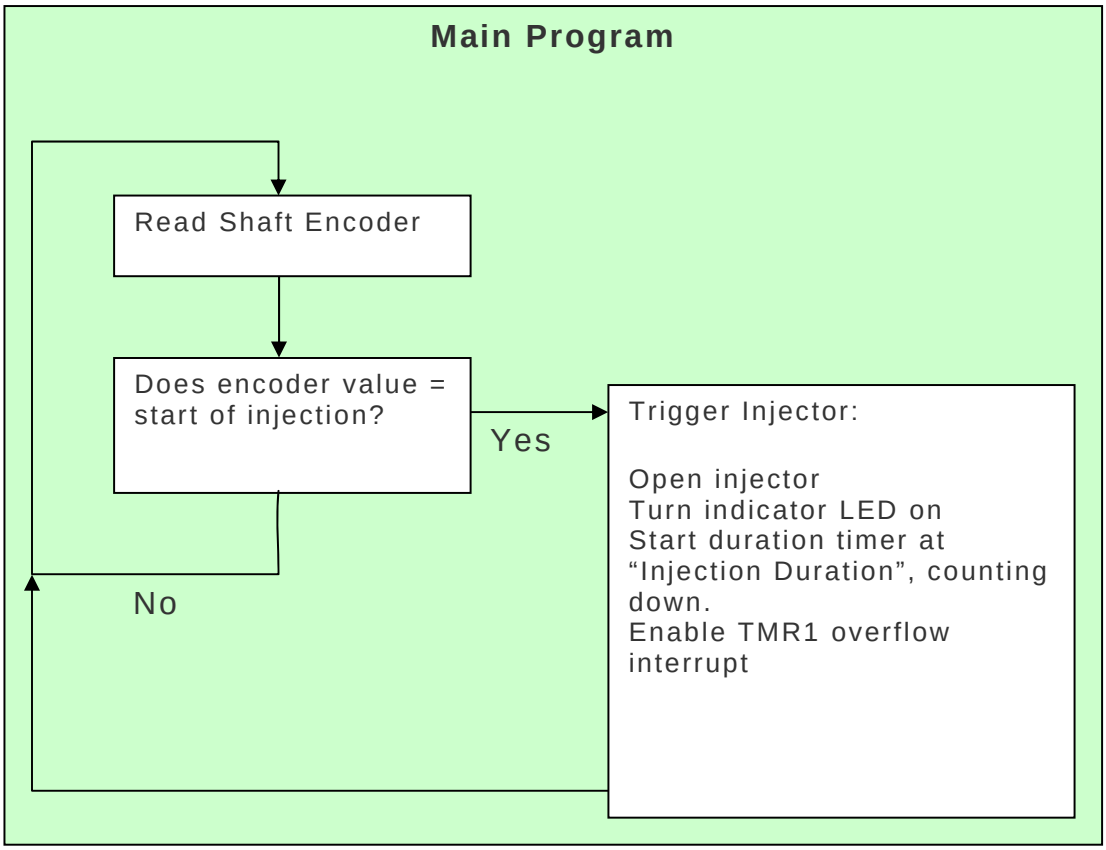

Figure 3.37: Main microcontroller program structure.

The interrupt service routine programming is shown in Figure 3.38 and when called it determines the cause of the interrupt. If TMR1 caused the interrupt, the “Close Injector” routine is called, switching off the injector and the indicator LED, resetting the timer and disabling TMR1 as a source of further interrupts. If a “serial port receive” event triggered the interrupt, the received data is analysed and then the required action is performed. This may be to enable or disable the injector in order to start or stop the engine, or to trigger the “Log Data” process to record analogue sensor values from the engine. By controlling the injector in this way, the open duration of the injector was entirely independent of the engine rotational speed, allowing more flexible control of the engine.

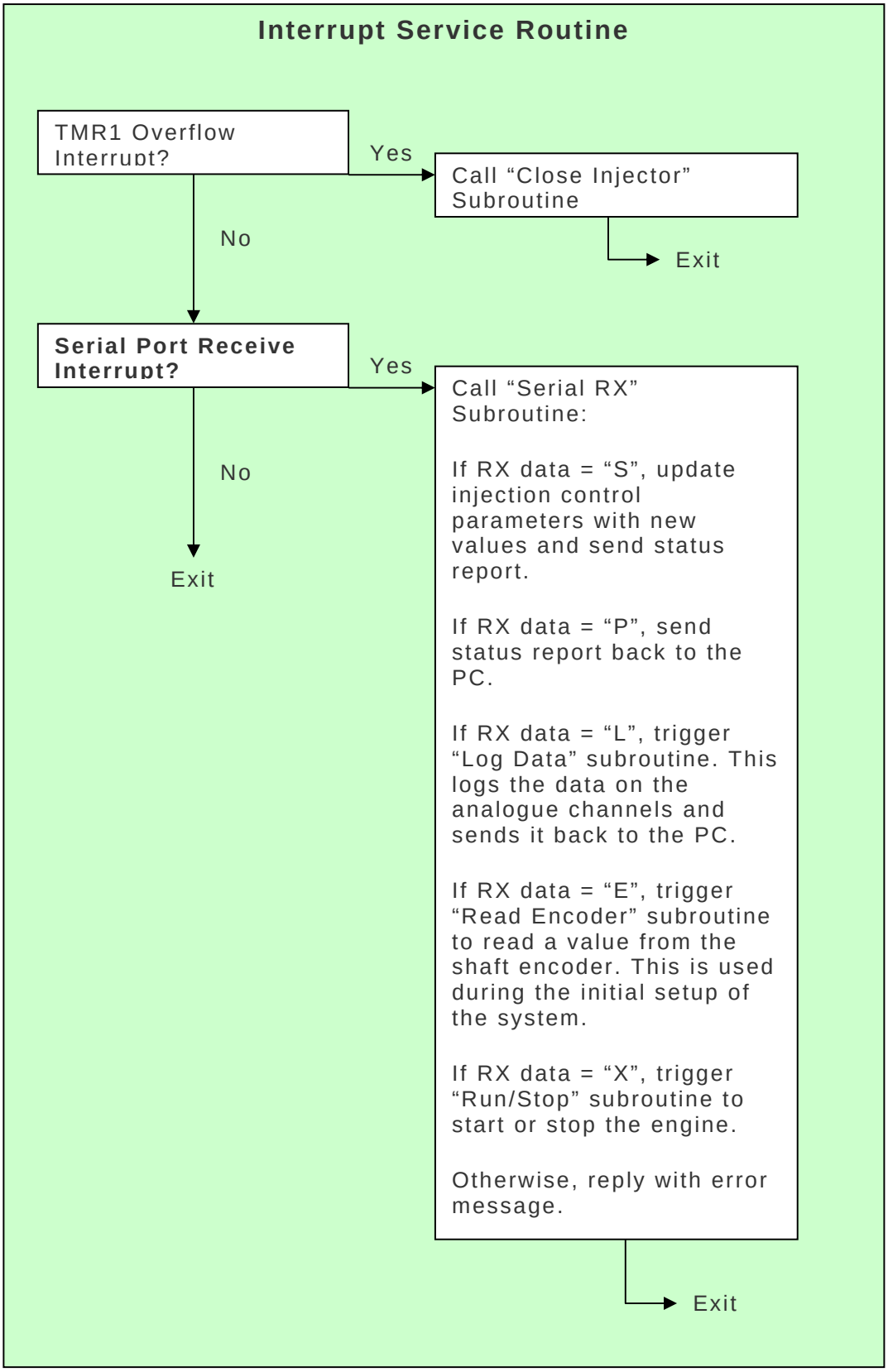

Figure 3.38: Interrupt service routine program.

The microcontroller has several embedded hardware functions which enable interaction with other systems and devices. The functions used in this application are shown in Table 3.9.

3.4.2 High level hydrogen injection control loop

The high level hydrogen injection control loop software was written in Matlab and ran on a PC to send and receive control data from low level hydrogen injector control loop via the PC's serial port.

The Matlab software allowed the timing and duration of fuel injection to be set and allowed analogue engine sensor data to be sampled. This data was plotted within the PC user interface and could be saved in a variety of formats, including MS Excel and Matlab .mat files.

The user interface for the high level hydrogen injection control loop is shown in Figure 3.39. The "Injector Control" box (top left) was used to specify the crank angle at which the injector should open and the time it should remain open in milliseconds. Clicking the "Set" button sent these settings to the microcontroller which then used these values every cycle until instructed otherwise.

The top-right box contains the data logging and saving controls. Figure 3.39 shows the result of clicking the "Log Data" button with the data shown in the plot window logged by the low level hydrogen injection control loop and then transmitted back to the PC. Clicking the "Save Data" button saved this data with the file name and path specified in the boxes below the buttons. The data shown in the plot window in Figure 3.39 was generated by a signal generator connected to the analogue input port of the low level hydrogen injection control loop to test its operation.

Table 3.9 Low level hydrogen injector control loop microcontroller hardware functions.

Hardware Function	Configuration Setting	Connection	Purpose
USART	Asynchronous bi-directional serial port. Baud Rate 19.2kbps, 8 data bits, 1 stop bit, no parity, no handshaking.	Connected to PC serial port via MAX232CPE voltage level converter.	Allows communication between PC and hardware module.
A/D Converter	Voltage reference on Pin 5. High-speed data acquisition on Channel 0 (Pin 2) with 8-bit resolution. Low speed data acquisition on Channel 1, Channel 2 and Channel 4, with 10-bit resolution. These channel numbers are those on the microcontroller only. The channels have been renumbered on the assembled module to make connecting inputs more intuitive.	5V Zener diode voltage reference on Pin 5. All data channels connected to screw terminals on enclosure.	Allows data collection from engine sensors. High-speed channel is intended for use with cylinder pressure sensor to record pressure profile over full cycle. Low speed channels can be used to collect temperature data, for example.

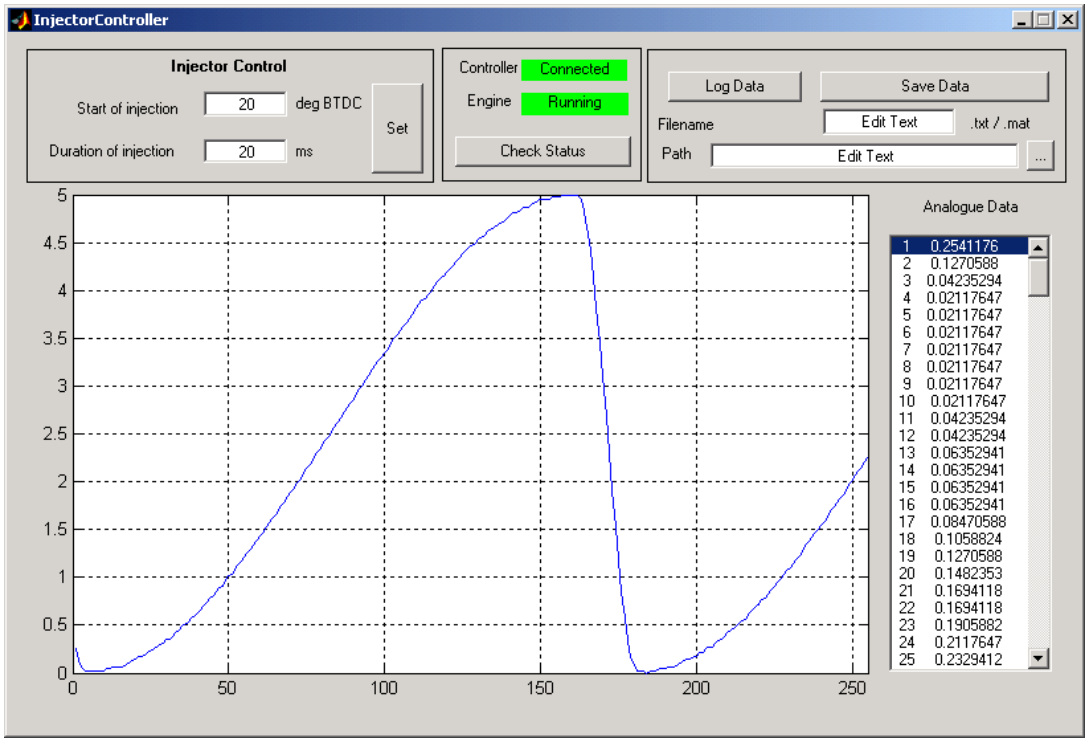

Figure 3.39: High level hydrogen injection control loop user interface.

To set up the camshaft encoder, the engine was held at top dead centre at the end of the exhaust stroke. The encoder value was then read and the resulting value stored as TDC. All injection timing was then calculated from this datum value.

The software included the facility to scale the analogue data before saving or displaying it, so that the data could be plotted as actual values, e.g. 0-100 bar, rather than a simple voltage value.

The analogue inputs from the engine sensors were required to be in the range of 0-5 V sharing a common ground connection. The low level microcontroller could log a maximum of 256 data points with single-byte (8-bit) precision at a maximum of 20 kHz. This allowed a cylinder pressure trace, for example, to be taken over a whole cycle, sampling every 2.8 crank angle degrees.

It was found that to fully analyse the engine cylinder pressure data to determine performance through identifying parameters such as maximum cylinder pressure, crank angle at maximum pressure, rate of pressure rise, pressure at ignition point and ignition angle, it was necessary to have a sampling resolution of 1 crank angle degree or less. This was important also to provide data with sufficient accuracy to validate simulation models used to explore a wider operational range than that possible through experimentation. Therefore, it was decided not to use the data sampling facility provided with the developed high level hydrogen injection control loop but to implement an additional high speed data acquisition loop and analysis system. This is shown in schematic form in Figure 3.40 which indicates the use of the separate data acquisition and analysis system which was used to sample engine sensor data with 0.5 crank angle degree resolution.

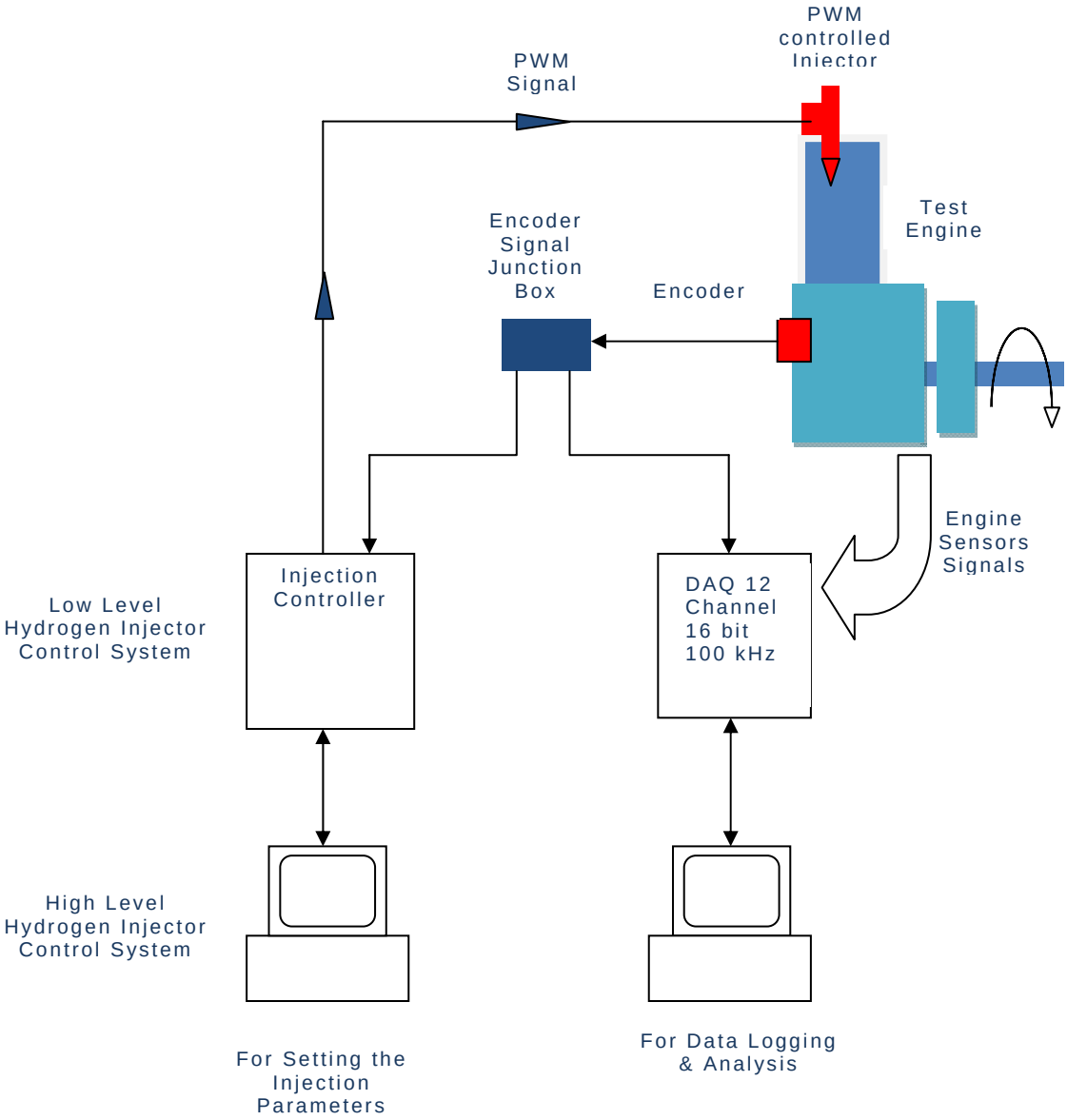

Figure 3.40: Integration of high and low level hydrogen injector control loop with the data acquisition system.

3.5 Conclusion

This chapter has described the engine and monitoring system which was designed and constructed to conduct experiments on HCCI and DIH_2 hydrogen fuelled operation. The engine test rig comprised a single cylinder compression ignition engine capable of running on these hydrogen operational modes. The instrumentation and acquisition of engine sensor data was an important element of the test rig setup so that accurate data could provide a detailed understanding of the engine performance during these modes. A high speed system was developed, capable of monitoring all relevant engine variables at 0.5 crank angle degree resolution and thereby enabling detailed analysis to be carried out.

Two main hydrogen fuel injection systems were designed and implemented with the engine test rig. These systems were prototypes for research purposes and would require further re-engineering for example in component tolerances and material selection before they would be suitable for commercial application. A HCCI injection system operating at a hydrogen pressure of 6 bar was designed and implemented using a fast acting solenoid injection valve in the engine air inlet manifold. Two DIH_2 injectors were designed, one which was a solenoid controlled hydraulic system and the other a hydraulically controlled and actuated system. The solenoid controlled hydraulic injector was found to be the most flexible design and therefore was developed further and used on the engine test rig. This DIH_2 injector had significant leakage problems due to manufacturing limitations, but this did not impact on the characterisation of the injector and the determination of the quantity of fuel injected into the engine. However, it prevented the originally planned wider range of operational testing to be conducted because of potential safety concerns.

It was important to characterise the properties of and amount of hydrogen delivered by HCCI and DIH_2 injection systems and it was therefore necessary to design and build an injector test rig and to conduct the characterisation process. The static and dynamic delivery performance of both injection systems were measured using this test rig, which at the start

of hydrogen injection had atmospheric pressure and temperature. The results produced were invaluable in the initial setting up of the injection control system on the engine since it is critical to know the relationship between fuel flow and pulse width. Since HCCI injection takes place within the air inlet manifold the conditions within the injector test rig were close to those found in engine operation. However, the injector test rig did not emulate in-cylinder conditions in terms of pressure and temperature for DIH_2 injection, since this would take place within the engine cylinder at approximately 27 bar and 260^{o}C. It was still found to be useful in order to get an initial insight into the characteristics of the DIH_2 injector to aid the setup and engine calibration.

Finally, a hydrogen injection control system capable of being implemented with both HCCI and DIH_2 injection systems was designed and implemented. It was found that the use of an 8-bit microcontroller within the low level control module was sufficient for engine injection control requirements. However, a higher resolution of data was necessary to monitoring engine operation and to retrieve data of use for detailed analysis.

Chapter 4

Experimental testing of hydrogen engine operation: results and analysis

"Think wrongly if you please, but in all cases think for yourself"
Doris Lessing

This chapter presents the methodologies, procedures and results obtained from the testing carried out with the hydrogen fuelled engine test rig under HCCI and DIH_2 modes of operation. Experimental results of dual fuel operation (hydrogen + diesel oil) are also presented as this mode of operation has a great potential for immediate use in the industry, namely on board ships.

4.1 Objectives of engine testing and methodology

The objectives of the test were to:

(a) prove that hydrogen can be used as a fuel for compression ignition engines operating under HCCI and DIH_2 modes;

(b) ascertain how the hydrogen impacted on the engine combustion in terms of cycle pressure development and thus on the component design; understand the limitations to the use of hydrogen use as a fuel in commercial CI engines;

(c) compare the HCCI and DIH_2 modes of operation in terms of thermal efficiency; and

(d) collect data to validate the simulation model developed to study operational conditions that were not practically feasible with the test engine.

4.1.1 Testing procedures

The hydrogen fuelled engine was tested using the engine test rig described in Chapter 3. Taking advantage of the installed instrumentation and high

speed data acquisition system it was possible to analyse test data in real time.

For each mode of operation the engine was tested systematically at different loads at constant speed, allowing engine cycle analysis.

A second set of tests were performed at constant load whilst varying the inlet air temperature, thus investigating the effect of the air temperature on the engine performance.

In order to have a reference set of values to compare with the HCCI and DIH_2 modes of operation tested, the engine was first run on diesel fuel using its conventional injection system. The DIH_2 mode that was tested only at one load due to safety problems related to the injector hydrogen leakage.

4.1.2 Engine operation and safety

For the testing, the engine was started with diesel fuel and run until the engine components were sufficiently hot. For switching to the HCCI mode of operation, hydrogen port injection was initiated and the diesel injection jerk pump rack was simply pulled out, thereby reducing diesel oil injection to zero. For the DIH_2 operation mode, the engine had to be stopped and the diesel injector was exchanged rapidly for the hydrogen injector.

Since the test engine had a modest compression ratio (17:1), and because of the high self-ignition temperature of hydrogen, pre-heating of the intake air was necessary to obtain stable running. An air heater with a simple PID controller was installed in the engine inlet manifold, as described in Chapter 3. This was used to maintain the air inlet temperature at approximately 90ºC for the hydrogen fuelled tests.

In this way, sufficiently high temperatures were reached inside the engine cylinder for the air-hydrogen cylinder charge to self-ignite.

4.1.3 Instrumentation set up and operation

Prior to testing, all the monitoring equipment was calibrated and checked to avoid erroneous readings. The data logging and monitoring software was

checked and the values of fuel densities and net calorific values were set. Special care had to be taken with the brake hydraulic oil temperature, as continuous testing over long periods produced an increase of the hydraulic oil temperature affecting the oil viscosity and therefore causing an engine load drift. Therefore all the measurements were taken within a time frame sufficiently short to overcome this undesirable effect.

4.2 Data logging and treatment

The raw data from the various transducers installed on the engine was logged in a .DAT file format. This allowed the data of each cycle to be available for further analysis after testing. The analysis of the logged raw data was performed using the software described in Chapter 3 in analysis mode, so that the raw data could be treated with the various analysis tools. Filters, averaging, FFT, and zoom features were available in the software. After the identification of the sets of data for further analysis, these sets were exported as .CSV files. The common averaging of data gave results that allow a reduction of noise as well as a representative data of the cylinder pressure history. The online data acquisition software included the capability of producing this averaging on a crank angle or time basis, with up to fourteen averages.

4.2.1 Cylinder pressure measurement data

There are a number of factors that can affect the quality of the acquired cylinder pressure data. Resonances, hysteresis, frequency response and thermal stability are some of those factors.

The cylinder pressure sensor was connected to the combustion chamber by a small channel of 2 mm diameter and 60 mm length. The resonance frequency of gas through the channel was determined in order to exclude such frequencies from the measured data. The resonance frequency of the gas in the channel is inversely proportional to its length and the order of the harmonic and is given by:

$$\upsilon = \frac{(2\mathrm{K}-1)C}{4\mathrm{L}} \qquad \text{(Hz)} \qquad (4.1)$$

C is the speed of sound of hydrogen (468 m/s to 520 m/s);

K is the harmonic index (1, 2, …)

L is the length of the channel.

Therefore the 1st harmonic the resonance frequency the first harmonic would be 7.8 kHz. A FFT analysis of the pressure trace was made to verify if a harmonic component with this frequency was present which could mask the pressure trace signal. No resonance frequencies were identified and the pressure transducer diaphragm resonant frequency was 120 kHz, which was well above the resulting resonance frequency of the gas pressure waves through the channel. Also the frequency response of the pressure transducer covers a range between 0.1 Hz and 25 KHz, allowing the discrimination of phenomena with a wide frequency range.

Investigation of the other sources of error was not performed as they were stated by the pressure transducer manufacturer.

4.2.2 Cylinder pressure sampling rate

There was the need to determine the maximum frequency of interest, f_m, because the signal was to be recorded at discrete values of time. Therefore there is the potential for the generation of false readings, or aliases.

The sampling rate theorem states that does not state that to avoid aliasing and provide an accurate representation of the original waveform, the sampling rate, f_s, must be greater than twice the maximum frequency for the signal, f_m:

$$f_s > 2 \times f_m \qquad (4.2)$$

If the sampling rate restriction is met, then the original wave form can be recovered using the series (Marks, 1991):

$$f(t) = \frac{1}{\pi} \sum_{n \to -\infty}^{+\infty} f(n\Delta T) \frac{\sin[\pi(t/\Delta T - n)]}{t/\Delta T - n}, \qquad (4.3)$$

$f(t)$ is the reconstructed function, $f(n\Delta T)$ is the discretely Sampled values of the function, N is an integer corresponding to each sample and ΔT is the sampling period ($1/f_s$).

One important characteristic of this equation is that it assumes an infinite set of sampled data and is hence an infinite series, whereas the actual sets of sampled data are finite. However, because the set sampling rate is high (the data points per sample at 2500 rpm were in excess of 3000) the series is convergent, allowing the reconstruction of the original signal with a finite number of samples.

In any case, since the data acquisition system was able to sample data up to 100 kS/s, to make sure that no aliasing phenomena was present the sampling frequency was set to 50kS/s. Once the function was decomposed by FFT analysis into its harmonics values, it was reconstructed again to check if all the values lay on top of the data points that constitute the original function. If a point calculated by the reconstructed function does not coincide with the original data, then an harmonic would be producing some distortion. Using the above procedure, it was checked that no aliasing phenomena or resonance was present, and therefore that no data distortion occurred.

An FFT of the pressure–volume sampled data was performed to determine the maximum frequency of interest for the signal. With 2000Hz, this was well below the resonance frequency of the pressure transducer.

As discussed by Den Hartog (1956), Churchill (1987) and Kamen (1987), any periodic function f(t) can be represented by the sum of a series of sine and cosine waves multiplied by a constant value which, in symbolic form, this can be written as:

$$f(t) = a_1 \sin \omega_0 t + a_2 \sin 2\omega_0 t + \ldots + a_n \sin n\omega_0 t + b_0 + b_1 \cos \omega_0 t + b_2 \cos 2\omega_0 t + \ldots + b_n \cos n\omega_0 t$$

(4.4)

$$a_n = \frac{2}{T}\int_0^T f(t)\sin(n\omega_0 t)dt \qquad (4.5)$$

$$b_n = \frac{2}{T}\int_0^T f(t)\cos(n\omega_0 t)dt \qquad (4.6)$$

and T is the period, f(t) is the function of time, ω_0 is the angular velocity, t is time and n = 0, 1, 2, … ∞

Since the pressure versus volume function is odd, it can be represented entirely with a series of sine terms, which is the Fourier sine series.
Having done the FFT analysis for the pressure versus volume function which the frequencies and respective amplitudes are listed on table 4.1, and substituting the amplitudes and angular frequencies, and then substituting various values of time, it was found that the values encountered by this substitution fall on top of the pressure versus volume function. Such a result is indicative of good quality data which has not been distorted by the aliasing phenomena.

Table 4.1: Cylinder pressure trace main harmonic components their frequencies and amplitudes.

Harmonic Frequency (Hz)	Harmonic Amplitude (bar)
6.1035	7.0740
24,4141	6.9689
42,7246	5.7053
54.9316	4.2352
73.3420	3.9820
91,5527	3.1997
109.8633	2.2380
122.0703	1.9773

4.3 Methodology of engine testing

The in-cylinder pressure variation was examined to compare the combustion process for the hydrogen fuelled HCCI and DIH_2 modes with the conventional diesel fuelled engine operation. Figure 4.2 shows full cycle cylinder pressure plots for the three operational modes with the engine at the same speed and load. Comparing the pressure traces, a significant difference in the combustion process between the three modes of operation can be seen.

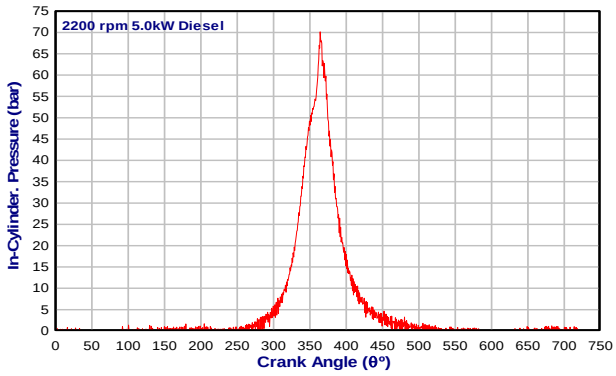

Diesel oil operation

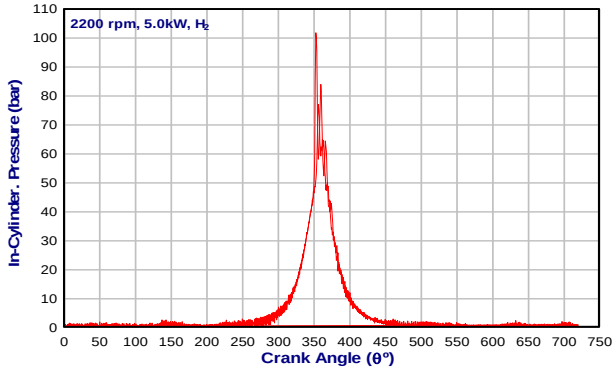

HCCI hydrogen operation

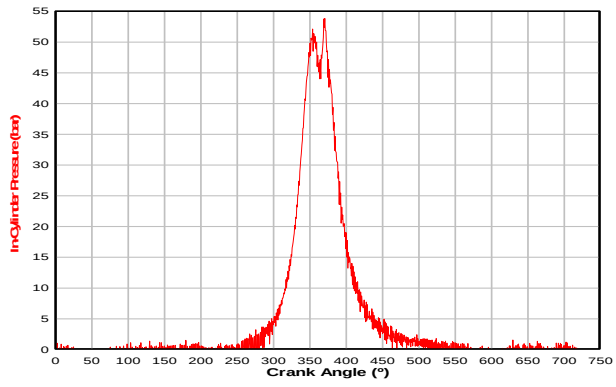

DIH_2 hydrogen operation

Figure 4.1: In-cylinder pressure traces for Diesel, HCCI and DIH_2 operation at 2200 rpm and 5 kW.

The implemented engine testing methodology was the same for all the operation modes (Diesel, HCCI and DIH_2), to allow an easier comparison of the results. The engine speed was set to be constant and equal to 2200 rpm for the majority of the testing, however some other speeds were tested to determine the effect of engine speed on the engine performance. While maintaining a constant speed, the engine load was varied and other operational variables such as maximum combustion pressure, angle of maximum combustion pressure, and exhaust gas temperature were recorded, and thermal efficiency and IMEP calculated.

4.4 Diesel fuel operation characterisation

The engine was tested in conventional Diesel fuel mode of operation and variables such as the magnitude of the maximum combustion pressure, angle of maximum pressure, IMEP, exhaust gas temperature and rate of pressure rise were recorded as a reference condition. It was decided that the control of such variables while testing the engine operating under HCCI and DIH_2 mode should be observed in order to maintain the engine component´s mechanical and thermal integrity.

Table 4.2: Maximum observed values of T_{EXH} , P_{MAX} and P_{IGN} at (a) 5800 W, (b) 3380 W, (c) 1770 W engine load. (2200 RPM, Ta= 21°C.)

Brake Load (W)	1770	3380	5080	5800
T_{EXH} (°C)	318	335	363	372
P_{MAX} (bar)	47.5	55.5	68.5	76.0
P_{IGN} (bar)	46.0	46.5	47.8	48.8

From Figure 4.3 and Table 4.2 it is possible to observe an increase of the ignition pressure of the cylinder charge with the increase in load. As expected, maximum combustion pressure and exhaust gas temperature increase with load. Figure 4.4 shows the engine thermal efficiency as a function of load, showing a maximum value of approximately 26% at 5800

W. This value served as a reference of comparison with the other modes of operation at the same load.

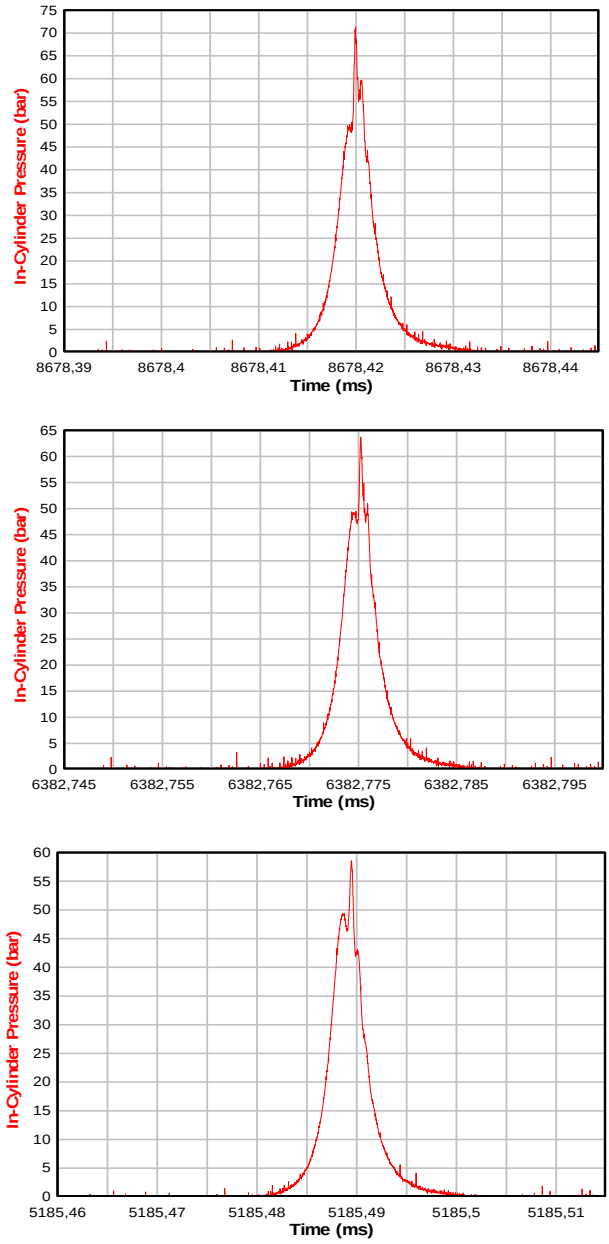

Figure 4.2: Cylinder pressure diagram for diesel operation at (a) 5800 W, (b) 3380 W, (c) 1770 W engine load. 2200 RPM, T_a= 21°C.

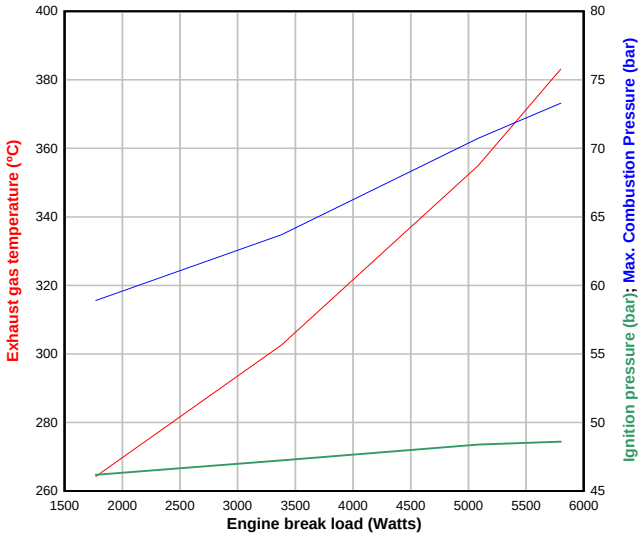

Figure 4.3: Exhaust gas temperature, ignition pressure and maximum combustion pressure at (a) 5800W, (b) 5080W, (c) 3380W, (d) 1770W.

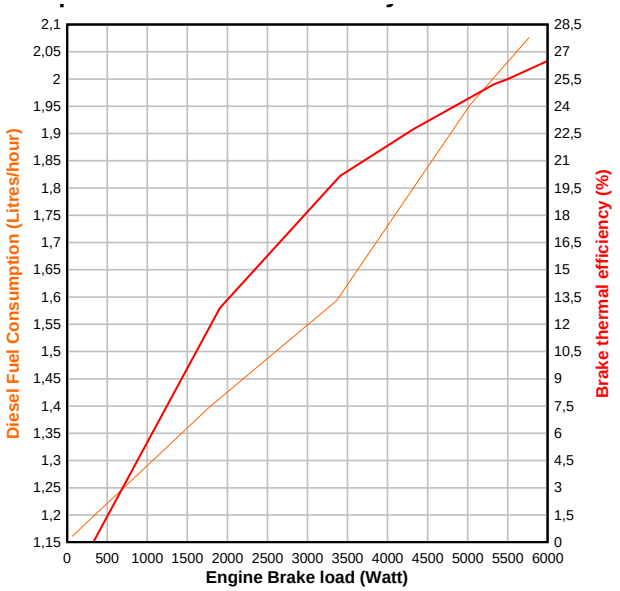

Figure 4.4: Diesel fuel consumption and brake thermal efficiency as a function of engine load. (2200 RPM, Ta= 21°C.)

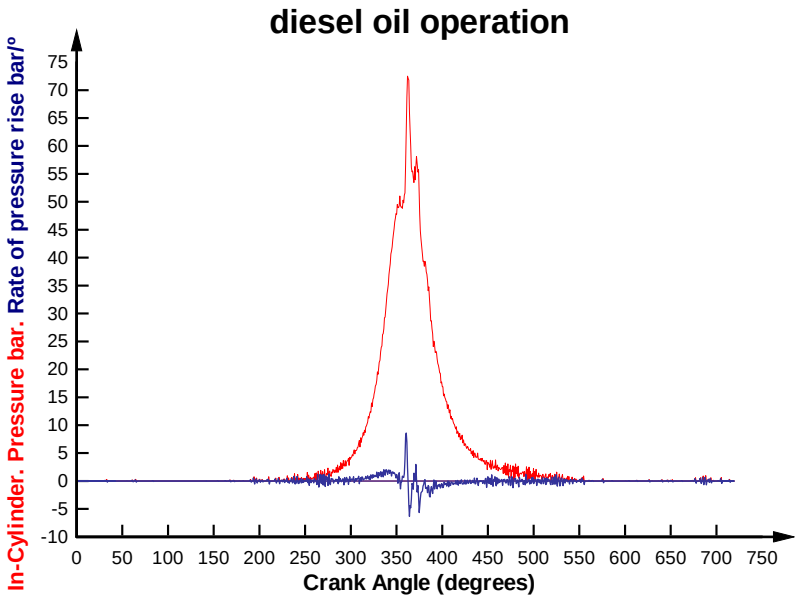

Figure 4.5: Open pressure diagram and its derivative of test engine operated in diesel mode at 5.8 kW load.

Figure 4.5 shows the pressure plot for diesel operation, as well as the rate of pressure rise. The maximum rate of pressure rise is 8.59 bar/°CA and the development of combustion from ignition to its maximum pressure takes approximately 6.4°CA.

4.5 Dual fuel operation characterization

Having the test rig with the hydrogen port injection system, testing of the engine in dual fuel (hydrogen and diesel) mode is possible. A series of such tests were carried out to generate experience with the test rig and as part of the development of commercial dual fuel engine technology, described further in Appendices A and B. Although dual fuel operation is not the main focus of this thesis, this section will present a summary of the results obtained during these initial tests.

Dual fuel engines run simultaneously on two different fuels, typically one gaseous and one liquid, where the liquid is used as a source of ignition for the pre-mixed cylinder charge. In addition to more flexibility in the fuel

supply one can, if the combustion properties of the two fuels complement each other, obtain a better engine performance than with either of the fuels alone.

The operation of diesel engines in dual fuel mode with a gaseous fuel inducted in the intake air is particularly attractive if the gaseous fuel can improve the diesel combustion, since this may improve on some of the weak points of this engine type, such as high particulate matter (PM) emissions. This is particularly attractive if using diesel fuels of low quality with poor ignition and combustion properties, such as bio-oils or heavy fuel oils. In the case of biofuels, minimising the need for costly fuel processing is of great importance, and an engine which can use, for example, unprocessed vegetable oils directly will provide a substantial advantage in the overall energy balance.

Diesel engines operating in dual fuel mode with natural gas have been studied by a number of authors (See Appendix A for a short overview), and such systems with hydrogen as the inducted fuel have also been reported (see e.g. Roy et al., 2010; Varde and Frame, 1983; Saravanan et al., 2007,2008). In general, it is reported that engine fuel efficiency is comparable to that under normal diesel operation and nitrogen oxides (NOx) emissions are similar or slightly lower. Substantial advantages have, however, been seen in the particulate matter emissions, with reductions of above 50% frequently reported. Lower PM emissions follows naturally from the substitution of diesel with a pre-mixed fuel (which does not produce PM), however changes in the in-cylinder processes will also influence this, potentially further enhancing the PM reductions. Studying the combustion process and interaction between the two fuels in dual fuel engines is therefore worthwhile, in order to fully understand the mechanisms governing the formation of emissions.

4.5.1 Experimental setup

The experimental setup was based around the same system as described above. The hydrogen injection rate was adjusted to avoid knock,. The

fraction of energy supplied by the hydrogen gas is therefore limited by the knock detection system based on the knock intensity.

4.5.2 Test results

One of the first tasks carried out was the characterisation of the engine operation for different amounts of hydrogen injection into the inlet air manifold. The hydrogen flow rate was varied from 1 to 9.8 dm3/min, and the diesel oil consumption was adjusted automatically as hydrogen flow rate changed by normal, simple action of the speed governor. This was repeated for a range of engine loads to provide an extensive data set of engine performance parameters for varying operating conditions. Table 4.3 shows an example of the percentage of energy based on hydrogen and on diesel fuel as a function of load.

Table 4.3: Energy share ratios for hydrogen and diesel fuel at different engine loads for a constant hydrogen flow of 6.0 dm^3/min.

Load (%)	Diesel Fuel (%)	Hydrogen energy (%)
0	75.0	25.00
25	84.2	15.01
50	88.0	12.0
75	90.9	9.1
100	92.9	7.1

4.5.2.1 Combustion and energy efficiency

Figure 4.6 shows the brake thermal efficiency values for all the engine test loads and hydrogen flow rates as well as those under normal diesel operation. A clear trend towards increased efficiency with increasing hydrogen flow rate can be seen. This increase in thermal efficiency indicates a substantial improvement in the combustion process.

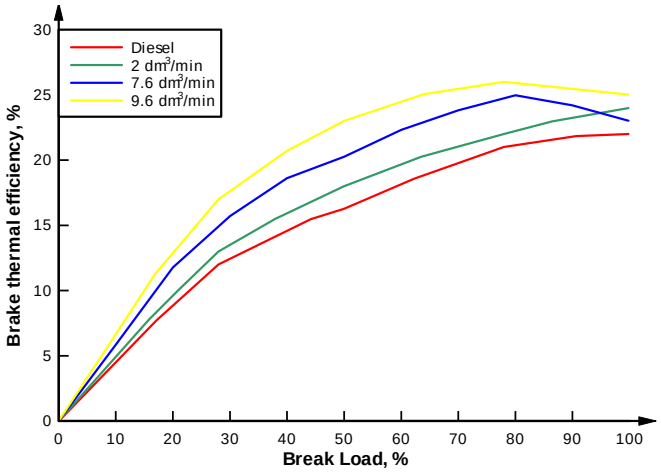

Figure 4.6: Brake thermal efficiency as a function of load for various hydrogen flow rates.

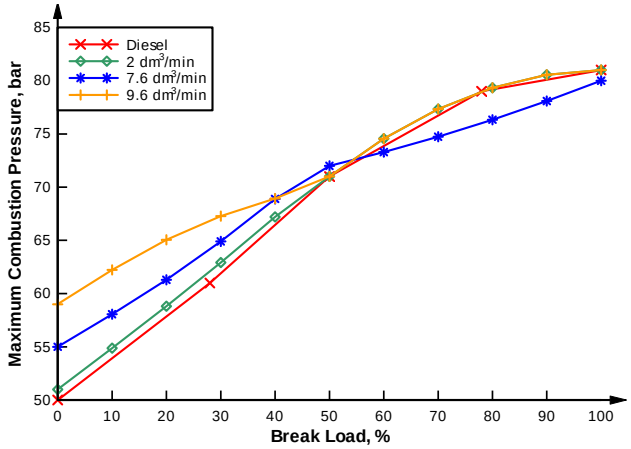

Figure 4.7: Maximum combustion pressure for different hydrogen flow rates compared with diesel-only operation.

In Figure 4.7 the variation of maximum in-cylinder gas pressure at varying loads and for different hydrogen flow rates is presented. Under stable dual fuel operation, i.e. without knocking, the peak gas pressure differs only very little from that under normal diesel operation. This indicates that the dual fuel engine will have similar performance as a conventional diesel engine in terms of noise, and no mechanical challenges are expected (which can be the case in relation to e.g. bearing loads when using very fast-burning fuels creating high rates of pressure rise).

Figure 4.8 shows the variation of exhaust gas temperature for different hydrogen flow rates and for different brake loads. It was found that the operation with hydrogen results in slightly higher exhaust gas temperatures, and this temperature increases with the hydrogen flow rate.

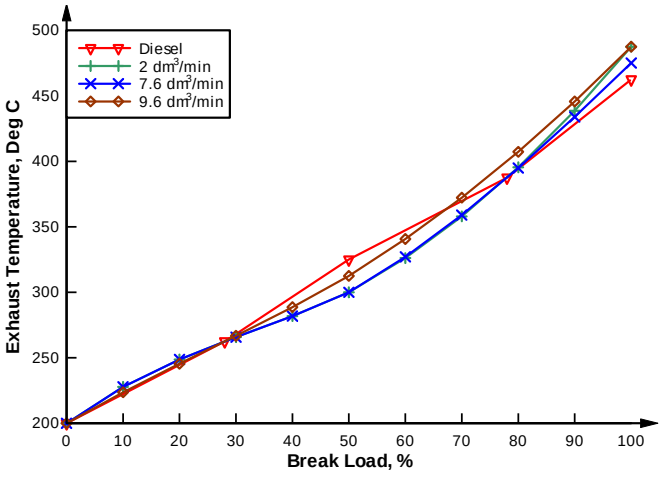

Figure 4.8: Comparison of exhaust gas temperatures between diesel and various hydrogen flows.

4.5.2.2 Exhaust gas emissions

Although hydrogen is only injected during the induction stroke, i.e. when the intake valves are open and exhaust valves are closed, some hydrogen may pass through the engine and into the exhaust. This is known as hydrogen slip. Figure 4.9 shows the hydrogen slip expressed in ppm at the exhaust gases. As can be seen from the figure, the level of hydrogen in the exhaust gases is generally higher than for diesel operation for the cases with hydrogen injection, however the level of unburnt hydrogen in the exhaust is in all cases acceptably low. Regarding this effect, the use of port injection results in a better use of hydrogen energy and also in a system much safer than hydrogen fumigation system as engine manifold is not full of an hydrogen air mixture, and therefore the cylinder is not scavenged with such mixture.

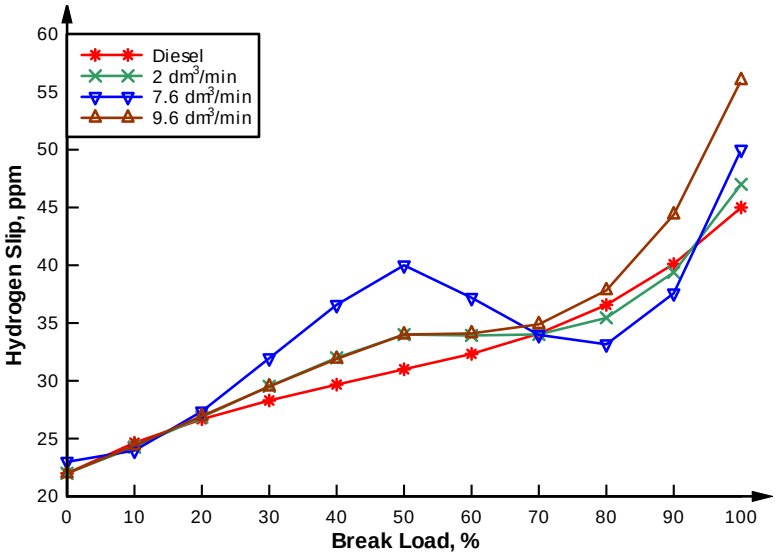

Figure 4.9: Hydrogen slip into the exhaust gases for different hydrogen flow rates and engine loads.

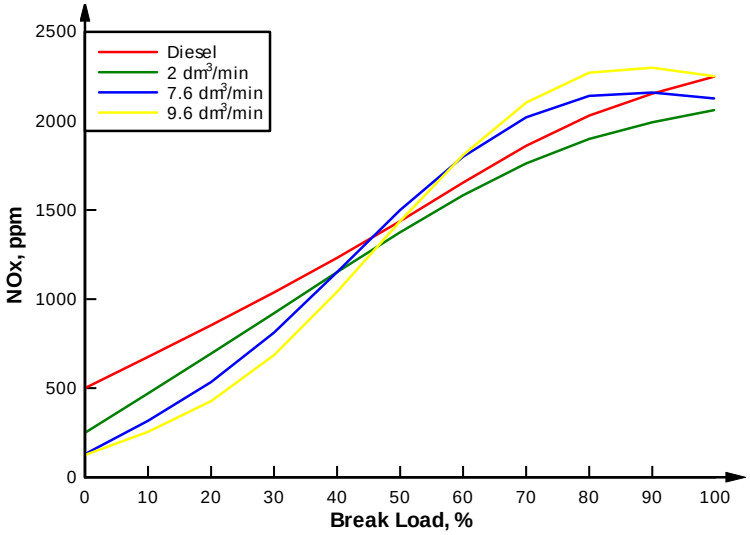

Figure 4.10: Comparision of the effect of hydrogen addition on the NOx emissions for different engine loads.

Figure 4.10 shows the variation in NOx concentration in the exhaust gases for various engine loads and hydrogen flow rates compared with those resulting from normal diesel operation. It can be seen that for up to 50% load hydrogen injection resulted in a slight reduction of NOx compared with the emissions resulting from diesel operation. But for engine loads above

50%, injection of hydrogen results in a small increase of NOx production. However, it can be observed that for 100% engine load the NOx emissions in dual fuel mode are approximately the same as for diesel operation.

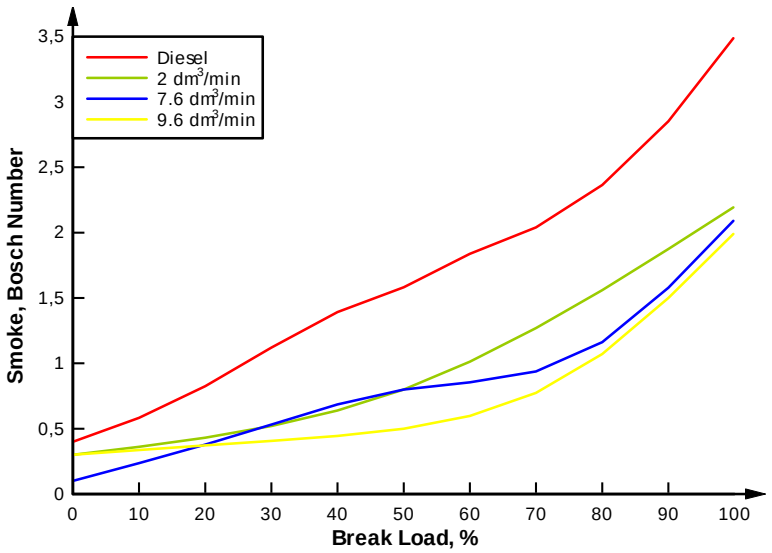

Figure 4.11: Particulate matter emissions compared for various hydrogem flowrates and diesel operation.

As has been reported by other researchers, the use of hydrogen has a strong impact on the formation of particulate matter, and the test results for the current system are shown in Figure 4.11. The smoke emissions are found to be lower for any hydrogen flow rate and throughout the tested load range. It can be seen that the higher the flow rate of hydrogen, the lower the emissions of particulate matter are, as one would expect. At full load and for a hydrogen flow rate of 9.6 dm3/min, the measured Bosch smoke number is found to be 2 for the dual fuel engine, compared with 3.9 for diesel operation. Notably, it can be seen that even a small hydrogen flow rate (providing in the order of 5% of the fuel energy) leads to a substantial reduction in particulate matter. This indicates that the combustion of the diesel fuel is improved by operating the engine in dual fuel mode, and the higher the hydrogen flow rate the lower the carbon content of the exhaust gases.

4.6 HCCI operation characterization

The HCCI mode of operation was tested at a constant speed of 2200 rpm and at the following loads: 1600W, 2100W and 4132W, corresponding to different equivalence ratios. This procedure allowed investigations into the interdependency between the various variables involved.

During the tests, the HCCI engine operation exhibited very high thermal efficiency values, approaching 49%, making the initial results very encouraging. However, this mode of operation produced varying and high rates of cylinder pressure rise and reduced operational stability, even at constant load.

4.6.1 Inlet air temperature and ignition control

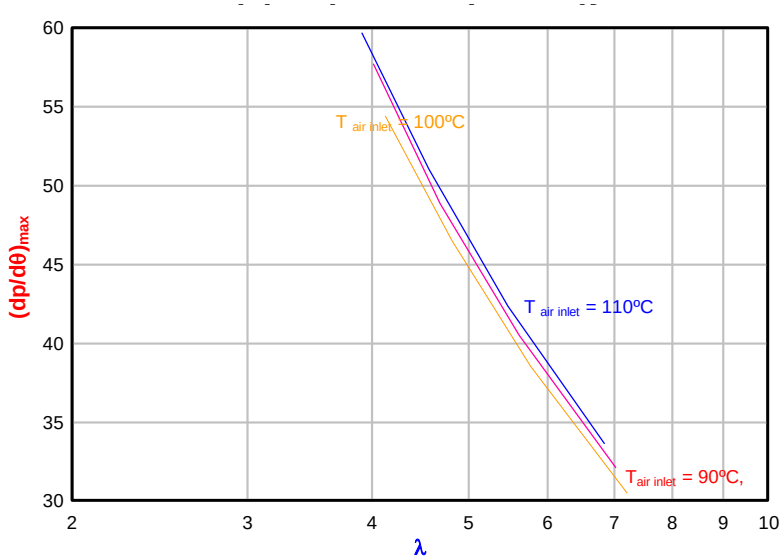

Figure 4.12: Dependence of the RPR as a function of T_{air} inlet and λ.

Figure 4.12 shows the maximum rate of cylinder pressure rise as a function of λ and inlet air temperature T_{air}. It can be seen that the maximum rate of cylinder pressure rise is not significantly affected by the temperature of the air at the cylinder inlet, but that the excess air ratio λ has a strong influence. As a reference, the rate of pressure rise in a medium speed Diesel engine should generally not be higher than 12 bar per crank angle degree. During the experiments on HCCI operation, rates of pressure rise

exceeding 40 bar/° were observed, with the highest values occurring for richer cylinder charges and lower speeds.

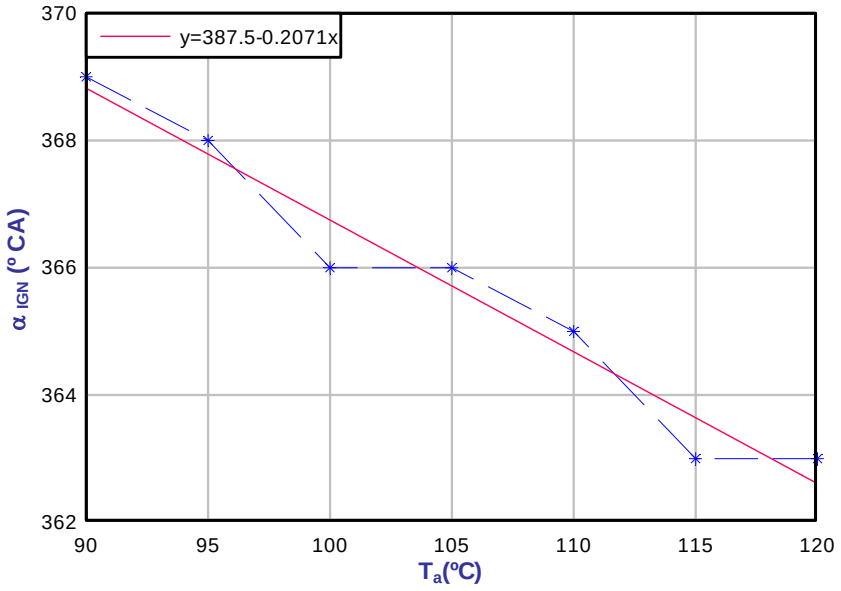

Figure 4.13: Angle of ignition as a function of air inlet temperature, T_{air}.

The ignition angle, $\alpha_{IGN,}$ is governed by the end of compression temperature, and is therefore influenced by the temperature of the air entering the cylinder. Figure 4.13 illustrates this dependence: higher inlet air temperatures will result in advanced ignition. For high pre-heating temperatures, the ignition can take place before the piston top dead centre, reducing the cycle efficiency drastically and increasing the mechanical loads on the engine bearings due to the fast combustion in the HCCI engine.

4.6.2 Operating characteristics and performance

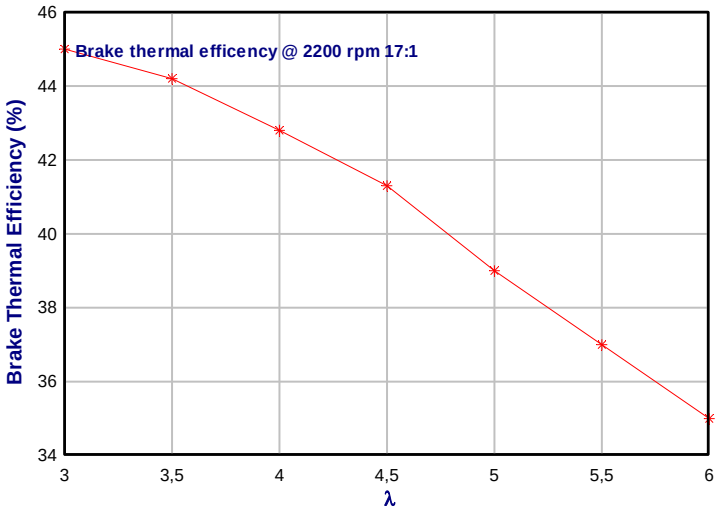

Figure 4.14: Brake thermal efficiency at constant speed (2200 rpm) for varying fuel air ratios.

Figure 4.14 shows the brake thermal efficiency of the engine for varying excess air ratios. It can be seen that the engine is able to maintain high fuel efficiency even for very lean cylinder charges.

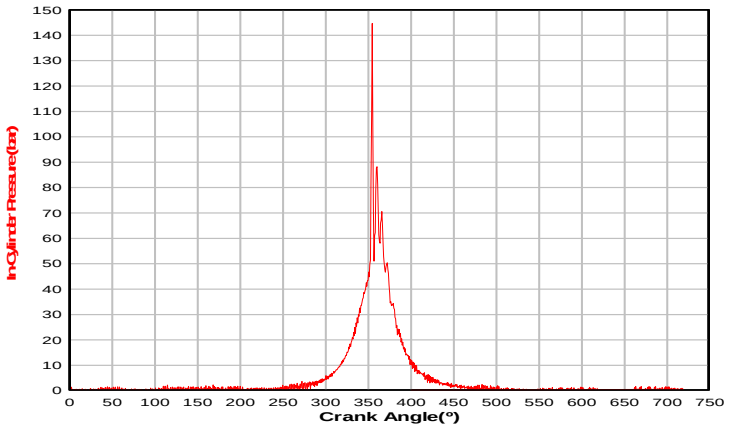

4132 Watt HCCI (6 Averages)

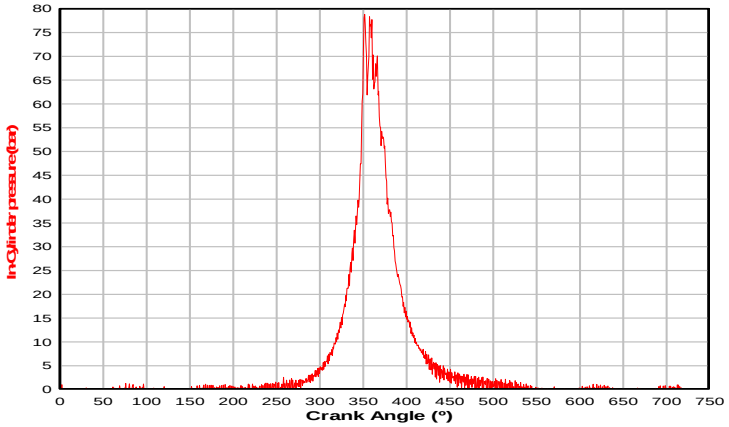

2100 Watt (6 Averages)

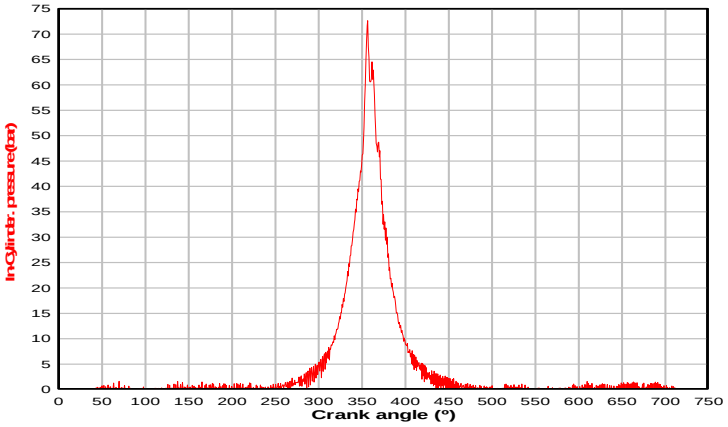

1600 Watt HCCI (6 Averages)

Figure 4.15: HCCI open cycle diagrams for different loads.

It can be observed in Figure 4.15, that the cylinder maximum pressure amplitude it is a function of the engine load, has it was observed that

higher combustion pressures are generated at higher loads but in any case accompanied by high rates of pressure rise, therefore explaining the difficulties encountered into control the engine speed and its lower thermal efficiency at lower loads .

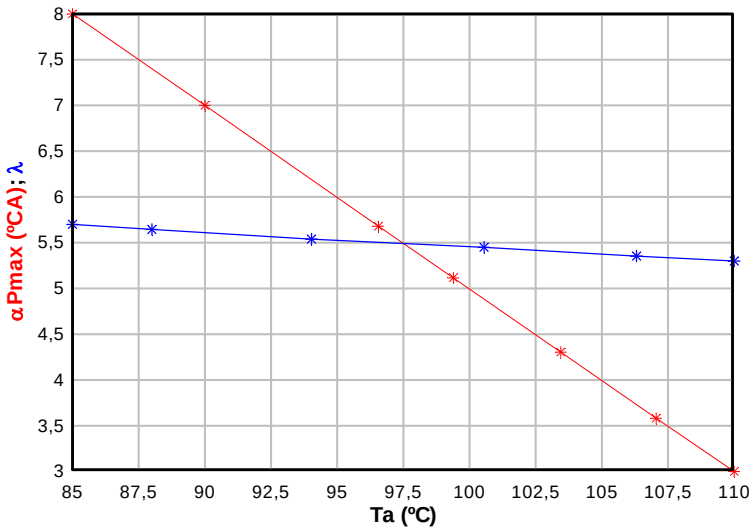

Figure 4.16: Effect of the air inlet temperature on the excess air ratio and angle of maximum pressure. (At constant speed of 2000 rpm, and mass flow rate 9g/minute of H_2.)

The effect of the air inlet temperature on the excess air ratio and angle of maximum pressure is illustrated in Figure 4.16. As expected, increasing inlet air temperature advances the angle of maximum pressure, which can move as much as 5º crank angle (BTDC), therefore affecting directly the engine efficiency and the mechanical loads on the bearings.

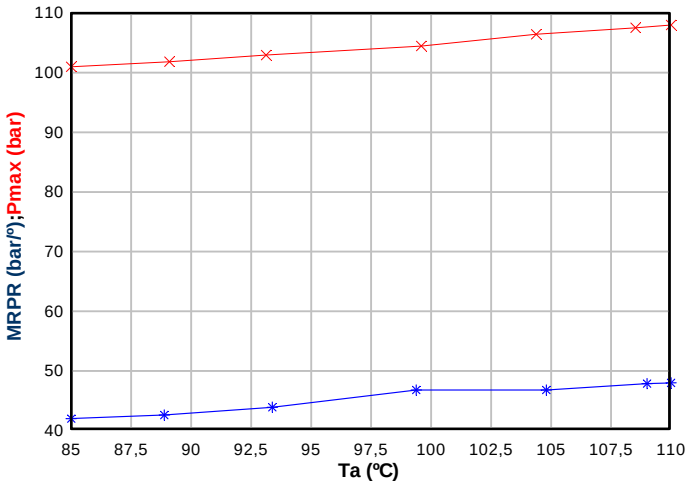

Figure 4.17: Effect of the air inlet temperature on the maximum combustion pressure and maximum rate of pressure rise. (At constant speed of 2000 rpm, and mass flow rate 9g/minute of H_2.)

Figure 4.17 illustrates the effect of air inlet temperature on the maximum combustion pressure and maximum rate of pressure rise. It can be seen that the rate of pressure rise has some dependence on the temperature of the air entering the cylinder, and this is accompanied by a linear increase of the maximum combustion pressure. Also, it was identified through the simulation that increasing the intake air temperature has a bigger influence on the final compression temperature than an increase in the compression ratio. This effect was also observed by (Rottengruber et al., 2004) using an experimental engine.

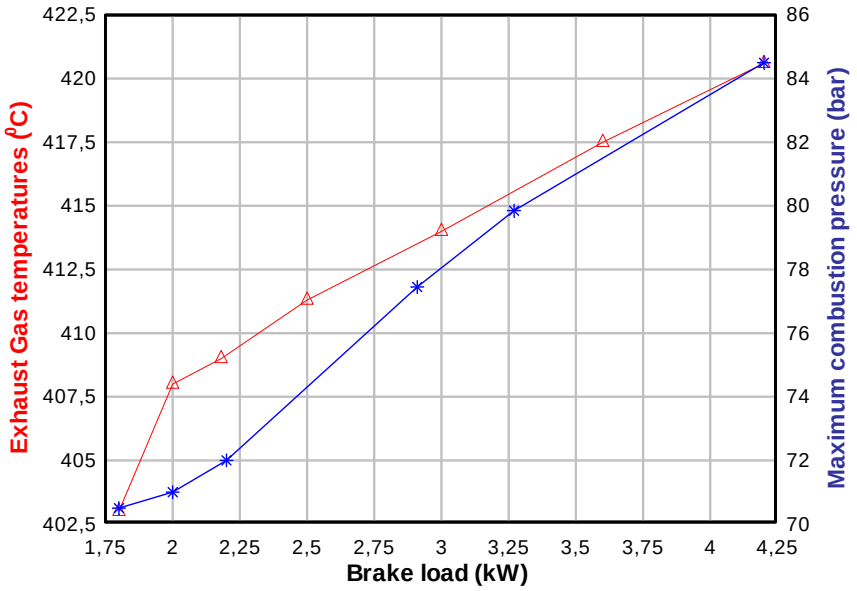

Figure 4.18: Exhaust gas temperature and maximum combustion pressure as a function of engine load (with constant T_a=90°C at 2200 RPM).

Figure 4.18 shows the exhaust gas temperature and maximum combustion pressure over the load range with constant intake air temperature and at constant speed. Considering that the tests were performed at constant speed, therefore with the same approximate exhaust gas flow, it can be observed that for break loads up to 2.2 kW the rate of heat loss through the exhaust is higher than for loads above 2.2 kW resulting in a lower thermal efficiency. A similar behaviour can be identified in what concerns the maximum combustion pressure. A possible explanation of this behaviour can be a characteristic of the engine particular combustion chamber design, however some authors (Rottengruber et al. 2004) mentioned the suitability of the HCCI mode for lower to moderate loads, and the suitability of DIH_2 for moderate to higher loads applications.

An increase in the average cylinder charge temperature causes a reduction in the ignition delay and an increase in the conversion rate of the hydrogen fuel. Therefore the heat release rates of consecutive operating cycles become more even, contributing for a better engine controllability through the reduction of the cyclic variations. However decreasing the ignition delay and increasing the conversion rate of the hydrogen fuel will result in

higher thermal and mechanical component loading, which must be considered at the design stage.

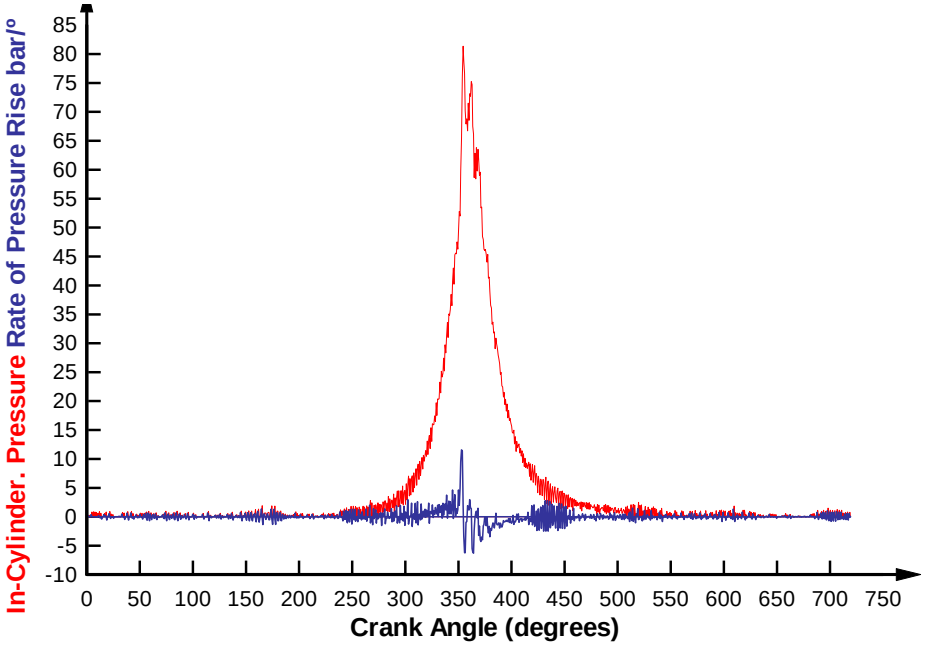

Figure 4.19: HCCI open pressure diagram and its derivative of test engine operated at 4.1kW load.

Figure 4.19 shows the in-cylinder pressure plot and its derivative, the rate of pressure rise, under HCCI operation. The maximum rate of pressure rise is 11.6 bar/°CA, taking place before TDC. The development of combustion from ignition to its maximum pressure takes only 4.2 °CA. A number of sharp pressure peaks after the maximum pressure peak can be observed, being the result of combustion generated pressure waves due to uncontrolled HCCI combustion characteristics.

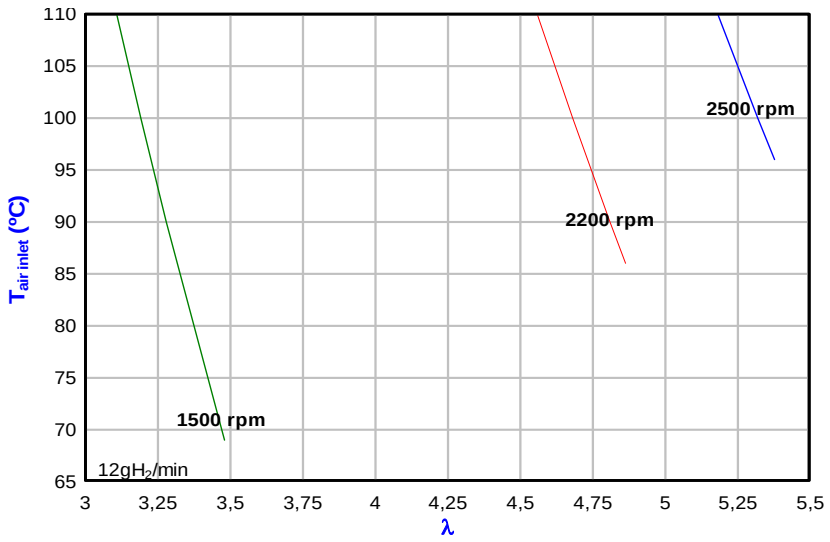

Figure 4.20: Required intake air temperature to sustain combustion as a function λ, and speed for a 17:1 compression ratio.

Figure 4.20 illustrates one of the most critical aspects of HCCI engine behaviour: the dependence of the air inlet temperature on the operational stability of the engine for varying excess air ratios. In order to use the temperature control of the intake air to control the ignition timing and combustion, it is critical to include the relationship between these variables in the engine control system. In particular, the variation of the minimum inlet air temperature required to sustain combustion for different speeds and loads must be studied in detail to achieve good engine control.

4.6.3 Emissions

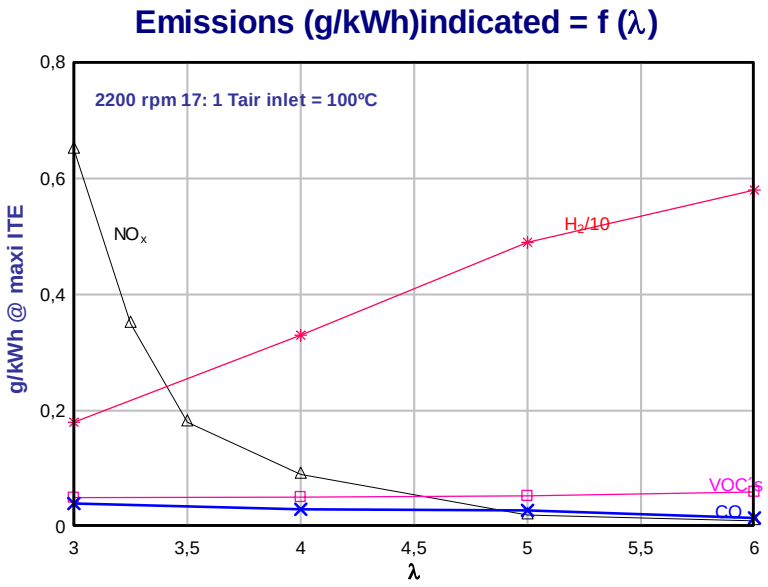

Figure 4.21: Emissions at constant speed (2200 rpm) and air inlet temperature (100ºC) as a function of air fuel ratio.

The exhaust emissions were measured while the engine was operated in hydrogen fuelled HCCI mode at a speed of 2200 rpm and T_a of 100ºC. The results of the test are presented in Figure 4.21. As can be seen, the NO_x emissions increase sharply for λ <3.5, and become negligible for higher values of λ. The NO_x levels are considerably lower that what would be expected for conventional diesel engine operation for all the cases investigated. The levels of CO and unburnt hydrocarbons (VOC) emissions are fairly constant over the investigated load range. The levels of these emissions are negligible for the hydrogen engine, with the only carbon source being the burning of the lubricating oil.

Figure 4.21 also shows the presence of some hydrogen in the exhaust gases, and this is due to hydrogen slip which occurs during the valve overlap period and the non-optimized hydrogen injection valve period. To minimise hydrogen slip, more accurate control of hydrogen injection is required. Values of exhaust emissions for the test engine operating in hydrogen fuelled HCCI and conventional diesel fuelled engine modes are shown in Table 4.4, illustrating the significant emissions reductions characteristics of HCCI engines.

Table 4.4: Comparison of emissions for DI Diesel and H_2 HCCI operation.

	H_2 HCCI engine	Diesel engine
NO_x	0.01 g/kWh	6.30 g/kWh
CO	~0.00 g/kWh	2.00 g/kWh
Particulate matter	~0.00 g/kWh	0.36 g/kWh
VOC´s	0.015 g/kWh	0.50 g/kWh

4.6.4 Operational stability

Because of the challenges associated with ignition timing control, operational stability is one of the main challenges in HCCI engines. Small variations in ignition timing can lead to large variations in the peak cylinder pressure and the cycle work output, and therefore have large influence on engine efficiency and emissions formation.

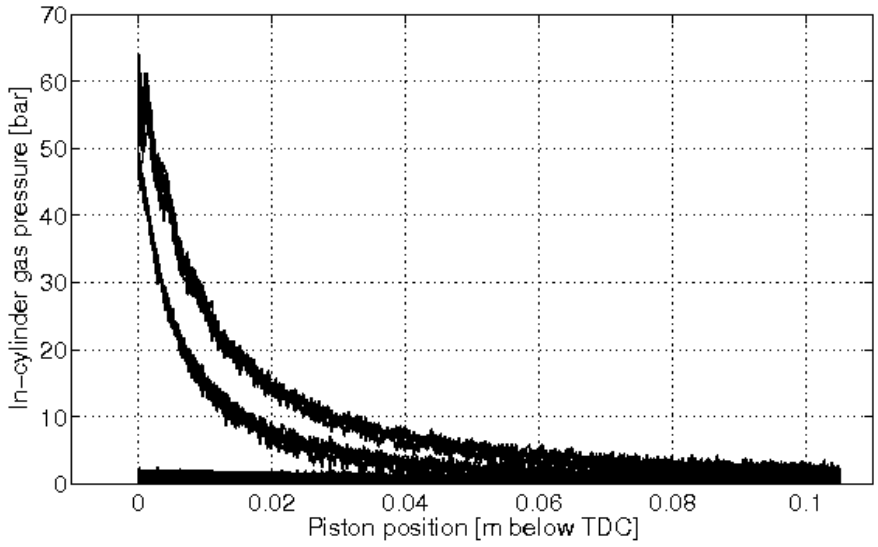

Figure 4.22: Cylinder pressure-volume plots for H_2 HCCI operation.

Figure 4.22 shows the pressure-volume plots for 10 consecutive cycles under HCCI operation. Some variation between the cycles can be seen, particularly around top dead centre, due to the poor control of the ignition timing in the HCCI engine.

Cycle-to-cycle variations in cycle work output (W) are commonly measured by the coefficient of variation, COV, defined as

$$COV_W = \sigma_W / \text{mean}(W), \quad (4.7)$$

where σ_W is the standard deviation of the cycle work and mean(W) is the mean work output from the cycles.

Sets of 100 consecutive cycles taken at different operating conditions were analysed to establish the extent of the cycle-to-cycle variations in cycle work and in-cylinder gas pressure. It was found that between the highest and the lowest loads tested the coefficient of variation in cycle work ranged respectively from 7% to 23%. These are acceptable values, particularly for the higher loads that tend to produce a more stable operation. The variations in peak in-cylinder gas pressure were higher, ranging from 15% to 25% over the same load range. This is due to the high pressure rise shortly after ignition resulting from a fast combustion of hydrogen, giving large variations in peak pressure from minor variations in ignition angle. This effect is not desirable as it can result in some engine instability during load variations.

4.7 DIH_2 operation characterization

Similarly as above the DIH_2 mode was tested in such a way to characterize the engine operation at constant load for different equivalence ratios or fuelling rates, as well as with different inlet air temperatures, thus giving knowledge of the interdependency between these variables.

4.7.1 Auto-ignition of the hydrogen jet

Due to the limited compression ratio of the test engine (17:1) the temperature at the end of compression was not sufficiently high for auto-ignition of the injected hydrogen jet. Therefore, heating of the air entering the cylinder was required as for the HCCI tests above. The temperature of the air entering the cylinder plays a key role in the control of the RPR and smoothness of the engine operation, and the relation between these variables is a critical aspect for developing appropriate engine control strategies.

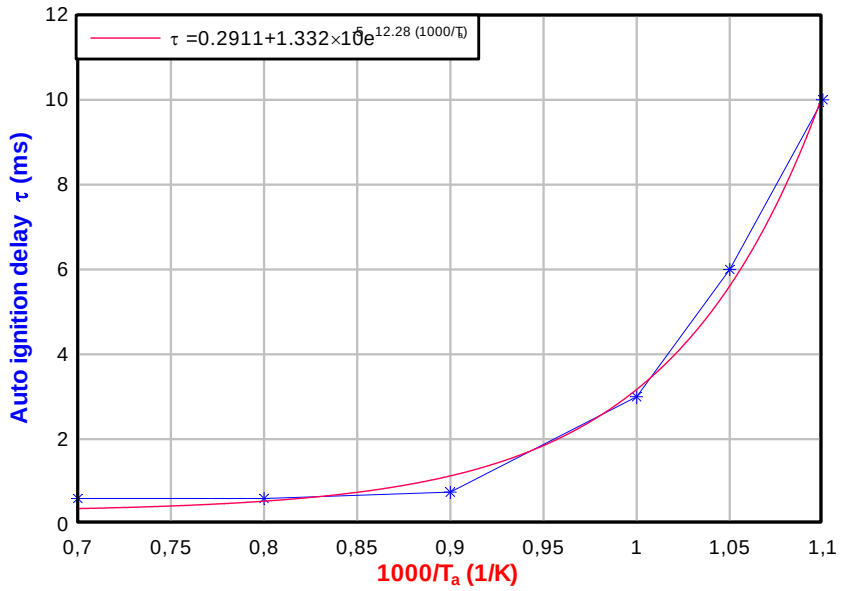

Figure 4.23: Effect of the end-of-compression temperature on the ignition delay of the hydrogen jet.

Based on the work of Tsujimura et al. (2003), Figure 4.23 illustrates the strong dependence of the hydrogen ignition delay on the end-of-compression temperature. For temperatures below 1100 K, the auto ignition delay increases sharply and becomes much longer than for temperatures above 1100K. This dependence follows an Arrhenius function. The auto ignition delay is therefore strongly dependent upon the temperature of the air entering the cylinder and the engine compression ratio, since these variables determine the end-of-compression air temperature.

According with Tsujimura et al. (2003) for end-of-compression temperatures below 1100K, the auto ignition delay is longer than that for Diesel fuel at the same operating conditions, but much shorter delays are produced for cylinder charge temperatures above 1100K. Due to the high diffusion of hydrogen the injected hydrogen is rapidly spread all over the combustion chamber volume, not requiring time for vaporisation of droplets, and therefore the combustion process proceeds very quickly after ignition. This gives the benefit of a fast combustion process, and the high rate of pressure rise is a characteristic of the hydrogen combustion. A third stage of combustion typical for diesel oil does not exist is practical terms because, due to the enhanced fuel-air mixing and low hydrogen quenching distance, the cylinder charge is completely combusted, even in combustion chamber crevices.

4.7.2 Engine tests

Various injection timings (start- and duration of injection) were tested. In order to study fully the characteristics of the DIH_2 engine, extensive work for optimization is required. However, here only a limited amount of optimization work could be carried out as the hydrogen injector was leaking badly into the hydraulic oil system, and its operating stability was deteriorating during the tests.

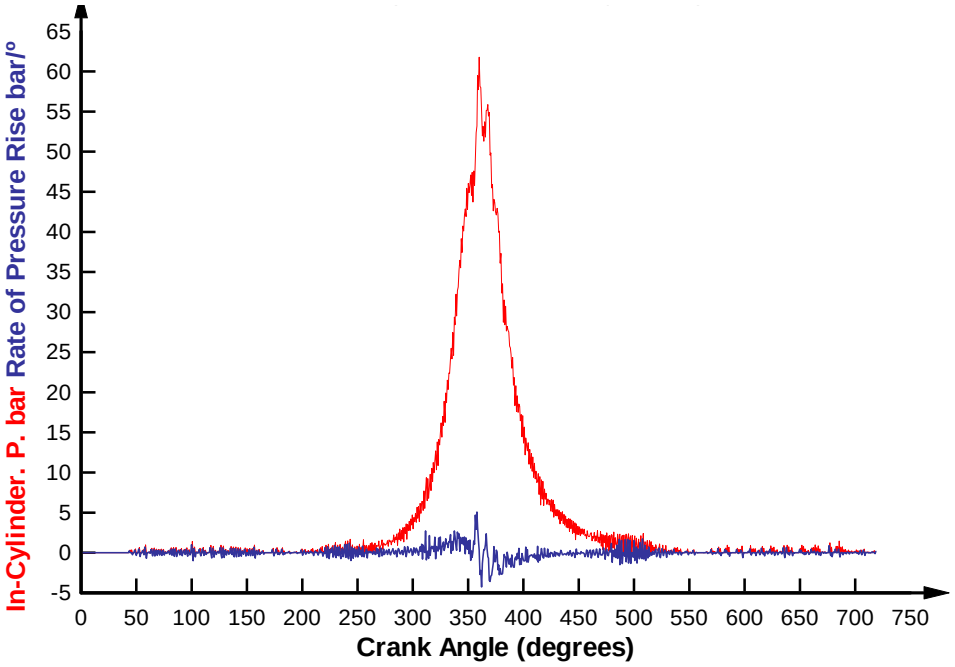

Figure 4.24: Cylinder pressure diagram and its derivative at 5.0 kW load.

Figure 4.24 presents the cylinder pressure plot and the rate of pressure rise under DIH_2 operation at 5.0 kW load. The maximum rate of pressure rise was found to be 5.1 bar/° and the development of combustion from ignition to its maximum pressure takes 5.6 °CA. Comparing with the results above, it is clear that the rate of pressure rise is significantly lower than for HCCI operation, as expected. A number of tests were carried out to understand the effect of the injection timing and duration on the engine operation.

Table 4.5 shows results for varying ignition timing and duration, indicating that the closer the injection is to the TDC, the higher the IMEP is, and as a consequence $dp/d\theta$ and P_{max} become smaller and T_{exh} increases as the cycle pressure diagram is shifted to the right. From the experimental results it is suggested that to take advantage of the fast hydrogen combustion the start of injection can be closer the TDC, resulting in a higher thermal efficiency.

Table 4.5: Combustion characteristics as a function of injection timing and duration (2000 rpm, λ = 5.395).

	10° injection duration, 10°BTDC start of injection	15° injection duration, 15°BTDC start of injection	20° injection duration, 20°BTDC start of injection
Dp/dθ (bar/ °θ)	4.2	4.8	5.0
Pmax (bar)	107	119	123
αPmax (°ATDC)	10°	5°	2°
IMEP (bar)	6.778	6.472	6.196
Texh (°C)	583	531	506
Pign (bar)	35.97	42.11	43.31

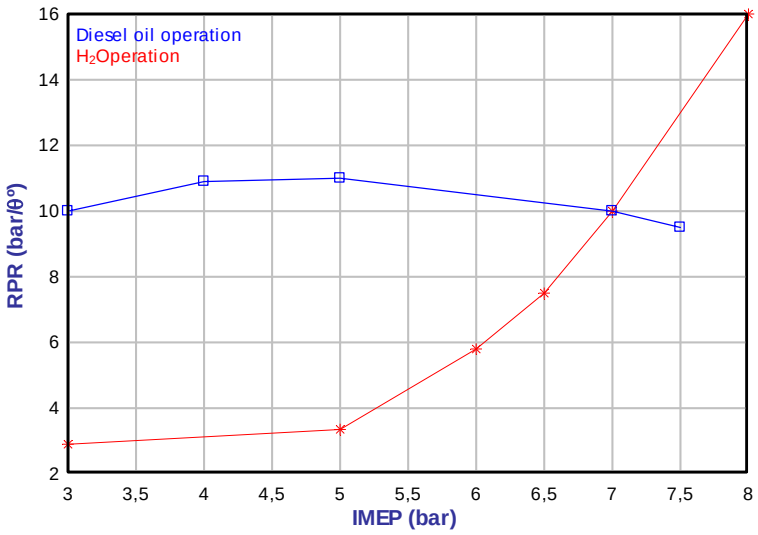

Figure 4.25: Rate of pressure rise as a function of engine load for diesel and DIH2 operation.

The rate of pressure rise, shown in Figure 4.25, was found to be almost constant and small for low loads, but increasing rapidly with increasing load. The rate of pressure rise was much lower than when the engine was operated with Diesel fuel over most of the load range, however the pressure rise rate increases rapidly at high loads for the DIH_2 engine. This behaviour is one of the limiting factors of the Diesel engine fuelled with

hydrogen, since the operation becomes noisy and the mechanical loads increase drastically for high engine loads.

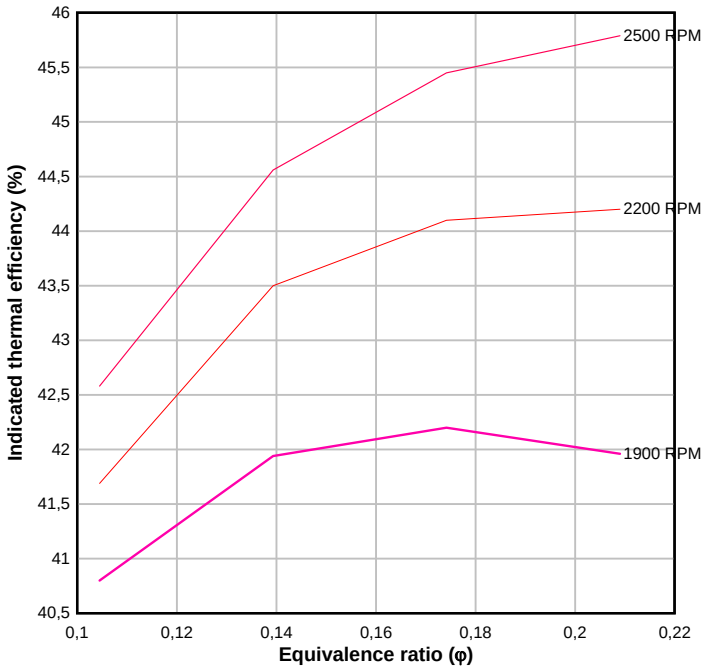

Figure 4.26: Indicated thermal efficiency for different equivalence ratios φ and different speeds.

Figure 4.26 shows the engine efficiency for different engine speeds and equivalence ratios. It can be seen that the fast combustion of hydrogen allows the engine to produce high indicated efficiencies at high speeds, indicating its potential for high power densities and low high-temperature emissions such as NO_x.

4.7.3 Emissions formation

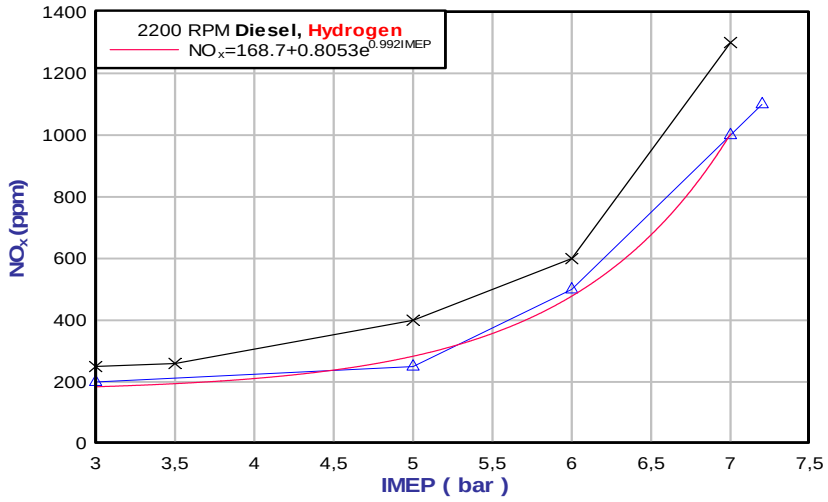

Figure 4.27: Emissions as a function of engine load under DIH_2 and DI Diesel operation.

Figure 4.27 shows the nitrogen oxide (NO_x) emissions for the engine under DIH_2 and conventional diesel engine modes for a range of loads. As expected, the NO_x formation increases sharply at higher loads, due to the higher temperature levels in the combustion chamber. The DIH_2 engine is seen to produce approximately 20% lower NO_x emissions compared with the same engine in conventional diesel mode. Despite of higher cylinder peak pressure characteristic of DIH_2 mode, resulting from the faster combustion of hydrogen, the results suggest that the enhanced fuel-air mixing in the combustion chamber results in a more homogeneous combustion with less high-temperature zones, therefore inhibiting the thermal NO_x formation. The time required for the combustion of the cylinder charge with hydrogen and the temperature developed during its combustion are therefore key parameters that can explain the lower NO_x emissions of the hydrogen fuelled engines.

4.8 Efficiency calculations and comparison

As described in Chapter 3, the engine data acquisition and monitoring software was designed to collect the variables required to calculate the engine thermal efficiency. On the instrumentation set-up menu of the software, the net calorific values of the fuels, as well as their densities are introduced, allowing online calculation of engine thermal efficiency. The other monitored and logged engine operational parameters were: exhaust gas temperature; air inlet temperature; air mass flow rate; hydrogen mass flow rate; diesel oil mass flow rate; and engine speed and power.

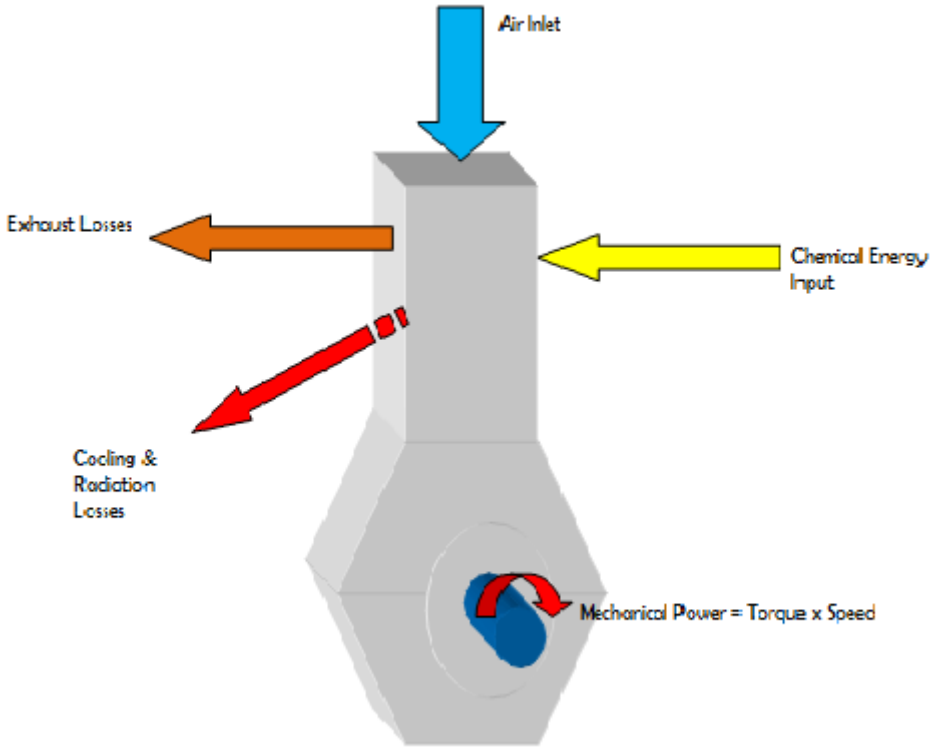

Figure 4.28: Engine energy flows considered for thermal efficiency calculation.

Figure 4.28 illustrates the energy balance of the engine during operation. Considering the difficulty in measuring the energy losses due to radiation, these were lumped with the engine cooling losses for these calculations.

Fuel heat input is given by:

$$Q_f = \dot{m} \times NCV \times C \qquad (4.8)$$

Exhaust gas heat is given by:

$$Q_{exh} = \dot{m}_{exh} \times C_p \times \Delta T \qquad (4.9)$$

Brake power:

$$Q_b = T \times \omega \qquad (4.10)$$

Mass flow of exhaust gases:

$$\dot{m}_{exh} = \dot{m}_{air} + \dot{m}_f \qquad (4.11)$$

The overall heat equation is then:

$$Q_F = Q_m + Q_{cool} + Q_{rad} + Q_{exh} \qquad (4.12)$$

Solving in order to determine the heat losses by radiation and cooling of the cylinder:

$$Q_{cool} + Q_{rad} = Q_f - Q_m - Q_{exh} \qquad (4.13)$$

Q_f - Fuel power input [kJ/s];

Q_b - Brake power [kJ/s];

Q_{exh} - Exhaust gas energy [kJ/s];

Q_{rad} - Radiation loss of energy [kJ/s];

Q_{cool} - Cooling energy loss [kJ/s];

Q_m - Mechanical energy at the engine shaft [kJ/s];

NCV - Net calorific value of the fuel [kJ/kg];

C - Specific fuel consumption [g/kWh];

$\dot{m}_f$ - Mass flow rate of fuel [kg/s];

$\dot{m}_{exh}$ - Mass flow rate of gases [kg/s];

$\dot{m}_{air}$ - Mass flow rate of air [kg/s];

C_p - Specific calorific value of the gases [kJ/kg K];

ω - Angular speed [rad/s] and

T - Engine torque [Nm];

4.8.1 Comparison of thermal efficiencies

In order to minimise the differences in terms of mechanical losses friction and hysteresis, which are dependent upon the engine speed, the engine was operated at a constant speed of 2200 RPM for the energy balance comparison. Table 4.6 summarises the results of the tests for thermal efficiency calculation.

Table 4.6: Comparison of engine energy balance and thermal efficiency at the maximum reached power at a speed of 2200 RPM.

LOSSES	Diesel DI (Diesel oil)	HCCI (H_2)	DIH_2 (H_2)
Shaft [%]	27.9	48.0	42.8
Cooling [%]	42.2	20.4	17.3
Exhaust [%]	35.3	31.6	39.9
Shaft Power [W]	9000	7076	10280

The highest thermal efficiency was observed for the hydrogen fuelled HCCI mode, followed by the DIH_2 mode. It can be seen that the cooling losses are significantly lower for DIH_2 operation compared with Diesel DI, leading to a large efficiency advantage. For the HCCI mode of operation, the efficiency is higher than in direct injection mode, but the power is considerably less than the other modes of operation, at just above 7 kW.

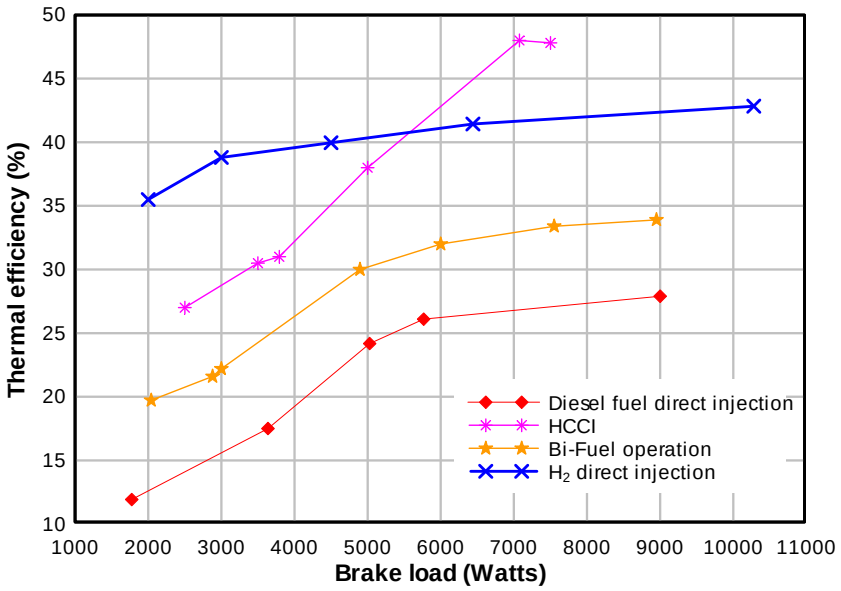

Figure 4.29: Comparison of brake thermal efficiencies of the test engine for four operating modes tested.

Figure 4.29 presents the measured thermal efficiency over the full load range for the four operating modes tested: Diesel DI, DIH_2, HCCI H_2 and dual fuel Diesel & H_2. It can be seen that DIH_2 mode of operation develops the highest power and a higher thermal efficiency throughout through the load range, despite the HCCI engine thermal efficiency is higher for its maximum rated power, it drops for lower loads. The maximum load achieved under HCCI mode is lowest due to the displacement of intake air with hydrogen, which is consistent with the results presented by Rottengrubber et al. (2004). Figure 22 also refers Dual fuel operation providing an efficiency improvement compared with the standard Diesel DI mode, having the lowest fuel efficiency. Dual Fuel operation allow existing Diesel engines to be fuelled with important hydrogen quantities therefore being a transition technology for the expansion of hydrogen. As a result of the present research, the author converted two marine Diesel engines of 4 MW to be operated with heavy fuel oil as the ignition source of the cylinder charge, and a mixture of natural gas and hydrogen.

4.9 Uncertainty of measured variables

Prior to the engine testing, the uncertainty associated with the data to be collected during the experimental work was calculated, since this helps to gain confidence in the quality of the results and also an understanding of the deviation between simulated and experimental results. The understanding of the causes of deviations should be considered to determine which part of the error is due to the model inaccuracy, and what is due to uncertainty in the measured data.

Since any experimental result involves some level of uncertainty that may originate from a lack of accuracy in measurement equipment, transducer hysteresis, transducers thermal instability, resonance frequencies and approximations in data reduction relations, uncertainty analysis is a vital part of the experimental program and measurement system design. All these individual uncertainties eventually translate into an uncertainty in the final results (the so called propagation of uncertainty). Uncertainty is also important for the model validation, since must be taken into consideration during the evaluation of the differences of the simulated and measured results. For this reason, great care was taken during the experimental system design to choose appropriate transducers, checking if their characteristics were adequate to monitor the variables involved.

4.9.1 Quantification of uncertainty

Since no statistical analysis of a series of observations was made, according with the *Guide to the Expression of Uncertainty in Measurement Binp et al, 1995,* a type B evaluation of standard uncertainty was used.

Assuming that all the uncertainties have the same level of confidence of 95%, and that all the variables are independent of each other, then the overall uncertainty associated with the thermal efficiency calculation can be obtained from the following equation:

$$W_R = \sqrt{\sum_{i=1}^{n}\left(W_{Xi}\frac{\partial R}{\partial x_i}\right)^2} \qquad (4.14)$$

W_R represents the overall uncertainty;

X represents the independent variable in the thermal efficiency equation; and

W_{Xi} – represents the uncertainty in that variable alone.

4.9.2 Uncertainty in thermal efficiency

The determination of thermal efficiency is one of the key aims of this research work and therefore the uncertainty of its measurement is of great importance. Uncertainty is included in the calculation of thermal efficiency through three different sources: uncertainty in the power measurement, fuel flow rate, and hydrogen heating value.

The thermal efficiency or fuel conversion efficiency is defined as the ratio of the work done by the engine divided by the energy input:

$$\eta_{th} = \frac{work.done}{Energy.input} \tag{4.15}$$

Rewriting expression (4.15) in terms of the rate of work, or power, and the rate of energy input it becomes:

$$\eta_{th} = \frac{Power.Output}{Energy.input.rate} \tag{4.16}$$

The power output can be calculated as the product of the engine torque and speed, and the energy input rate by the fuel heating value multiplied by the flow rate.

4.9.3 Measurement of thermal efficiency

The measurement of thermal efficiency using a volumetric fuel flow meter relies on the following equation:

$$\eta_{th} = \frac{N\tau}{\rho_g V_g Q_r} \qquad (4.17)$$

N is engine speed [rad/s]; τ is torque [Nm]; ρ_g is the gas density [kg/m^3]; V_g is volumetric flow rate [m^3/s]; and Q_r is the heating value per mass of fuel [J/kg].

The calculation of the mass fuel flow rate using a volumetric flow device also requires the determination of the gas density. Gas density is not a parameter that can be measured directly and has to be inferred from other gas properties. The density of gas can be determined using the ideal gas law, as shown in Equation 4.18.

$$\rho = \frac{P}{\frac{R_U}{M_m}T} \qquad (4.18)$$

ρ is gas density [kg/m^3]; P is gas pressure [Pa]; T is gas temperature [K]; R_U is the universal gas constant [J/mol K]; and M_m is the molecular weight [kg].

Pressure and temperature can be measured directly. Molecular weight must be known or can be calculated in the case of a mixture of gases with the use of gas chromatography.

Although using the ideal gas law provides a convenient method to calculate the gas density, it is only an idealization of the gas behaviour. Real gas behaviour approximates an ideal gas only at relatively low pressures and high temperatures. At other conditions, the density of the gas deviates from the ideal. To correct this, the concept of a compressibility factor, *Z*, is introduced, as shown in Equation 4.19, and is used to adjust the ideal gas law to fit actual gas behaviour.

$$\rho = \frac{P}{ZRT} = \frac{P}{Z\frac{R_U}{M_m}T} \tag{4.19}$$

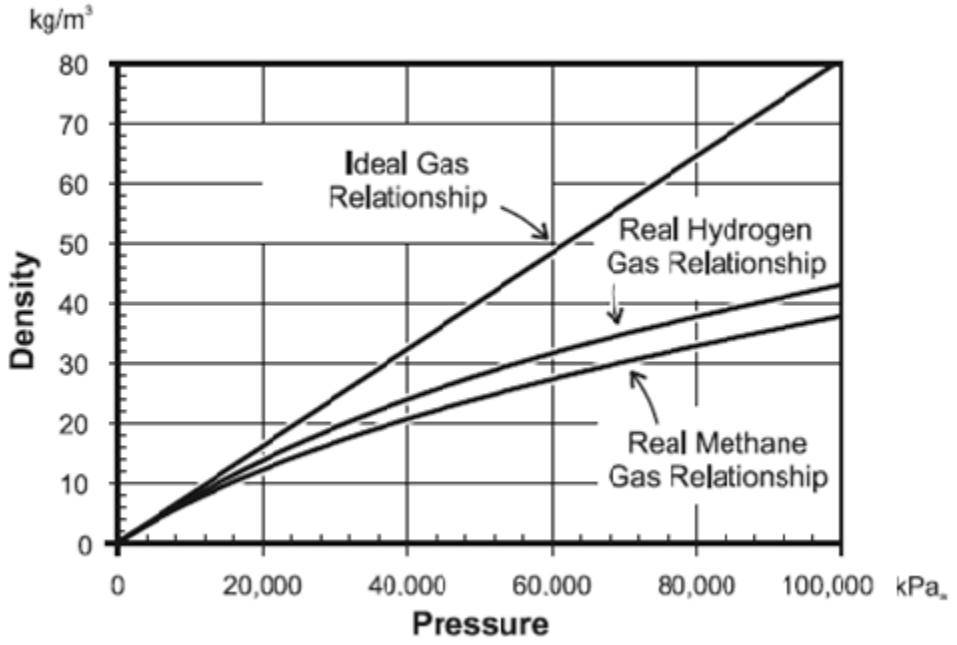

Figure 4.30: Hydrogen and methane density as a function of pressure @ 300K (Source:www.eere.energy.gov)

As can be seen in Figure 4.30, hydrogen density deviates from the ideal gas relationship substantially for pressures above 15,000 kPa.

4.9.4 Uncertainty in engine power calculation

The calculation of power is usually dependent on two measurements: speed and torque. The measurement of speed is most likely the least uncertain of all the measurements made on the engine. Speed is typically measured digitally, through one or two encoders fitted on the engine camshaft and crankshaft. The test engine had one encoder fitted at the rear end of the camshaft with a resolution of 10 Bit and uncertainty equal to ±1/2LSB.
Torque measurement was made trough the use of the developed hydraulic pressure, generated by a hydraulic pump with fixed displacement. The

hydraulic pressure was continuously measured and multiplied by the volumetric pump efficiency and hydraulic pump flow, which is a function of pump speed, resulting therefore into shaft power:

$$P = N_H \times v_H \times \eta_H \,, \quad (4.20)$$

N_H is pump speed [rev/s]; v_H is the unitary volume of the pump [3.6 cm^3/rev]; and η_H is the volumetric efficiency of the pump.

The hydraulic pump efficiency as a function of load was included into the online data acquisition and analysis software, thereby accounting for all the pump inefficiencies as a function of load.

4.9.5 Uncertainty in fuel mass flow rate

The measurement of fuel flow rate is required to calculate thermal efficiency, and the specific calculation method used depends on what method is used to measure fuel flow rate, i.e. what type of flow meter is used. The hydrogen mass flow rate was measured using a Dwyer GFM-1107 mass flow meter with totalizer, shown in Figure 4.31. It is based on a straight tube sensor with a restrictor flow element to provide high accuracy (+/-1.5% of full scale) and repeatability (+/- 0.5% of full scale).
The principle of operation of the transducer is based on dividing the flow by shunting a small portion of the flow through a capillary stainless steel sensor tube. The remainder of the gas flows through the primary flow conduit. The geometry of the primary conduit and the sensor tube are designed to ensure laminar flow in each branch. According to principles of fluid dynamics the flow rates of a gas in the two laminar flow conduits are proportional to one another.

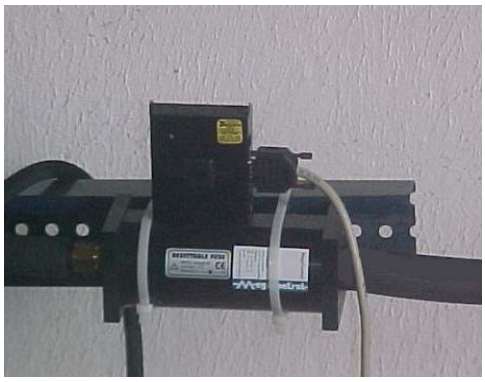

Figure 4.31: Hydrogen flow meter.

Therefore, the flow rates measured in the sensor tube are directly proportional to the total flow through the transducer. In order to sense the flow tube, heat flux is introduced at two sections of the sensing tube by means of precision wound heating coils. Heat is transferred through the thin wall of the sensor tube to the gas flowing inside. As gas flow takes place, heat is carried by the gas stream from the upstream coil to the down stream coil windings. The resultant temperature dependent resistance differential is detected by a Wheatstone bridge and amplified. The measured gradient at the sensor windings is linearly proportional to the instantaneous rate of flow taking place. An output signal is generated that is a function of the amount of heat carried by the gases to indicate mass molecular based flow rates.

The volumetric flow must be converted to a mass flow rate. A great deal of uncertainty can enter into the calculation of mass flow rate due to the compound measurements required to calculate the gas density. Pressure and temperature measurements are needed and taken into account by the flow meter, also needed is the knowledge of the hydrogen molecular weight, and lower calorific value.

4.9.6 Uncertainty in the volumetric flow measurement

The thermal efficiency equation for use with a volumetric flow meter was developed previously. It is shown here explicitly as a function of measurable variables:

$$\eta_{th} = \frac{NV_H \eta_H \rho_H}{\rho_g V_g Q_r} \qquad (4.21)$$

Taking partial derivatives of the above expression and substituting their values for a particular test condition and their individual uncertainties (Kubesh et al., 2002; Wheeler et al., 1996) the calculated uncertainty associated with the thermal efficiency is calculated by:

$$\left(\frac{\partial \eta_{th}}{\partial V_H}\right) = N_H \rho_H p_H \rho_g^{-1} V_g^{-1} Q_r^{-1} \qquad (4.22)$$

$$\left(\frac{\partial \eta_{th}}{\partial V_N}\right) = V_H \rho_H p_H \rho_g^{-1} V_g^{-1} Q_r^{-1} \qquad (4.23)$$

$$\left(\frac{\partial \eta_{th}}{\partial \eta_H}\right) = V_H N_H p_H \rho_g^{-1} V_g^{-1} Q_r^{-1} \qquad (4.24)$$

$$\left(\frac{\partial \eta_{th}}{\partial p_H}\right) = V_H \rho_H N_H \rho_g^{-1} V_g^{-1} Q_r^{-1} \qquad (4.25)$$

$$\left(\frac{\partial \eta_{th}}{\partial \rho_g}\right) = V_H \eta_H p_H N_H \rho_g^{-2} V_g^{-1} Q_r^{-1} \qquad (4.26)$$

$$\left(\frac{\partial \eta_{th}}{\partial V_g}\right) = V_H \eta_H p_H N_H \rho_g^{-2} V_g^{-1} Q_r^{-1} \qquad (4.27)$$

$$\left(\frac{\partial \eta_{th}}{\partial Q_r}\right) = V_H \eta_H p_H N_H \rho_g^{-2} V_g^{-1} Q_r^{-1} \qquad (4.28)$$

and

$$W_R = \left[\left(\frac{\partial \eta_{th}}{\partial V_H} \times W_{VH} \right)^2 + \left(\frac{\partial \eta_{th}}{\partial N} \times W_N \right)^2 + \left(\frac{\partial \eta_{th}}{\partial \eta_H} \times W_{\eta H} \right)^2 + \left(\frac{\partial \eta_{th}}{\partial p_H} \times W_{pH} \right)^2 + \left(\frac{\partial \eta_{th}}{\partial \rho_g} \times W_{\rho H} \right)^2 + \left(\frac{\partial \eta_{th}}{\partial V_g} \times W_{Vg} \right)^2 + \left(\frac{\partial \eta_{th}}{\partial Q_r} \times W_{Q_r} \right)^2 \right]^{\frac{1}{2}} \quad (4.29)$$

It results from the above calculations that the uncertainty associated with the engine thermal efficiency is 0.0065, summarised in Table 4.7 for the test conditions registered during the experiments. Therefore, the thermal efficiency values calculated from the experimental results have an uncertainty of ± 0.65%.

Table 4.7: Units and values used for the determination of uncertainties.

Parameter	Symbol	Units	*Values*
Engine / pump speed	N	rev/s	*36.666*
Brake oil pressure	P_h	Pa	*$12x10^6$*
Pump volumetric efficiency	η_h	-	*0.98*
H_2 flow rate	V_s	m^3/sec	-
Pump unit displacement	V_H	cm^3/rev	*3.6*
H_2 density (NPT)	ρ_g	Kg/Nm^3	*0.08988*
Oil temperature	T_h	K	*298*

The value of ±0.65 % represents a relatively low level of uncertainty, especially when compared with the values stipulated by the standard ISO 15000, that sets a maximum value of 2 % uncertainty for brake torque, 2 % uncertainty for speed and 3 % for specific fuel consumption.

A closer inspection of the uncertainty composition reveals that the individual uncertainty of the hydrogen flow meter (±1.5 %), and the hydraulic pressure transmitter (±1.0 %) are the main contributors for this result.

The hydrogen temperature and pressure uncertainties were considered and combined in the hydrogen flow meter uncertainty calculation. If the

hydrogen flow meter measured mass flow instead of volumetric flow, the result could be improved, since no conversion calculations would be necessary.

4.9.7 Uncertainty associated with other measurements

The pressure transducer used for the cylinder pressure measurement was a fibre optic based transducer as described in Chapter 3, with a useful frequency response range of 0.1 to 25Hz and a maximum housing temperature of 300ºC, which corresponds an uncertainty of ±1.0% FS under combustion conditions. Therefore the pressure measurements uncertainty would be ±3.0 kPa.

Table 4.8: Summary of uncertainties associated with the transducers.

Hydrogen Flow meter	± 1.5%
Hydraulic pressure transmitter	± 1.0%
Cylinder pressure transducer	± 1.0%
Speed sensing system	10Bit ± ½ LSB
Exhaust gas temperature	± 1.0%
Diesel oil flow meter	± 1.5%

4.10 Conclusion

Within the scope of this research project, it was successfully proven that combustion of the hydrogen in a compression ignition engine is possible by using any of the three modes (HCCI, DIH_2 and Dual-fuel). In addition, the concept of converting a commercial high speed diesel engine to hydrogen operation was developed and the tests were conducted on the designed test bench, operating safely and in acceptable running behaviour.

By means of parameter variations, the influences of the various engine operating parameters on thermal efficiency, pollutant emissions, and

combustion development were studied. The high power, lower emissions potentials of CI hydrogen fuelled engines was proven.

This chapter also presented the methodology of the data treatment as well as the data derived from engine tests carried out to characterise each mode of operation in reference to the diesel fuelled engine.

The performed Dual-fuel operation tests showed a clear efficiency advantage over the diesel oil operation, with brake fuel efficiency improvements of up to 5 percentage points. Nitrogen oxides emissions were comparable to those under normal diesel operation however the emissions of particulate matter dropped significantly even for small amounts of hydrogen fuel inducted in the intake air.

The results confirm that dual fuel engines have a significant potential to improve internal combustion engine performance and reduce exhaust gas emissions formation. More detailed studies of the mechanisms governing the in-cylinder processes in dual fuel engines are therefore worthwhile in order to optimise the design of such engines. Similarly, the use of alternative fuels, such as bio-oils with poor combustion characteristics, should be studied to identify potential performance advantages realisable with hydrogen injection.

Higher flow rates of hydrogen can be achieved, but a control of the Diesel fuel must be implemented, in such way that the increase of hydrogen flow rate, will lead to a proportional decrease of the Diesel flow rate, controlling in this way the amount of energy per cycle. This type of control is achieved by introducing a transfer function, which above 50% hydrogen energy per cycle becomes the governing fuel, this implies a transfer of the PID function, from the diesel governor to the hydrogen governor.

It was found that for HCCI as well as for DIH_2 modes of operation the effect of the temperature of the air entering the engine cylinder has a major impact in the control of the rate of cylinder pressure rise and this on the mechanical bearing loads. It was further found that at higher loads the controllability of the engine is improved but that the rate of pressure rise can be high.

From the energy balances carried to characterise each mode of operation of the engine it is noticeable that the HCCI mode is characterised by a high efficiency, but the power is limited by the amount of hydrogen the cylinder volume can receive. By comparing the losses of heat between the various modes of operation at the same speed, it was concluded that exhaust losses are less predominant on the HCCI mode than on Diesel or DIH_2 , this fact can be due to a lower heat input per cycle, and therefore to the lower temperatures reached at the HCCI exhaust. However DIH_2 operation is characterised by lower cooling losses as the combustion takes place closest the TDC than the other modes of operation tested. This comparison of heat losses, can be criticised as the power conditions was not equal for all the tested modes, and the HCCI mode operation was not optimised in terms of control The HCCI mode is characterised by an unstable ignition angle that calls for extensive research to keep it inside acceptable angle variations not endangering the engine controllability. It can be concluded that the higher the air temperature at the cylinder inlet, the sooner can be the ignition of the cylinder charge, therefore contributing for lower engine efficiency in case of a too early ignition. The direct injection of hydrogen using high injection pressure allows the control of the ignition angle and if optimised, can lead to very high thermal efficiencies and high engine controllability. It was found also that most of that intake air temperature has a greater effect of the final end of compression temperature that the engine compression ratio, therefore the use of methodologies for controlling the cylinder charge at the beginning of compression are very important. Also it was concluded that cyclic variation are better controlled when the inlet air temperature is above 70ºC, which necessarily has a negative effect on the NO_x formation. Also it was realised that the increase in the average mass temperature at the time of the start of injection causes a reduction of the ignition delay, and an increase in the speed of the combustion process of the injected fuel, resulting in heat release rates of the consecutive operating cycles more even. However, a decrease in the ignition delay results in higher peak pressures, and therefore in higher mechanical loads on the bearings. The operation of the engine in a Dual-

fuel mode, allows the immediate use of hydrogen with important economic and environment benefits due to the improved exhaust emissions. Hydrogen can be seen as an energy carrier, which can be produced from renewable or waste based energy and therefore used as fuel into existing diesel engines without major modifications of the engine. The controllability of the dual fuel mode operated engine is satisfactory for hydrogen percentages of 50% of the energy per cycle. Above that value, a transfer function of the engine governing actions (PID) needs to be implemented.

Chapter 5

Modelling and simulation

« Curiosity has its own reason for existing! »

Albert Einstein

This chapter presents of the models used for simulation of the HCCI and DIH_2 hydrogen operated engine, as well as the injector's dynamic simulation model used during this research work. A full-cycle simulation model was developed to investigate the performance of the HCCI and DIH_2 engine cycles, but also to serve as a tool for the initial set up of the various test engine runs and finally to develop practical improvements and recommendations for future work. The model flexibility allowed the observation of parameters that are experimentally difficult or expensive to monitor.

The simulation model allowed the study of the interactions between various operational variables. The model was kept relatively simple as the increase in accuracy would require more detailed sub models without major benefits to the objective of this research work. As a result, the present simulation model was not developed for in-cycle crankshaft angular speed variation prediction, since engine and hydraulic brake pump inertia terms where not considered. The simulation program has a resolution of 0.5 degree of crank angle.

5.1 Modelling of hydrogen HCCI and DIH_2 engines

The modelling of compression ignition engines has been investigated and developed extensively for decades, with varying levels of accuracy, depending on the modelling objectives ranging from engine dynamics, combustion development to emissions prediction.

The approach followed to model the HCCI and DIH_2 engine cycle was initially to use a standard air cycle for compression ignition engines. Then a

number of improvements around this formulation were implemented to bring the model closer to the CI engine operation and to HCCI and DIH_2 respectively.

The mathematical model was programmed using the numerical computation tool box Matlab, which allowed the use of specialised algorithms for solving the model ordinary differential equations, and also the construction of a unique and friendly graphic interface.

The following sections describe the details of the simulation model.

5.1.1 Modelling objectives

Engine modelling and simulation was used to reproduce engine operation and predict its performance. The development of the model was made based on the actual test engine main characteristics, i.e. bore, stroke, connecting rod length, piston offset, speed, maximum combustion pressure, compression pressure, compression ratio, valve angles, valve dimensions, air inlet temperature, exhaust gas temperatures, specific fuel consumption, etc.

The objective was to develop a simulation model as close to the actual test engine as appropriate for the research study. Therefore, the simulation of the thermodynamic cycle to correlate important cycle events with the piston position and to determine the engine cycle process parameters was pursued. The model should also allow the investigation of possible improvements and solutions for problems specific to the CI engine operated with hydrogen.

Secondary objectives implemented included data output capability in an appropriate format to allow detailed analyses and production of high-quality graphics. Data logging with a resolution of at least 1° crank angle was implemented, matching the data acquisition installed on the engine, and a comprehensive user-friendly human interface was produced.

5.1.2 HCCI and DIH_2 engine model differences

The differences between HCCI and DIH_2 engine operation necessarily affect the engine model, however the two modes of operation have in common the fact that ignition of the cylinder charge occurs due to the high temperature reached during the compression stroke. The HCCI cycle power output is limited by the amount of hydrogen that forms the cylinder charge, because of its high stoichiometric volume at the cylinder charge pressure and the displacement of intake air. The DIH_2 cycle has a much higher limit concerning the amount of hydrogen per cylinder charge; in practice physical component constraints limit the amount of hydrogen that can be injected in each cycle.

In the HCCI mode of operation, the cylinder charge can be considered a homogeneous mixture of hydrogen and air. In contrast, the cylinder charge of a DIH_2 hydrogen engine is a stratified charge (despite the hydrogen diffusion characteristics), where air is compressed during the main part of the compression stroke, the hydrogen being injected only when the self ignition temperature has been achieved and determined by the engine crank angle.

The cylinder charge ignition in the HCCI engine takes place somewhat erratically, depending very much on the heat transfer characteristics of the cylinder to the cylinder charge, ambient air temperature, charge conditions, etc. The simulation model included a heat loss calculation from the combustion chamber components, cylinder head and liner to try and predict this behaviour.

The turbulence of the in-cylinder air and fuel charge is an important factor in conventionally fuelled engines, however this was not modelled, as for HCCI the cylinder charge is considered homogeneous and for DIH_2 the high diffusion and short quenching distance of hydrogen would produce a close to homogeneous cylinder charge within a very short time period. With DIH_2 engine operation, combustion coincides with the precise timing of hydrogen injection as no fuel vaporization or preparation timing phases are required

for modelling ignition of hydrogen. However, combustion chamber heat losses are not so critical in determining the fuel ignition as for the HCCI mode of operation.

For HCCI engine operation the cylinder hydrogen charge is introduced at low pressure through inlet port injection, typically below 6 bar, and air and hydrogen are then compressed until the ignition temperature is reached. A modified polytropic compression exponent was determined and used for the working fluid since this is a hydrogen and air mixture which is compressed. For DIH_2 operation, hydrogen at 90 bar is injected near the top dead centre, into a compressed hot air atmosphere.

5.2 Simulation program description

In the following section the simulation program structure is presented. The decomposition of the simulation program according to various levels of detail shows the interaction between various program blocks and the overall program structure.

5.2.1 High level program structure

Figure 5.1 shows the high level structure of the simulation program which is described in the next paragraphs. The inputs of the simulation program can be grouped into, engine parameters, engine ambient conditions and model parameters. As a result of the resolution and number of iterations, the thermodynamic cycle is calculated and the results are displayed graphically and numerically. Using the implemented cursor facility it is possible to analytically analyse details of the graphic outputs.

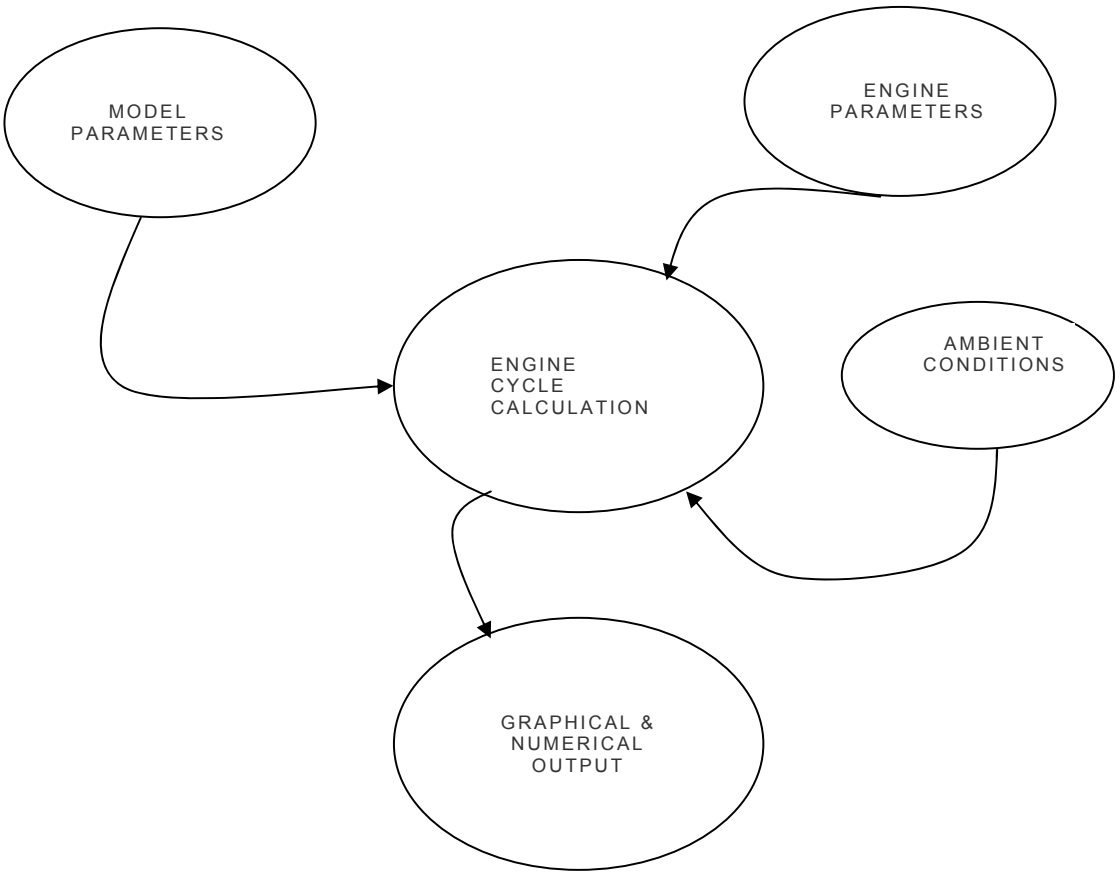

Figure 5.1: Simulation model structure.

5.2.2 Model parameters

Constant model parameters that are required, such as polynomials coefficients, constants and tables, are grouped together in the program and allow the initiation of the iterative engine simulation.

5.2.3 Engine parameters

These parameters define the engine geometry and include the following: stroke, connecting rod length, piston offset, piston cylinder head ratio, piston crown area, bore, compression ratio, clearance volume, exhaust valve maximum diameter, exhaust valve minimum diameter, inlet valve dwell angle, exhaust valve dwell angle, inlet valve opening angle, inlet valve closing angle, exhaust valve opening angle, exhaust valve closing angle, and engine speed. These parameters also include the start of injection and duration of injection for DIH_2 operation, as well as pulsed injection frequency and duty cycle for the pulsed injection.

5.2.4 Ambient conditions

These parameters define the ambient conditions of the simulation run, including: atmospheric pressure and temperature, exhaust back pressure, fuel net calorific value, fuel specific gravity, specific fuel consumption, and ignition delay.

5.3 Engine cycle calculation

This part of the simulation performs the calculation of the thermodynamic cycle using the model and engine parameters at the ambient conditions. The engine cycle calculation model can be decomposed into the following structure, as shown in Figure 5.2.

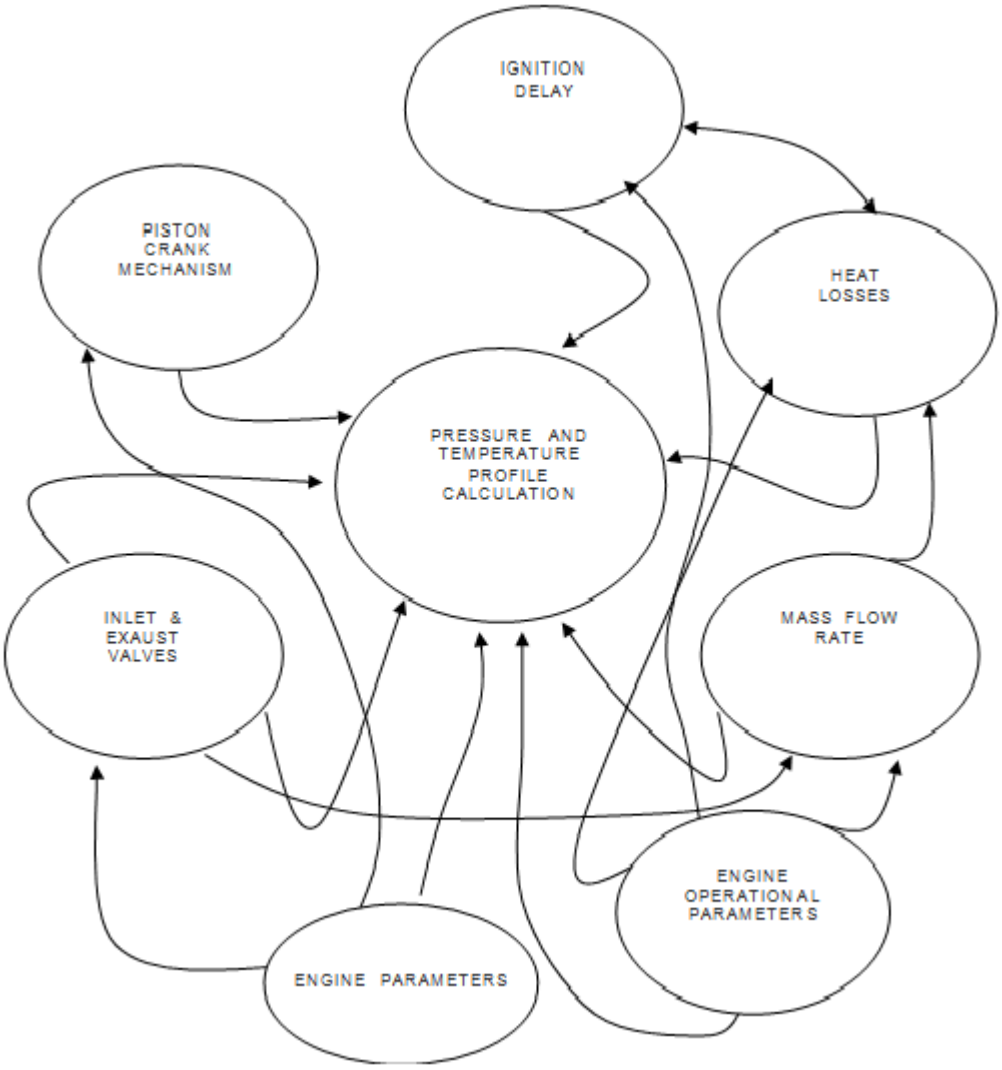

Figure 5.2: Engine cycle model structure.

5.3.1 Piston crank mechanism

For the thermodynamic simulation of the engine cycle it is vital to know the precise cylinder volume at any crankshaft angular position.

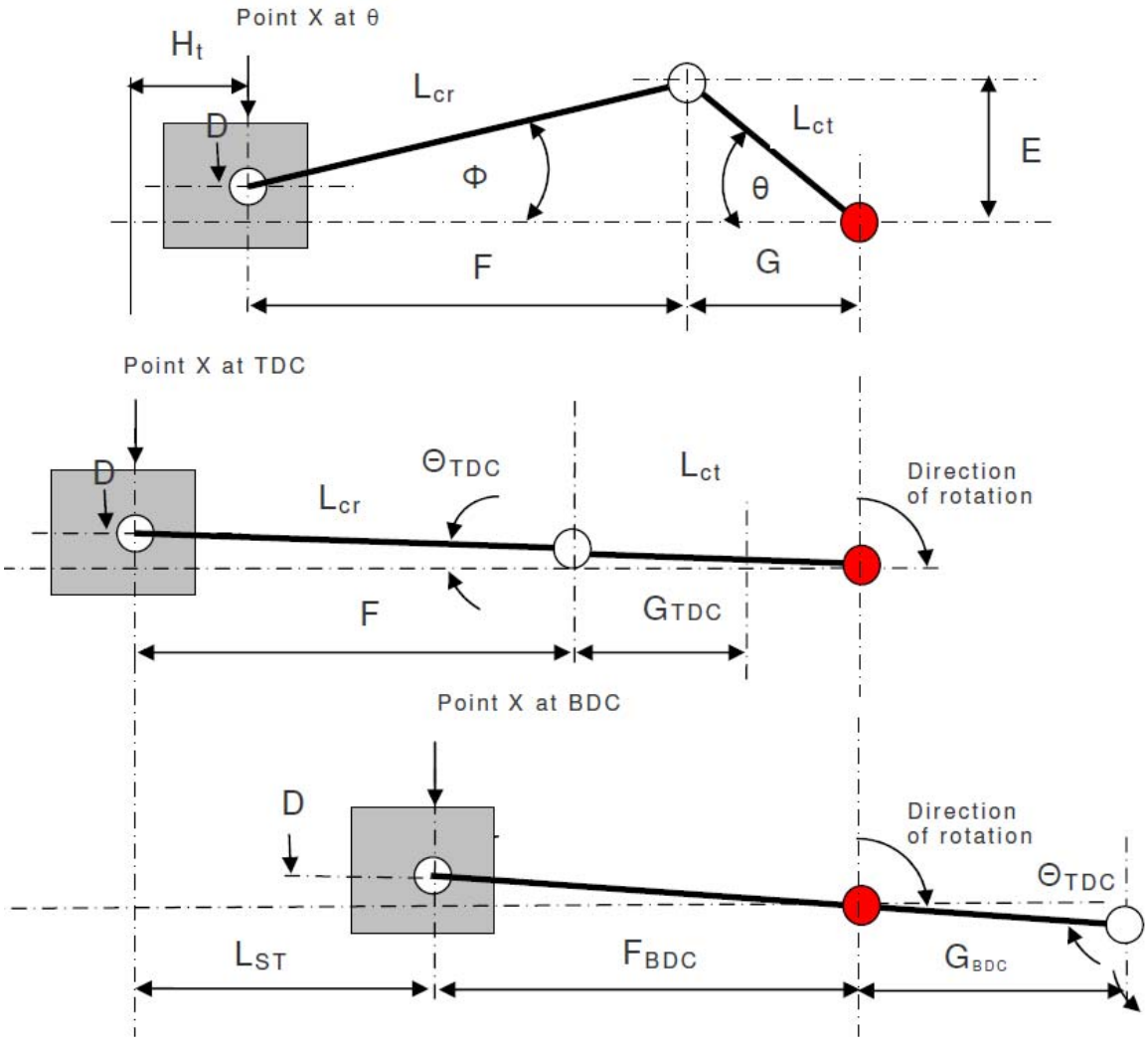

Figure 5.3: is a representation of the piston crank mechanism.

Figure 5.3 is a representation of the piston crank mechanism and the variables shown are:

L_{cr} is the connecting rod with a length (m);F is the projected length of the connecting rod (m); Lct is the length of the crank (m); G is the crank

projected length over the piston axis (m); E is the crank projected length over a perpendicular to the piston axis direction (m); θ is the crank angle referred to TDC (rad); ϕ is the angle defined between the connecting rod and the piston axis (rad); D, P and Q define the position of the connecting rod pin centre; L_{st} is the stroke length (m).

At any given crankshaft angle, θ, after the TDC position of the crank, the connecting rod centre line assumes an angle ϕ, to the centre line. This angle is designated as the "angle of obliquity" of the connecting rod. The bearing location where the connecting rod attaches to the piston is denominated the "small end" and may be offset by an amount D to the cylinder centre line. The offset is positive if that offset is positive toward the direction of the crank rotation, as in Figure 5.3. The direct implication of the offset is that when the crank is at the top dead centre, the piston will be not at its top dead centre, in this case the piston TDC and BDT will occur at crank angles respectively θ_{tdc} , and θ_{bdc}. Using the nomenclature and Figure 5.3, it is possible to derive the piston position as a function of the crank angle θ. With the piston at TDC:

$$F_{tdc} + G_{tdc} = \sqrt{(L_{cr} + L_{ct})^2 - D^2} \ , \tag{5.1}$$

$$\theta_{tdc} = \tan^{-1}\left(\frac{D}{F_{tdc} + G_{tdc}}\right), \tag{5.2}$$

and

$$G_{tdc} = L_{ct}\cos\theta_{tdc} \ . \tag{5.3}$$

Therefore

$$F_{tdc} = -L_{ct}\cos\theta_{tdc} + \sqrt{(L_{cr} + L_{ct})^2 - D^2} \ . \tag{5.4}$$

With the piston at BDC:

$$F_{bdc} = \sqrt{(L_{cr} - L_{ct})^2 - D^2} \ , \tag{5.5}$$

$$\theta_{bdc} = \tan^{-1}(\frac{D}{F_{bdc}}), \quad (5.6)$$

and $$G_{bdc} = L_{ct}\cos\theta_{bdc} \ . \quad (5.7)$$

The stroke of the piston from TDC to BDC is then given by

$$L_{st} = F_{tdc} + G_{tdc} - F_{bdc} \ . \quad (5.8)$$

If the gudgeon pin offset and/or cylinder axis offset is zero, i.e., if D is zero, then:

$\theta_{tdc} = 0$
$\theta_{bdc} = 0$
$F_{tdc} = L_{cr} + L_{ct}$
$G_{tdc} = L_{ct}$
$F_{bdc} = L_{cr} - L_{ct}$

And the length of the stroke becomes:

$$L_{st} = F_{tdc} + G_{tdc} - F_{bdc} = L_{cr} + L_{ct} - (L_{cr} - L_{ct}) = 2L_{ct} \quad (5.9)$$

Considering a position within the cylinder of any point on a piston with respect to its motion from its TDC position to a point where the crank has turned through an angle θ from the TDC angular position of the crank. If for convenience such a position is marked as X and is located at the small end bearing centre and its location down the cylinder from its TDC position is H_t as illustrated in the upper sketch of Figure 5.3, the length H_t is:

$$H_t = (F_{tdc} + G_{tdc}) - (F + G), \quad (5.10)$$

$$E = L_{ct}\sin\theta \ , \quad (5.11)$$

$$G = L_{ct}\cos\theta \ , \quad (5.12)$$

and

$$F = \sqrt{L_{cr}^2 - (E - D)^2} \ . \quad (5.13)$$

Therefore,

$$H_t = \sqrt{(L_{cr} + L_{ct})^2 - D^2} - \sqrt{L_{cr}^2 - (L_{ct}\sin\theta - D)^2} - L_{ct}\cos\theta \,, \qquad (5.14)$$

and the angle of obliquity of the connecting rod is given by:

$$\Phi = \tan^{-1}\left(\left(\frac{E - D}{F}\right)\right) = \tan^{-1}\left[\left(\left(\frac{L_{cr}}{L_{ct}\sin\theta - D}\right)\right) - 1\right]^{\frac{1}{2}} \qquad (5.15)$$

5.3.2 Heat losses

The derivation of a global heat transfer coefficient has been researched extensively, but without consensus on the most adequate methodology. A widely used methodology recommended by Blair (1999), which is based on Annand´s work, Annand et al. (1963) was implemented in the simulation model.

The heat losses from an engine combustion chamber are illustrated in Figure 5.4.

Annand et al. (1963) developed one of the most widely used and accurate methods for deriving the heat transfer in spark ignition engines while Eichelberg, Woschni and others developed models for the calculation of cylinder heat transfer of diesel engines.

The method implemented in this research is based on Annand´s methodology as hydrogen combustion using homogeneous charge compression ignition and direct injection is closer to constant volume combustion than to constant pressure and volume combustion.

This approach separates out the convection and radiation terms, and this distinguishes it from the heat transfer theories of the other researchers. The expression of the Nusselt number, Nu, leads to a conventional derivation for the convection heat transfer coefficient, C_h.

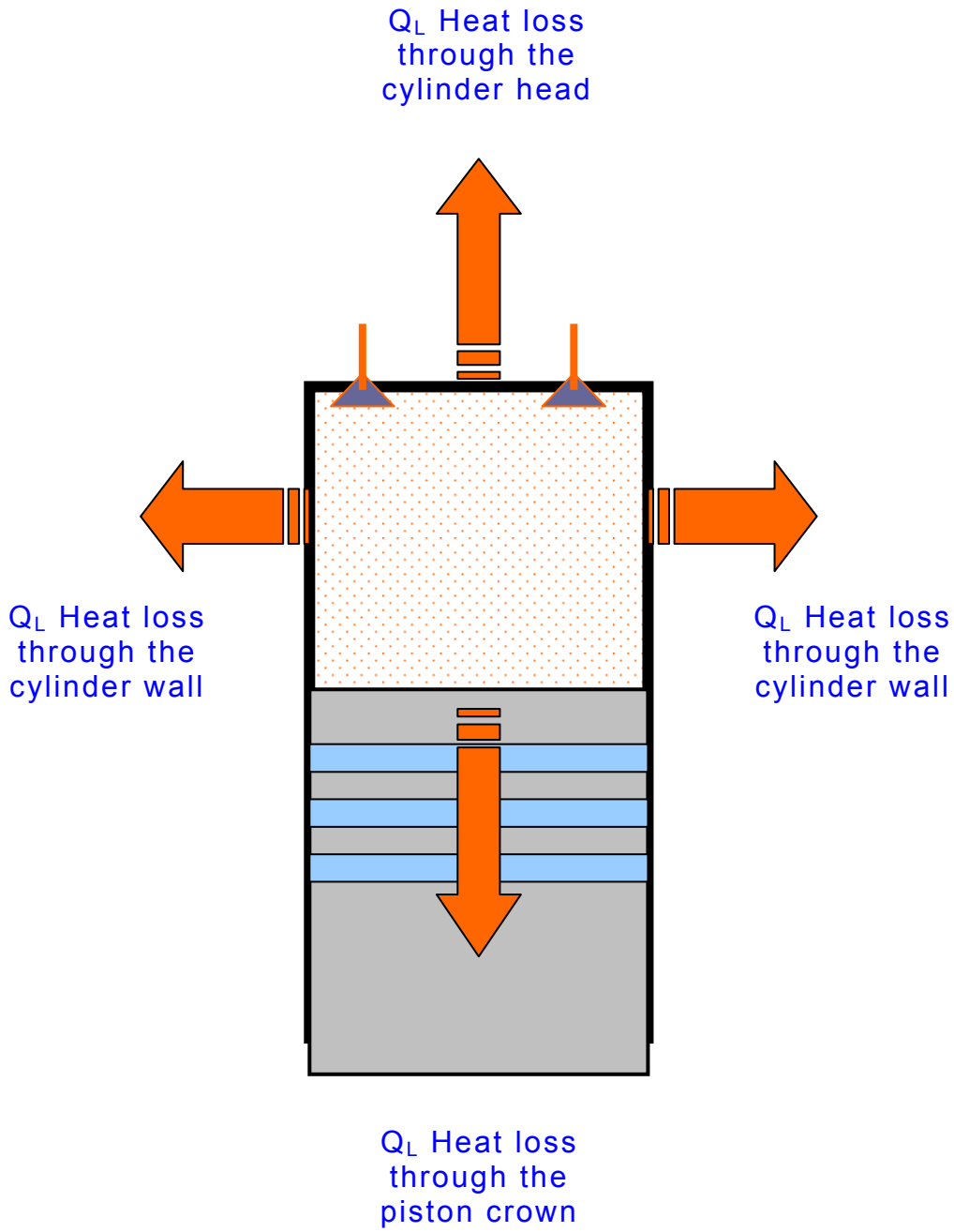

Figure 5.4: Engine cylinder heat losses.

Annand recommends the following relationship between the Reynolds and Nusselt numbers for a four stroke engine:

$$N_u = a\,\mathrm{Re}^{0.7} \quad , \tag{5.16}$$

the constant a has a value of 0.46. The Reynolds number is calculated by:

$$\mathrm{Re} = \frac{\rho_{cy} C_p d_{cy}}{\mu_{cy}} \quad , \tag{5.17}$$

The working fluid density is derived from the prevailing cylinder pressure, temperature and gas properties using Equation 5.18.

$$\rho_{cy} = \frac{p_{cy}}{R_{cy} T_{cy}} , \tag{5.18}$$

p_{cy} is the typical cylinder pressure (Pa), and T_{cy} is the prevailing cylinder temperature (K).

During the compression stroke, the gases inside the cylinder will be a mixture of air and hydrogen if the engine is operated as a HCCI engine. For DIH_2 operation, the gases will mix only after the compression and injection have taken place. From the induction stroke to the exhaust of the gases, the gas constant varies, as do other gas properties. Therefore, tracking of the gas constant during the process is very important. The viscosity of the gases inside the cylinder with temperature and pressure, but according to research by Blair (1999), little accuracy is lost if the expression for the viscosity of air is used. A good approximation of μ of air can be expressed as:

$$\mu = 7.457 \times 10^{-6} + 4.1547 \times 10^{-8} T - 7.4793 \times 10^{-12} T^2 , \tag{5.19}$$

The mean piston velocity is a function of the piston stroke and the engine speed and is given by

$$C_p = \frac{2 L_{st} N}{60} , \tag{5.20}$$

L_{st} is piston stroke (m) and N is the engine speed (rpm).

Once the Reynolds number is calculated, the convection heat transfer coefficient, C_h, can be obtained from the Nusselt number as follows:

$$C_h = \frac{C_k Nu}{d}, \tag{5.21}$$

C_k is the thermal conductivity of the in-cylinder gas (W/m^{2}K) and T_{cy} is the instantaneous gas temperature (K).

The parameter C_k represents the thermal conductivity of the gas in the cylinder that can be assumed equal to that of air at instantaneous cylinder temperature (Blair, 1999) and it may be determined by:

$$C_k = 6.1944\times10^{-3} + 7.3814\times10^{-5} T - 1.2491\times10^{-8} T^2 \tag{5.22}$$

Annand also considers the radiation heat transfer coefficient, C_r, to be given by:

$$C_r = 4.25\times10^{-9} \times \frac{T_{cy}^4 - T_{cW}^4}{T_{cy} - T_{cw}}, \tag{5.23}$$

T_{cw} is the average cylinder wall temperature (K).

It should be noted that C_r is much smaller than C_h, which is why it is neglected by many researchers when a reasonable simplification is desired. This is particularly the case for this research since hydrogen flame radiation is extremely small due to the fact that hydrogen combustion do not produce radiating particulate matter normally originated by the combustion of hydrocarbon fuels. However due to the lubricating oil combustion some particulate may exist, although negligible without any impact on the simulation results.

The value of T_{cw} is the instantaneous average temperature of the cylinder wall, the piston crown and cylinder head surfaces. The infinitesimal heat transfer dQ_L during a crankshaft angle interval $d\theta$, corresponding to an interval dt can be calculated for the mean value of that transmitted to the total surface exposed area to the cylinder gases by

$$dQ_L = (C_h - C_r)(T_{cy} - T_{cw})A_{cw}dt\,, \tag{5.24}$$

$$dt = \frac{d\theta}{360} \times \frac{60}{N} \tag{5.25}$$

and the surface area of the cylinder, A_{cw} is the summation of the cylinder head, piston crown and cylinder liner areas.

It should be noted that the heat transfer coefficients increase dramatically when combustion is taking place, but that is when a minimum surface area is exposed, and as the combustion of hydrogen is extremely fast, the time of exposure of the combustion chamber surfaces to high temperatures is very short.

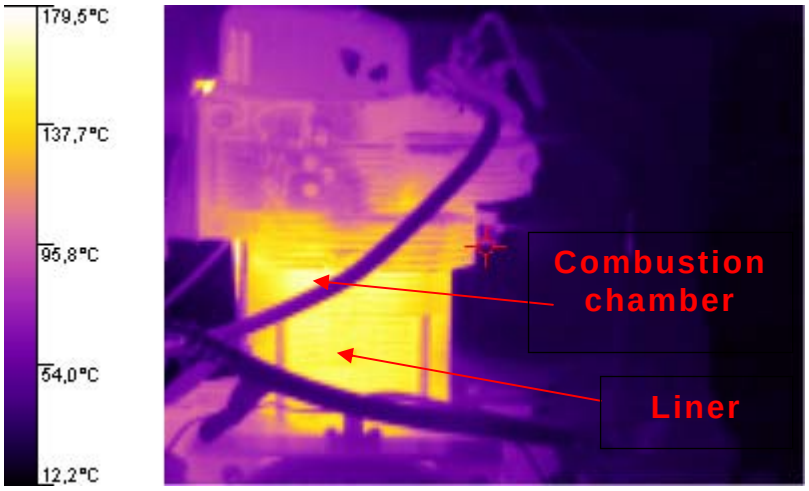

Figure 5.5: Engine cylinder head and liner thermal image.

Figure 5.5 shows the thermal image of the test engine cylinder and it is evident that there is a greater heat flux in way of the combustion chamber, and its distribution along the cylinder liner.

The average temperatures measured using the thermal imaging camera was used in the engine model, and the assumption was made that the piston crown temperature was the same as the combustion chamber temperatures. This assumption and the temperature measured were applied to HCCI and DIH_2 simulated modes of operation.

5.3.3 Cylinder valves modelling

To model a diesel engine it is essential to calculate the geometrical passage areas exposed by the valves at any crank angle. There are two aspects to this requirement. The first is the exposed area at any particular valve lift, and the second is the valve lift characteristic as a function of the crank angle.

A representation of the intake and exhaust valves and manifolds is shown in Figure 5.6.

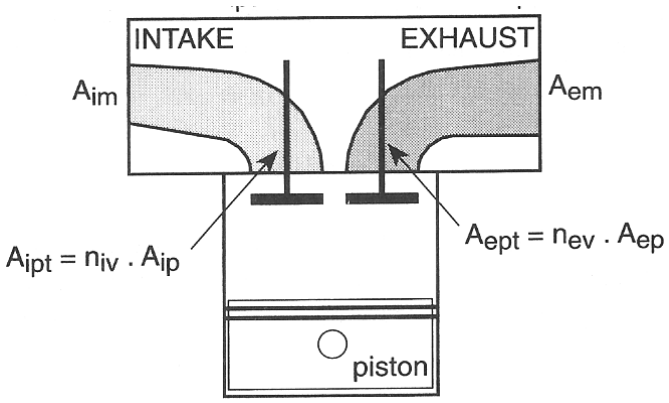

Figure 5.6: Valve apertures (Blair, 1999).

The intake and exhaust manifold areas are denoted by A_{im} and A_{em} respectively. The flow areas across the ports of the valves are A_{ip} and A_{ep} for an intake and exhaust valve, respectively. The total flow areas are

$$A_{ipt} = n_{iv} A_{ip}, \tag{5.26}$$

and

$$A_{ept} = n_{ev} A_{ip}, \tag{5.27}$$

n_{iv} and n_{ev} are the number of intake and exhaust valves respectively. Therefore, the intake manifold to valve area ratio can be defined as:

$$C_{im} = \frac{A_{im}}{n_{iv} \times A_{ip}} = \frac{A_{im}}{A_{ipt}}, \tag{5.28}$$

and exhaust manifold to valve area as:

$$C_{em} = \frac{A_{em}}{n_{ev} \times A_{ep}} = \frac{A_{em}}{A_{ept}} \quad . \tag{5.29}$$

These ratios are critical to the performance of an engine since they determine the amplitude of any pressure wave created in the ducting by the cylinder state conditions.

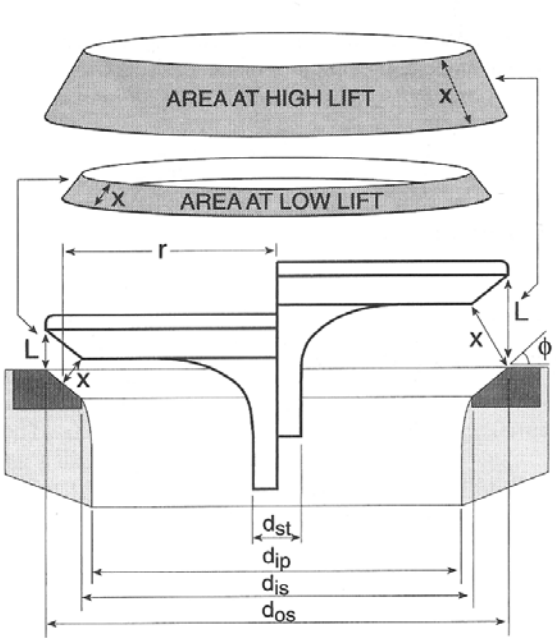

Figure 5.7: Valve geometry (Blair, 1999).

The inflow or outflow of any valve depends on the areas which correspond to the side areas of a frustum of a cone. Therefore, according to Figure 5.7, the controlling aperture areas for the exhaust and intake ports at the values are defined as follows:

$$A_{ept} = n_{ev} \frac{\pi}{4} (d^2_{ip} - d^2_{st}), \tag{5.30}$$

$$A_{ipt} = n_{ip} \frac{\pi}{4} (d^2{}_{ip} - d^2{}_{st}) \quad (5.31)$$

Poppet valve aperture geometry

Referring to Figure 5.8, the aperture geometry of the poppet valve is a function of the lift L, above the seat, and the angle ø, which is defined by the inner and outer diameters d_{is} and d_{os} respectively. Therefore, a manifold to valve curtain area, A_t, models the side surface area of a cylinder of diameter d_{is} and lift height L and is given by:

$$A_t = \pi \times d_{is} \times L \quad (5.32)$$

The area of passage is defined as the area of a frustum of a cone defined by the side length dimensions *x*, the valve seat angle ø, the inner and outer seat diameter d_{is} and d_{os}, and the radius r, all of which are dependent upon the value lift L.

The side surface of a frustum of a cone A_s, defines the maximum geometrical flow area and is given by:

$$A_s = \pi(\frac{d_{major} + d_{minor}}{2})x, \quad (5.33)$$

x, is the length of the sloping side and d_{major}, d_{minor} are the cone top and bottom diameters.

As can be seen in Figure 5.8, *x* has two distinct values dependent on valve position. When the valve lift is very small, *x* is no longer normal to the valve seat at angle ø. Therefore, minimum valve lift is given by:

$$L_{\lim} = \frac{d_{os} - d_{is}}{2\sin\phi\cos\phi} = \frac{d_{os} - d_{is}}{\sin 2\phi} \quad (5.34)$$

For the first stage of the poppet valve lift where $L \leq L_{\lim}$, the valve curtain area A_t is a function of *x* and *r* and can be calculated by:

$$X = L\cos\phi \quad , \tag{5.35}$$

$$r = \frac{d_{is}}{2} + x \cdot \sin\phi \text{ , and} \tag{5.36}$$

$$A_t = \pi \cdot L \cdot \cos\phi (d_{is} + L \cdot \sin\phi \cdot \cos\phi) \text{ .} \tag{5.37}$$

For the second stage of poppet valve lift where $L > L_{lim}$ the valve curtain area A_t is given by:

$$A_t = \pi(\frac{d_{os} + d_{is}}{2})\sqrt{(L - \frac{d_{os} - d_{is}}{2}\tan\phi)^2 + (\frac{d_{os} - d_{is}}{2})^2} \text{ .} \tag{5.38}$$

Since the valves of the test engine have a conventional seat angle of 45°, Equation (5.38) simplifies to

$$A_t = \pi(\frac{d_{os} - d_{is}}{2})\sqrt{(L - \frac{d_{os} - d_{is}}{2}) + (\frac{d_{os} - d_{is}}{2})^2} \text{ .} \tag{5.39}$$

In practice, for valve lift more than 40% of the inner valve seat diameter, resulting losses that are characterised by a discharge coefficient C_d. Therefore, the effective area of the valve throat restriction becomes A_{tc}, which is defined as follows:

For $A_t < A_p$:

$$A_{tc} = C_d \times A_t \quad , \tag{5.40}$$

and for $A_t \geq A_p$:

$$A_{te} = C_d \times A_p \quad , \tag{5.41}$$

A_t is valve throat area and A_p is valve minimum area (m^2).

Poppet valve lift

Valves cannot instantly lift or drop, therefore the valve commences its lift at a crank angle V_o and upon closing returns to zero lift at a crank angle V_c. To model the valve operation, the precise valve timing must be known to compute the valve aperture areas at any instant during crank shaft rotation.

The poppet valve lift can be described in five different phases, as shown in Figure 5.8.

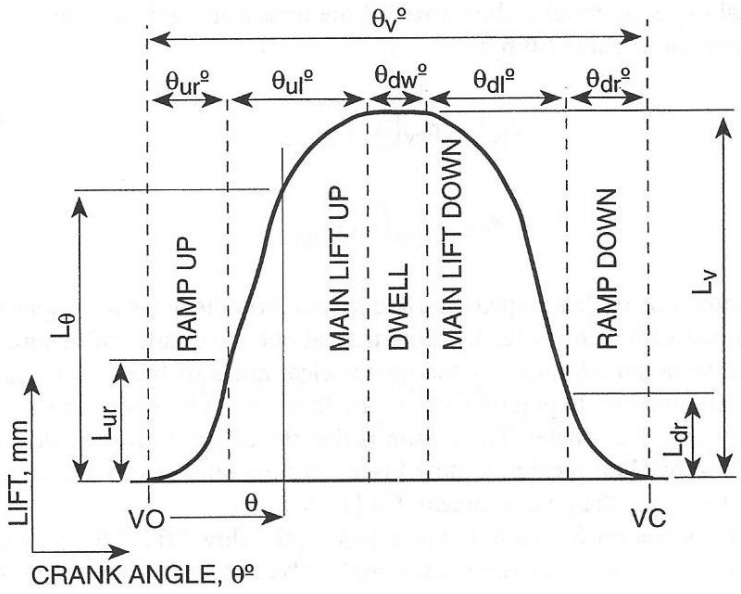

Figure 5.8: Valve lift characteristics as a function of crank angle (Blair, 1999).

The ramp up phase has a duration of $\theta°_{ur}$, with the valve lift going from 0 to L_{ur}. The main lift up phase is from the end of the ramp up to the beginning of the dwell period around the maximum lift point. This period is θ_{ur} and the valve lifts from L_{ur} to L_v. The dwell phase occurs around peak lift when the valve remains at L_v for a period θ_{dw}. The main lift down phase corresponds to the valve drop from the end of dwell phase to beginning of the final ramp down phase. It lasts for θ_{dw} degrees and the valve falls from the lift L_v to L_{dr}. The ramp down is the final phase and lasts for θ_{dr} with the lift decreasing from L_{dr} to zero.

It is quite usual for engines to have valve opening and closing ramps which are similar in crank angle duration and valve displacements L_{ur} and L_{dr}.

Acceleration characteristics of a poppet valve

Assuming that the movement of the valve at any point of its lift is given by dL, over an infinitesimal time interval dt, when the engine speed is N. Since the engine rotates dθ degrees during dt then

$$\frac{dt}{d\theta} = \frac{60/N}{360} = \frac{1}{6\mathrm{N}}. \tag{5.42}$$

Assuming that the valve lift is in mm, the valve velocity C_v is given by:

$$C_v = \frac{1}{1000} \times \frac{dL}{dt}. \tag{5.43}$$

therefore

$$C_v = \frac{1}{1000} \times \frac{dL}{d\theta} \times \frac{d\theta}{dt} \tag{5.44}$$

hence

$$C_v = \frac{6\mathrm{N}}{1000} \times \frac{dL}{d\theta}. \tag{5.45}$$

Defining the valve velocity variation as dC_v during the time interval dt, then the acceleration is given by:

$$a_v = \frac{dCv}{dt} \times \frac{1}{g}, \tag{5.46}$$

where $g = 9{,}81 m/s^2$. Therefore

$$a_v = \frac{dCv}{d\theta} \times \frac{d\theta}{dt} \times \frac{1}{g}. \tag{5.47}$$

Hence

$$a_v = \frac{6\mathrm{N}}{9{,}81} \times \frac{dCv}{d\theta}. \tag{5.48}$$

A lookup table of valve lift L_v at one degree increments was required to model the lift of the engine valves. Figure 5.9 shows lift L_1, L_2 and L_3 and from Equation (5.49) the mean valve velocity for the two crank angle intervals is given by:

$$C_{v1} = \frac{6\mathrm{N}}{1000} \times \frac{L_2 - L_1}{\theta_2 - \theta_1}, \tag{5.49}$$

$$C_{v2} = \frac{6\mathrm{N}}{1000} \times \frac{L_3 - L_2}{\theta_3 - \theta_2}. \tag{5.50}$$

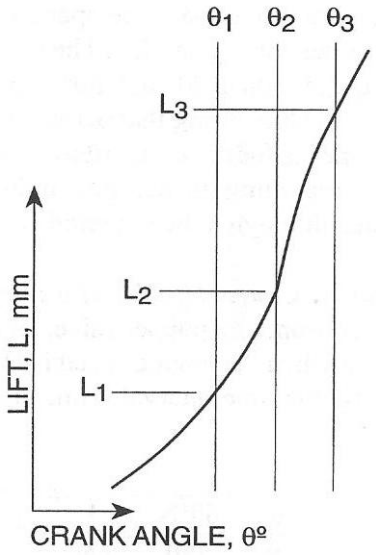

Figure 5.9: Three adjacent points on a valve lift curve (Blair, 1999).

Therefore the mean acceleration for the lift process as a motion from the median point of the first element, to the median point on the second element is given by

$$a_{v12} = \frac{6\mathrm{N}}{9{,}81} \times \frac{C_{v2} - C_{v1}}{0.5\left[\left(\theta_2 + \theta_3\right) - \left(\theta_1 + \theta_2\right)\right]} \tag{5.51}$$

From this, the valve lift can be calculated for each crank angle increment at any given engine speed.

Valve lift characteristics

While developing the simulation model, the option of creating a realistic valve lift profile was assumed rather than using the measured engine data of valve lift versus crank angle. The reason was that no angle marks were available on the engine flywheel, and incorrect angle measurements could produce an unrealistic valve lift profile.

Since the design of the valve train is a very specialized process, it was decided to inspect various engine valve lift versus crank angle data to implement a numerical method of modelling the valve lift. Mathematically, there is no single function capable of accurately representing the entire specific lift function. Reverting to the concept of specific lift and specific angle and referring to Figure 5.7, specific lift and specific angle are given by:

$$L_s = \frac{L_\theta}{L_v}$$

$$\theta_s = \frac{\theta}{\theta_v}$$

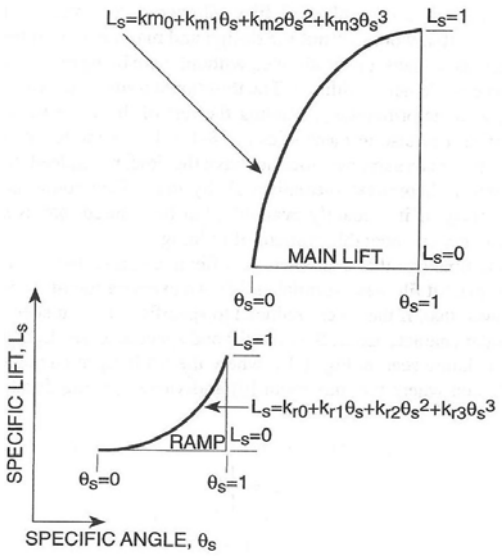

Figure 5.10: Specific lift characteristics of a poppet valve (Blair, 1999).

Figure 5.10 shows the specific lift and specific angle relationships for a ramp period and a lift period. The same polynomial relationship is used for

the “ramp down” as is used for the “ramp up”, and similarly for the “main lift up” and the “main lift down”. The relationship linking specific lift and angle is a third-order polynomial in each case, the coefficients of which are determined from an analysis of measured data. The functions are the following:

For ramp up and ramp down:

$$L_s = K_{ro} + K_{r1}\theta_s + K_{r2}\theta_s^2 + K_{r3}\theta_s^3 \ . \tag{5.52}$$

For main lift up and main lift down:

$$L_s = K_{mo} + K_{m1}\theta_s + K_{m2}\theta_2^2 + K_{m3}\theta_s^3 \tag{5.53}$$

Procedure for modelling valve lift characteristics

The procedure for modelling valve lift characteristics can be carried out in the following steps.

Step 1: Opening and closing angles of the valves are “designed” i.e., numerical values are assigned to V_o and V_c as crank angles referring to the engine TDC, as θ = 0°.

Step 2: Calculate the valve opening duration using:

$$\theta_v = V_c - V_o \tag{5.54}$$

Step 3: Set the duration of the “dwell angle” θ_{dw} as the number of crank angle degrees, typically in the range of 0° to 10°.

Step 4: The “ramp up” and “ramp down” periods, θ_{vr} and θ_{dr} are calculated by assuming they take place over a number of crank angle degrees. Similarly, the main lift periods, up and down, θ_{ul} and θ_{dl}, are each a number of crank angle degrees.

The sum of all these angles must be equal to θ_v (see Figure 5.8). According to Blair (1999), the main lift periods are identical for each ramp period. Therefore:

$$\theta_{ul} = \theta_{dl} = \frac{\theta_v - \theta_{dw} - \theta_{ur} - \theta_{dr}}{2} \tag{5.55}$$

Step 5: Assign the valve lifting associated with the up and down ramp periods, i.e., L_{ur} and L_{dr} as a fraction of the maximum lift L_v. These will be greater than 50% of L_v for CI engines.

The valve lift ratios for the up and down ramp periods are defined as C_{ur} and C_{dr} respectively.

Ramp lift ratios

The ramp lift ratios are defined as

$$C_{dr} = \frac{L_{dr}}{V_v}, \tag{5.56}$$

$$C_{ur} = \frac{L_{ur}}{L_v}. \tag{5.57}$$

The valve lift curve can be computed by considering each element in sequence as shown in Figure 5.10, starting with valve opening and the opening "ramp up".

Valve lift commences at

$$\theta = 0^{o} \qquad L_\theta = 0 \tag{5.58}$$

The opening ramp up period at any angle such as

$$0 < \theta \le \theta_{ur} \tag{5.59}$$

Therefore the specific angle is calculated by

$$\theta_s = \frac{\theta}{\theta_{ur}} \tag{5.60}$$

Inserting θ_s into Equation (5.53) to calculate L_s. Hence the valve lift is given by

$$L_\theta = C_{ur} \times L_s \times L_v \tag{5.61}$$

Main lift up period

For

$$\theta_{ur} < \theta \leq \theta_{ur} + \theta_{ul} \,, \tag{5.62}$$

the specific angle is given by

$$\theta_s = \frac{\theta - \theta_{ur}}{\theta_{ul}} \,. \tag{5.63}$$

Inserting θ_s into Equation 5.53 and calculating L_s, the value of the actual lift, L_θ is found by

$$L_\theta = L_{ur} + L_s (L_v - L_{ur}) \,. \tag{5.64}$$

The dwell period

For

$$\theta_{ur} + \theta_{ul} < \theta \leq \theta_{ur} + \theta_{ul} + \theta_{dw} \tag{5.65}$$

and specific angle θ_s=1, the value of the actual lift, L_θ, is simply the maximum lift: $L_\theta = L_v$

Main lift down

For

$$(\theta_{ur} + \theta_{ul} + \theta_{dw}) < \theta \leq (\theta_{ur} + \theta_{ul} + \theta_{dw} + \theta_{dl}) \,, \tag{5.66}$$

The specific angle θ_s is

$$\theta_S = \frac{\theta_{ur} + \theta_{ul} + \theta_{dw} + \theta_{dl} - \theta}{\theta_{dl}} \,. \tag{5.67}$$

The angle is calculated in reverse to obtain the valve drop. Inserting the specific angle θ_s into Equation 5.53 and calculating Ls, the value of the actual lift, L_θ is found by:

$$L_\theta = L_{dr} + L_s (L_v - L_{dr}) \,. \tag{5.68}$$

The ramp down

For

$$\theta_{ur} + \theta_{ul} + \theta_{dw} + \theta_{dl} < \theta < \theta_v \ , \tag{5.69}$$

the specific angle is

$$\theta_s = \frac{\theta_v - \theta}{\theta_{dr}} . \tag{5.70}$$

It should be noted that the values of angle and lift are determined by their position from the start of the down ramp, i.e. the computation is operated in reverse for “ramp down” by comparison with “ramp up”.

The final point at θ_v is not calculated, but is reserved for a positive ”shut” in the next segment below. Inserting θ_s (Equation 5.52) the specific lift L_s is then calculated. The value of the actual lift, L_θ, is found by:

$$L_\theta = C_{dr} \times L_s \times L_v \tag{5.71}$$

Valve shutting

For

$$\theta = \theta_v \qquad L_\theta = 0$$

The use of the positive zeroing of the valve lift curve, at opening and closing, takes care of the numerical problems caused by the polynomial coefficient K_{ro} in Equation (5.52) not being an actual zero.

This problem is evidenced on air flow graphs and charge mass graphs by showing abrupt “cuts” corresponding to discontinuities of the functions on their connecting transition points. There are some methods for smoothing these abrupt cuts, but the routines implemented on the model were not sufficiently robust to create the desired smoothing of the graphs.

As expected, there will be some function problems due to the fact that those values of lift are calculated from different functions, giving rise to unacceptably high levels of velocity and acceleration of the valve.

5.3.4 Ignition delay

Ignition delay is dependent on the auto ignition temperature of the hydrogen, and for a gaseous injection of hydrogen this is solely dependent

on the temperature of the cylinder charge. This dependence was modelled using experimental data derived by Tsujimura (1999) and is given by the following expression:

$$\tau = 0.2911 + 1.332 \times 10^{5} \times e^{12.28\left(\left(\frac{1000}{T_a}\right)\right)} \tag{5.72}$$

This expression, which is a function of the cylinder charge temperature, was used to define the ignition crank angle.

For cylinder charge temperatures below the hydrogen self ignition temperature, there is no ignition and therefore no combustion. For cylinder charge temperatures above the self ignition temperature, combustion takes place and is affected by a delay given by the expression above. Therefore, the angle of ignition is a function of the ignition delay and the cylinder charge temperature.

In the case of DIH_2 it was assumed that the cylinder charge temperature is always above 1100 K, the self-ignition temperature of hydrogen, therefore resulting in extremely short ignition delays.

5.3.5 Mass flow calculation

The cylinder conducts an intake stroke, in which a mass of fresh air is induced through the inlet valve into the cylinder from the atmosphere. Therefore, this variable varies with atmosphere pressure and temperature. The ambient conditions T_a and P_a influence directly the air density, and can be expressed by

$$\rho_a = \frac{P_a}{R_a T_a}. \tag{5.73}$$

Therefore, the volumetric efficiency, η_v, of the engine, which is an input parameter of the simulation program, is related directly to the mass of air supplied through the inlet manifold and inlet valve during the intake

period, divided by mv_{ref} which is the mass required to fully fill the cylinder with a swept volume V_{sv} under the cylinder prevailing condition. Therefore:

$$\eta_v = \frac{m_a}{m_{vref}}, \tag{5.74}$$

$$m_{vref} = \rho_a V_{sv} . \tag{5.75}$$

Assuming that the cylinder has induced a mass of fresh air at standard conditions of pressure and temperature, the reference density ρ_{dref} is given by

$$\rho_{dref} = \frac{P_{dref}}{R_a T_{dref}} \tag{5.76}$$

The delivery ratio, DR, of the engine is defined as the mass of air supplied through the inlet valve during the intake period divided by the mass of air, m_{dref}, with a perfect suction into the swept volume and at standard reference density ρ_{dref}. The delivery ratio is then defined as:

$$DR = \frac{m_{as}}{m_{dref}} \tag{5.77}$$

where

$$m_{dref} = \rho_{dref} V_{sv} \tag{5.78}$$

5.3.5 Combustion

The CI engine air fuel ratio

Hydrogen (H_2) as a CI engine fuel has the following stoichiometric equation

$$2H_2 + \left[O_2 + \frac{79}{21} N_2 \right] \begin{matrix} \leftarrow \\ \rightarrow \end{matrix} 2H_2O + \frac{79}{21} N_2 \qquad (5.79)$$

Therefore the air fuel gravimetric ratio is given by

$$AFR = \frac{1 \times 32 + 1 \times \frac{79}{21} \times 28}{2 \times 1 \times 2} = 34.332 .$$

Unlike for diesel fuels, particulate matter emissions are not produced by the hydrogen combustion, allowing operation with richer cylinder charges if required. Also, due to the hydrogen physical properties such as, high dispersion, lower explosive limit, low quenching distance and high flame speed, its possible to run CI engines with very high air fuel ratios.

Cylinder trapping conditions

The air trapping point is considered the point where the intake valve closes, therefore the total mass of air available for combustion is dependent on the pressure and temperature conditions at the trapping point, which is given by:

$$m_{tr} = \frac{P_{tr} \times V_{tr}}{R_{tr} \times T_{tr}} , \qquad (5.80)$$

and:

$$V_{tr} = V_{ivc} + V_{cv} . \qquad (5.81)$$

Considering that air is the prevailing gas inside the cylinder there is little error assuming that $R_{tr}=R_a$. The dominant variable of the trapping process is the pressure inside the cylinder P_{tr}. The trapping pressure is directly controlled by the pressure wave dynamics of the intake and exhaust system (Blair, 1999).

Pressure and temperature profile calculation

The CI engine cycle can be represented by five processes, corresponding to the air-standard dual cycle as shown in Figure 5.11:

Adiabatic and isentropic compression 1-2;

Constant volume heat addition (combustion) 2-3;

Constant pressure heat addition (combustion) 3-4;

Adiabatic and isentropic expansion 4-5;

Constant volume heat rejection, exhaust process 5-1;

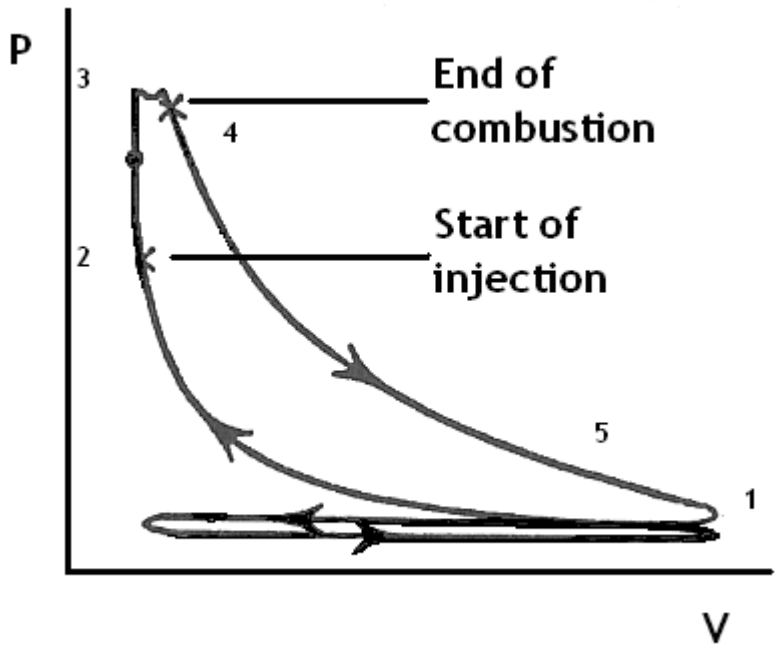

Figure 5.11: Four stroke CI engine pressure volume cycle.

To perform the calculation of the dual cycle, data from the engine parameters related to the engine geometry are used in Equation 5.14 to define the piston position H_t at any crank angle, thus allowing the calculation of cylinder volume and temperature profiles.

To simplify the calculation of the various equations an incremental method was used. The volume increment is approximated by:

$$V_{step} = V_n + \left[\frac{V_{n+1} + V_1}{2}\right] \qquad (5.82)$$

and the temperature increment is approximated by:

$$\frac{dT}{d\theta} = T_{n+1} - T_n \tag{5.83}$$

Adiabatic and isentropic compression

It was assumed that only air is compressed, however this is not exactly correct in the case of the HCCI engine since a mixture of air and hydrogen is compressed. A correction factor using the ratio of the specific heats was therefore implemented, using the following expression recommended by Blair (1999):

$$k = 1.4373 - 1.318 \times 10^{-4} \times T + 3.12 \times 10^{-8} \times T^2 - \frac{4.8 \times 10^{-2}}{\lambda}, \tag{5.84}$$

T is the average cylinder charge temperature and λ is the average excess air factor. The mass of air trapped in the cylinder, m_{ta}, is given by

$$m_{ta} = \frac{P_1 V_{sv}}{R T_1}, \tag{5.85}$$

V_{sv} is the swept volume, R is the air universal constant, and T_1 and P_1 are the initial temperature and pressure.

5.4 Engine simulation program structure

The simulation program was implemented using Matlab (The MathWorks Inc., 2006). The implemented program structure is presented in Figure 5.12 and its respective functions are described below.

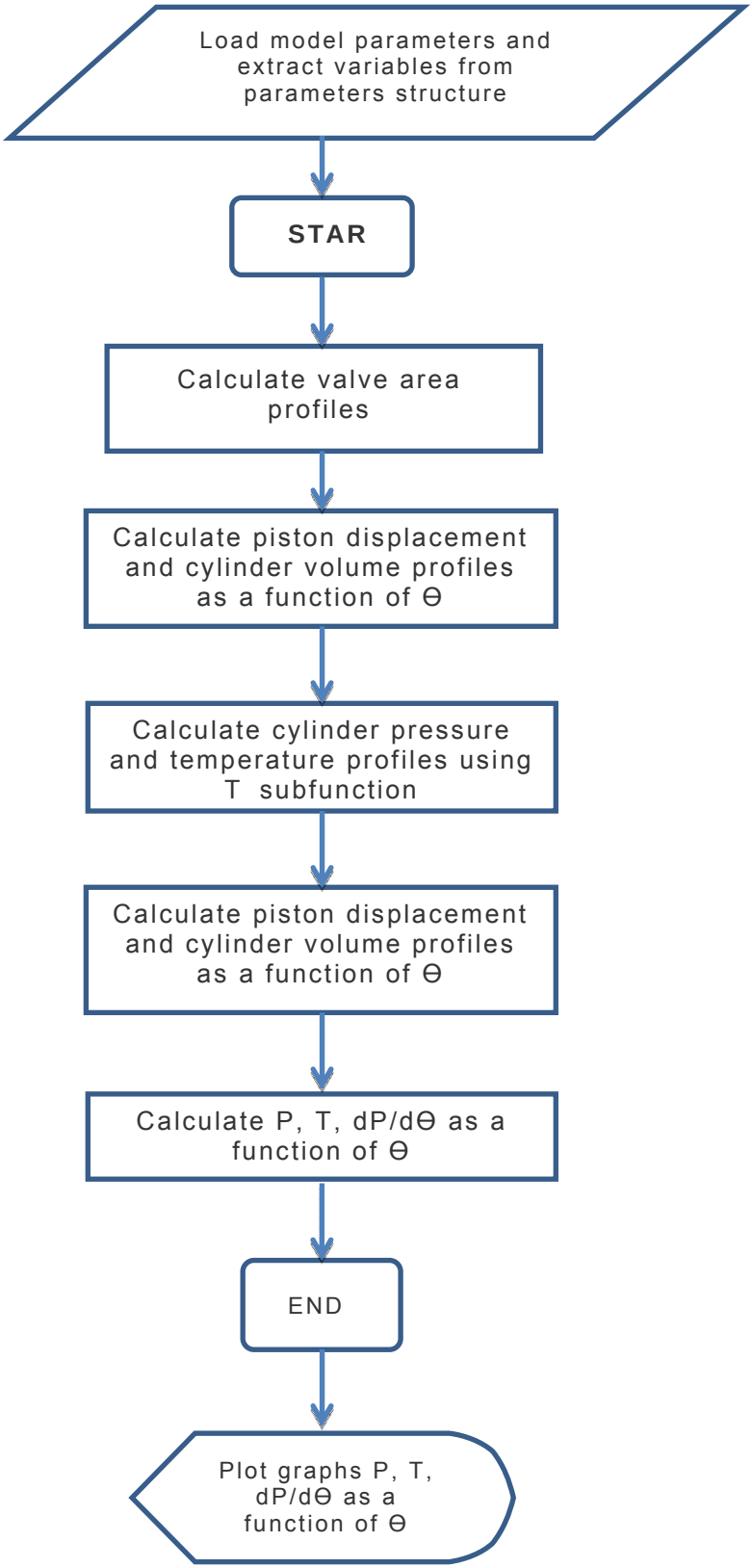

Figure 5.12: Simulation program process.

Function Main Engine Cycle

This function calculates the working fluid temperature and pressure as a function of crank angle, engine speed and ambient conditions. The input variables of this function are:

RPM: Engine speed (rpm);

P_a: ambient air pressure (Pa);

T_a: ambient air temperature (K);

Q_{in}: combustion energy input function (J/s);

Function Barrel

In order to calculate the flow through valves and other parameters, it is necessary to shift the engine cycle and other parameters, so that the initial state is one of known, quasi-static conditions. For this state, the inlet and exhaust valves are both closed and the in-cylinder pressure is known or can be predicted reliably.

The Barrel function is used to shift all crank-angle related values calculated so far to a suitable point to enable further calculations. The same function will then be used to restore the cycle to its original position on the crank angle axis. The cycle is shifted so that the initial condition is immediately before the exhaust valve opens.

Function Pressure

This function calculates the cylinder pressure profile over a complete engine combustion cycle. The initial cylinder pressure is the variable P_{start}. The function uses an iterative process to calculate the results for the input (θ) range, using the inlet and exhaust valve area profiles given by the variables i_{av} area and e_v area, previously defined.

The engine speed is given by the variable omega in rad/sec, and the cylinder volume is given as a function of theta by volume. The data is shifted to give the starting point where inlet and exhaust valves are closed,

starting immediately after inlet valve closes, and assumes that cylinder pressure is atmospheric.

Function data

This function returns engine parameters. If an input argument is supplied, it also plots a graphical representation of the valve timing,

Function Engine model

This function contains the whole engine model as separate sub-functions, and is divided into three distinct intervals:

From beginning of cycle until start of injection.

From start of injection until end of combustion.

From end of combustion until exhaust valve opens.

Calculations are made for each of these cycle periods.

Functions valve lift and area

The valve lift function calculates the valve lift profile based upon the duration as defined by the opening and closing angles. The valve area function calculates the valve areas in relation to the crank angle for given valve dimensions and lift profiles. The methods implemented are those given by Blair (1999), as described above.

5.4.1 Simulation program interfaces

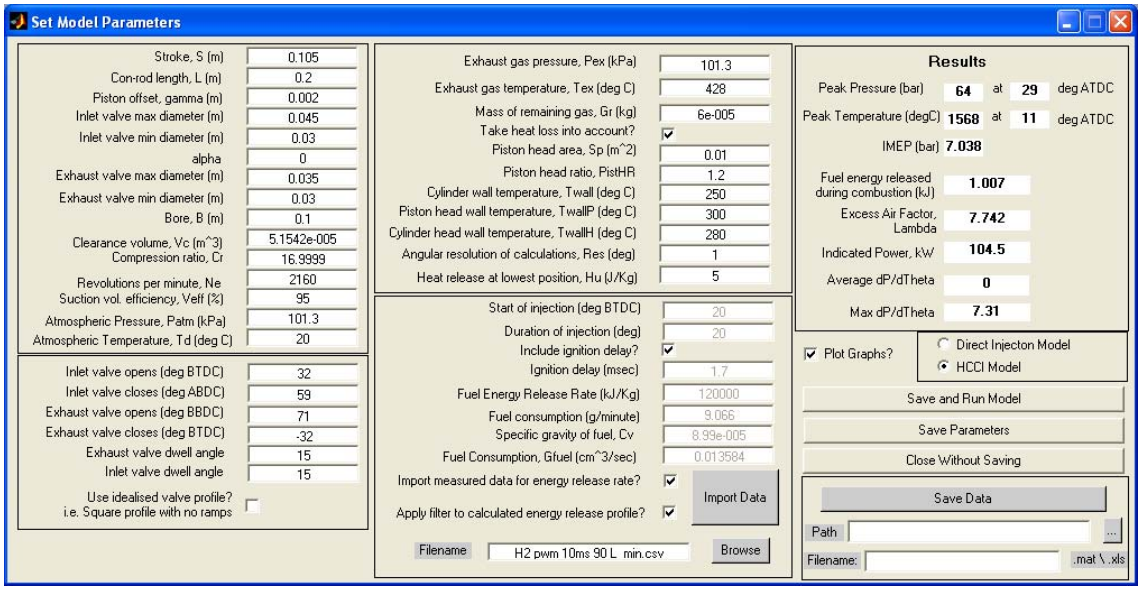

Figure 5.13: Simulation program human interface.

The simulation program was designed to have a graphical user interface as shown in Figure 5.13. This allows the geometric engine parameters, injection timing, valves timing, and all the other parameters to be defined.

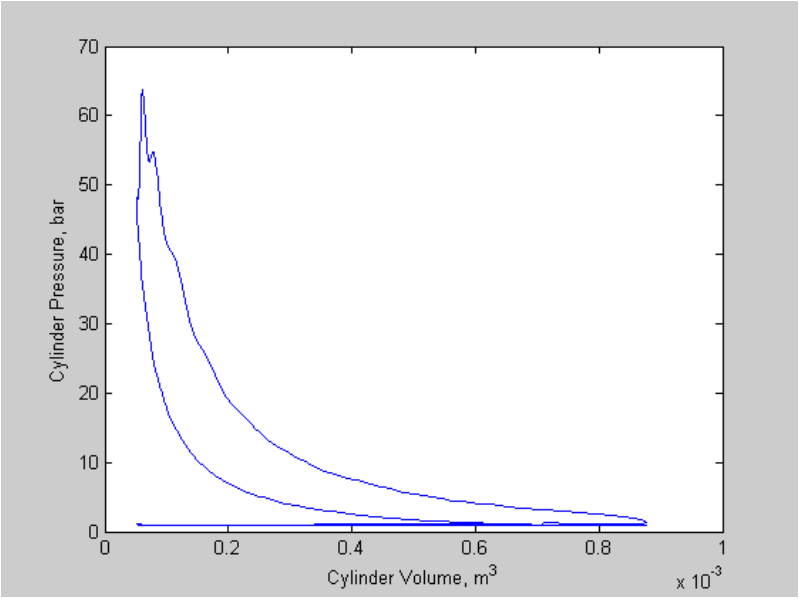

Figure 5.14: Pressure volume diagram.

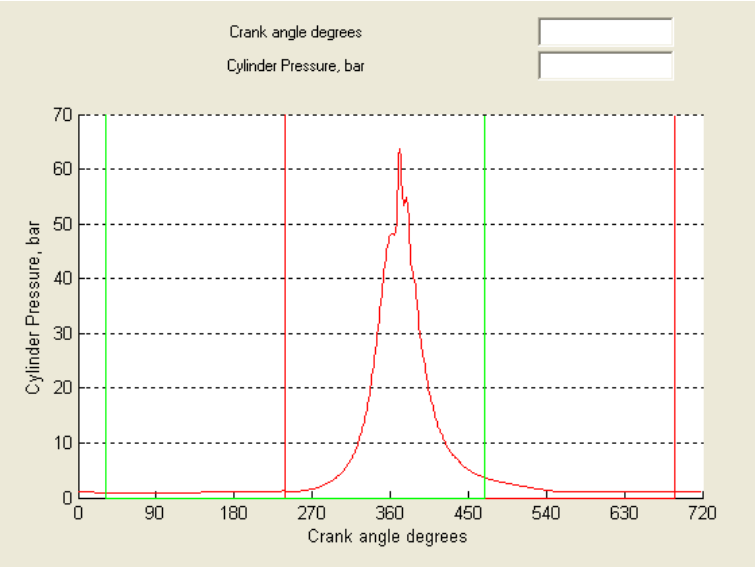

Figure 5.15: Open pressure diagram pressure as a function of the crank angle

A pressure volume diagram, an open pressure diagram and a temperature angle diagram are shown in Figures 5.14, 5.15, and 5.16 respectively. These are the basic output diagrams of the simulation program.

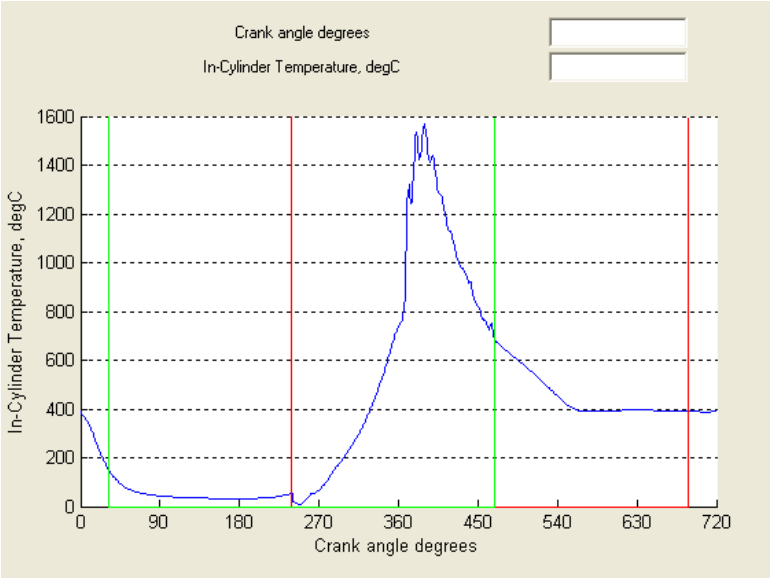

Figure 5.16: In-cylinder temperature as a function of the crank angle.

Complementary simulations are performed on the basis of the pressure and temperature diagrams, allowing further graphical interpretation of the cycle. This includes rate of pressure rise as a function of the crank angle,

as shown in Figure 5.17, rate of energy release as a function of the crank angle as shown in Figure 5.18, and rate of energy received from the combustion chamber as a function of the crank angle, as shown in Figure 5.19. These are all diagrams related to heat transfer and provides cycle analysis information essential to investigate hydrogen combustion.

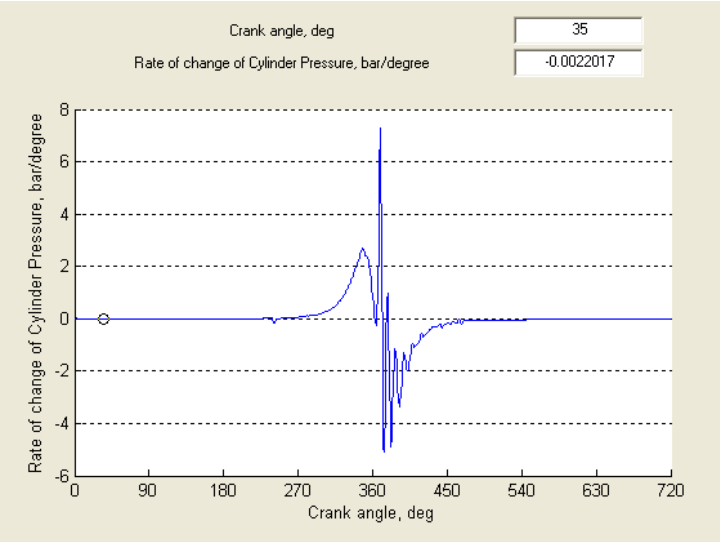

Figure 5.17: Rate of pressure rise as a function of the crank angle.

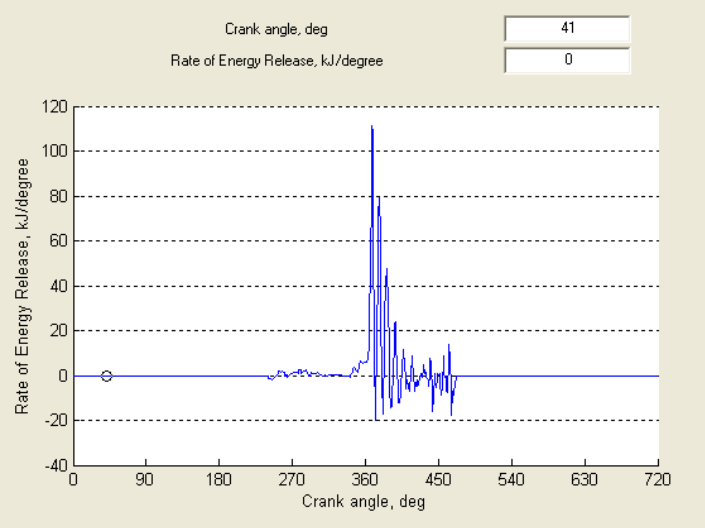

Figure 5.18: Rate of energy release as a function of the crank angle.

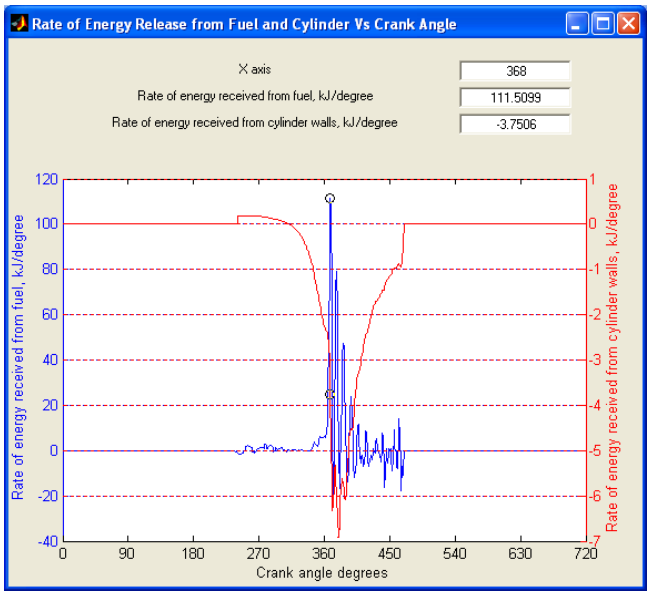

Figure 5.19: Rate of energy transfer fuel combustion and combustion chamber walls.

Another set of diagrams which can be drawn are related with the air flow through the engine and valves settings. These diagrams are illustrated in Figures 5.20, 5.21, and 5.22.

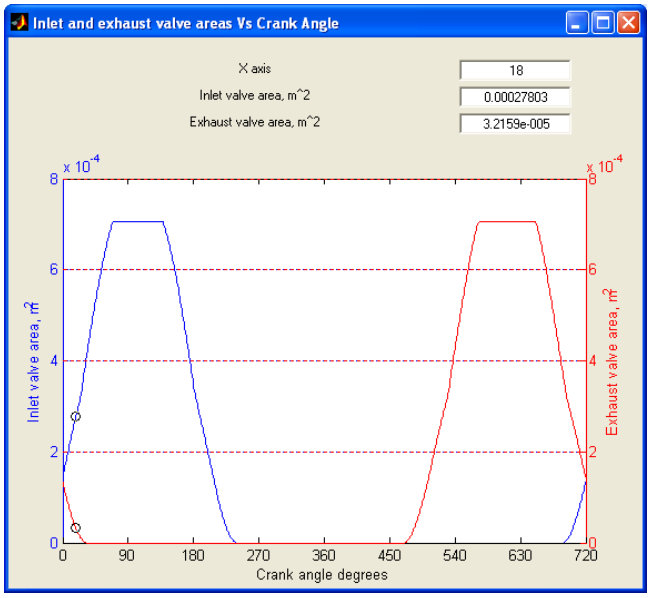

Figure 5.20: Inlet and exhaust valve areas as a function of crank angle.

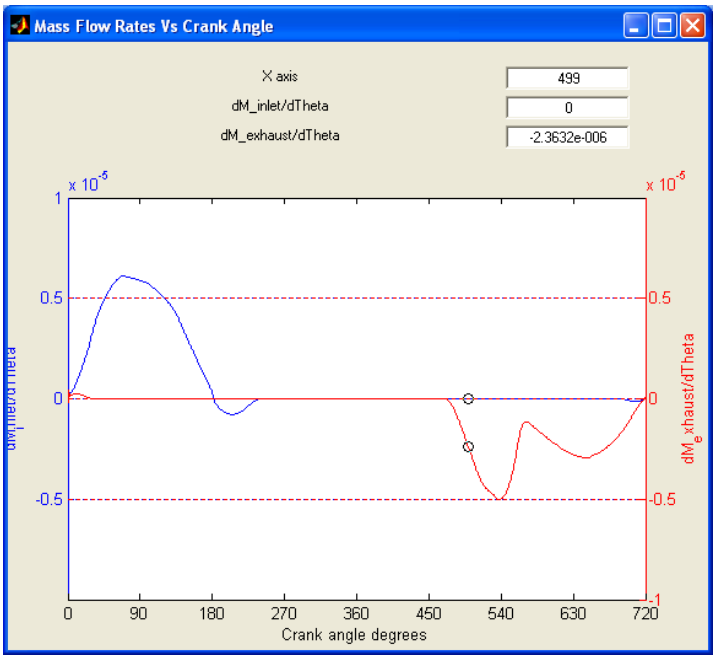

Figure 5.21: Variation of induced mass of air and exhaust gases as a function of rank angle.

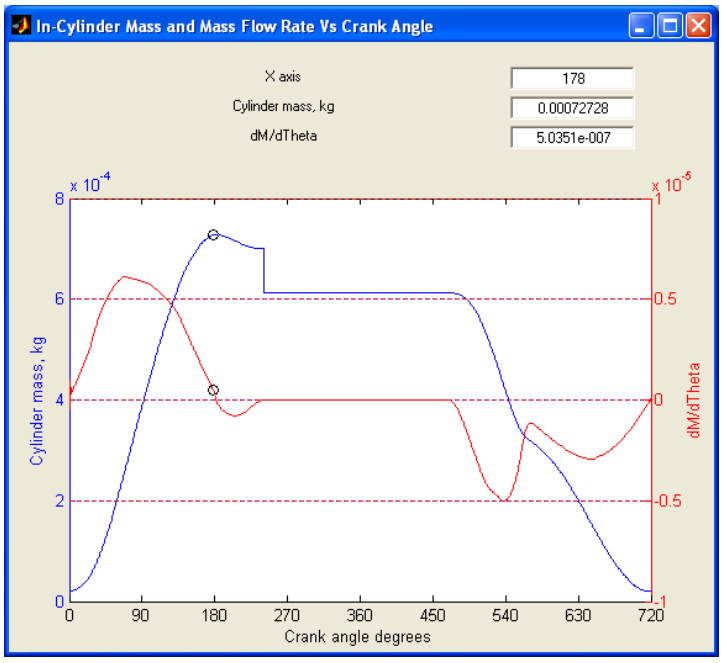

Figure 5.22: Cylinder air mass flow rate and its variation with the crank angle.

5.5 Hydrogen injectors modelling

The next sections present the design of the hydrogen injectors used for HCCI and DIH_2 engine operation. Since each injector has a different design and requirements, their development work is presented separately. The injection control system is also presented.

5.5.1 HCCI injector design considerations

The design of the injector for the homogeneous charge compression ignition mode of operation is simpler than that of the DIH_2 injector, as the pressures, temperatures and time available for injection are less restrictive than for the direct injection injector.

The HCCI injector used first was a pulse width modulated, two way, normally closed, solenoid valve, as shown in Figure 5.23. It is made from corrosion resistant materials and used to inject gaseous hydrogen into the engine intake air manifold. Pulse width modulation allows fuel quantity to be controlled with an opening and closing timing precision of +/-25 microseconds.

Figure 5.23: HCCI Hydrogen injection valve.

The valve assembly is composed of the valve body, which holds the solenoid armature, ball poppet and seat, as shown in Figure 5.23.

With the solenoid de-energised, the supply pressure, assisted by a spring, forces the solenoid ball poppet on its seat, barring gas flow. When the solenoid is energised, the ball poppet is lifted off the seat and held against the stop. Gas then passes through the valve seat and outlet port of the injector.

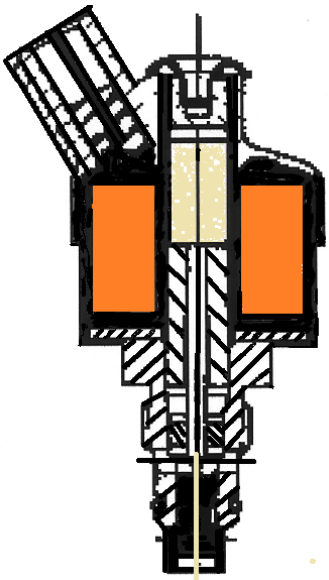

Figure 5.24: Cross section of the solenoid valve.

Figure 5.25 shows the injection valve fitted on the engine air inlet manifold where a pressure gauge and thermocouple were fitted to monitor the hydrogen pressure and temperature.

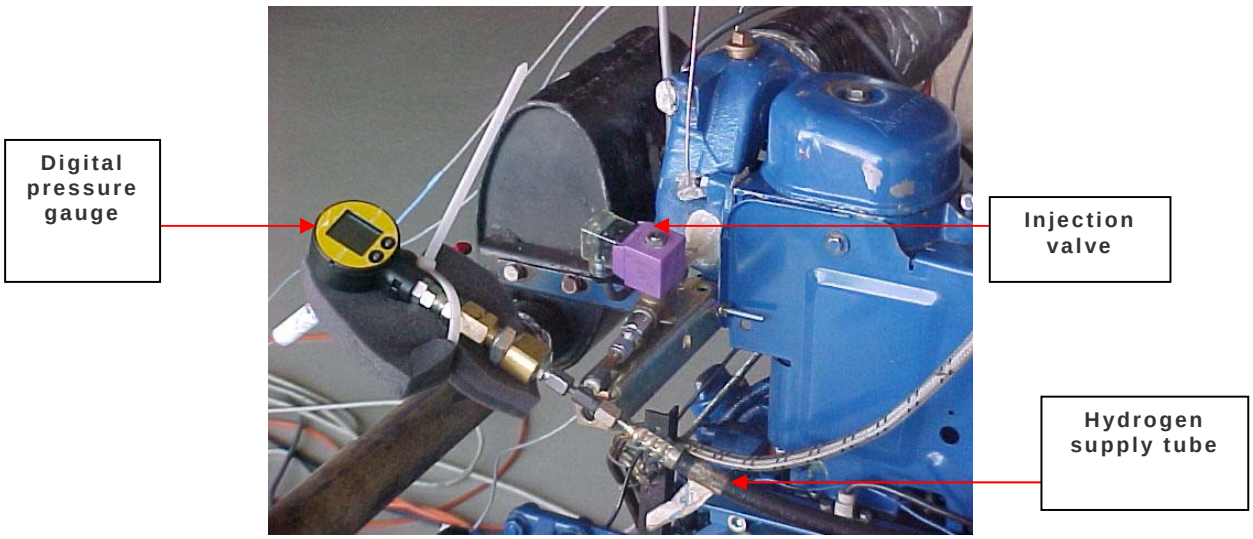

Figure 5.25: HCCI injection valve fitted on the engine.

As referred before, the electronically controlled fuel injection valve is used also as a fuel-metering device. Gaseous fuelling consistency between injectors and cycles is just as important as with direct injection injectors. The steady gaseous flow rate is defined by the following expression:

$$Q_{steady} = C_d \cdot A \cdot V_t \ , \tag{5.86}$$

C_d is the coefficient of discharge, A is the area of throat at valve seat (m^2), and V_t is the velocity at the throat (m/s).

For sonic flow, the velocity of gas through the orifice is given by:

$$V_t = \sqrt{\frac{\gamma \cdot P_t}{\rho_t}} \ , \tag{5.87}$$

γ is the ratio of specific heats, P_t is the pressure at the throat (Pa), and ρ is the density at the throat.

Therefore, the steady mass flow rate is given by

$$Q_{steady} = \frac{K \cdot A \cdot P_1}{\sqrt{T_1}} \ , \tag{5.88}$$

P_1 is absolute inlet pressure (Pa), T_1 is absolute inlet temperature (K), and K is a constant given by injector manufacturer (0.214),

provided that

$$\frac{P_2}{P_1} \leq r \ , \tag{5.89}$$

P_2 is absolute outlet pressure (Pa) and R is the critical pressure ratio,

and

$$r = \left(\frac{2}{\gamma + 1} \right)^{\frac{\gamma}{\gamma - 1}} \ . \tag{5.90}$$

Therefore, the ratio of manifold absolute pressure to absolute supply pressure cannot exceed the critical pressure ratio to maintain the sonic

flow characteristic. The time delay of this valve is 3.0 ms to open and 2.0 ms to close.

5.5.2 DIH_2 injector design

The production of a hydraulic high speed injection system for engine speeds above 1000 rpm is problematic because of the dynamic response of the injector, the lubrication of the moving parts, and the prevention of hydrogen leakage.

Assuming that hydrogen behaves as an ideal gas and flows isentropically between the hydrogen manifold and the nozzle hole exit, then there is no energy loss during the flow process. Assuming also that the enthalpy is dependent only on the temperature, using the relationship between the specific heat at constant pressure and the specific heat ratio, the following energy equation can be written:

$$\frac{1}{2}u_e^2 + \frac{k}{k-1}\frac{p_e}{\rho_e} = \frac{k}{k-1}\frac{p_o}{\rho_o}, \tag{5.91}$$

p is pressure (Pa), ρ is density (kg/m^3), u is internal energy (kJ/kg). and k is specific heat ratio.

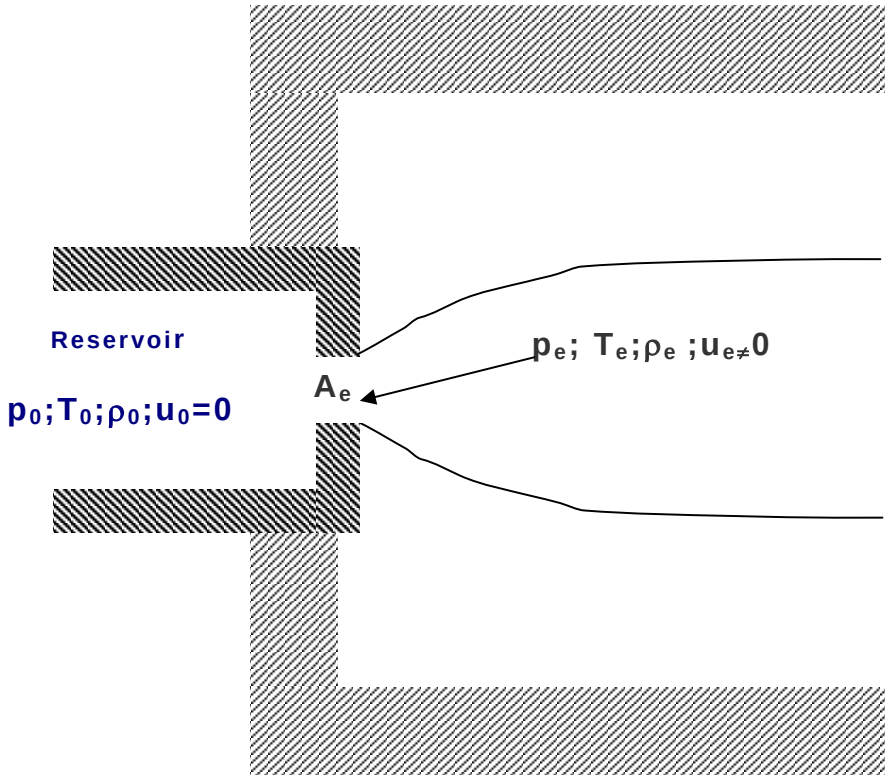

Figure 5.26: Isentropic jet development of hydrogen injection.

Figure 5.26 shows a schematic diagram of the hydrogen manifold and nozzle exit. The subscripts "e" and "o" refer to the conditions at the exit of the nozzle hole, and inside the hydrogen manifold respectively.

The flow velocity and the mass flow rate at the nozzle can be derived based on figure 5.26:

$$u_e = \sqrt{2\frac{k}{k-1}\frac{p_o}{\rho_o}\left[1-\left(\frac{p_e}{p_o}\right)^{\left(\frac{k-1}{k}\right)}\right]} \tag{5.92}$$

$$m_e = \overset{*}{\rho}_e u_e A_e = A_e\sqrt{2\frac{k}{k-1}p_o\rho_o\left(\frac{p_e}{p_o}\right)^{\frac{2}{k}}\left[1-\left(\frac{p_e}{p_o}\right)^{\left(\frac{k-1}{k}\right)}\right]} \tag{5.93}$$

As the flow velocity at the exit of the nozzle hole approaches the speed of sound, in compressible flow theory under choked flow conditions (Yunus A. et al. 1998), the critical pressure, critical density, critical velocity and critical temperature are given respectively:

$$p = p_o\left(\frac{2}{k+1}\right)^{\frac{k}{k-1}} \tag{5.94}$$

$$\rho = \rho_o\left(\frac{p}{p_o}\right)^{\frac{1}{k}} = \rho_o\left(\frac{2}{k+1}\right)^{\frac{1}{k+1}} \tag{5.95}$$

$$u = \sqrt{k\frac{p}{\rho}} = \sqrt{\frac{2\mathrm{k}}{(k+1)}\frac{p_o}{\rho_o}} \tag{5.96}$$

$$T = T_o\left(\frac{2}{k+1}\right) \tag{5.97}$$

Neglecting the energy losses due to viscosity at the nozzle hole, the maximum mass flow rate is expressed by equation (5.98) as follows:

$$m = \rho_0 u A_e = \rho_o A_e\left(\frac{p_o}{\rho_o}k\right)^{\frac{1}{2}}\left(\frac{2}{k+1}\right)^{\frac{k+1}{2(k-1)}} \tag{5.98}$$

In practice, because there are friction losses due to viscosity, at the entry of the nozzle, the flow velocity is smaller than the critical velocity, and as a consequence, the discharge coefficient is also less than one, varying

according to the geometry of the nozzle hole. Therefore, it is necessary to investigate the discharge coefficients for varying flow conditions.

5.5.3 Under-expanded gas flow in the proximity of a nozzle hole

The pressure at the nozzle exit is higher than the cylinder pressure, causing the hydrogen to expand as it is injected. Since hydrogen flows near the nozzle exit as if it emanated from a nozzle diameter hole larger source than the actual nozzle (Tsujimura et al., 2003), the nozzle is referred as having a pseudo-diameter. Figure 5.27 shows a schematic diagram of the under-expanded jet behaviour just downstream of the nozzle exit. In the immediate region downstream of the nozzle exit, the over pressure causes the flow to accelerate and expand, generating expansion waves, that form a barrel shaped shock profile. In the hydrogen barrel shaped shock volume, the flow reaches a supersonic speed, being capped by a so called Mach disc, that has several times the diameter of the orifice. It can be assumed that the hydrogen pressure drops to the ambient gas pressure at the Mach disc and the ambient gas cannot be entrained into the barrel shaped shock volume.

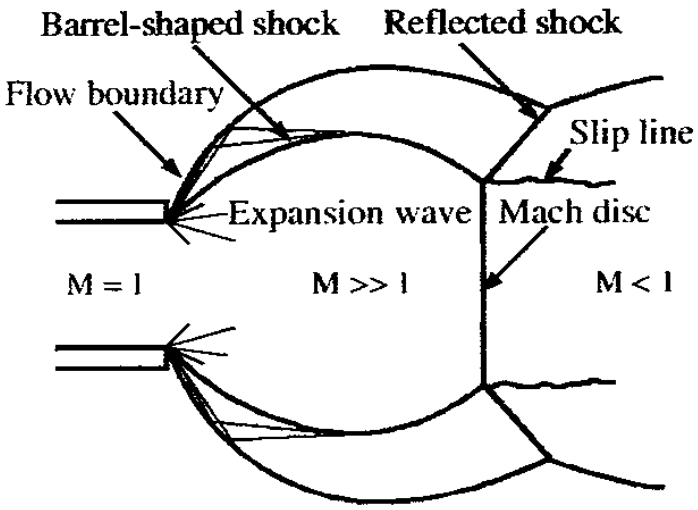

Figure 5.27: Schematic diagram of the under-expanded jet behaviour at the nozzle hole exit (Ewan et al., 1986).

Table 5.1: The under-expanded flow equations.

	Nozzle exit	*Barrel shaped shock*	*Mach disc*
Pressure	p^*	$p^*<p<p_a$	$p_{MD}=p_a$
Density	ρ	$\rho <<$	$\rho_{MD} = p_0 / R_o T_{MD}$
Temperature	T^*	------	$T_{MD} = T_o$
Velocity	u^*	$>>u^*$	$u_{MD} = \sqrt{kR_o T_{MD}}$
Mach number	1	>>1	1

In Table 5.1 the equations for under-expanded flow are summarised.

Therefore the mass flow rate at the Mach disc is given by:

$$\dot{m} = \frac{\pi}{4} d_{MD^2} \rho_{MD} U_{MD} \,, \tag{5.99}$$

since

$$U_{MD} = K\left(\frac{P_{MD}}{\rho_{MD}}\right). \tag{5.100}$$

Therefore

$$\dot{m} = \frac{\pi}{4} d_{DN}^2 \rho_{MD} \left(\frac{P_{MD}}{\rho_{MD}} \right), \tag{5.101}$$

the subscript MD stands for Mach Disc.

According to (Ewan et al., 1986) flow conditions at the nozzle hole exit are related with those at the Mach Disc as follows:

$$\dot{m} = \frac{\pi}{4} d_{e2} C_D \rho_o \left(k \frac{p_o}{\rho_o} \right)^{1/2} \left(\frac{2}{k+1} \right)^{\frac{(k-1)}{2(k-1)}}, \tag{5.102}$$

$$\left(\frac{d_{MD}}{d_e} \right)^2 = C_D \frac{p_o}{p_a} \left(\frac{T_{MD}}{T_D} \right)^{1/2} \left(\frac{2}{k+1} \right)^{\frac{(k-1)}{2(k-1)}}, \tag{5.103}$$

the subscript *a* refers to the ambient conditions inside the injection volume.

Assuming that the temperature at the reservoir is approximately the temperature at the Mach Disc, the diameter of the Mach disc is given by:

$$d_{MD} = d_c \left[C_D \frac{p_o}{p_a} \left(\frac{2}{k+1} \right)^{\frac{1}{2}} \right]^{\frac{1}{2}}. \tag{5.104}$$

The direct injection of hydrogen into a diesel engine cylinder is a process different compared to the injection of a diesel liquid fuel since there is no evaporation and the inertia of the particles or droplets does not have the same magnitude, the momentum theory must be modified for hydrogen. This fact of the particles low inertia affects the penetration of the jet into the cylinder volume. Also, the injection process of a gaseous fuel is related to the auto ignition and consequent combustion. The injection of a highly pressurised jet into a pressurised atmosphere has been investigated (Ewan et al., 1996), but there is a limited amount of data available, therefore a modified momentum theory is presented to derive a gas jet penetration correlation.

Momentum theory applied to the jet penetration is based on momentum conservation, i.e., the jet entering the compressed atmosphere of the cylinder, changes its momentum due to the cylinder pressure, also called ambient atmosphere. Momentum theory (Wakuri et al., 1960) is often used to analyse the spray penetration, but for application to gaseous fuels, some modifications are needed which require some assumptions to be made. These are: (a) the spray dispersion angle is constant during its development process, (b) the velocity differences between the fuel and the ambient gas entrained into the spray are negligible, (c) the momentum at the nozzle exit is constant up to the spray tip, and (d) the velocity profile of the spray is uniform. Assuming that hydrogen is injected through the Mach disc, as shown in Figure 5.28, the spray correlation x' based on momentum theory is modified to estimate the jet penetration as follows:

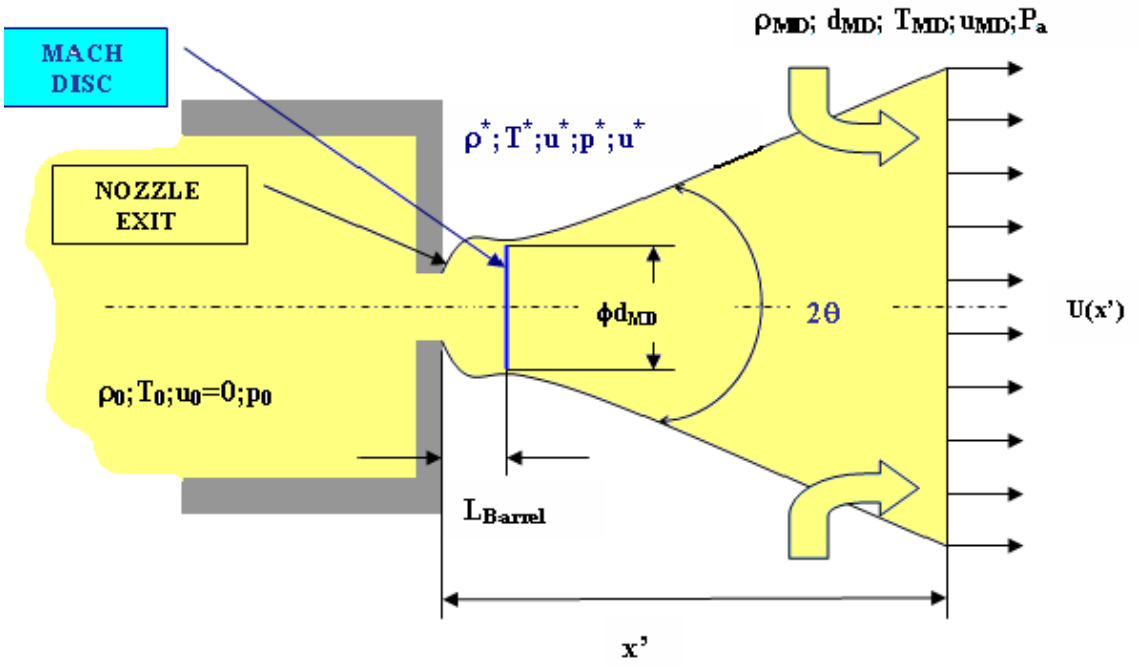

Figure 5.28: Schematic diagram of the jet development model (Tsujimura T. et al., 2003).

$$x' = a'\left[C_p k \frac{p_0}{\rho_a}\left(\frac{2}{k+1}\right)^{\frac{(k-1)}{2(k-1)}}\right]^{0.25}\left(\frac{d_e t}{\tan\theta}\right)^{0.5} + L_{BARREL}\,, \qquad (5.105)$$

(Tsujimura T. et al., 2003)

a' is the experimental constant, θ is the jet dispersion angle (rad) , and L_{BARREL} is the distance between the actual nozzle exit and the Mach disc (m).

The length of the barrel shaped shock profile can be represented by means of the following equation (Ewan et al. 1986):

$$L_{BARREL} = 0.77 d_e + 0.068 d_e^{1.35}\frac{p_f}{p_a}\left(\frac{2}{k+1}\right)^{\frac{k}{k-1}}. \qquad (5.106)$$

Figure 5.30 presents a schematic diagram of the jet development model.

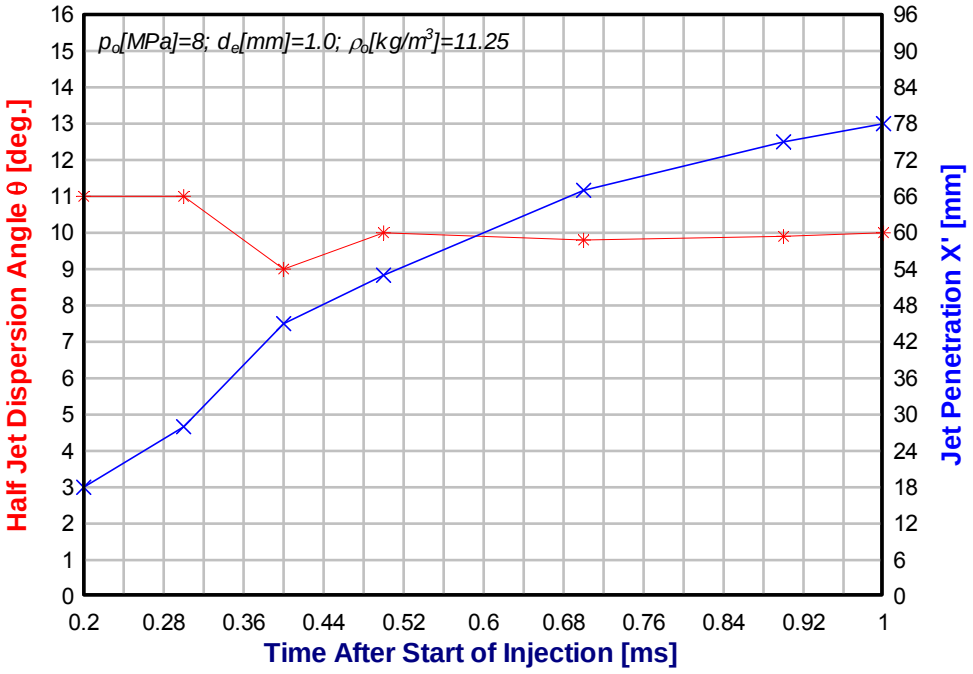

Figure 5.29: Profile of jet penetration and half jet dispersion angle for an orifice with 1.0 mm diameter derived from experimental data (Tsujimura et al., 2003; Shao et al., 2003).

As a consequence of the presented theory, one can say that the ambient density increase, results in a decrease of the spray penetration, as shown in Figure 5.29, and that the hole diameter has a significant influence over the jet penetration volume just after the start of injection. According to Rottengrubber et al. (2004), the number of holes in the hydrogen injector does not significantly affect behaviour of the hydrogen jet, and this was confirmed by using only one hole injector nozzle.

5.5.4 Injector hydraulic actuation modelling

With the objective of understanding the dynamics of the hydrogen hydraulic injector, a dynamic simulation model was created using Simulink. With this dynamic simulation model, the variables that govern the injector dynamics were identified, enabling injector design decisions to be made.The injector speed of response is influenced by two main injector

components, the hydraulic solenoid valve and the actuator piston. The forces that act on the actuator piston are shown in Figure 5.30.

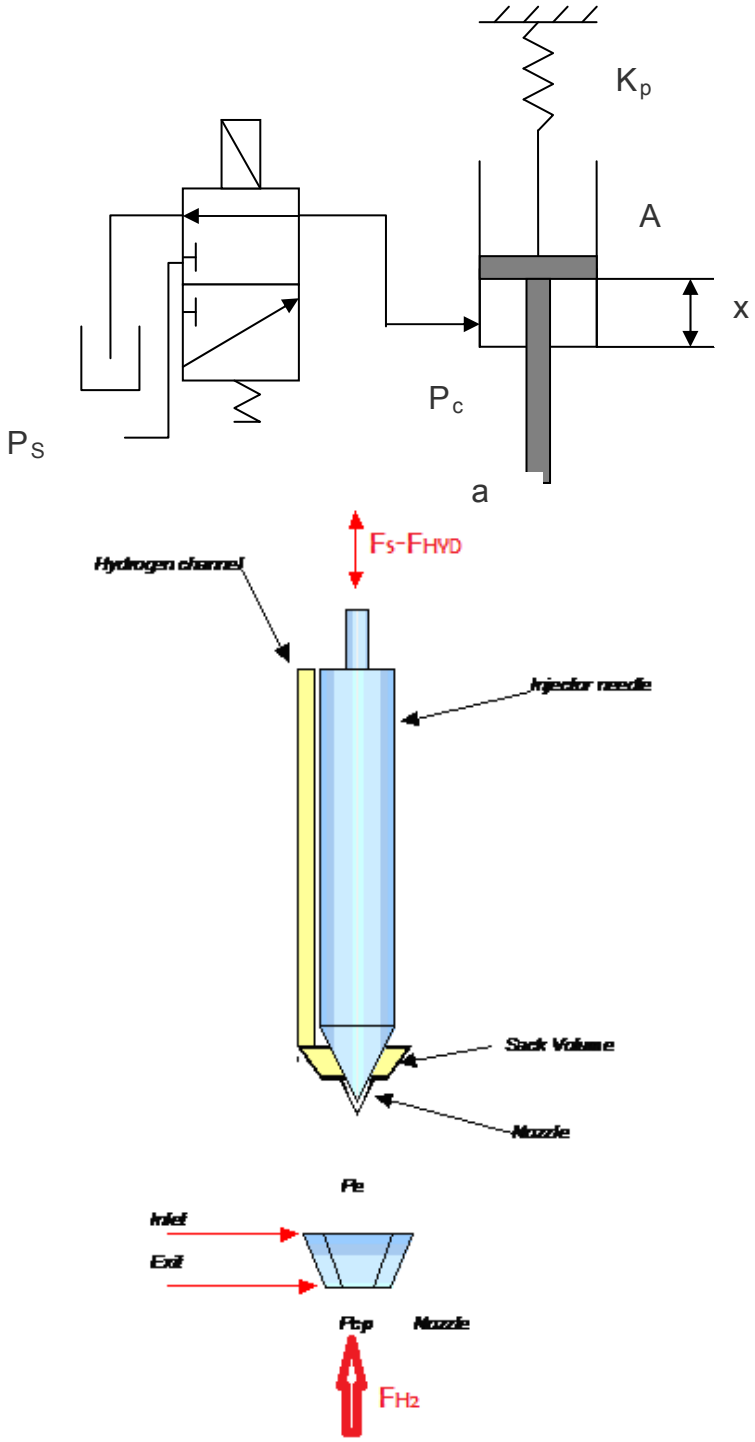

Figure 5.30: Top - Injector hydraulic actuator free body diagram. Bottom Forces acting on the needle

Therefore, the Newton second law of motion in vertical direction equation is given by

$$\frac{dv}{dt} = \frac{1}{m_t}(F_S - F_{H_2} - F_{hyd}), \tag{5.107}$$

m_t is the mass of the needle actuator group (kg) and

$$F_S = K \cdot X, \tag{5.108}$$

K is the spring elastic constant (N/m);

$$F_{H_2} = P_{H_2} A_{SACK}, \tag{5.109}$$

P_{H2} is the hydrogen supply pressure (Pa) and A_{SACK} is the lateral area of the cone inside the sack volume (m^2); and

$$F_{hyd} = (A - a) \times P_{HYD}, \tag{5.110}$$

A is the area of the piston (m^2), a is the cross section area of the piston rod (m^2), and P_{HYD} is the hydraulic oil pressure (Pa).

Applying the momentum equation to the piston and spring movement depicted at figure 5.32, the speed of response of the injector can be represented by the following equation:

$$V(t) = \frac{1}{m}\int_{t=1}^{t=t}\left[(K \times X) - \left(P_{H_2} \times A_{SACK}\right) - \left((A - a)P_{HYD}\right)\right]dt, \tag{5.111}$$

V is the velocity of the needle actuator group (m/s) and X is the vertical displacement (m).

It can be concluded from this analysis that to increase the speed of response of the injector it is required to reduce the mass of the actuator assembly, increase the spring stiffness for a fast closing, and increase the hydraulic pressure to increase the opening response.

To model the hydraulic poppet valve as illustrated in figure 5.33, it is necessary to consider the armature response as a function of the solenoid force, as well as the effect of hydraulic and spring forces.

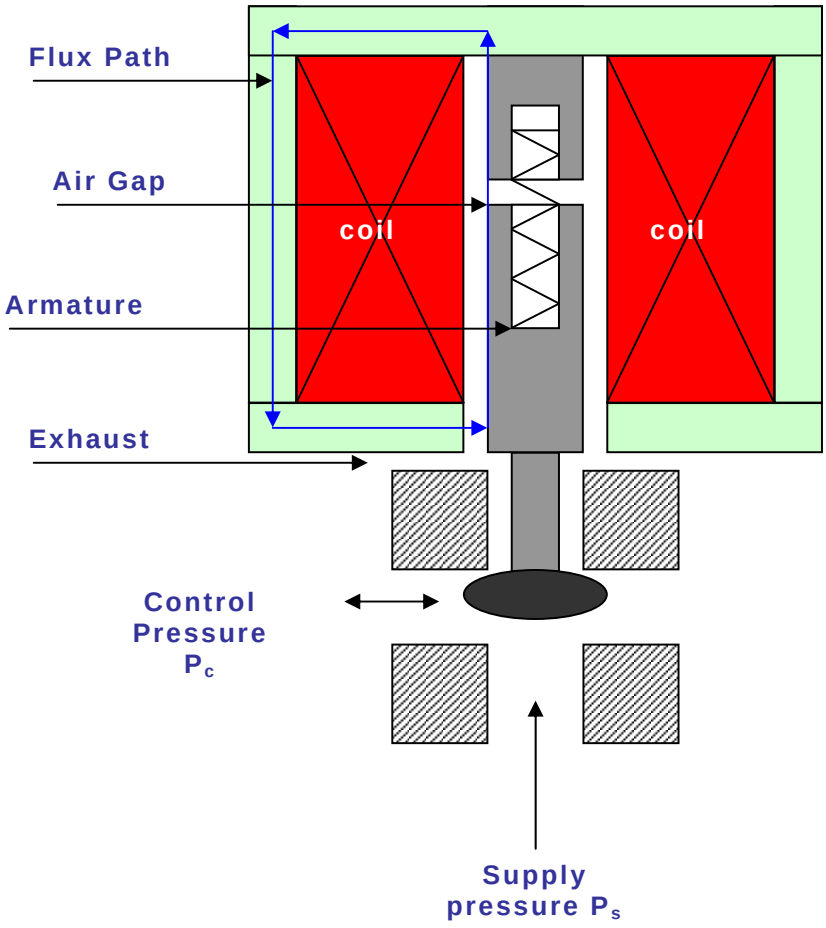

Figure 5.31: Cross section of solenoid actuated hydraulic valve.

Figure 5.31 illustrates the cross section view of a typical solenoid valve which will be used to derive its magnetic circuit equations. The enclosure armature and pole piece are made of mild steel, and the coil is wound around the armature/pole axis. With no current, the internal spring forces press the armature and ball downwards, against the hydraulic force. This blocks the supply pressure P_s, and opens a path from control pressure to exhaust. When the solenoid is energized, the armature and pole come together and the ball opens the supply port and blocks the exhaust port.

According to Faraday´s law, the magnetic flux can be determined, assuming eddy currents and leakage flux are negligible. Therefore

$$\varphi = \frac{v_{sol} - iR}{N}, \tag{5.112}$$

φ is magnetic flux (Wb); v_{sol} is solenoid voltage (V); i is solenoid current (A); R is coil resistance (Z); and N is number of turns.

The magneto motive force required to develop this flux is decomposed into two components; one for steel and another for the air gap. Although the majority of the induction is concentrated at the air gap, the nonlinear properties of the steel components, such as saturation, and hysteresis, may limit the solenoid valve performance.

Therefore the magneto motive force can be expressed as follows:

$$MMF = MMF_{air} + MMF_{steel} \tag{5.113}$$

$$MMF_{air} = H_{air} \times g \tag{5.114}$$

$$MMF_{steel} = H_{steel} \times L_{steel} \tag{5.115}$$

MMF is the magneto motive force (N); H is the magnetic field intensity (A/m); g is the length of the air gap (m); and L_{steel} is the magnetic circuit length in steel (m).

Within the steel, the flux density B is a nonlinear function of H, dependent upon the material properties. Assuming that the steel path has a uniform area A, which relates to φ, B and the air gap, the flux density can be calculated as

$$B = \frac{\varphi}{A} = \mu_0 \times H_{air} , \tag{5.116}$$

A is the cross section area in the air gap (m^2) and μ_0 is the magnetic permeability of air (H/m).

The solenoid force, F_{sol}, and respective current, *i*, are given by:

$$F_{sol} = \frac{0.5 \times B^2 \times A}{\mu_0} \text{ , and} \tag{5.117}$$

$$i = \frac{MMF}{N} . \tag{5.118}$$

The armature response to the solenoid force, as well as to the hydraulic and spring forces, is given by

$$mX'' = F_{sol} + A_0 P_s - K_s X - C_v X' \quad , \tag{5.119}$$

X is armature position (m), M is mass (kg), A_0 is the supply orifice area (m^2),P_s is the supply pressure (Pa), K_s is the spring constant (N/m), and C_v is the damping rate.

The net oil flow directed from the valve to the actuator is equal to the difference between the supply flow and the exhaust flow which causes the valve needle to lift from its seat.

$$q_{net} = q_s - q_{exh} \tag{5.120}$$

$$q_S = K_0 A_0 \text{sign}(P_S - P_C)\sqrt{|P_S - P_C|}, \text{ for } X > 0 \tag{5.121}$$

$$q_S = 0, \text{ for } X = 0 \tag{5.122}$$

$$q_{exh} = K_0 A_0 \sqrt{P_C} \text{ for } X > balltravel \tag{5.123}$$

$$q_{exh} = 0, \text{ for } X = balltravel \tag{5.124}$$

P_C is the control pressure (Pa) and K_0 is the flow coefficient.

The actuating assembly moves the piston against the spring as a function of the control pressure developed behind it. Neglecting the leakage, the variation of the control pressure as a function of time can be expressed as:

$$P_C' = \frac{\beta}{V}\left(q_{net} - X_P' A_P\right), \tag{5.125}$$

$V = X_P A_P$ is fluid volume (m^3), X_P is actuator piston position (m); and A_P is actuator piston area (m^2).

The equation of motion is dominated by the relatively large hydraulic and spring forces, neglecting the existence of leakages and according with the equation of motion (5.126):

$$M_P X_P'' = P_C A_P - K_{SP} X_P \quad , \tag{5.126}$$

M_P is the net actuator mass (kg) and K_{SP} is the spring constant (N/m).

5.5.4.1 Assumptions for the hydraulic injector simulation

In the absence of detailed information on the mechanical and electrical properties of the solenoid valve, the basic timing information from the manufacturer was used as the basis of the solenoid model. Therefore, it was assumed that, time constants for the valve to reach the fully open position was 3 ms and to reach fully closed position was 2ms. The displacement of the armature between fully open and fully closed is assumed to be proportional to the elapsed time.

The hydraulic oil pressure upstream of the solenoid valve and the injector is assumed to be constant since an accumulator is included in the hydraulic circuit. The injector control pressure, P_c, is assumed to range between the upstream hydraulic pressure, P_{hyd}, when the solenoid valve is fully open and atmospheric pressure, P_{atm}, when the valve is fully closed.

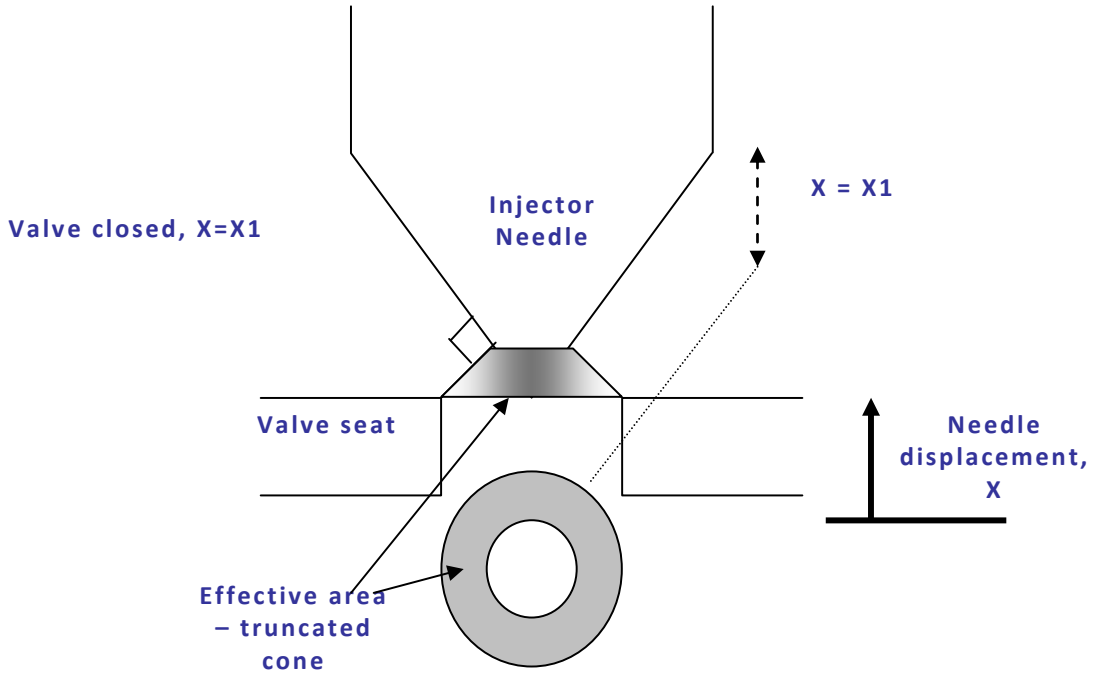

Figure 5.32: Definitions of angles of passages of the injector nozzle

The area of passage for the injector nozzle, as illustrated in Figure 5.32, can be calculated by:

$$A_o = \pi\left(\left(R\sqrt{R^2 + (Rtan\varphi)}\right) - (R - Xsin\varphi sin\varphi)\sqrt{(R - Xsin\varphi sin\varphi)^2 + (Rtan\varphi - Xsin^2\varphi)^2}\right)$$

(5.127)

R is nozzle hole radius (m), θ is needle tip angle (rad) and Φ is θ/2.

The maximum area is the nozzle area, given by:

$$A_{o\,Max} = \pi R^2$$

For non-choked flow, mass flow through the orifice is given by

$$\dot{m} = K_{nv} A P_1 \sqrt{\frac{2M}{RT}\left(\frac{\gamma}{\gamma - 1}\right)\left[\left(\frac{P_2}{P_1}\right)^{2/\gamma} - \left(\frac{P_2}{P_1}\right)^{(\gamma+1)/\gamma}\right]}. \quad (5.128)$$

For choked flow condition we have the mass flow expressed by:

$$\dot{m} = K_{nv} A P_1 \sqrt{\frac{\gamma M}{RT}\left(\frac{2\gamma}{\gamma - 1}\right)^{(\gamma+1)/(\gamma-1)}}, \quad (5.129)$$

K_{nv} is the flow coefficient, A is the orifice area (m^2), P_1 is the H_2 upstream pressure (Pa), P_2 is the in-cylinder pressure (Pa) and T is the upstream H_2 temperature (K).

Choked flow occurs when ratio P_1/P_2 exceeds the critical pressure ratio P_c, given by

$$P_c = \left(\frac{\gamma + 1}{2}\right)^{\gamma/(\gamma-1)} \quad (5.130)$$

5.5.5 DIH_2 injector dynamic simulation

A direct injection injector for gaseous fuels has various objectives to meet:

a) Accurate metering capability. This is the characteristic of the injector to deliver consistently the same amount of hydrogen, when actuated with the same input. This allows the fuel delivered to the engine to be accurately controlled by the Electronic Control Unit, using a control pulse width signal.

b) Good dynamic response. This is characterised by its capability to cope with injection speed and consistency of opening and closing times.

c) The injector should be able to inject the hydrogen at the appropriate pressure.

d) The injector should not have any leakage.

e) The injector should be constructed with materials compatible with hydrogen.

f) The injector moving components should be adequately lubricated.

To achieve the three first requirements, a simulation model using Simulink was developed using the equations presented above. The structure of the simulation model is shown in Figure 5.33.

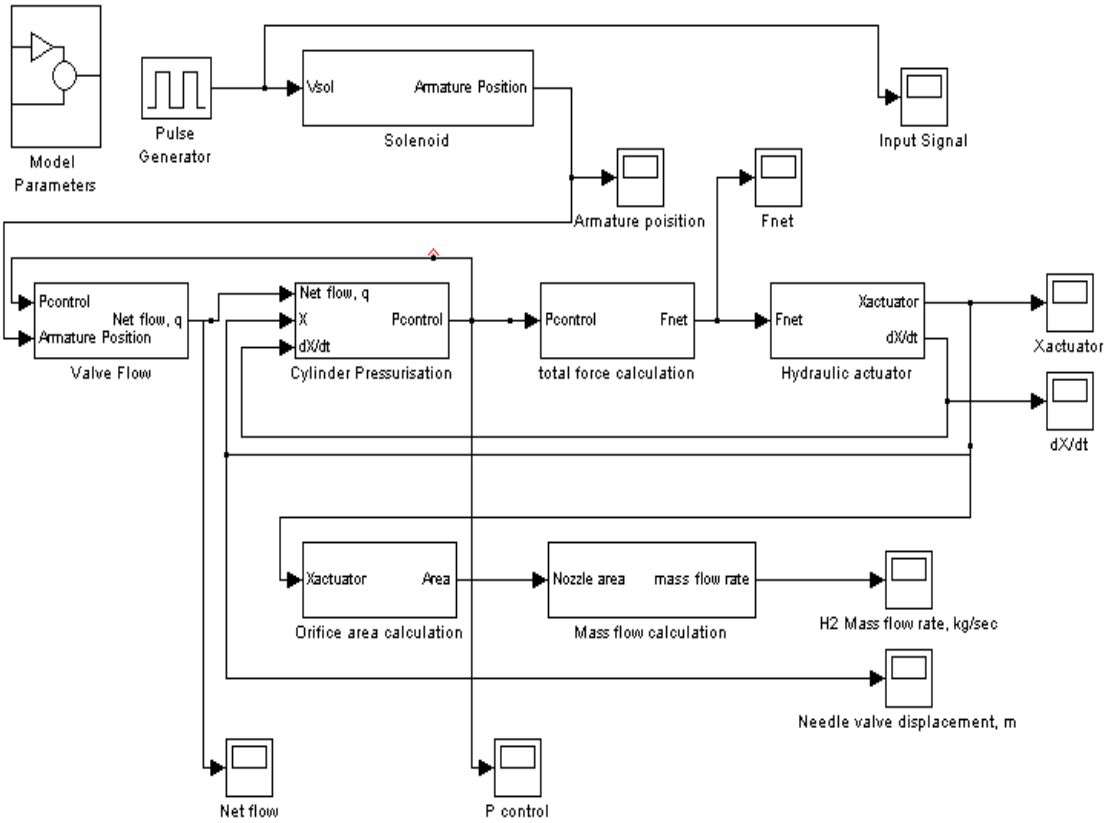

Figure 5.33: Block diagram of hydraulic injector model.

The model is subdivided into the following sub model blocs: orifice area calculation; inlet valve flow; exhaust valve flow; valve flow; total force

calculation; solenoid; critical pressure ratio calculator; choked flow calculation; subsonic flow calculation; mass flow calculation; hydraulic actuator; and cylinder pressurization.

The model parameters used are shown in Figure 5.34, and the structure of the sub models is shown in Figures 5.35-5.44.

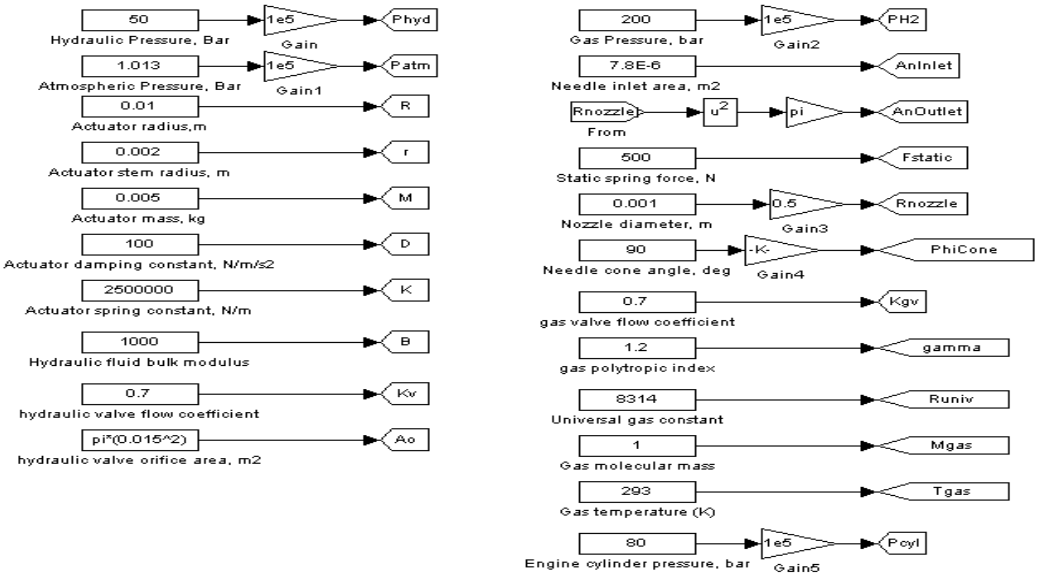

Figure 5.34: Simulation model parameters.

Cylinder pressurization

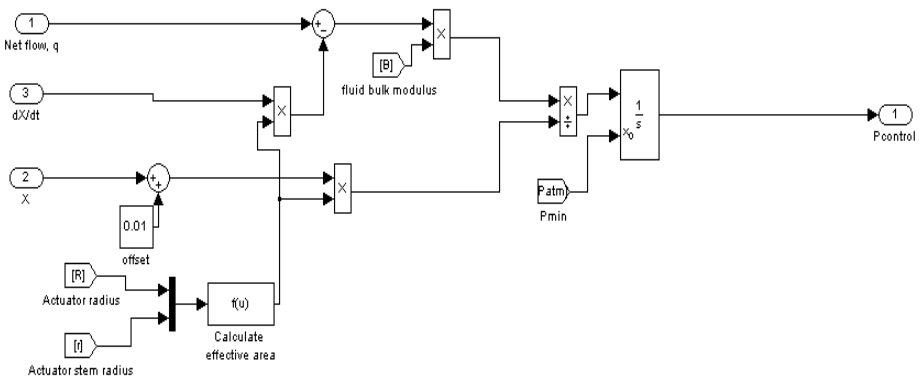

Figure 5.35: Cylinder pressurization.

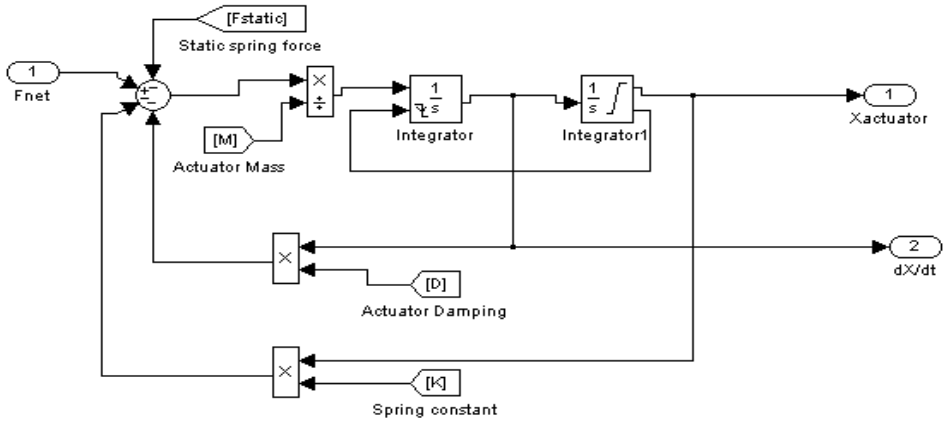

Figure 5.36: Hydraulic actuator sub model.

Flow calculation

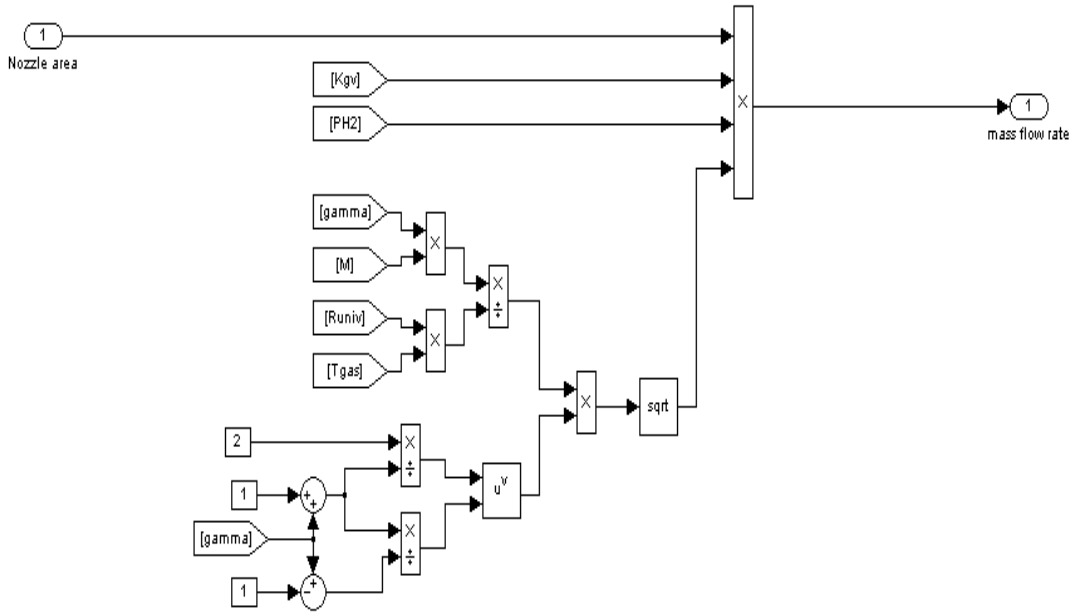

Figure 5.37: Choked flow sub model.

Critical pressure calculation

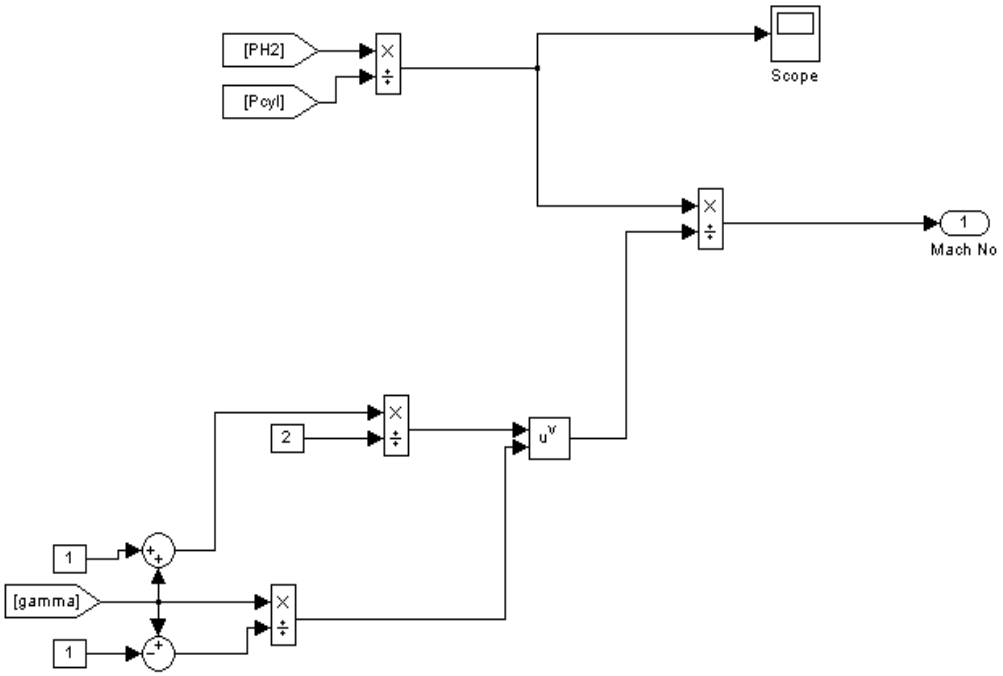

Figure 5.38: Critical flow calculation block.

Subsonic flow calculation

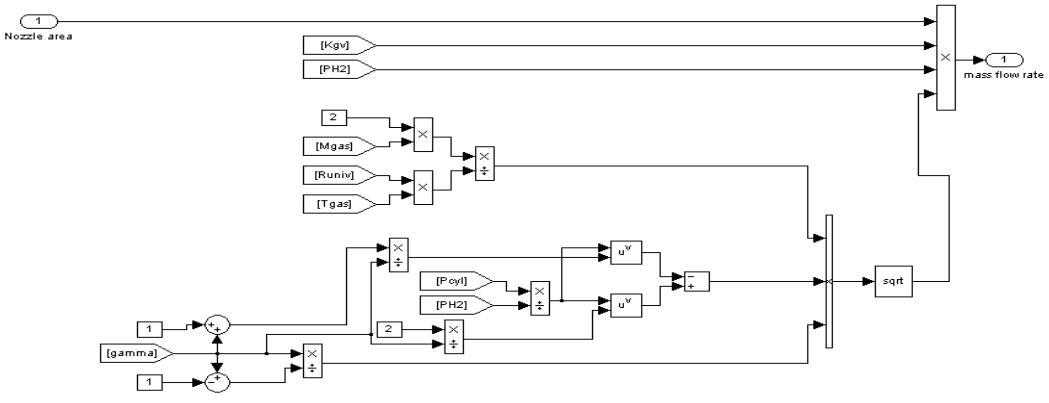

Figure 5.39: Subsonic flow model.

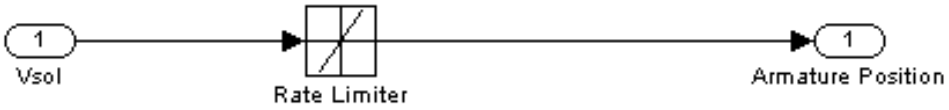

Figure 5.40: Solenoid sub model.

Resultant force sub model

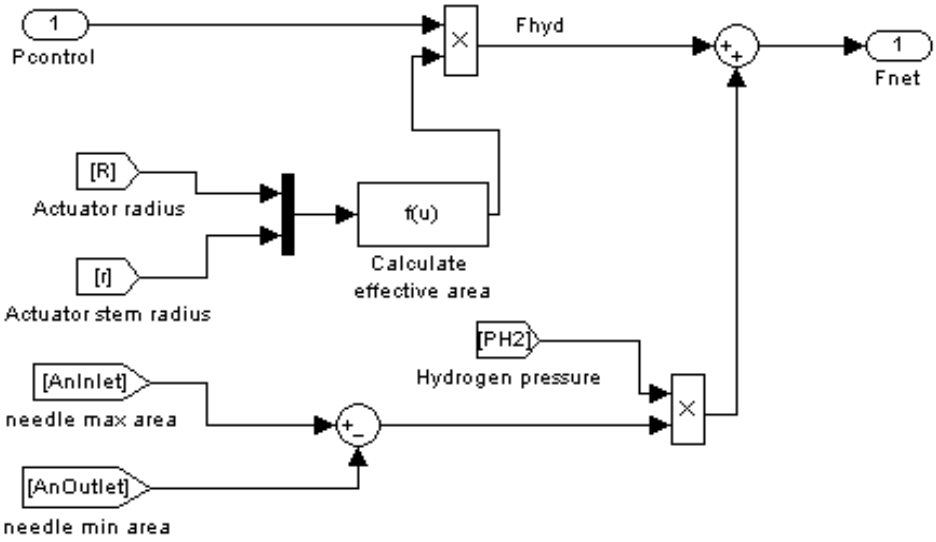

Figure 5.41: Resultant force calculation sub model.

Overall valve flow model

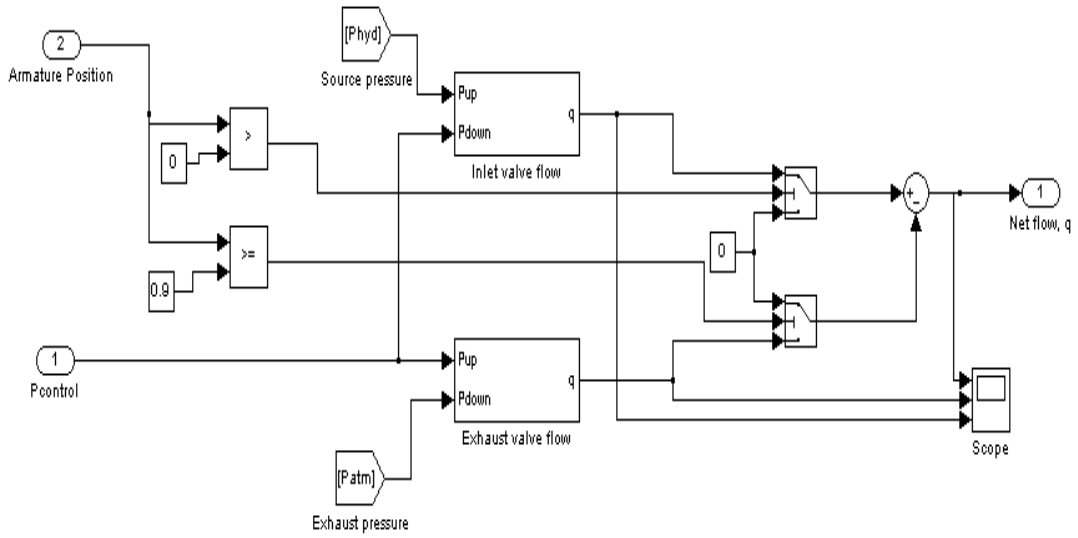

Figure 5.42: Overall valve flow model.

Inlet valve flow

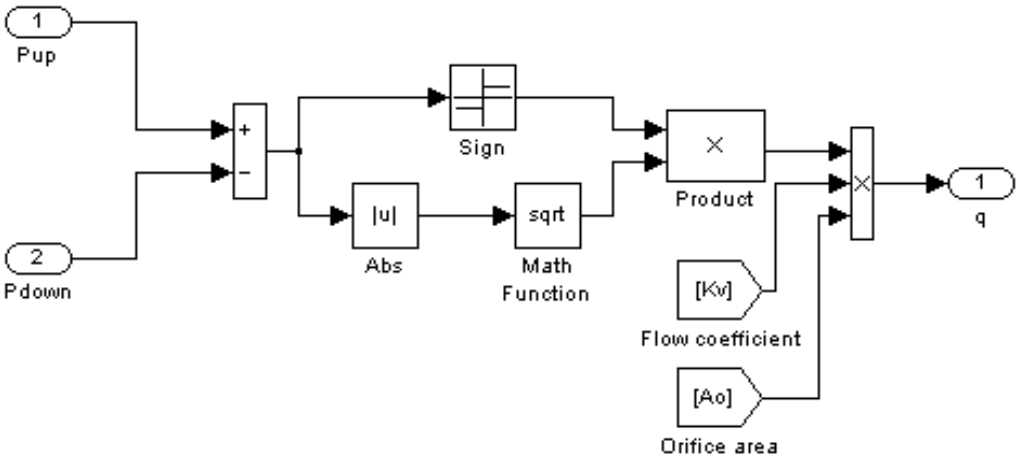

Figure 5.43: Inlet valve flow sub model.

Injection valve sub model

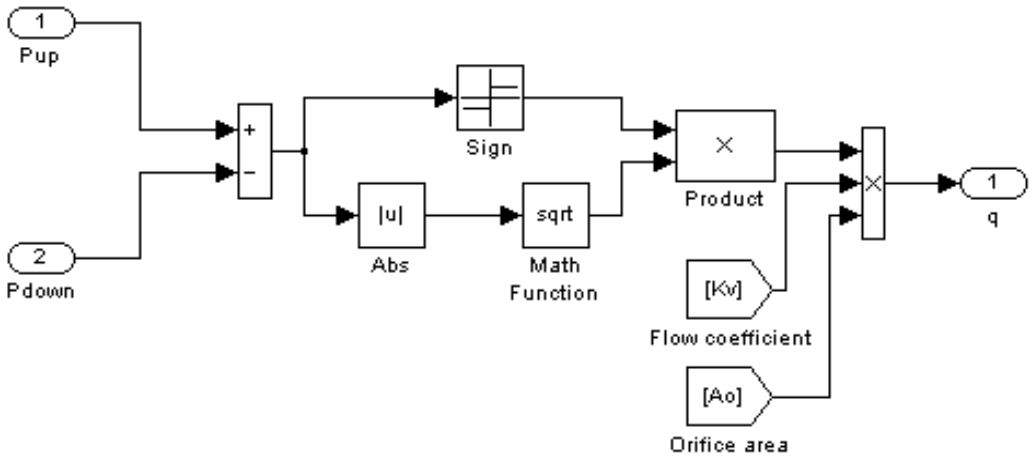

Figure 5.44: Injection (exhaust) valve sub model.

5.6 Summary

The results obtained from a simulation program depend on the suitability of the sub-models used, and assumptions made during the modelling phase. The accuracy of the model is a trade-off between time and effort; therefore it is a balance between effort and accuracy of the results to select the most relevant sub-models. The developed simulation program was oriented towards the research needs, therefore considered the most important sub-models, such as valve modelling, cylinder charge mass variation, Cp variation with temperature, heat release, heat losses, injection timing adjustment, ambient conditions, and a good graphic display capability. While a number of sub-models are generic and were easily adopted from existing models of reciprocating engines, there is a great deal of controversial models used for hydrogen engines, in particular in what concerns the adequacy of certain standard approaches to model heat release and heat losses in hydrogen fuelled engines. It was identified that despite the connection between some sub-models of the air flow calculation and valve lift polynomials revealed some discontinuities, it was very useful as the influence of those discontinuities was not relevant. The

program was found suitable and fundamental for the research carried out, revealing how the engine would perform under operating conditions that could not be achieved with the actual test engine.

This chapter presented the main sub-models of the simulation program, as well as the simulation program structure and functionalities. All the simulation results of this research were based on the sub-models introduced, and their results and conclusions are presented into **Chapter 6 "Performance analysis through simulation"**.

As the simulation work developed during this research is divided into two different systems, engine modelling and injection system modelling, the chapter presents these two systems models separately. The first modelled with the Matlab programming language, the second modelled using Simulink simulation block tools. In what concerns the engine models, further detailed investigations based on experimental work, can lead to even better results through model block improvements, being a recommendation for future development, in particular on the cylinder charge ignition, flame development and injection optimization knowledge .

Most of the engine sub-models used are based on commonly recommended modelling approaches and the engine heat loss model was based on the behaviour of constant volume combustion rather than constant pressure combustion as it was found to be more appropriate for hydrogen due to its combustion behaviour. The injector models introduced in this chapter were used to perform dynamic simulations studies and their results are presented on next chapter. The model of the injector for direct injection of hydrogen is a valuable design tool, and revealed the power of the simulation as the results obtained from practice coincided with the expected results from simulation in particular for setting up of the DIH_2 injection system.

Chapter 6

Performance analysis through simulation

« There is no such thing as a failed experiment, only experiments with unexpected outcomes. »

Buckminster Fuller

This chapter describes the HCCI and DIH_2 engines performance analysis and possible design improvements using the developed simulation program produced from the mathematical models presented in Chapter 5. By using the simulation program, the limitations of the test engine in relation to design and operating variables could be studied. In this chapter, a DIH_2 injector dynamic simulation program is also presented. Simulation results and possible improvements of the engine and injector operation are presented and discussed. For the two modes of engine operation, the research was oriented to study the following: The effect of injection timing and pulsed injection on the control of the rate of pressure rise (RPR) and angle of ignition; the effect of equivalence ratio, compression ratio, air inlet temperature and pressure on engine performance; and the effect of engine speed on the ignition and combustion processes. For the DIH_2 injector, the simulation study was oriented towards identifying the limitations of the prototype DIH_2 injector.

6.1 Hydrogen HCCI model analyses

Data from the test engine was used for the model input parameters. The parameters were divided into geometric and operational.

The geometric parameters included: stroke, bore, connecting rod length, exhaust valve timing, exhaust valve inner and outer diameters, inlet valve

timing, inlet valve inner and outer diameters, compression ratio, clearance volume, speed, volumetric efficiency, inlet valve dwell angle, exhaust valve dwell angle, piston head area, piston head ratio, and piston off-set .

The operational parameters used were: exhaust gas pressure, exhaust gas temperature, cylinder wall, piston head and cylinder head wall temperatures, start of injection, duration of injection, fuelling rate, and lower fuel heating value.

6.1.1 Validation and evaluation of the HCCI model

The HCCI model program was validated by comparing simulated and test data collected at a number of different engine loads. For a set constant fuel rate, injection timing, engine speed, and ambient air temperature and pressure, the following data was recorded: cylinder pressure data, rate of pressure rise, ignition timing, exhaust gas temperature, and power output from the engine.

The output variables that served to compare the test engine with the simulation model were: maximum combustion pressure (P_{max}); angle of maximum combustion pressure (A_{Pmax}); lignition pressure (P_{ign}); angle of ignition (A_{ign}); exhaust gas temperature (T_{Exh}); the maximum rate of pressure rise (MRPR); rate of pressure rise (RPR); engine thermal efficiency; indicated mean effective pressure (IMEP); and brake power (P_b).

To assess the accuracy of the simulation model for HCCI mode of operation, the engine was tested with known ambient and operational conditions that were replicated in the simulation model.

The input variables for the simulation model were: ambient air temperature (T_{ainlet}), ambient air pressure (P_{ainlet}), hydrogen mass fuel rate (m_{H2}), and engine speed (N_e).

The engine was warmed up and the load and temperatures stabilised for ten minutes at each load, prior to recording test data.

The data was taken from the test engine using the developed data acquisition system. Six data sets were recorded at each operating point, and the data was averaged and filtered to remove noise within Labview.

For the tests the engine load was 5.6kW, which was the maximum load achieved in HCCI mode, and the operating conditions were:

$T_{air\ inlet}$ = 90ºC, P_a=101.5 kPa; m_{H2}=7.698g/min ; N_e=2250rpm. Table 6.1 shows the engine test data recorded and the simulation data at this operating point and conditions.

Table 6.1: Comparison between simulated and measured results for HCCI mode of operation.

Variable	Test engine	Engine simulation model	Error
P_{max} (bar)	84.7	86.4	2.0%
AP_{max} (CAº)	354.4º	358º	3.6º
IMEP (bar)	3.6	3.3	7.0%
MRPR (bar/CAº)	63.0	35.6	43.5%
RPR (bar/CAº)	8.1	9.2	12.2%
P_{ign} (bar)	33.0	31.2	5.4%
A_{ign} (CAº)	348	352	4
T_{exh} (ºC)	418	469	10.8%
P_{exh} (bar)	2.0	2.2	10%
Thermal efficiency (%)	36.4	39.5	7.9%
Power (kW)	5.6	6.1	7.8%

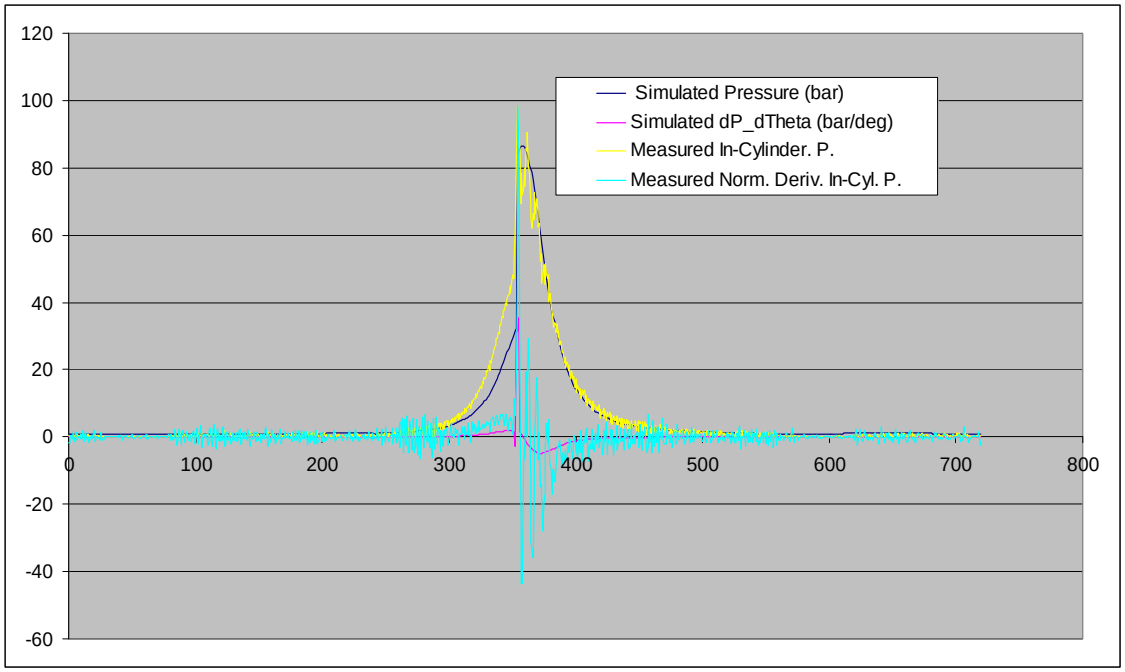

Figure 6.1: Comparison between predicted and measured pressure traces and their derivatives for the HCCI compression ignition engine.

It can be seen by the results presented in Table 6.1 and Figure 6.1 that the RPR and the MRPR have deviations from the average that are not acceptable. The inaccuracies in the simulated results for the parameters are because of the problems in accurately modelling the combustion process. Apart from these parameters, the model output seems to be sufficiently accurate for the purpose of this research work.

6.1.2 Hydrogen HCCI engine operation analysis

As identified during the tests, the HCCI mode of operation can reach thermal efficiencies in the order of 50%, while the emissions are kept to a minimum. Nevertheless it has certain problems that require a design effort if the hydrogen HCCI engine is to become a commercial option in the future.

Problems like difficulty to start, engine control and load limit will be addressed in the following sections.

Due to physical and economic limitations of the experimental engine and testing, simulation was used to explore possible improvements.

In the following section, the control of the ignition angle is characterised and three different systems that can contribute to effecting control of ignition are proposed. The control of the ignition angle through the addition of a second fuel with different ignition properties (see for example Olsson et al, 2000) does not seem practical.

6.1.3 Problems associated with HCCI operation

6.1.3.1 Hydrogen slip during the valve overlap period

Hydrogen slip results in inefficient hydrogen use and the presence of unburnt hydrogen in the exhaust gases. The maximum power developed by the engine is limited by the amount of hydrogen induced and the amount of slip.

This problem can only be slightly improved for HCCI operation by reducing the valve overlap period, i.e. the period when both inlet and exhaust valves are open. Decreasing the valve overlap period increases the amount of residual gases trapped inside the cylinder, which can lead to a drop in engine power and poor combustion. A small amount of this so called internal exhaust gas recirculation can have the advantage of reducing the NOx emissions. However, this should not be above 30% of the exhaust mass flow rate, otherwise the penalty in specific fuel consumption and exaggerated displacement of oxygen in the cylinder becomes too high.

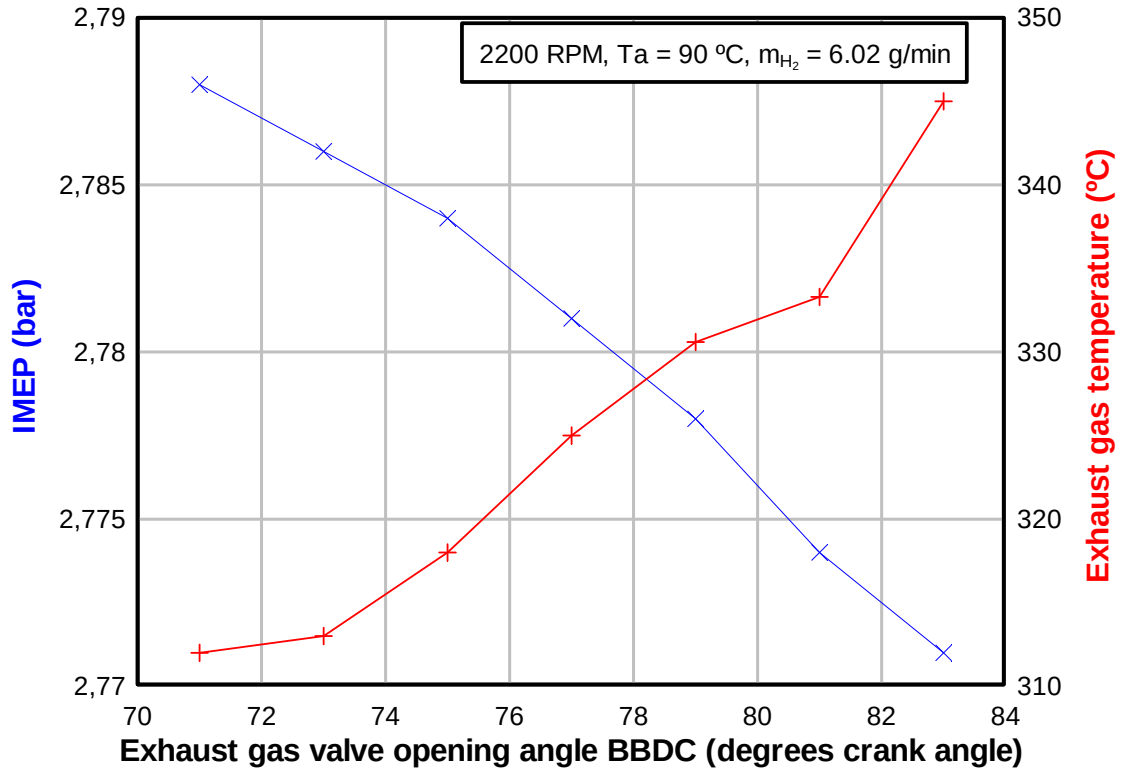

Figure 6.2: Simulated exhaust gas internal recirculation by reduction of valve overlap period.

The simulation program was run for different degrees of valve overlap to study the effects on engine performance. Figure 6.2 shows the results for a hydrogen flow rate of 6.02 g/min and an air inlet temperature of 90ºC. There are two obvious effects resulting from the reduction of the valve overlap period. One is a decrease in the indicated mean effective pressure, therefore a decrease in power and engine thermal efficiency, and the other is a substantial increase of the exhaust gas temperature.

6.1.3.2 High rates of pressure rise.

As mentioned before, the cylinder charge ignition angle of the HCCI engine is dependent on when the ignition temperature is reached during the compression stroke, and it is therefore influenced by the air inlet temperature. Figure 6.3 shows the angle of ignition for different inlet air

temperatures for an engine running at 2200 rpm and with a hydrogen flow rate of 6.2 g/min.

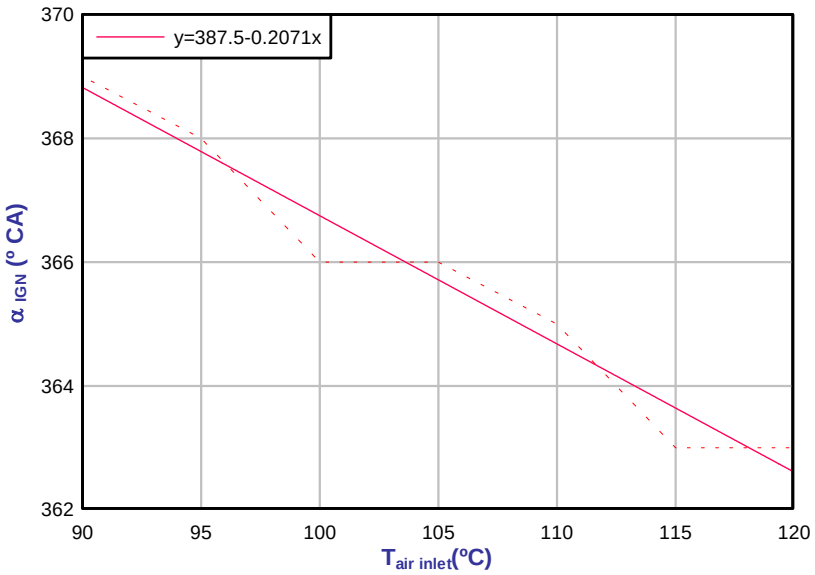

Figure 6.3: Simulated angle of ignition for different air inlet temperatures.

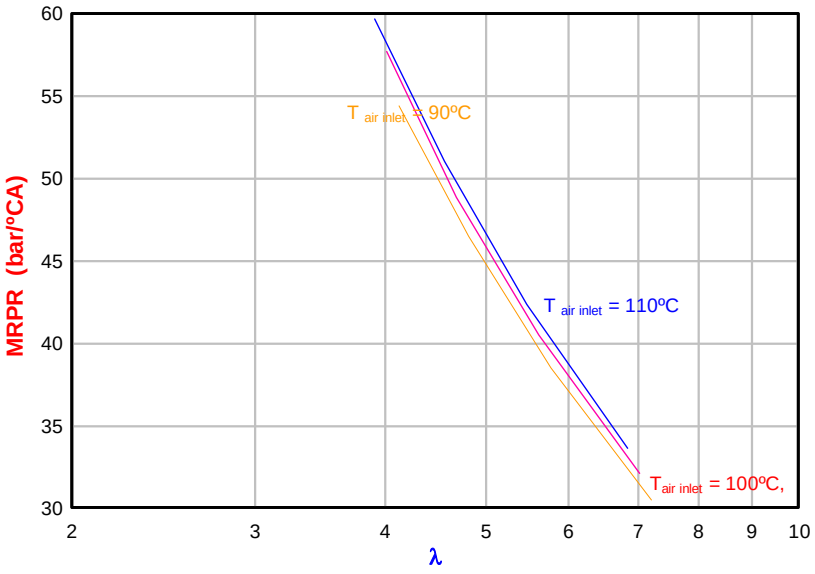

Figure 6.4: Dependence of the MRPR as a function of Tair inlet and λ.

Figure 6.4 shows the rate of pressure rise for different air inlet temperatures and the relationship with excess air ratio λ and cylinder inlet temperature $T_{air\ inlet}$. This is an important engine operating parameter, since it indicates the level of piston force transferred to the engine crankshaft. It can be seen from Figure 6.4 that the rate of pressure rise depends heavily on the excess air ratio and to some degree on the temperature of the air at the cylinder inlet.The maximum rate of pressure rise for HCCI engine operation is more than the double that of diesel operation, and above the maximum recommended 12 bar/°. It is therefore critical that the operating characteristics of the HCCI engine are taken into account in the mechanical design of the engine.

6.1.3.3 Power limitation of the HCCI engine

The power output of the HCCI engine is limited by the volume of hydrogen that can be induced per stroke. Theoretically, for a stoichiometric hydrogen-air mixture, the (gaseous) hydrogen makes up approximately 30% of the cylinder displacement volume. Induction of a larger quantity of hydrogen using port injection can not increase engine power. Due to the low density of hydrogen, a stoichiometric hydrogen-air mixture has an energy content of approximately 83% of that of a gasoline-air mixture. This reduces the engine power output of a pre-mixed hydrogen engine by around 30% compared to a gasoline engine.

A possible way to get around this limitation would be the injection of hydrogen into the cylinder at a pressure slightly higher than the one used with port injection during the first degrees of crank angle while the piston is starting the charge compression, in this case it might be considered to fall in the category of direct injection engine.

6.1.4 Possible design improvements using simulation

Following the results presented for HCCI operation, design improvements are recommended to ensure that the engine can operate reliably. These are:

a) Stronger piston rings and higher load bearings, to withstand the higher dynamic shock loads. b) An inlet air heating system utilising the exhaust gas heat. c) Hydrogen injection control ensuring injection only after exhaust valve closing, to avoid hydrogen slip. d) Control of the temperature of the air at the engine inlet, the excess air ratio, and the injection duty cycle, using engine knock as a feedback signal. e) Flame screens fitted on the air manifold, and a connecting pipe fitted between the crank case and the inlet manifold, to improve safety by removing blow-by hydrogen.

Results from the test engine and simulation study show that the HCCI operation has a number of problems that need to be addressed, namely:

- Poor combustion control.
- Maximum power limited by the amount of hydrogen induced.
- Hydrogen slip during the valve overlap period.
- High rates of pressure rise.
- Safety issues, such as air inlet manifold backfires.

6.1.4.1 Combustion control and dependence of the inlet air temperature

These problems are characterised by the absence of any timed ignition mechanism able to ignite the cylinder charge at a pre-defined crank angle.

The ignition timing on the HCCI engine is dependent on the temperature of the cylinder charge; therefore the test engine performance is sensitive to the air temperature entering the cylinder. Increasing inlet air temperature leads to advanced ignition, and vice versa, as shown in Figure 6.3.

This problem can be solved by increasing the engine compression ratio to an extent that the self-ignition temperature of the hydrogen-air charge is reached at a certain desired angle without heating of the inlet air. If this solution is implemented, an intake air heating system may not be necessary, and the engine will be able to start without pre-heating. If a variable compression ratio system is implemented, this can be adapted to control ignition timing based on the actual local temperature of the ambient air.

Another option involves the use of two different fuels; in this case, hydrogen and another fuel with a different ignition temperature. Varying the composition of the fuels mixture can allow the ignition angle to be controlled (Olsson et al, 2000).

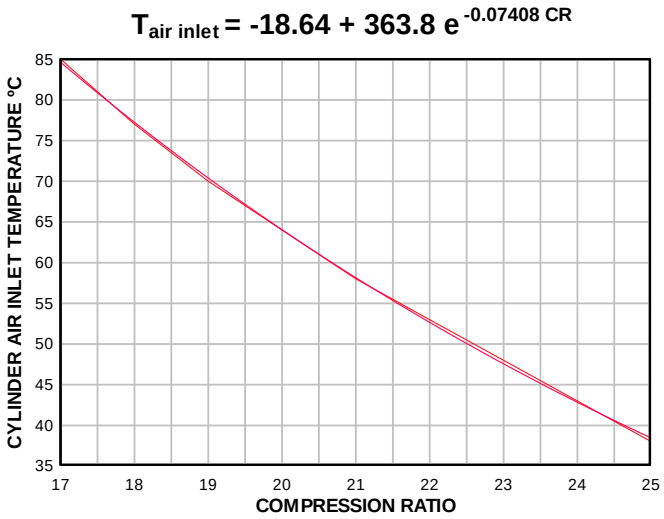

Figure 6.5: Simulated relationship between the minimum cylinder air inlet temperature required to maintain combustion and the engine compression ratio.

Figure 6.5 shows the simulated relationship between the compression ratio and the required inlet temperature for a constant speed of 2200 rpm and hydrogen mass flow rate of 9g/minute. This relationship shows that a compression ratio of the order of 25:1 could ensure combustion with a temperature of the air at the cylinder inlet of 38ºC.

Operating an engine with such high compression ratio results in the control of its combustion process being performed by the quantity of hydrogen injected in the inlet port i.e. becomes a PWM controlled process, independent of the air inlet temperature.

However, increasing the compression ratio to 25:1 will require stronger engine components.

Figure 6.6 shows the effect of inlet air temperature over the indicated power and mean effective pressure. As expected, an increase in inlet air temperature results a decrease in the engine power output due to the reduced density of the cylinder charge.

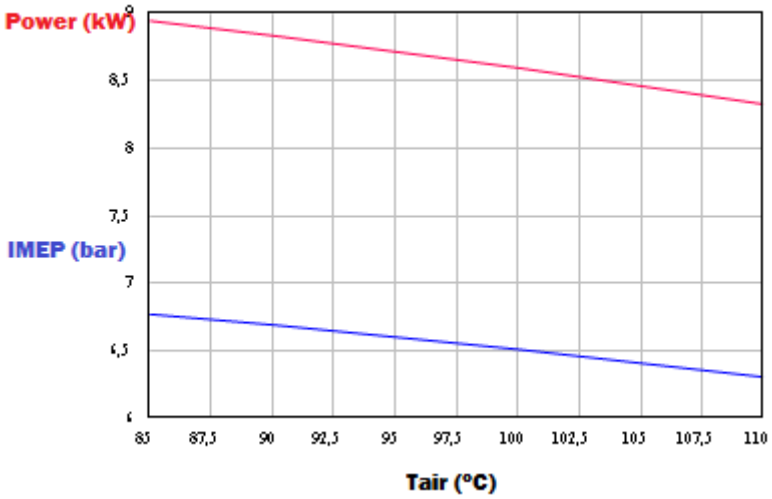

Figure 6.6: Simulated effect of the air inlet temperature on the IMEP and indicated power.

6.2 Hydrogen direct injection engine model validation

The DIH_2 engine model is basically the same as that used for the HCCI engine, as the engine used for testing is the same. The model shares the same routines and sub models presented previously.

By selecting the mode DIH_2 mode of operation, the DIH_2 injection parameters are enabled, and the model assumes that the chosen quantity of hydrogen is being introduced in the cylinder according with the injection timing and duration set. With respect to the ignition delay and timing, the model assumes that ignition will take place only when the self ignition temperature of hydrogen is reached. Therefore it is dependent on the operational and ambient conditions set as inputs. The DIH_2 model program was validated through a comparison between simulated and test data collected from a number of simulation runs and comparative engine tests. Data was acquired for a set constant fuel rate, injection timing, engine speed, and ambient air temperature and pressure. Cylinder pressure data, rate of pressure rise, ignition timing, exhaust gas temperature, and power output were recorded from the engine.

To assess the accuracy of the simulation model for the DIH_2 mode of operation, the engine was tested with known ambient and operational conditions that were replicated in the simulation model.

The input variables used for the simulation model were: ambient air temperature, ambient air pressure, hydrogen mass fuel rate, and engine speed.

The output variables that served to compare the test engine with the simulation model were: maximum combustion pressure (P_{max}), angle of maximum combustion pressure (AP_{max}), ignition pressure (P_{ign}), angle of ignition (A_{ign}), exhaust gas temperature (T_{Exh}), rate of maximum pressure rise (MPRP), rate of pressure rise (RPR), engine thermal efficiency, indicated mean effective pressure (IMEP) and brake power (P_b).From the DIH_2 simulation model other variables are also available, such as the excess

air factor (λ), the maximum combustion temperature (T_{max}), rate of heat release (RHR), air mass flow rate and polytropic index (n).

The engine was warmed up and the temperatures and pressures stabilised for ten minutes at each load, prior to recording test data.

The data was taken from the test engine using the developed data acquisition system, as described above.

Six data sets were recorded at each operating point. The data was averaged and filtered to remove noise within Labview. For the tests conducted at a load of 6kW, the operating conditions were:

Table 6.2: Comparison between simulated and measured results for the DIH_2 mode of operation at 6.0 kW load.

$T_{air\ inlet}$ = 90ºC, P_a=101.5 kPa; m_{H2}=7.698g/min ; N_e=2250rpm.

Variables	Test engine	Engine simulation model	Error
Pmax (bar)	78.8	81.7	3.5%
APmax (CAº)	364	369	5º
IMEP (bar)	4.0	4.1	3.0%
MRPR (bar/CAº)	72	28	60%
RPR (bar/CAº)	13.4	14.1	6.0%
Pign (bar)	40	42	4.7%
A_{ign}(CAº)	361	366	5º
Texh (ºC)	403	410	1.7%
Pexh (bar)	2.4	2.5	3.0%
Thermal efficiency (%)	39.0	41.0	4.8%
Power (kW)	6.0	6.4	5.0%

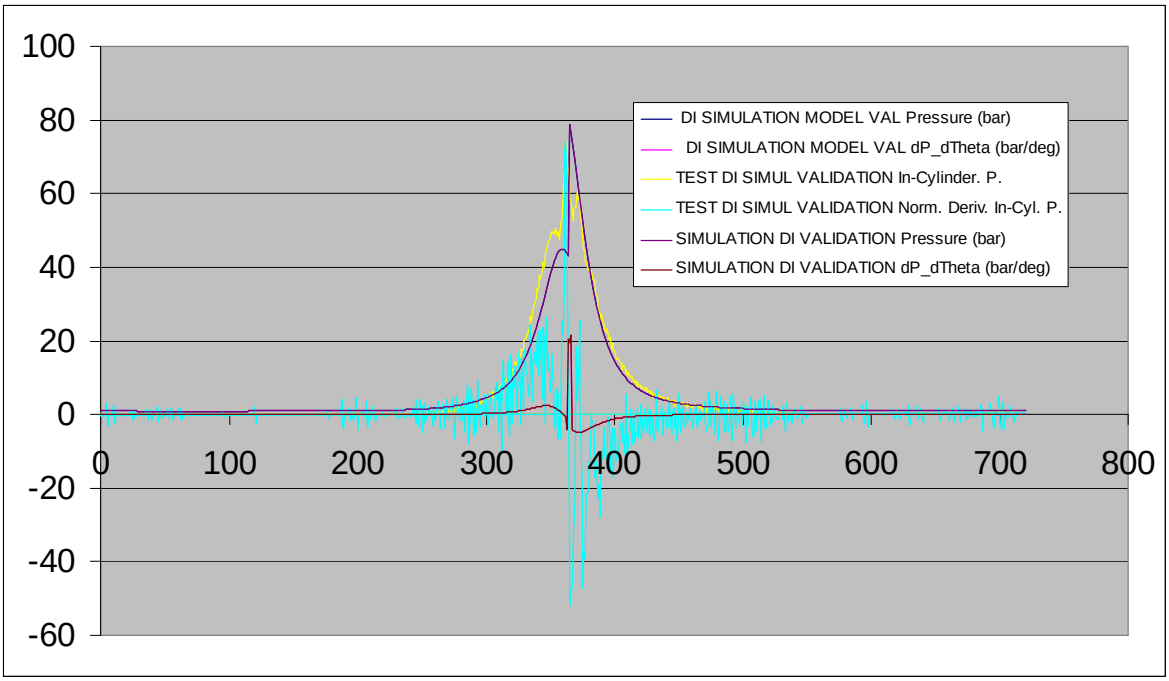

Figure 6.7: Comparison between predicted and measured pressure traces and their derivatives for DIH_2 mode operation.

It can be seen from the results presented in Table 6.2 and Figure 6.7 that only the RPR and the MRPR have deviations that are not acceptable. The inaccuracies in the simulated results are due to the challenges associated with accurately modelling the combustion process. Apart from these parameters, the model output seems to be sufficiently accurate for the purpose of this research work.

6.2.1 DIH_2 engine design and operational analysis

The diesel engine operated with direct injection of hydrogen has a number of advantages over the other modes of operation tested during this research. These are a higher power to weight ratio, very low exhaust gas emissions, no back firing and good control of the combustion process. It also has some problems that need to be overcome.

Like the HCCI mode of operation, the DIH_2 engine depends on the inlet air temperature to ensure combustion. This is particularly important in what regards ignition delay, affecting essentially the MRPR. The angle at which the ignition of the cylinder charge takes place during the cycle is not so

dependent on the air inlet temperature since the hydrogen is injected in the cylinder only when desired, at any crank angle after the ignition temperature has been reached. However, the mechanical loads related to the MRPR must be considered and it is important that measures to control this are taken.

One method to control high MRPR values is by using pulsed injection and appropriate inlet valve timing. Unfortunately, the hydrogen injector for direct injection which was manufactured for this research was not fast enough to perform pulsed injection. However, pulsed injection and modified inlet valve timing were investigated using the simulation model of the engine.

The ignition delay period forms the first phase of the combustion process, and is dependent on the properties of the hydrogen-air mixture. The second phase consists of the spread of the flame from the initial point of ignition to the main body of the cylinder charge. There is a rapid increase in pressure during this phase and the rate of pressure rise depends to some extent on the availability of oxygen next to the hydrogen spray, which in turn depends on the turbulence in the cylinder. Since hydrogen is injected into the cylinder in its gaseous phase, its mixing with air is extremely fast. Due to the very large excess of air, oxygen is available for combustion during this phase throughout the whole cylinder volume. Therefore, as the engine speed increases the rate of pressure rise also increases, and can result in engine knock. During the third phase of combustion the fuel burns as it is injected into the cylinder, giving more controlled combustion than in phase two. One of the main factors affecting the combustion in the controlled combustion phase is the gas motion (swirl and squish effects) which is governed by the shape of the combustion chamber.

6.2.2 Control of MRPR and engine optimisation

A number of tests and simulation studies were conducted to understand the effect of the injection timing and the use of pulsed injection over the thermodynamic cycle, and how these variables can help to control the MRPR.

Injection profile and timing

Injection is characterised by its timing, frequency of the injection profile (pulse), its injection duration, and by the angle at which the injection is started. These parameters are expressed in terms of the crank angle. The injection profile can be continuous, i.e. normal injection, being characterised by a single square-shaped pulse with rapid opening and closing and approximately constant fuel flow, or pulsed; where the injector is opened and closed a number of times during the injection angle, thus controlling the rate at which fuel is entering into the cylinder, and consequently the rate of heat release.

Unfortunately it was not possible to implement experimentally this solution, as the injector which was manufactured did not have a sufficiently fast dynamic response. High frequencies of operation, as well as accurate control, are essential requirements for pulsed injection. Therefore, this was investigated using the developed engine model and simulation program.

The frequency of the injection pulse profile during the injection angle depends on the engine speed and according to the Nyquist theorem Richards et al. 1979, the injection model needs to run at a frequency at least three times the injection frequency, if it is required to operate in the same time interval as the injection process under study. Another important aspect that was identified during the simulation study of pulsed injection was that, for high injection frequencies (typically above 1.0 kHz), if the

duty cycle is above 40%, then the pulsed injection approaches the continuous injection behaviour, therefore not producing any effect.

Each of the injection timing combinations resulted in a different engine cycle performance, and the simulation program was used to investigate the most appropriate optimal combination that can meet the objectives previously stated. In order to isolate the influences of the other engine parameters, from the injection timing results, all the engine operational parameters were kept constant.

The injection timing and duration simulation studies were performed for the conditions shown in Table 6.3:

Table 6.3: Operating parameters of the engine for injection timing and duration simulation studies.

Engine Parameters	**Values**
Ambient temperature (ºC)	80
Ambient pressure (kPa)	101.3
Engine speed (RPM)	2200
Exhaust gas back pressure (kPa)	101.3
Cylinder wall temperature (ºC)	250
Piston crown temperature (ºC)	300
Cylinder head temperature (ºC)	280
Angular resolution (CAº)	0.5
Ignition delay (ms)	1.2
Heat rate (kJ/kg)	18.0

The following tables and figures show the simulation results for continuous injection, pulsed injection and the optimised injection of hydrogen.

The following limits served as guide lines for the simulation:

Maximum combustion pressure of the same order as for diesel oil operation at corresponding loads;

Maximum rate of pressure rise of the same order as for diesel oil operation at corresponding loads <8°ca;

Angle of maximum pressure > 5°ca;

Continuous injection simulation

Three simulation studies were performed for continuous injection of hydrogen. The results are presented in Tables 6.4 to 6.6 and Figures 6.9 to 6.17.

Study 1: Continuous injection, duration 30°, start of injection 25° BTDC

Table 6.4: Engine performance for continuous injection, Study 1.

PB_{maxB} (bar)	98
α PB_{maxB} (θ°)	4
TB_{maxB} (°C)	1826
αTB_{maxB} (θ°)	3
IMEP (bar)	4.50
PB_{iB} (kW)	6.8
RPR (bar/°)	6.11
MRPR (bar/°)	61.86

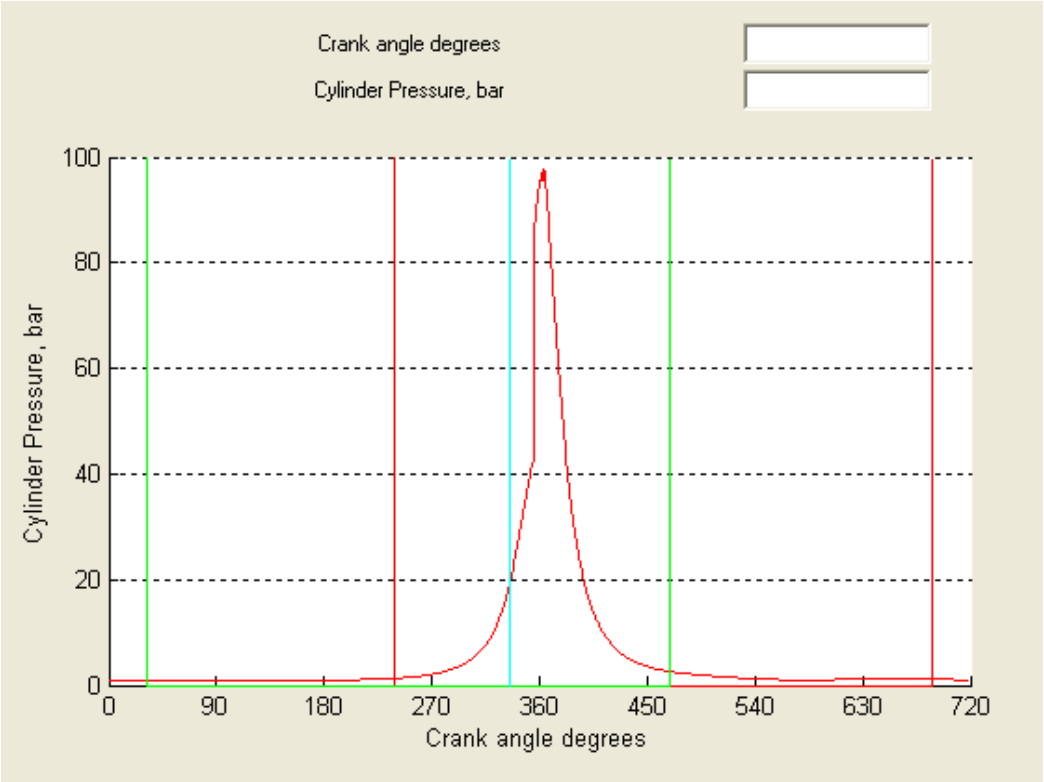

Figure 6.8: Open cycle diagram for Study 1.

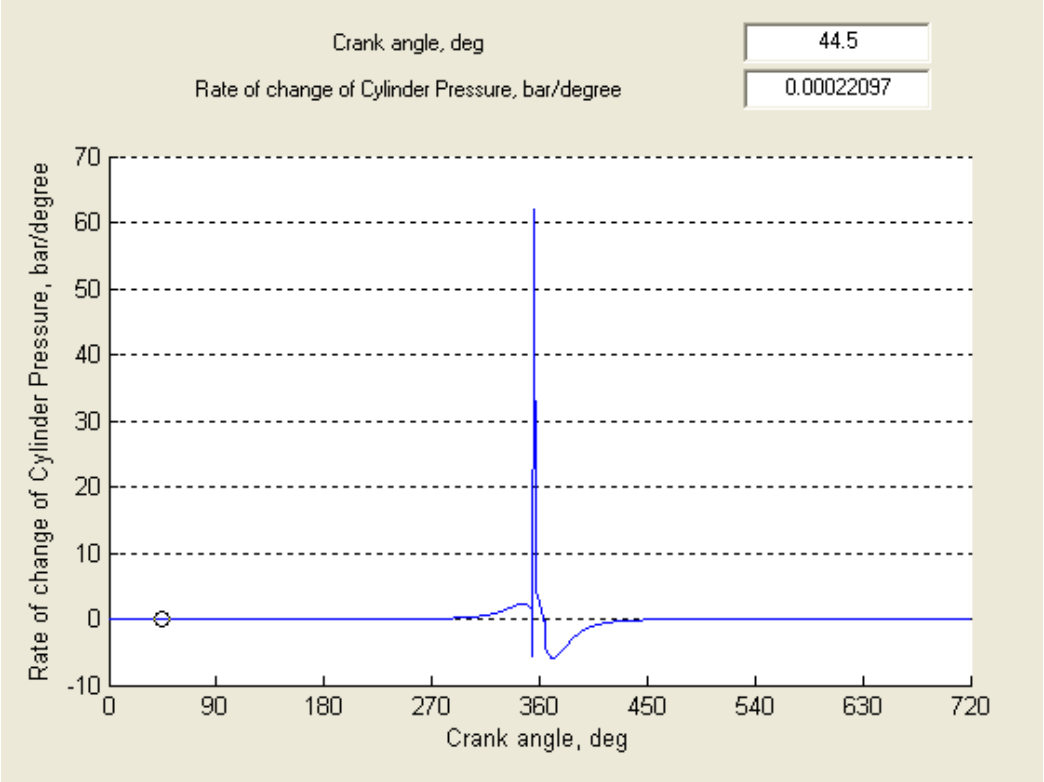

Figure 6.9: Rate of change of cylinder pressure for Study 1.

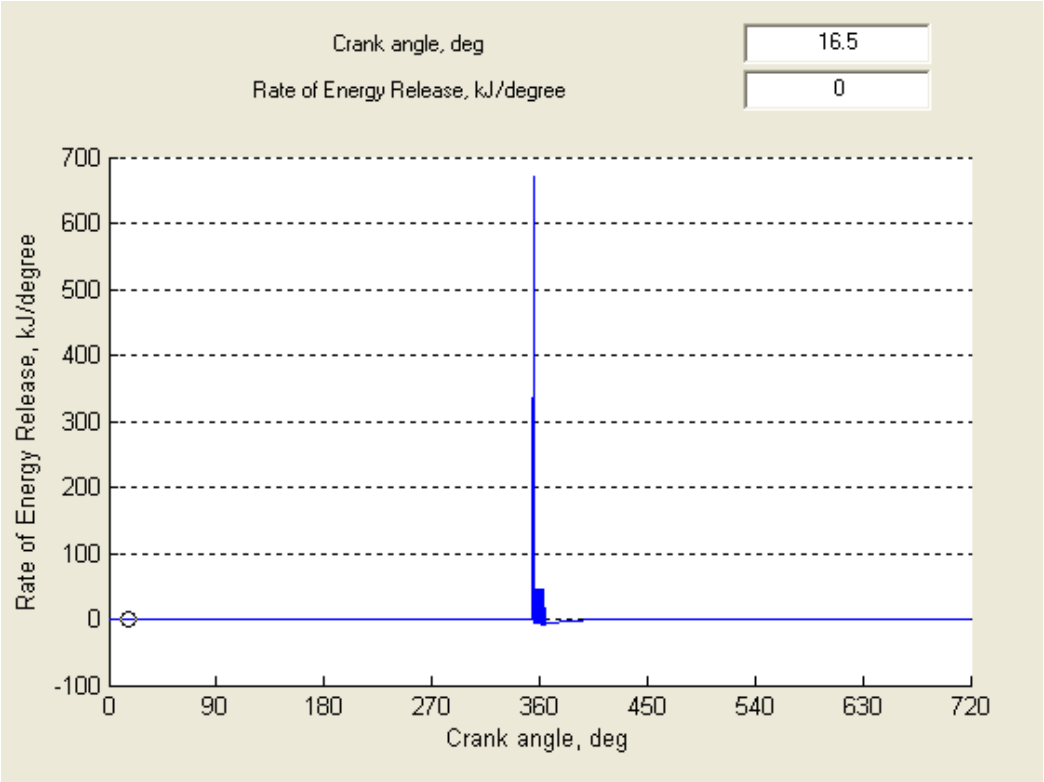

Figure 6.10: Rate of energy release diagram for Study 1.

Study 2:

Continuous injection, duration 25°, start of injection 25° BTDC

Table 6.5: Engine performance for continuous injection, Study 2.

PB_{maxB} (bar)	105
α PB_{maxB} (θ°)	-1
TB_{maxB} (°C)	1934
αTB_{maxB} (θ°)	-1
IMEP (bar)	4.53
PB_{iB} (kW)	6.85
RPR (bar/°)	13.73
MRPR (bar/°)	73.46

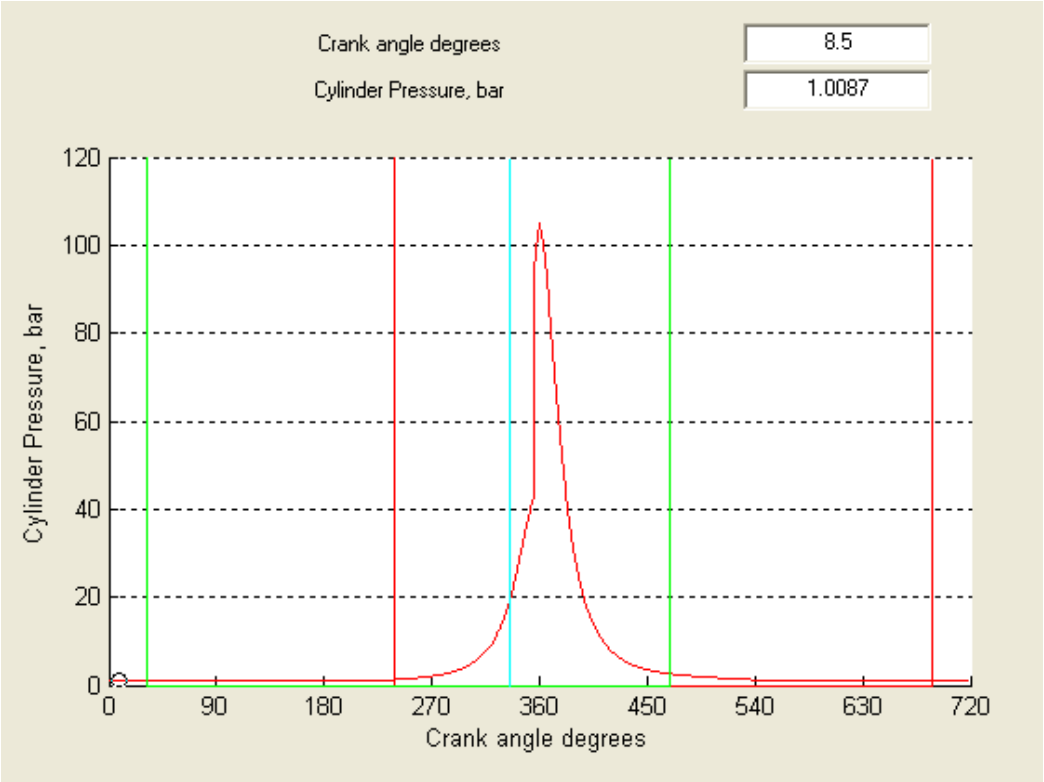

Figure 6.11: Open cycle pressure diagram for Study 2.

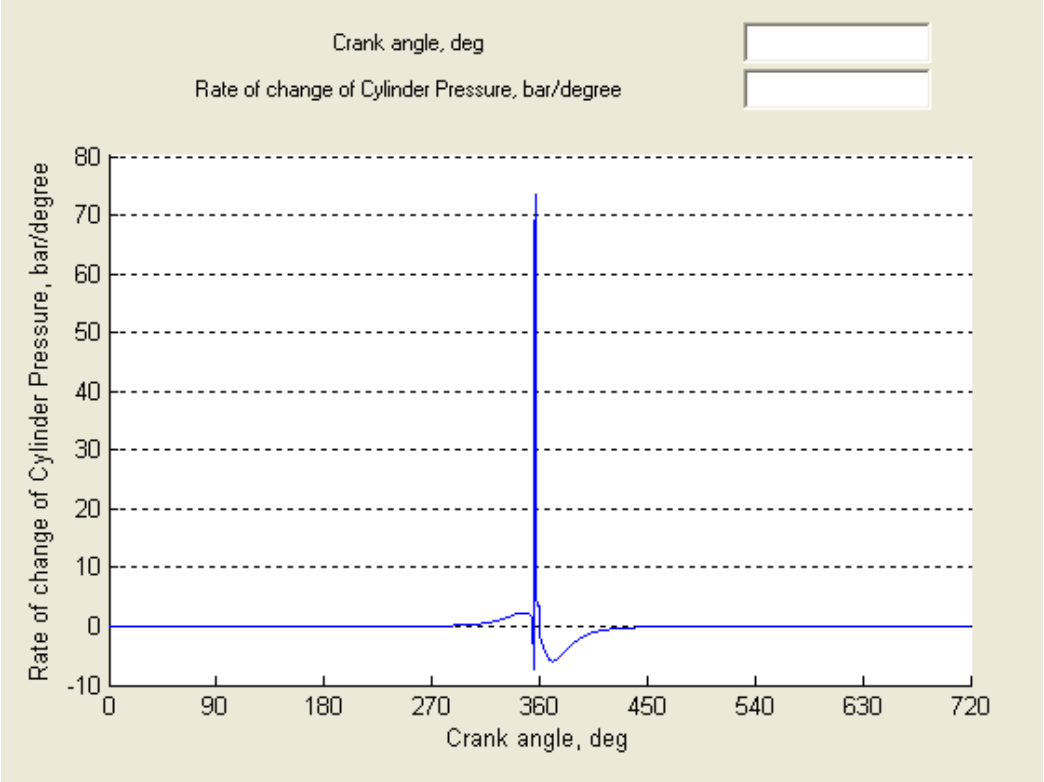

Figure 6.12: Rate of change of cylinder pressure diagram for Study 2.

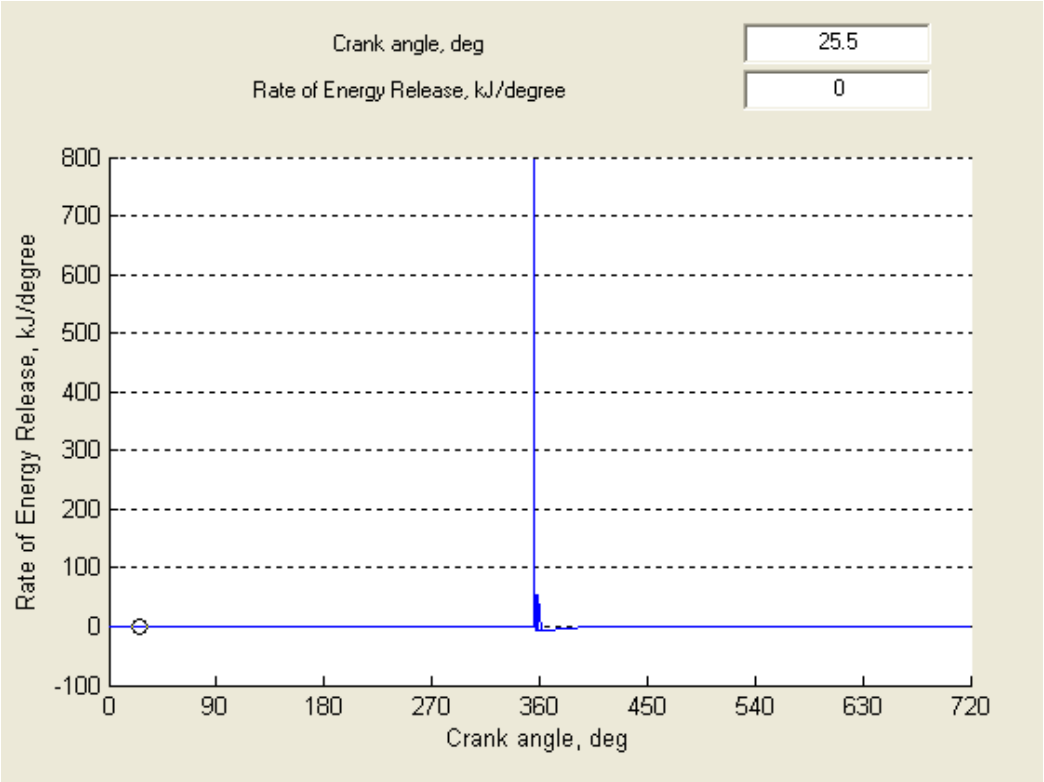

Figure 6.13: Rate of change of cylinder pressure for Study 2.

Study 3:

Continuous injection, duration 25°, start of injection 30° BTDC

Table 6.6: Engine performance for continuous injection, Study 3.

PB_{maxB} (bar)	107
α PB_{maxB} (θ°)	-4
TB_{maxB} (°C)	2009
αTB_{maxB} (θ°)	-3
IMEP (bar)	4.62
PB_{iB} (kW)	6.98
RPR (bar/°)	21.4
MRPR (bar/°)	85.31

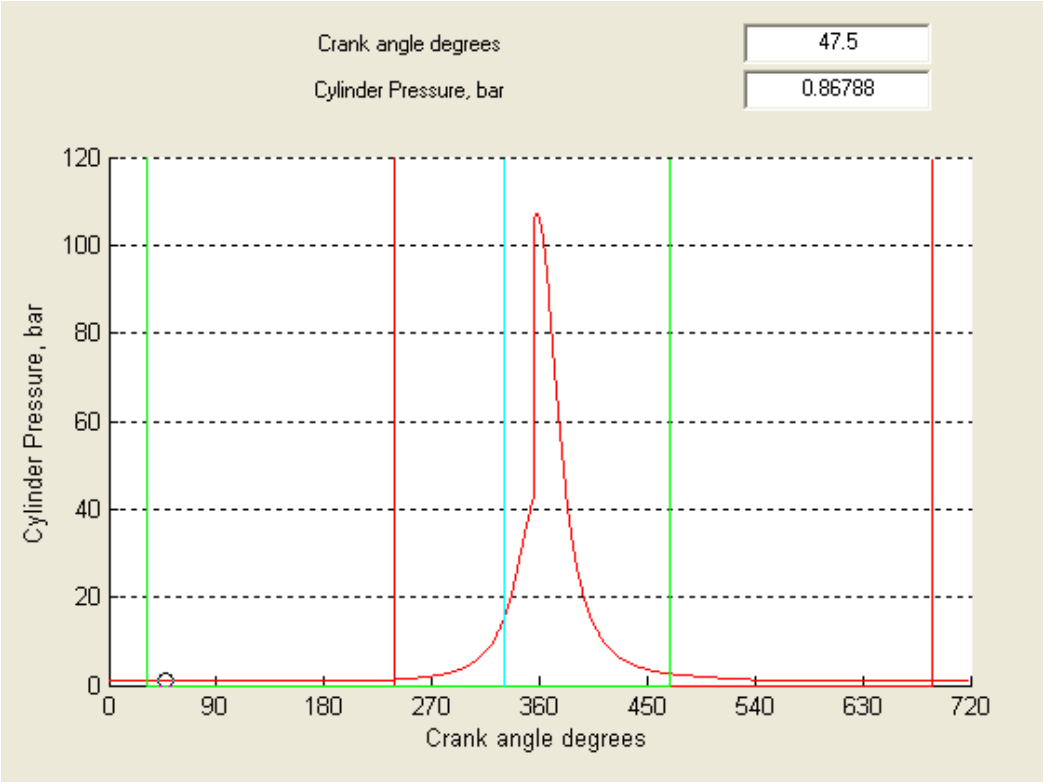

Figure 6.14: Open cycle diagram for Study 3.

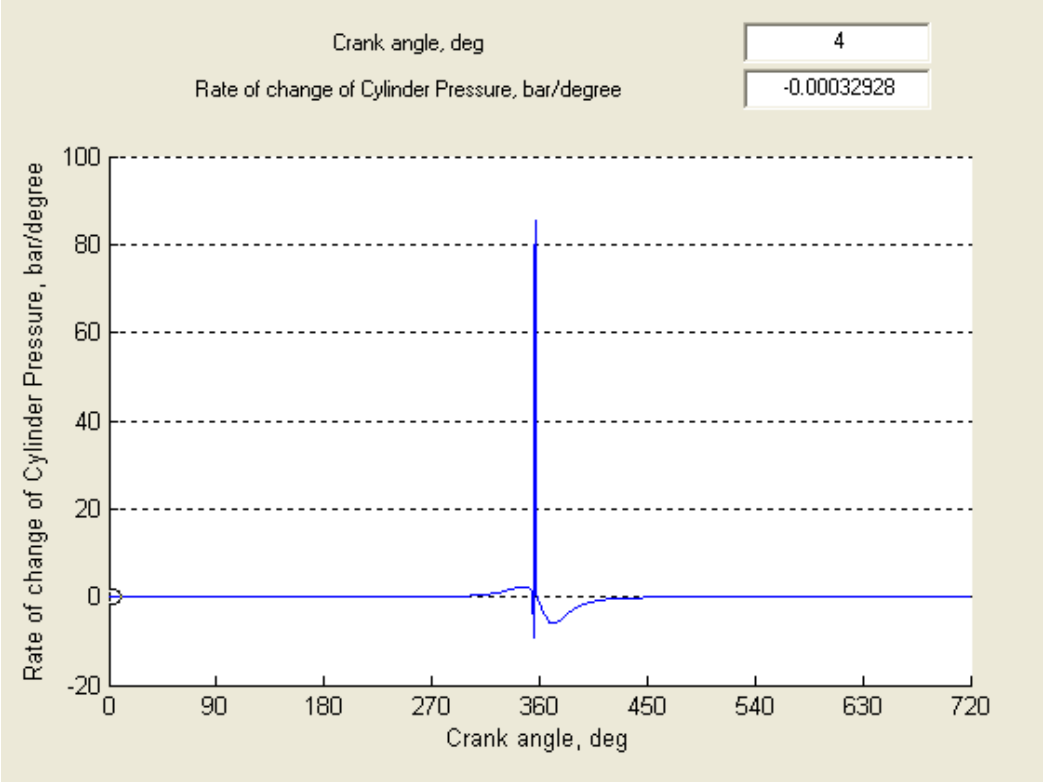

Figure: 6.15: Rate of change of cylinder pressure diagram for Study 3.

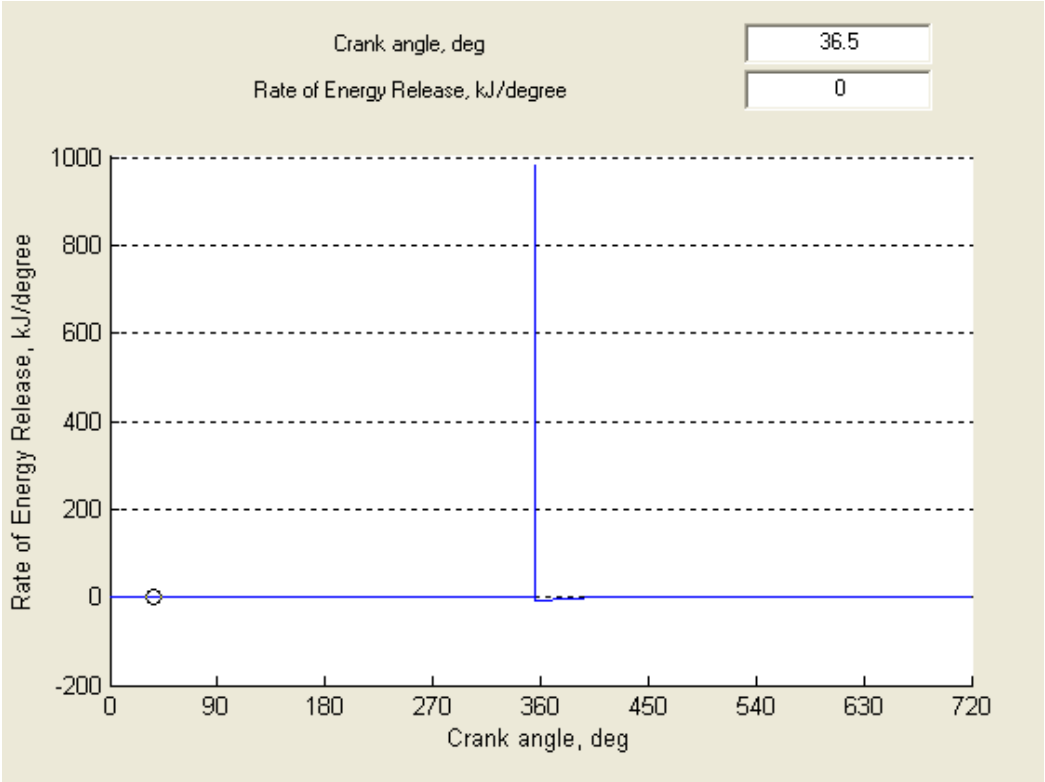

Figure 6.16: Rate of energy release diagram for Study 3.

Pulsed injection simulation

Five simulation studies were performed for the case of pulsed injection of hydrogen. The results are presented in Tables 6.7 to 6.11 and Figures 6.17 to 6.28.

Study 4:

Pulsed injection, duration 30°, start of injection = 25° BTDC

Table 6.7: Engine performance for pulsed injection, Study 4, frequency 10kHz, duty cycle 40%.

PB_{maxB} (bar)	95
α PB_{maxB} (θ°)	5
TB_{maxB} (°C)	1775
αTB_{maxB} (θ°)	3
IMEP (bar)	4.42
PB_{iB} (kW)	6.68
RPR (bar/°)	5.92
MRPR (bar/°)	58.92

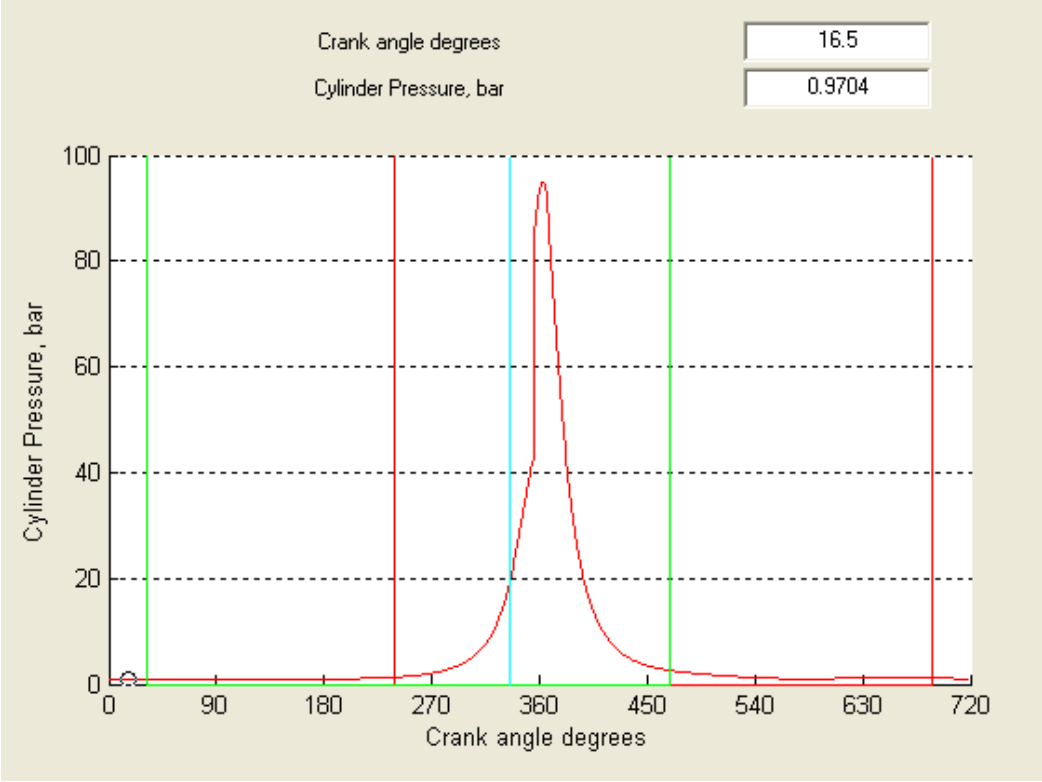

Figure 6.17: Open pressure diagram for Study 4.

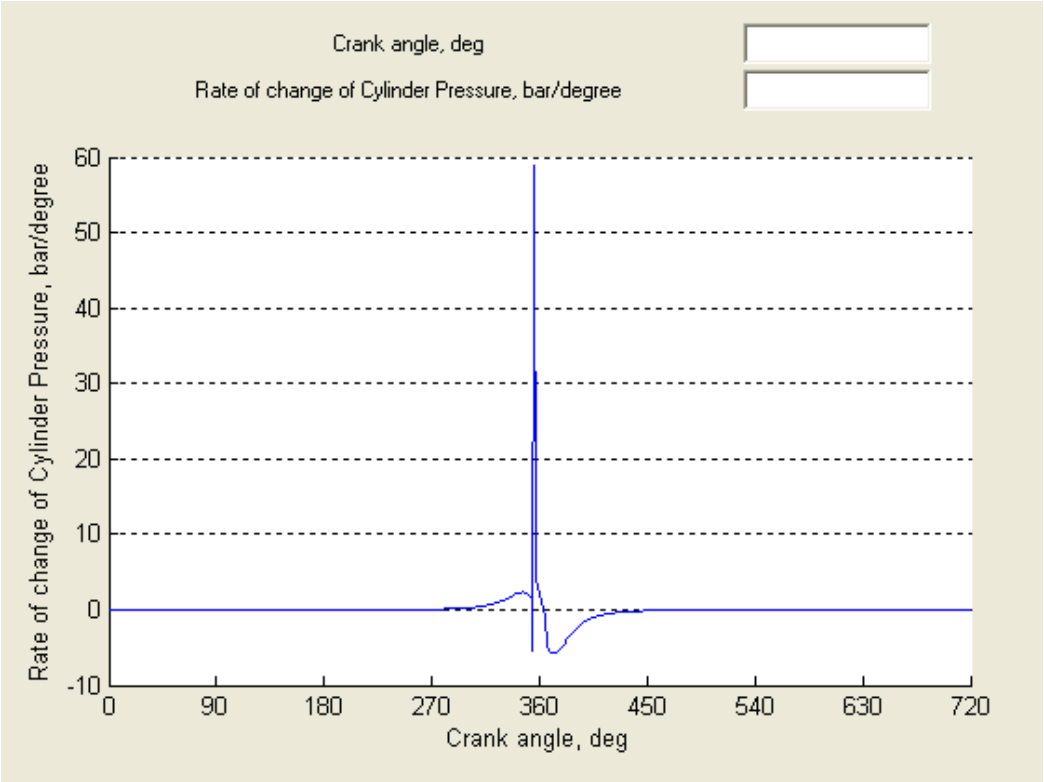

Figure 6.18: Rate of change of cylinder pressure diagram for Study 4.

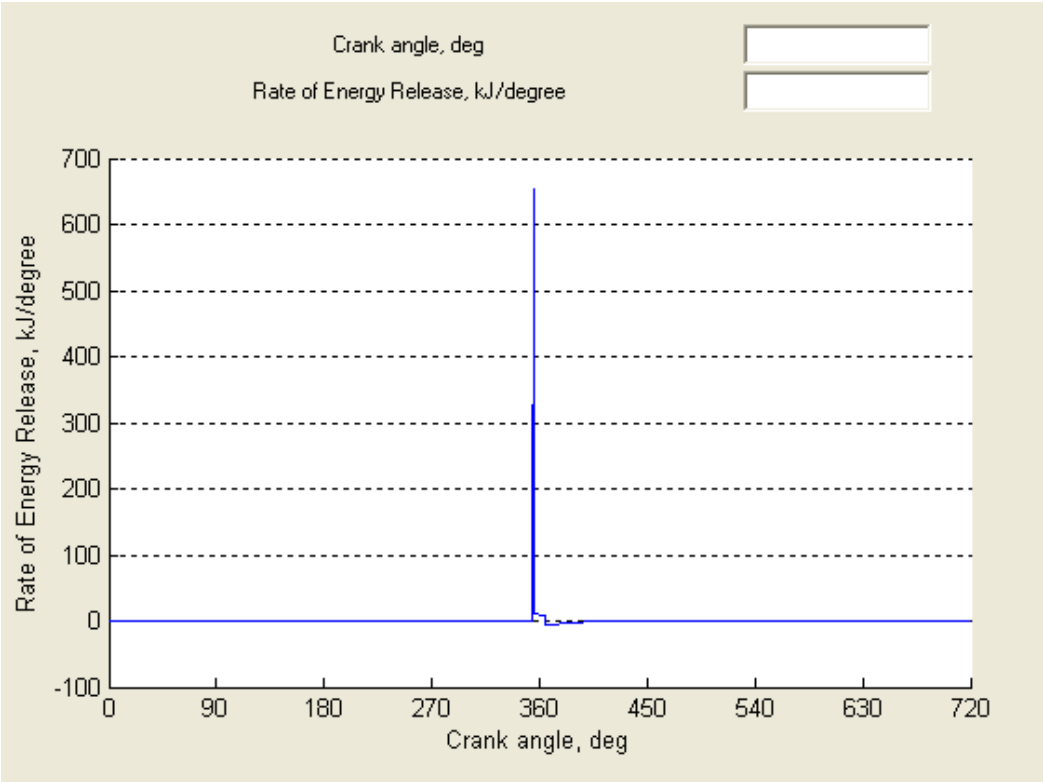

Figure 6.19: Rate of energy release diagram for Study 4.

Study 5:

Pulsed injection, duration 25°, start of injection = 25° BTDC

Table 6.8: Engine performance for pulsed injection, Study 5, frequency 10kHz, duty cycle 40%.

PB_{maxB} (bar)	104
α PB_{maxB} (θ°)	0
TB_{maxB} (°C)	1895
αTB_{maxB} (θ°)	0
IMEP (bar)	4.45
PB_{iB} (kW)	6.73
RPR (bar/°)	13.5
MRPR (bar/°)	72.45

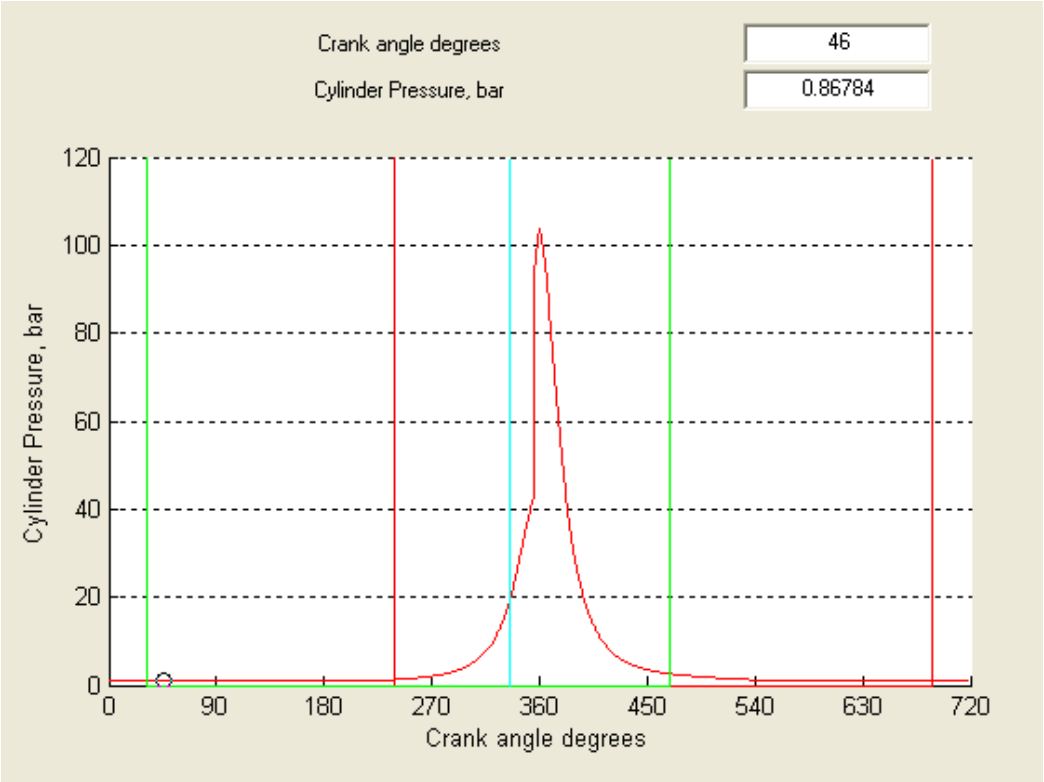

Figure 6.20: Open pressure diagram for Study 5.

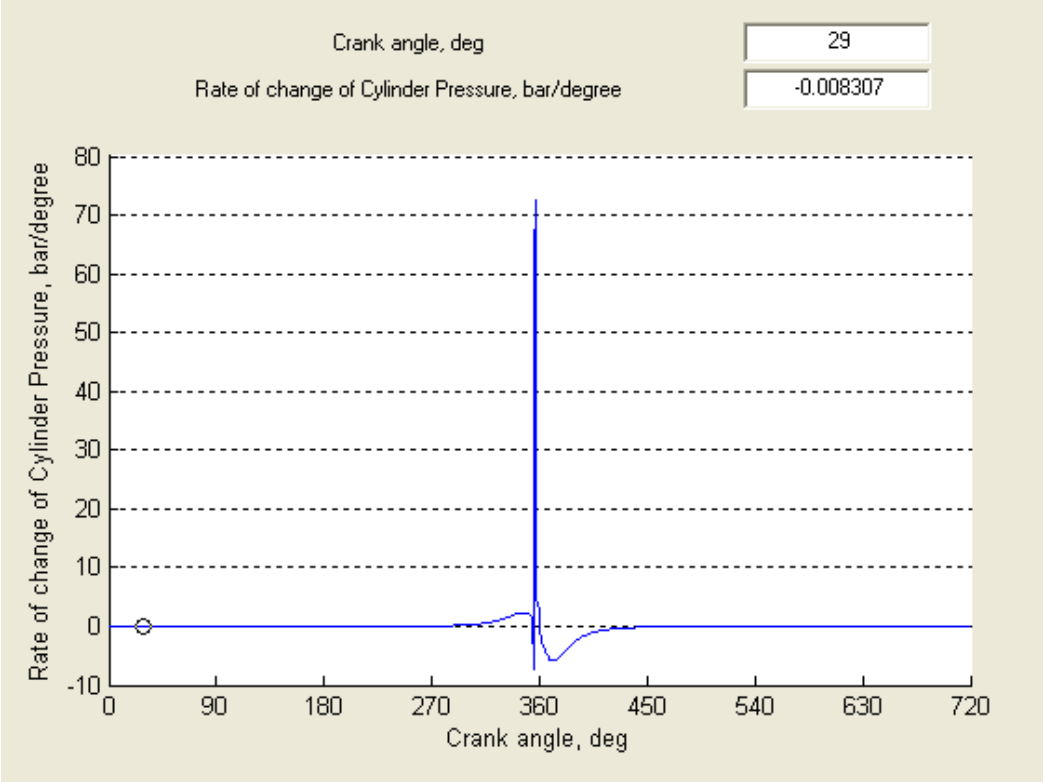

Figure 6.21: Rate of change of cylinder pressure diagram for Study 5.

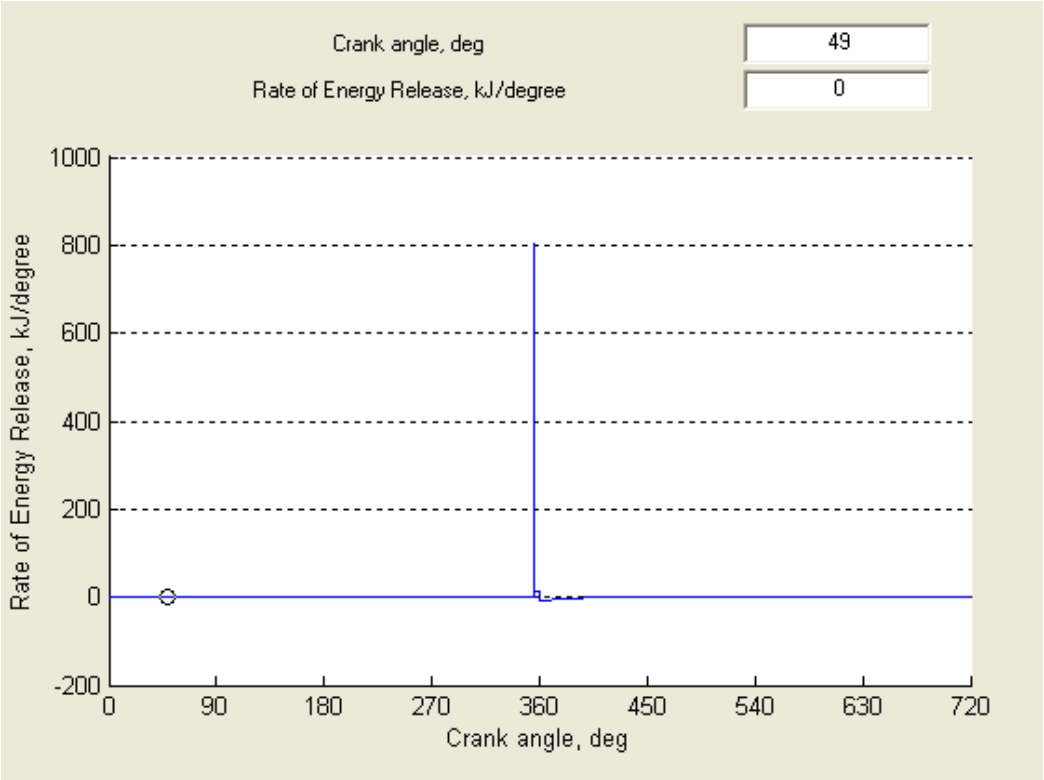

Figure 6.22: Rate of energy release diagram for Study 5.

Study 6: Pulsed injection, duration 25°, start of injection 30° BTDC

Table 6.9: Engine performance for pulsed injection, Study 6, frequency 10kHz, duty cycle 40%.

PB_{maxB} (bar)	107
α PB_{maxB} (θ°)	- 4
TB_{maxB} (°C)	2009
αTB_{maxB} (θ°)	- 3
IMEP (bar)	4.62
PB_{iB} (kW)	6.98
RPR (bar/°)	21.34
MRPR (bar/°)	85.31

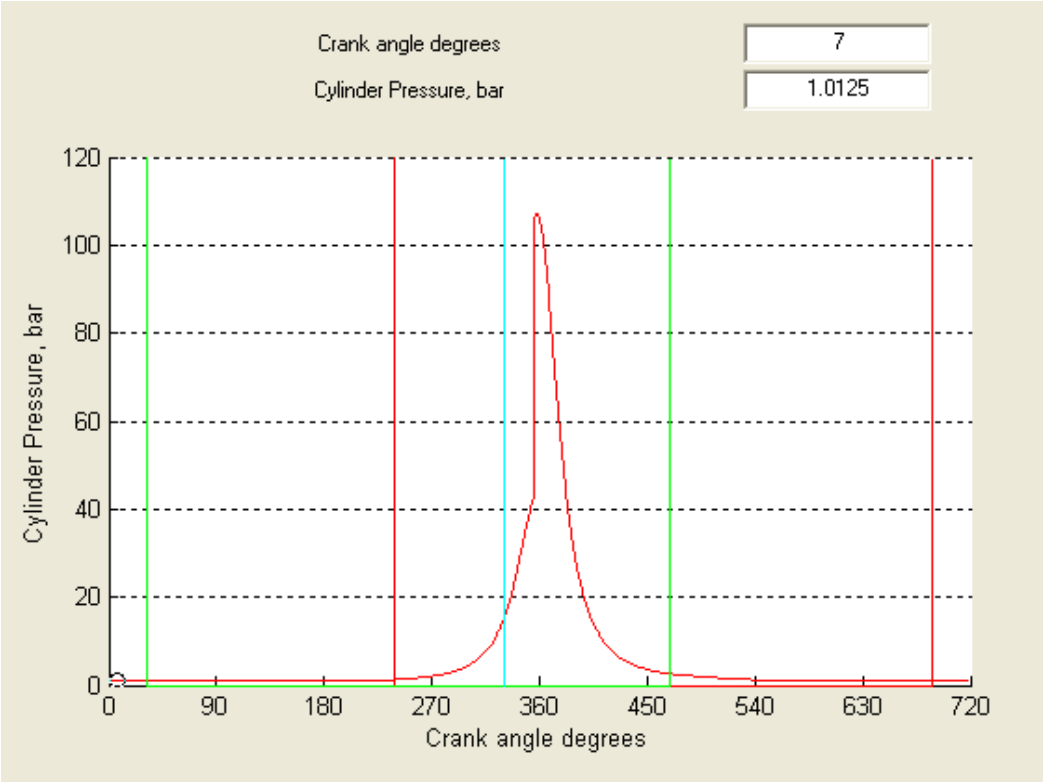

Figure 6.23: Open pressure diagram for Study 6.

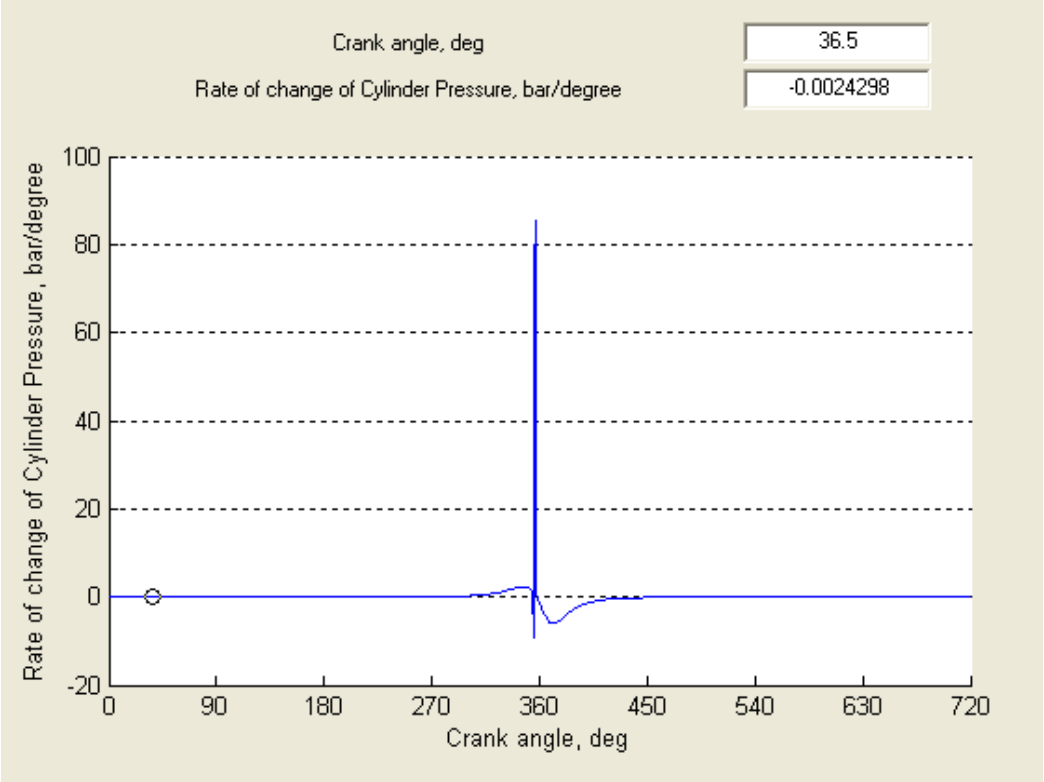

Figure 6.24: Rate of change of cylinder pressure diagram for Study 6.

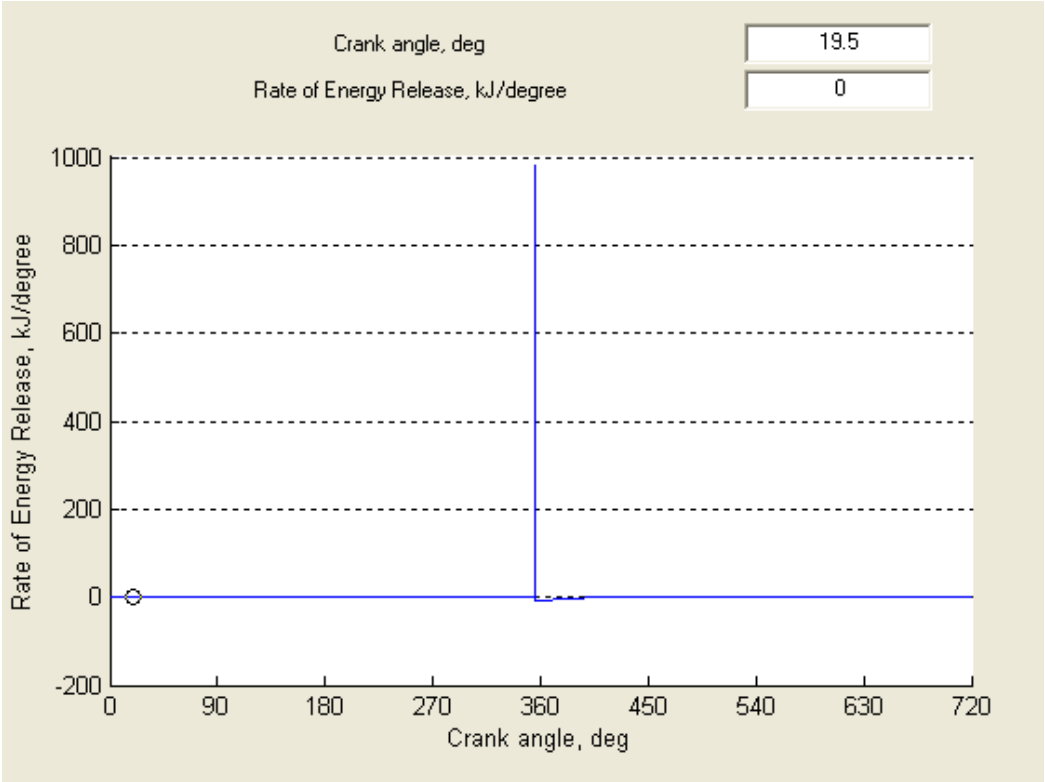

Figure 6.25: Rate of energy release for Study 6.

Study 7: Pulsed injection, duration 30°, start of injection 25° BTDC

Table 6.10: Engine performance for pulsed injection, Study 7, frequency 10kHz, duty cycle 40%.

Pmax (bar)	95
α Pmax (θ°)	5
Tmax (°C)	1785
αTmax (θ°)	3
IMEP (bar)	4.379
Pi (kW)	6.62
RPR (bar/°)	5.96
MRPR (bar/°)	58.39

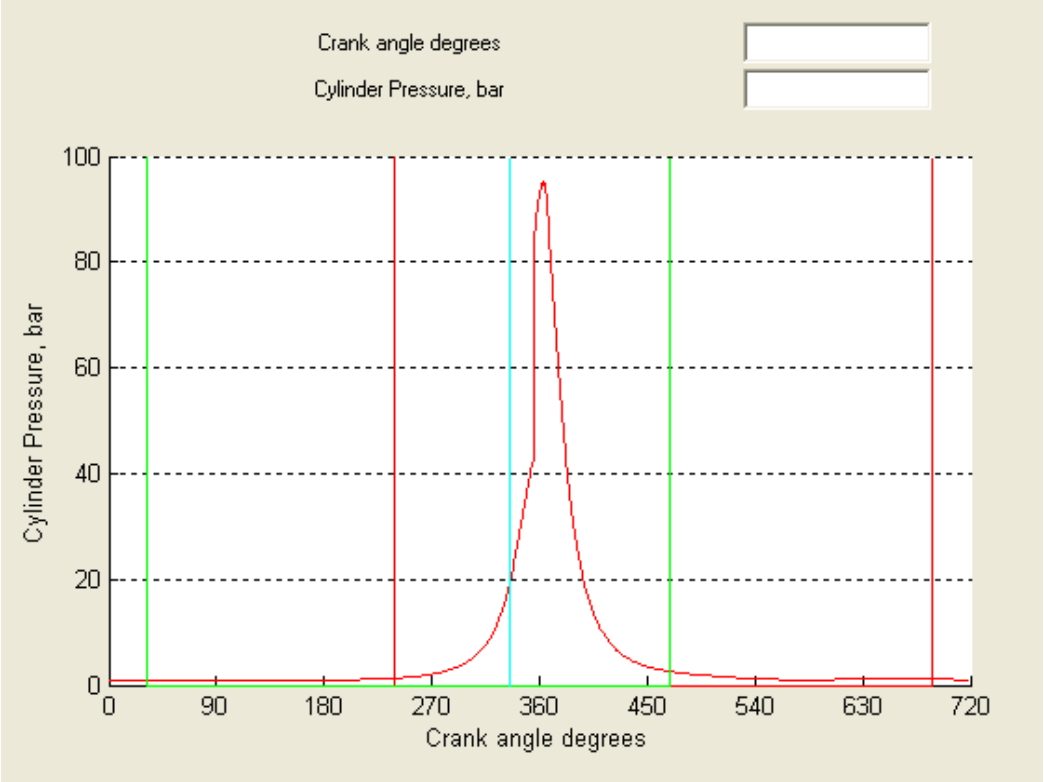

Figure 6.26: Open pressure diagram for Study 7.

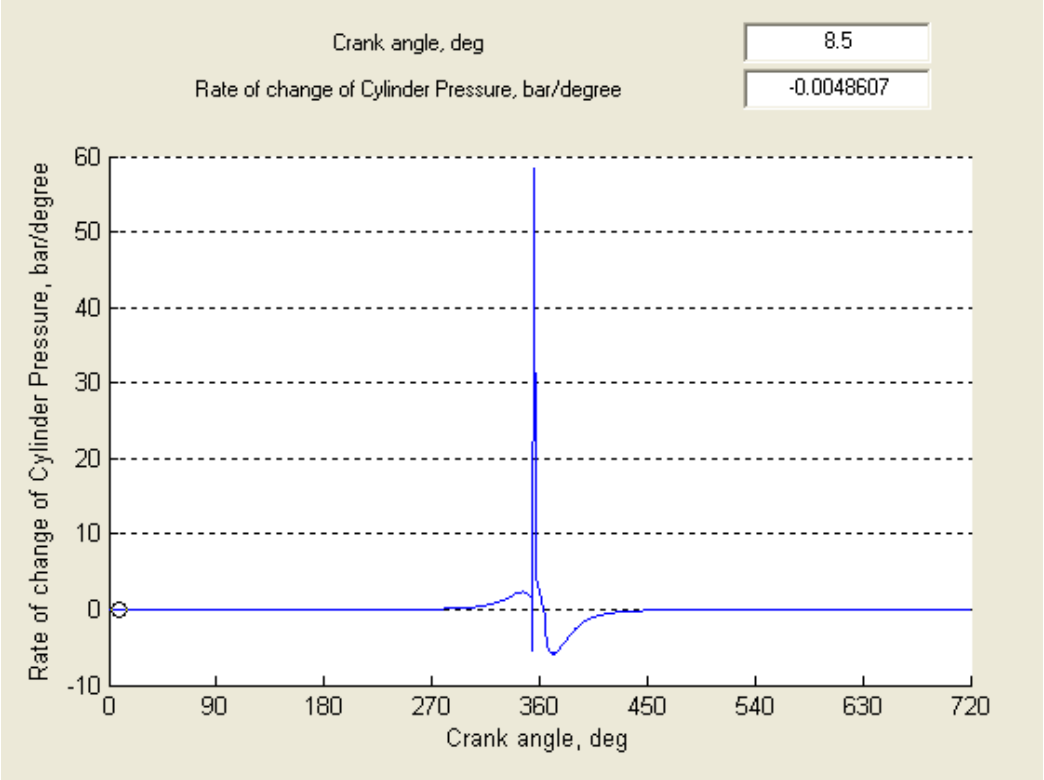

Figure 6.27: Rate of change of cylinder pressure diagram for Study 7.

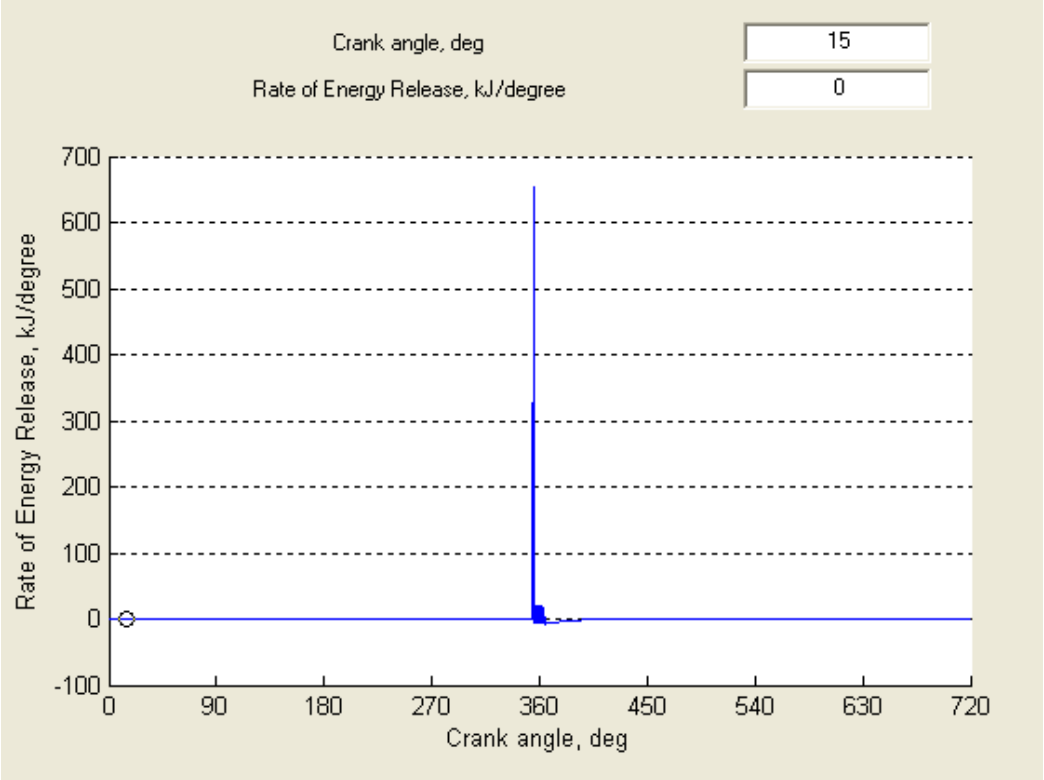

Figure 6.28: Rate of energy release diagram for Study 7.

Optimisation of injection to minimise MRPR

As already introduced, the MRPR (Maximum Rate of Pressure Rise) has a strong influence on mechanical loads of some components of the crankshaft connecting rod mechanism such as bearing shells and gudgeon pins, but it has a strong influence on the engine controllability. Therefore, the control of this parameter is of upmost importance to achieve a regular engine operation. It was identified during this research, that a too fast energy introduction results in high values of MRPR, therefore the controlled introduction of hydrogen into the cylinder, was an approach to follow, being implemented through simulation as a pulsed injection.

Study 8: Pulsed injection, duration 33°, start of injection 25° BTDC

Table 6.11: Engine performance for pulsed injection, Study 8, frequency 10kHz, duty cycle 40%.

P_{max} (bar)	91
αP_{max} (θ°)	8
T_{max} (°C)	1714
αT_{max} (θ°)	3
IMEP (bar)	4.42
P_i (kW)	6.68
RPR (bar/°)	5.44
MRPR (bar/°)	53

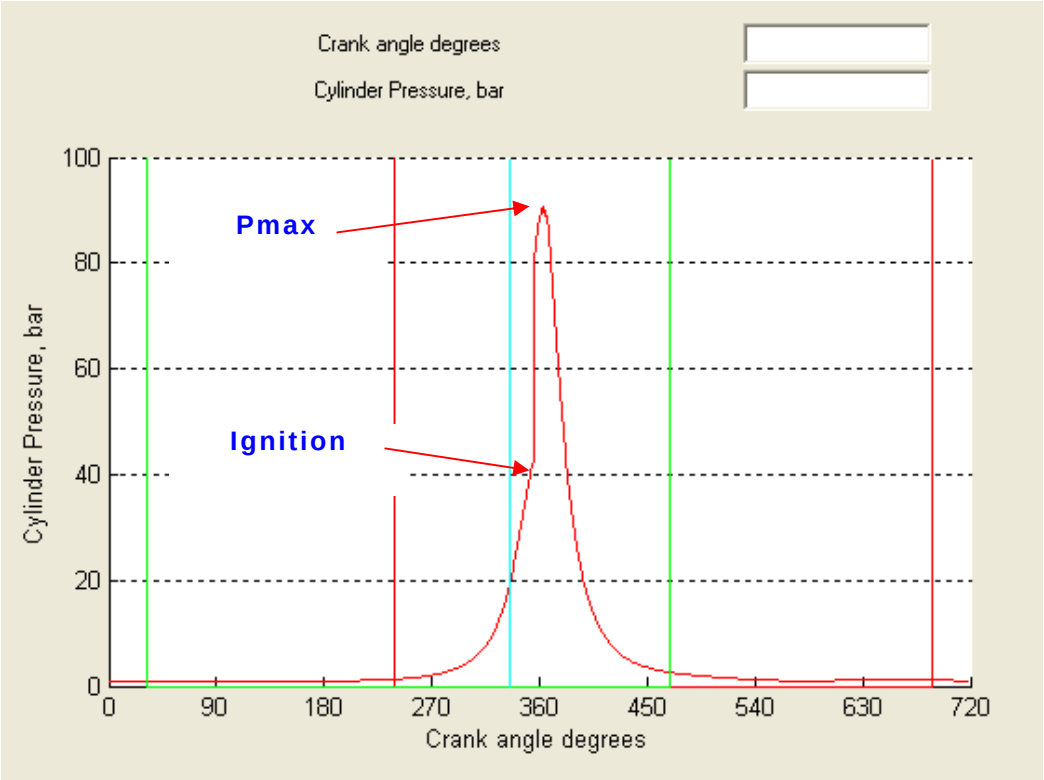

Figure 6.29: Open pressure diagram for Study 8.

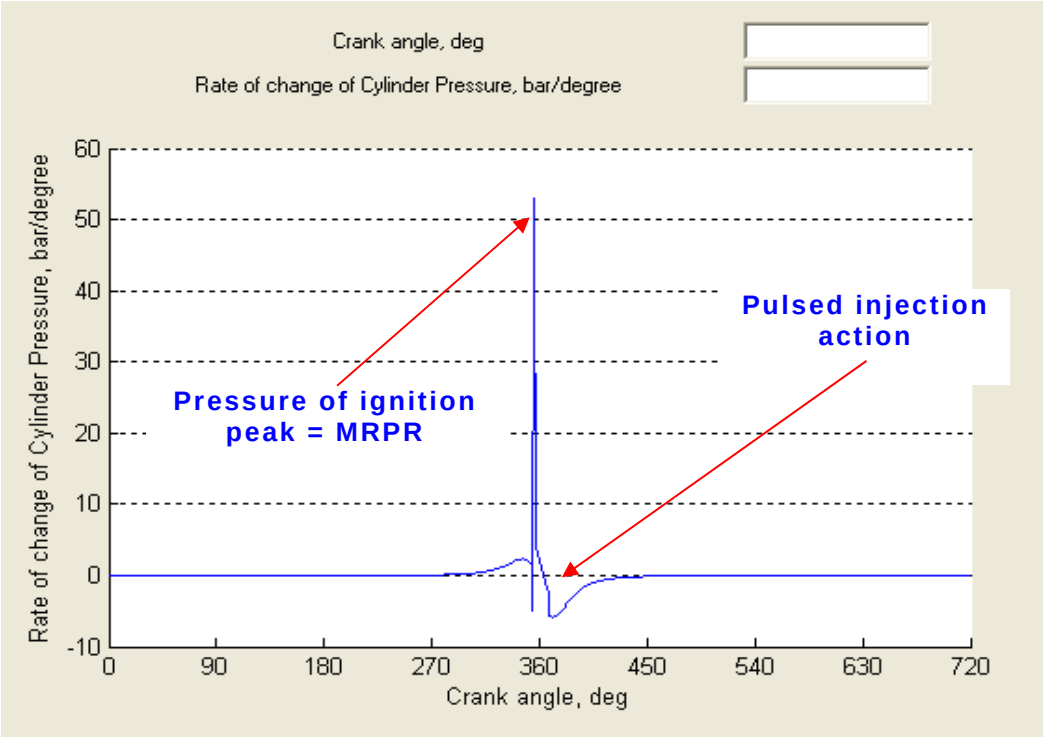

Figure 6.30: Rate of change of cylinder pressure diagram for Study 8.

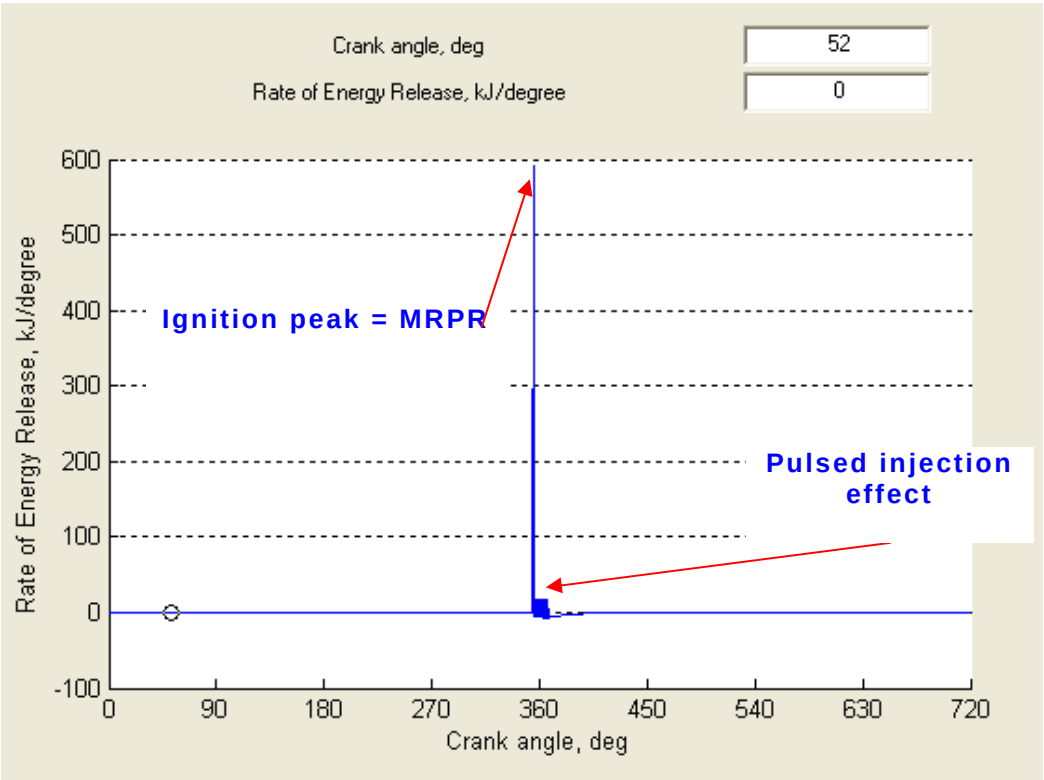

Figure 6.31: Rate of energy release diagram for Study 8.

By inspection of figures 6.29, to 6.31, it can be seen that the effect of pulsed injection resulted in a time extended energy input into the cylinder, controlling to some extent MRPR.

6.2.3 Comparison and conclusions regarding the simulated continuous and pulsed injection

The results of all injection timing and profile simulation studies are summarised in Table 6.12, showing the effects of injection angle and duration.

Continuous injection

Considering the results obtained from the simulation studies, it is possible to conclude that direct injection for a hydrogen fuelled CI engine should have the injection duration extended after top dead centre and that it should be pulsed. This injection arrangement will produce a cooler combustion, and the angle of maximum pressure will meet the objective of being 5º after top dead centre. Also the maximum combustion pressure will be of the same order of magnitude as when the engine is operated with diesel oil. It can be seen from the pressure diagrams that the operating cycle approaches the constant volume engine cycle, indicating that high efficiency can be achieved. As hydrogen CI engines require higher compression ratios to achieve the self ignition temperature of hydrogen than standard CI engines, it is expected that even higher cycle efficiencies can be achieved.

From the heat release diagrams it is possible to see that, as the injection starts at approximately top dead centre, the release of energy will be faster resulting in higher pressure, and therefore higher values of RPR. The use of pulsed injection has no apparent effect on the RPR values.

Injection timing plus pulsed injection

As noticed for the continuous injection, the injection timing is an important parameter in the control of engine RPR and MRPR. The simulation studies

show that the injection of the DIH_2 engine should be prolonged after the engine top dead centre and pulsed, thus resulting in a smooth combustion, with maximum cylinder temperatures around 1700ºC, and maximum cylinder pressures within the range experienced with diesel oil operation. Therefore DIH_2 operation will not create excessive thermal or mechanical loads on engine components, and as the developed peak temperatures are smaller than for the continuous injection, it is expected that the formation of thermal NO_x is extremely reduced, in particular because the thermal NO_x formation takes place above 1700ºC according to Richard (1980) and the time the cylinder charge temperature is above 1700ºC is extremely small when compared to hydrocarbon fuels Heywood (1972).

As can be seen from the figures of rate of energy release (RER) and MRPR (maximum rate of pressure rise), there is an initial peak of energy release, and only after that does the pulsed injection have some control. The pulsed injection control is only effective during the second phase of the combustion process; there is no evidence of any control during the ignition process. Therefore, it achieves only partially its main objective of controlling the MRPR originating from the first instant of injection.

It can be also recognised that with the advance of injection the maximum combustion temperature and pressure increases above acceptable values, particularly for the MRPR and RPR. The increase of the maximum combustion temperature T_{max} promotes the formation of thermal NO_x.

Comparing the results of the various simulations studies (see Table 6.12), it can be seen that the optimised injection profile and timing for the test engine was:

- start of injection 25º BTDC, duration of injection 33º, plus pulsed injection at 5 kHz.

This combination results in the lowest maximum combustion temperature, lower RPR, lower MRPR, while maintaining engine power output.

	Start of injection 25º Duration of injection 30º Pulsed injection	Start Injection 25º Duration Injection 33º Pulsed injection Optimized Injection	Start Injection 25º Duration Injection 30º	Start Injection 25º Duration Injection 25º	Start Injection 30º Duration Injection 25º
P_{max} (bar)	95	91	95	104	107
αP_{max} (θº)	5	8	5	0	- 4
T_{max} (ºC)	1785	1714	1775	1885	2009
αT_{max} (θº)	3	3	3	0	- 3
IMEP (bar)	4.38	4.42	4.42	4.45	4.62
PB_i (kW)	6.62	6.68	6.68	6.73	6.98
RPR (bar/º)	5.96	5.44	5.92	13.5	21.34
MRPR (bar/º)	58.39	53.07	58.92	72.45	85.31

Table 6.12: DIH_2 engine parameters for different injector profile and timing.

6.3 Effect of valve timing (Miller cycle) on DIH_2 engine performance.

Since MRPR is related to the temperatures of the cylinder and combustion chamber charge, any mechanism for controlling the temperature of the combustion chamber components internal to the engine is of interest. Therefore the effect of valve timing and use of the Miller cycle was investigated as such a possible mechanism.

The Miller cycle was first proposed in 1947 and is achieved by early inlet-valve closure to provide improved cooling before compression so as to reduce compression work (Miller, 1947). Miller et al. (1957) further proposed the increase of the boost pressure to compensate for the reduced inlet stroke duration, thus improving the engine thermal efficiency this effect is illustrated in figure 6.32.

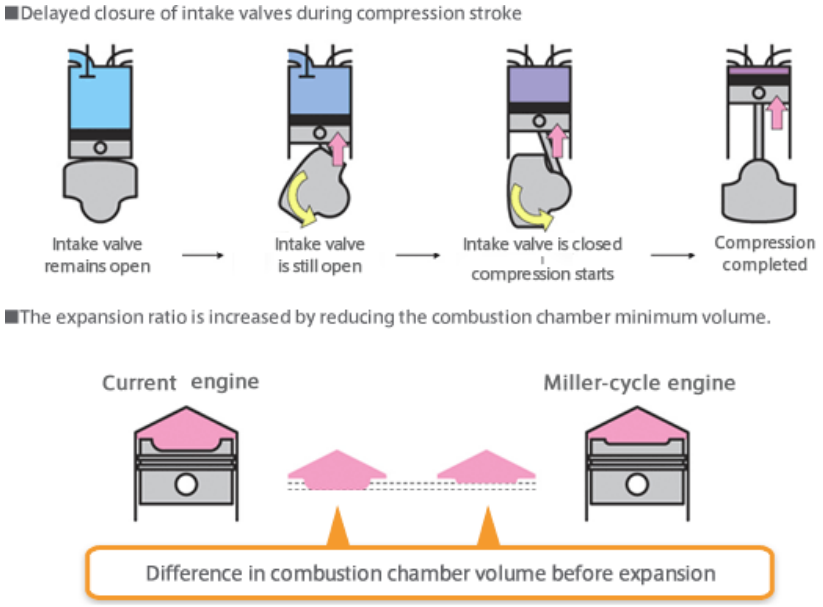

Figure 6.32 Miller cycle illustrations (Source Mazda Corp.)

As a result of the different inlet valve timing, the Miller cycle has lower combustion temperatures than a conventional engine cycle.

As a direct consequence of this new valve timing, the end-of-compression temperatures are lower. Therefore, maximum combustion temperatures are lower too, resulting in a lower MRPR and NO_x formation, which is a function of the temperatures during combustion, time, and turbulence.

For the Miller cycle, the compression stroke of the engine is shorter than the expansion stroke, allowing the compression ratio and the expansion ratio to be set independently. According to Wang et al. (2005), there are three different practical ways of implementing the Miller cycle:

a) Using a rotating valve between the air manifold, and the inlet valve (on the cylinder head) to control the intake air quantity. This is called early rotary valve closing (ERVC).

b) Closing the inlet valve before the termination of the suction stroke. This is called early inlet valve closing (EIVC).

c) Keeping the inlet valve open during a portion of the compression stroke, thus rejecting part of the charge and reducing the net compression ratio. This is called late inlet valve closing (LIVC).

6.3.1 Effect of the Miller cycle on the DIH_2 engine

The EIVC method to accomplish the Miller cycle was used as it was more readily simulated. Three different inlet valve timings were investigated:

Miller 1: the inlet valve opens 20° late and closes 20° early.

Miller 2: the inlet valve opens 25° late and closes 25° early.

Miller 3: the inlet valve opens 10° late and closes 10° early.

The thermal efficiency, indicated power, and the MRPR relationship to the hydrogen fuel rate (load) was plotted for each Miller valve setting and for the conventional valve setting for the DIH2 engine. The results are shown in Figures 6.33, 6.34 and 6.35.

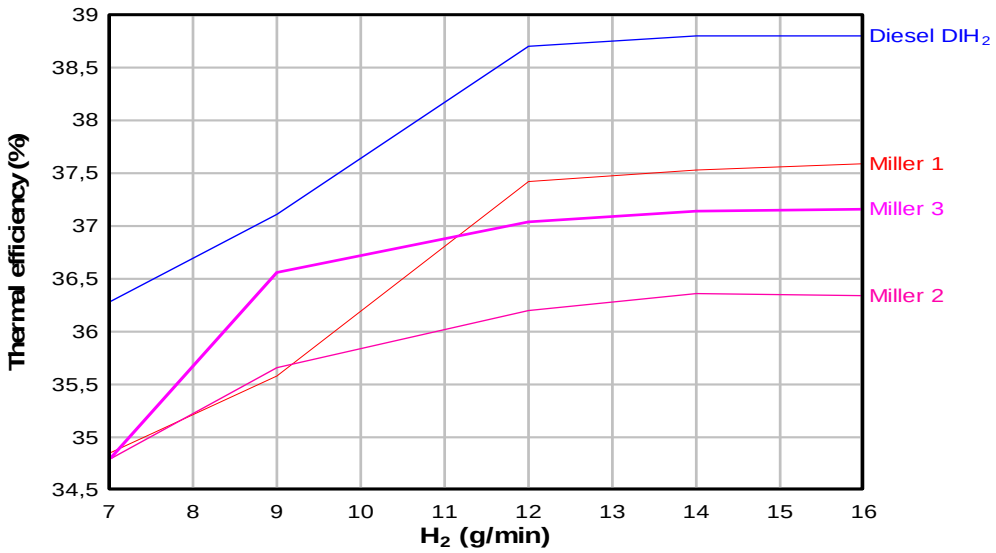

Figure 6.33: Relationship between thermal efficiency and hydrogen fuel rate for conventional and Miller cycle inlet valve settings.

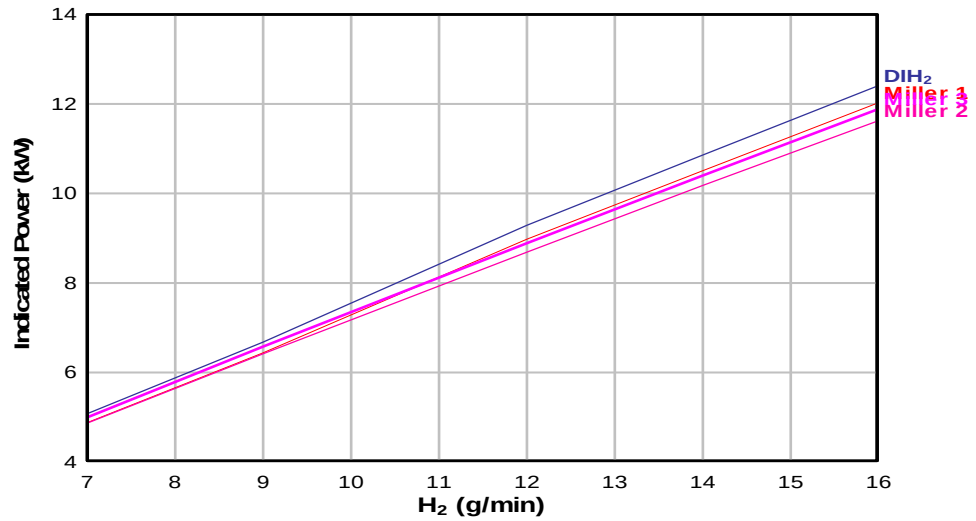

Figure 6.34: Relationship between indicated power and hydrogen fuel rate for conventional and Miller cycle inlet valve settings.

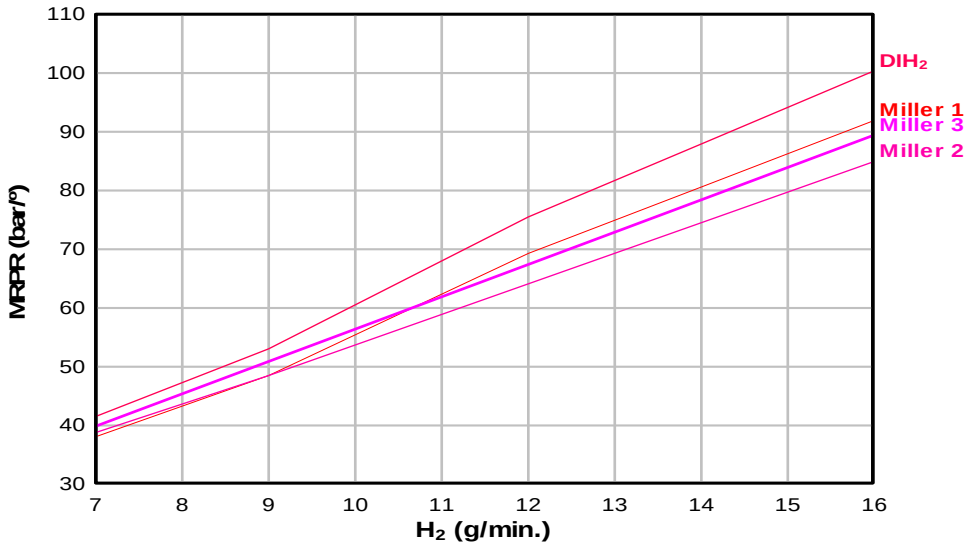

Figure 6.35: Relationship between MRPR and hydrogen fuel rate for conventional and Miller cycle inlet valve settings.

As can be seen from the results presented in Figure 6.35, the Miller cycle can be used effectively to reduce the MRPR, therefore improving the performance of a DIH_2 engine. The inlet valve setting corresponding with Miller1 has a significant effect on reducing MRPR whilst maintaining high engine thermal efficiency in comparison to the conventional valve timings, as shown in Figure 6.33.

For the Miller cycle, there is a slight reduction in indicated power (Figure 6.34), accompanied by a small reduction in thermal efficiency (Figure 6.33). If a Miller cycle is to be implemented for DIH_2 engine operation, a trade-off between a reduction in indicated power and thermal efficiency and the benefits of a reduction in MRPR needs to be made.

It was found that it was possible to achieve maximum combustion temperatures as low as 1463°C (for 7g/minute of H_2). This indicates the benefits the Miller cycle has in reducing NO_x formation and combustion chamber thermal stress. As an example, for full load (16g/minute) in standard DIH_2 mode, the peak combustion temperature is 2593°C whereas for the "Miller 2" cycle it is only 2482 °C (a difference of 111°C).

6.4 DIH_2 injector dynamic simulation

As has been discussed previously, a DIH_2 direct injection injector has various objectives to meet, namely:

a) Accurate metering capability. This is the ability of the injector to deliver consistently the same amount of hydrogen, when actuated with the same input. This allows the fuel delivered to the engine to be accurately controlled.

b) Good dynamic response. This is the ability of the injector to produce rapid and consistent opening and closing times.

c) The injector should be able to inject the hydrogen at the appropriate pressure.

d) The injector should not leak.

e) The injector should be constructed with materials compatible with hydrogen.

f) The injector should be auto lubricated.

To investigate the three first requirements, a simulation model using Simulink was developed using the equations presented in Chapter 5. The following paragraphs show the simulated dynamic response of the injector regarding the effect of inertia of its moving parts, duty cycle, actuation frequency, hydraulic pressure and static force or pre-load.

6.4.1 Effect of the inertia of the moving parts on the injector dynamic response

The inertia of the moving parts of the injector was studied to understand how it influences the dynamic response of the injector. The actuator mass was lumped together with the mass of the spring, and the mass was varied from 5 g to 50 g, whilst keeping all other injector parameters constant. The injector parameters were:

Table 6.13: Injector parameters for dynamic simulation.

Hydraulic pressure (bar)	50
H_2 pressure (bar)	200
Static spring force (N)	500
Cylinder pressure (bar)	80

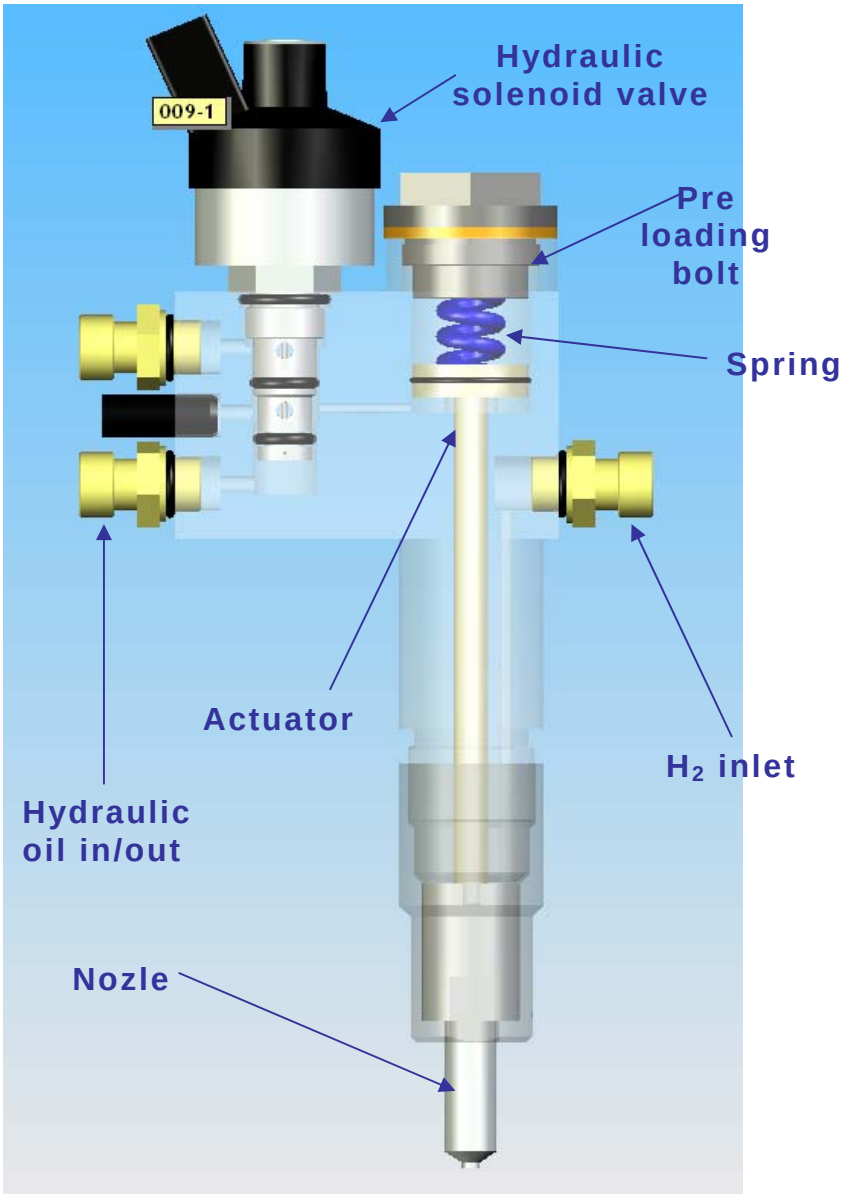

Figure 6.36: DIH_2 Injector view.

Figure 6.36 shows the arrangement of DIH_2 injector components, evidencing the hydraulic actuator and the three way solenoid valve.

Figure 6.37 and 6.38 show that injector actuator speed does not significantly change for a variation of the actuator mass between 5 g and 50 g.

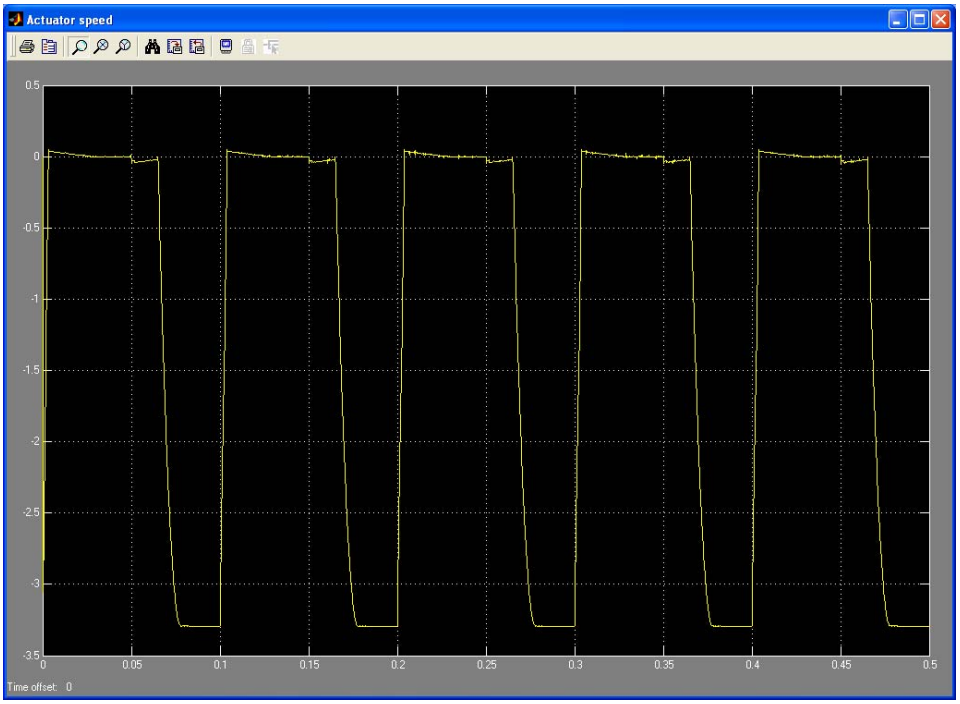

Figure 6.37: Injector actuator speed for an actuator and spring mass of 5 g.

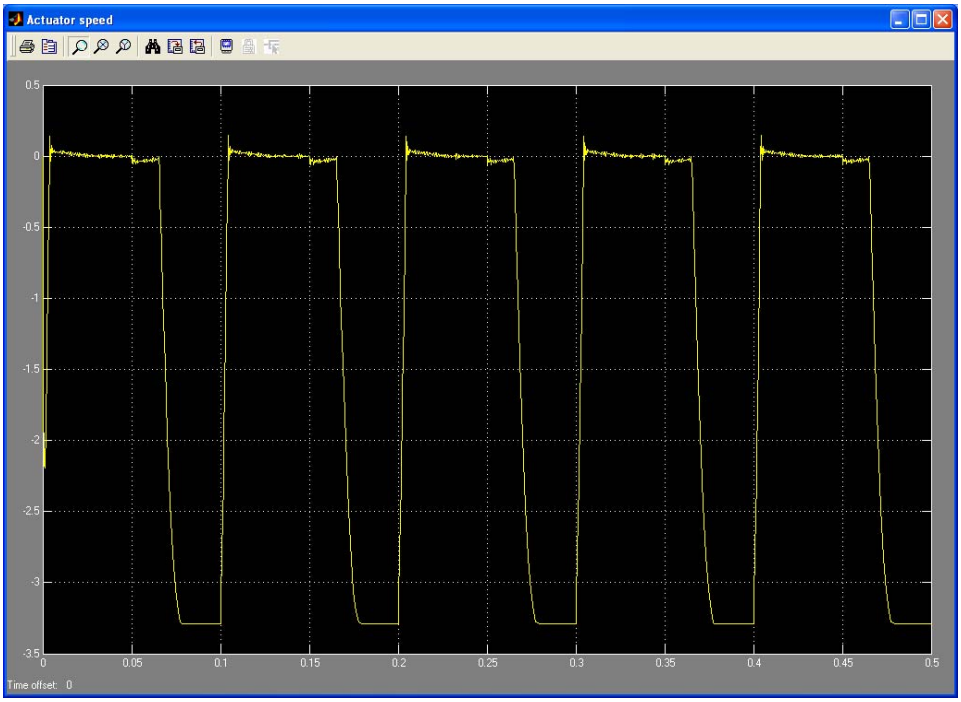

Figure 6.38: Injector actuator speed for an actuator and spring mass of 50g.

Figures 6.39 and 6.40 show that the injection needle displacement is not significantly influenced by an increase in actuator mass.

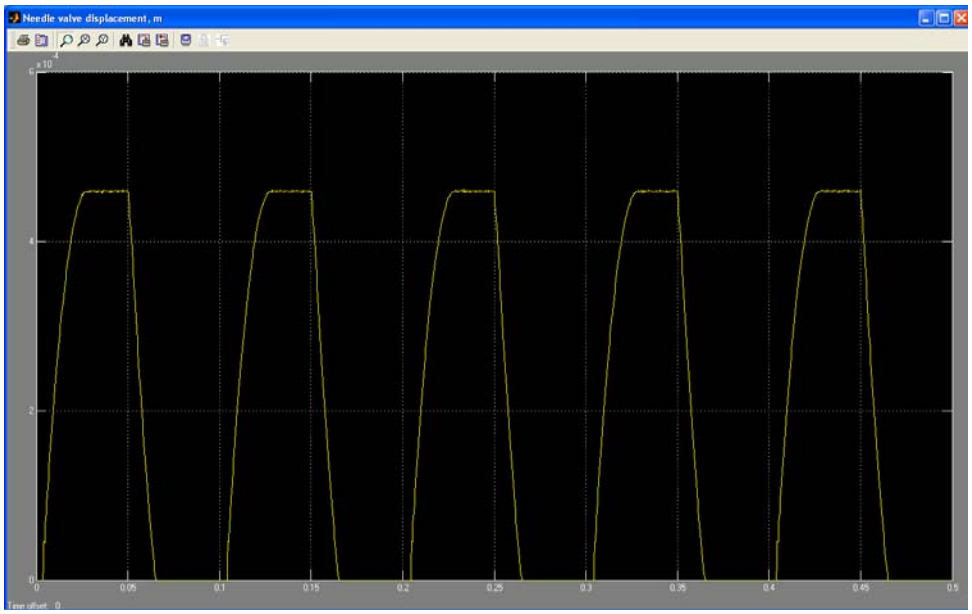

Figure 6.39: Injector needle valve displacement for an actuator and spring mass of 5 g.

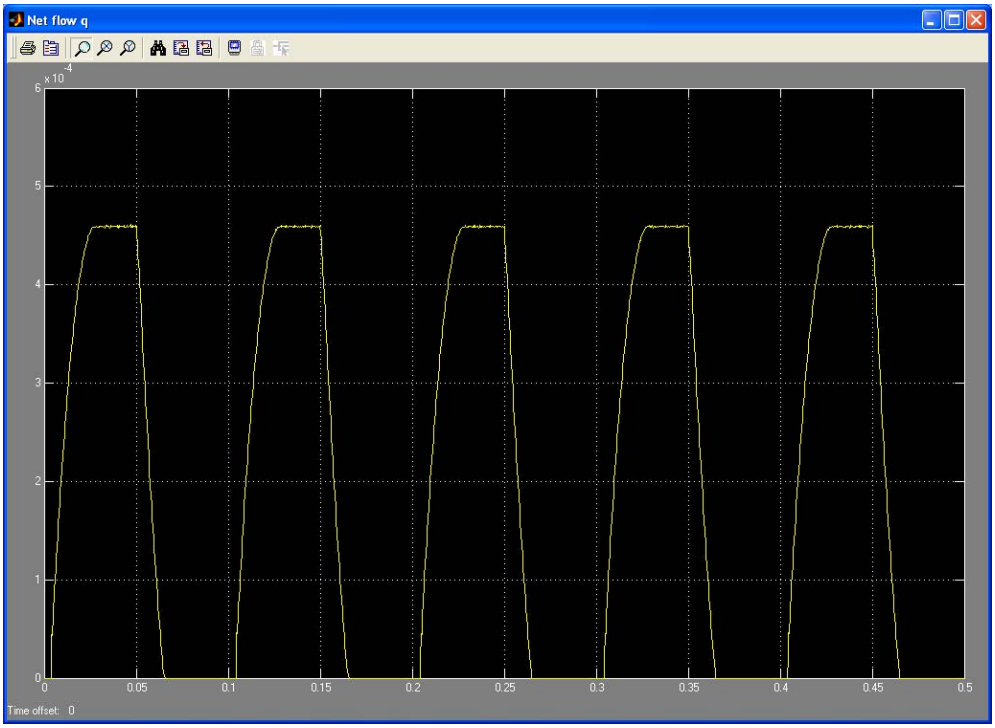

Figure 6.40: Injector needle valve displacement for an actuator and spring mass of 50 g.

6.4.2 Effect of duty cycle on the injector dynamic response

For values of duty cycle lower than 30%, the injector is not effective for regulation of mass flow. Despite the good speed of response of the actuator, there is no sufficient time for the flow to develop. As can be seen from the simulation graphs, the injector does the flow modulation in an acceptable way down to 10% duty cycle. For values of duty cycle lower than 10%, the injection flow rate per cycle is not regular, potentially making the engine run erratically.

Figures 6.41-6.44 show the actuator speed for a hydraulic pressure of 50 bar, H_2 pressure of 200 bar, static force of 500 N, cylinder pressure of 80 bar, actuator mass 5 g, period 0.0599 s (2000RPM), with the duty cycle varying from 5% to 30%.

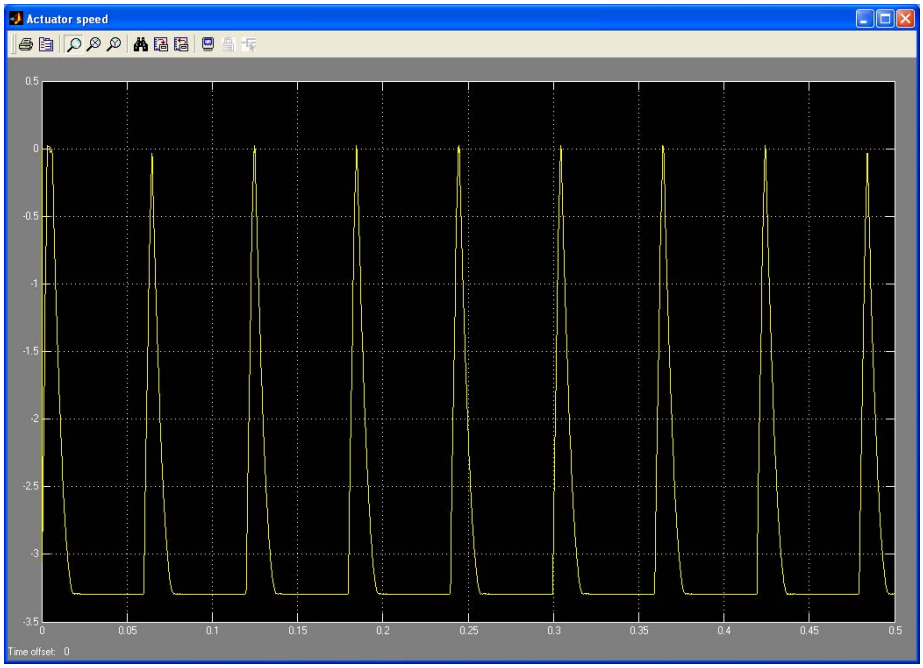

Figure 6.41: Actuator speed for a duty cycle of 5%.

In figure 6.41 can be observed that the injector is not sufficiently fast to open, not injecting any hydrogen.

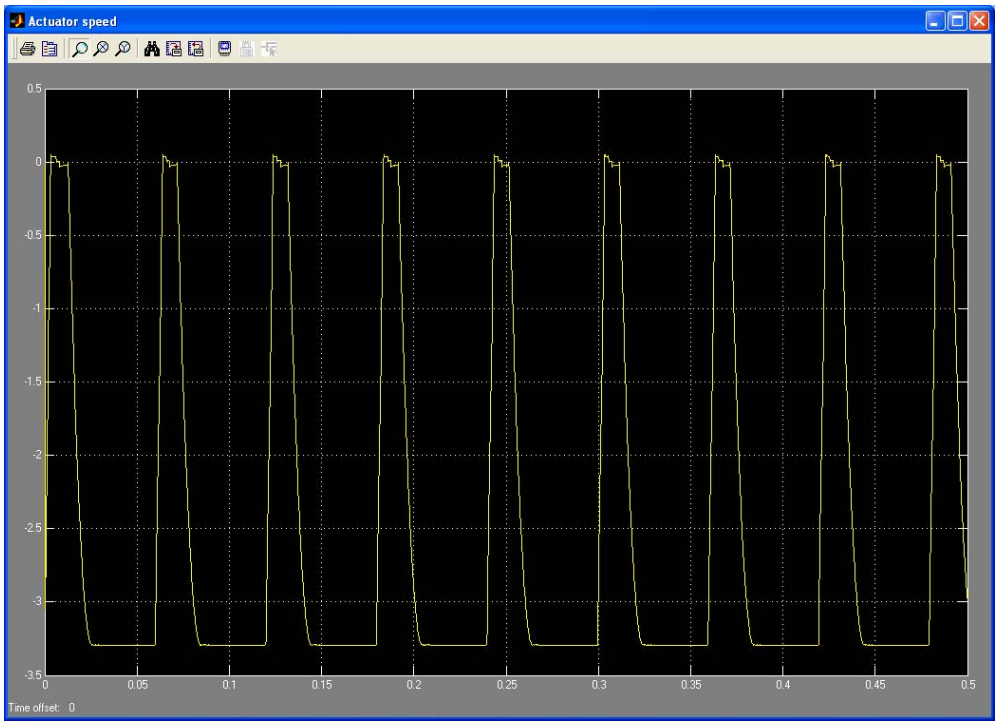

Figure 6.42: Actuator speed for a duty cycle of 10%.

Figure 6.42, shows that when the duty cycle is increased to 10%, the injector opens, but it does not have time to complete the injection.

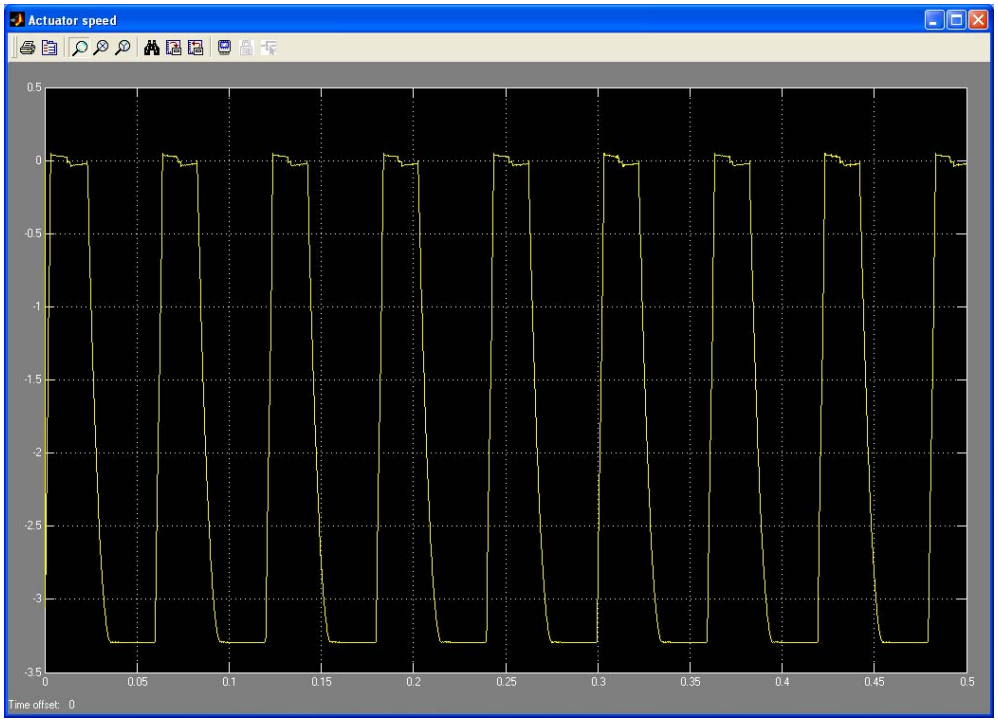

Figure 6.43: Actuator speed for a duty cycle of 20%.

In figure 6.43 the injector is opened for a bigger time, but still insufficient to complete the injection of hydrogen.

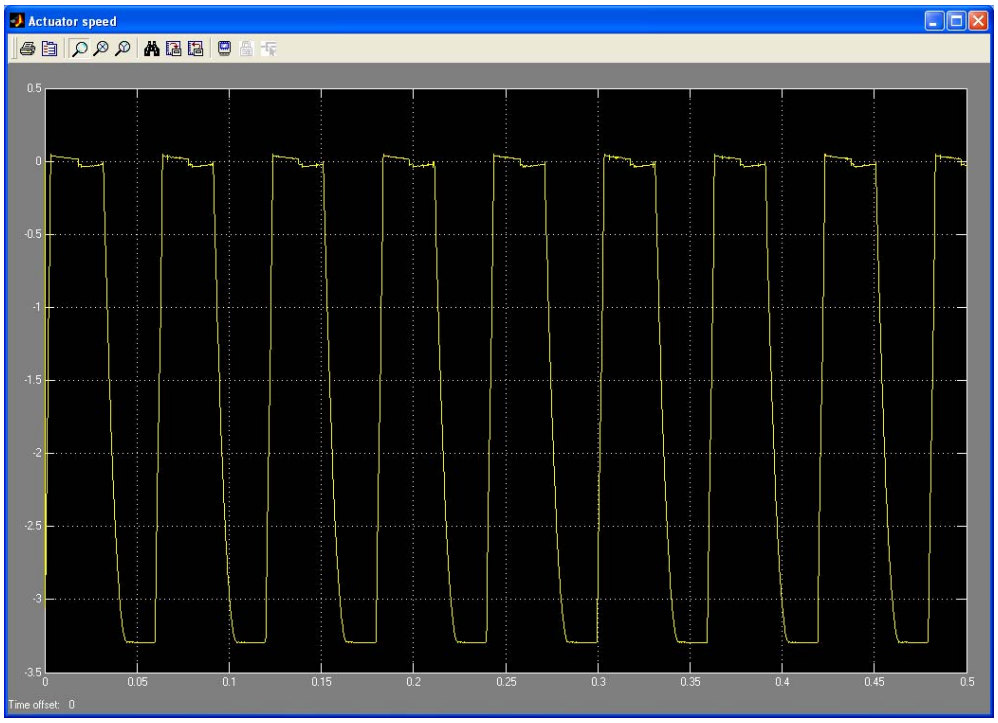

Figure 6.44: Actuator speed for a duty cycle of 30%.

Figure 6.44 shows that the injector response is complete, evidencing a good control of the injection cycles.

Figures 6.45 to 6.49 show the injector mass flow rate for varying duty cycle, with the other parameters constant.

Figure 6.45 shows mass low rate for a 5% Duty cycle, evidencing the irregular flow rate as a consequence of the poor response of the injector. Figures 6.46 through 6.49, show that an acceptable mass flow rate control is achieved only for Duty cycles above 30%. The precise control of the engine is a function of the mass flow rate and therefore of the amount of energy per cycle. To achieve such a control it is required to control accurately the time the injector is open, which is a function of the speed response of the hydraulic injector.

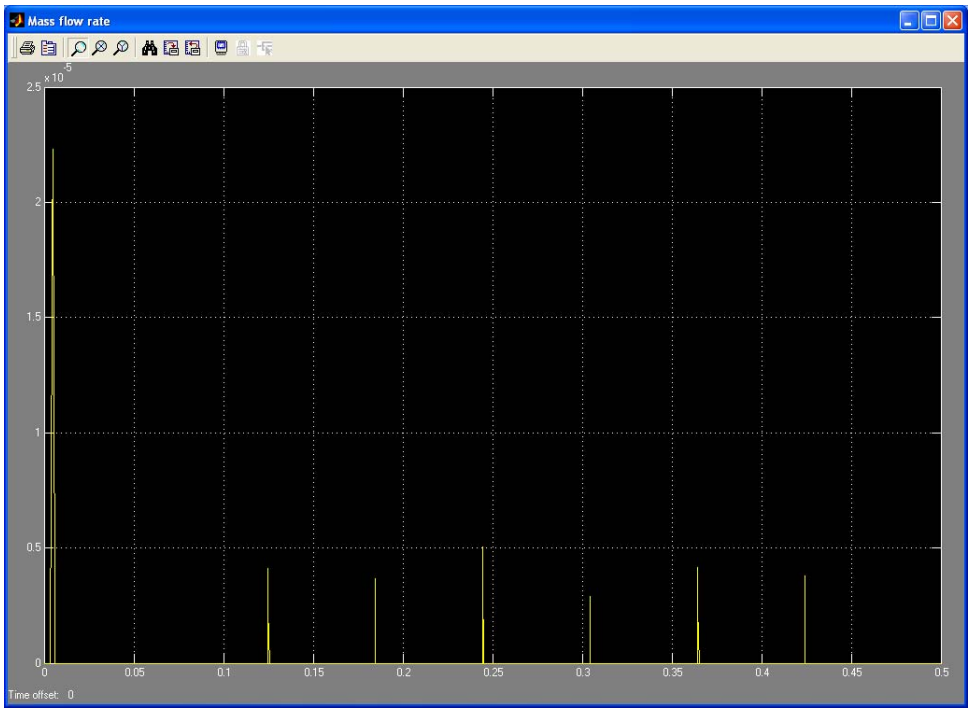

Figure 6.45: Injector mass flow rate for a duty cycle of 5%.

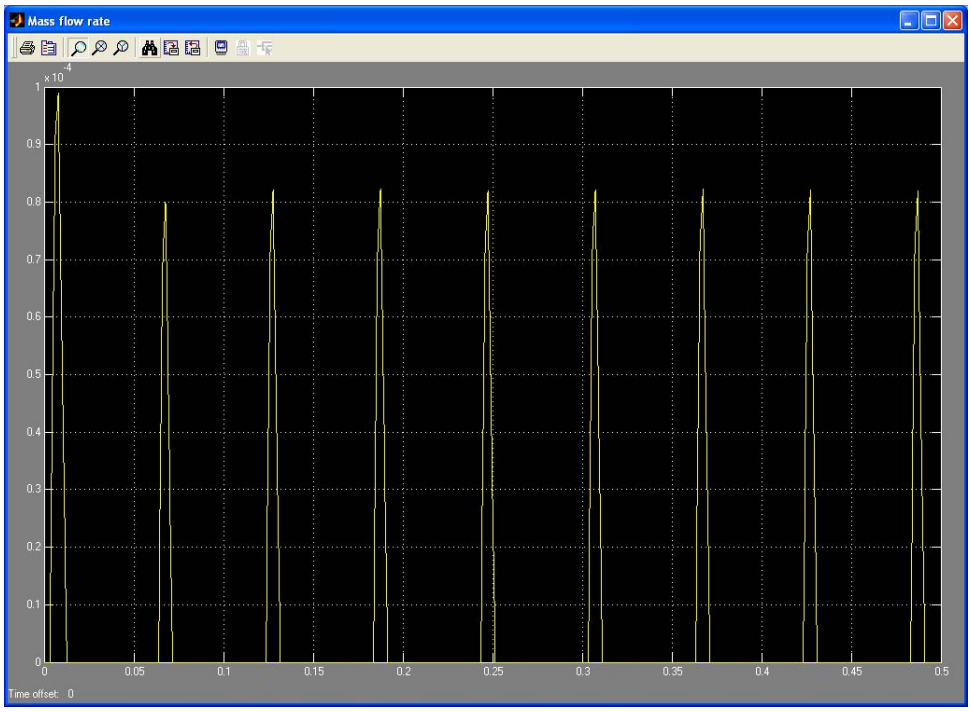

Figure 6.46: Injector mass flow rate for a duty cycle of 10%.

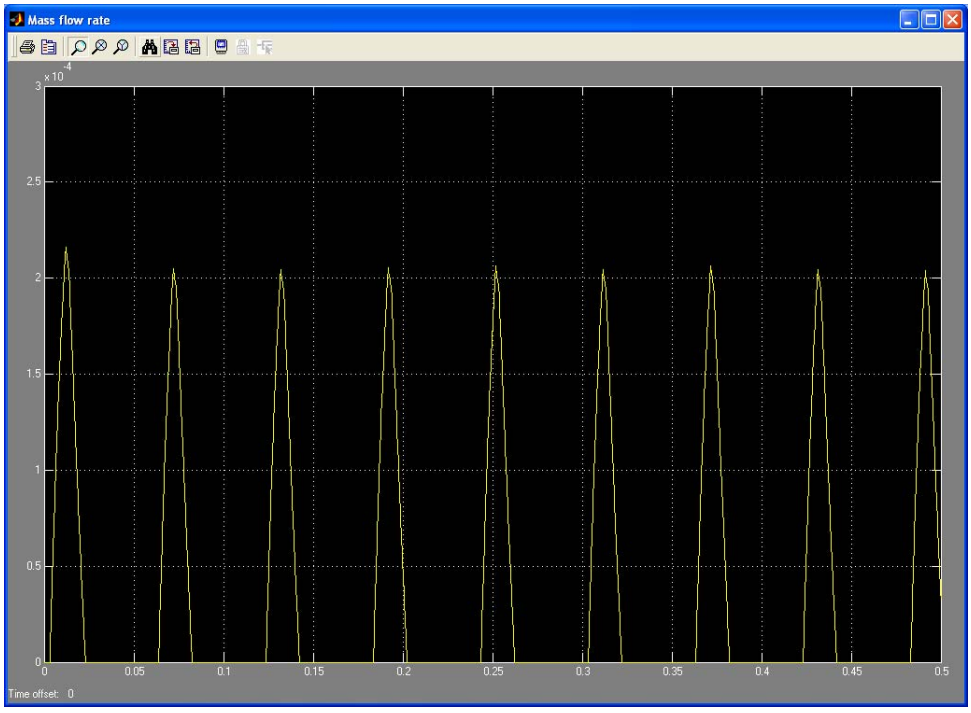

Figure 6.47: Injector mass flow rate for a duty cycle of 20%.

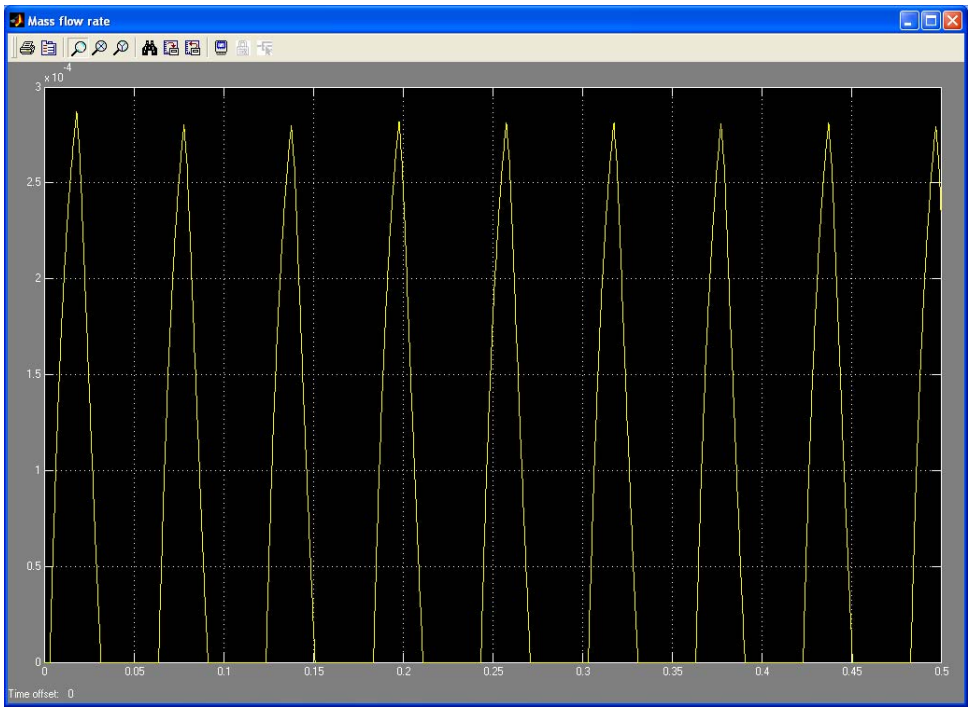

Figure 6.48: Injector mass flow rate for a duty cycle of 30%.

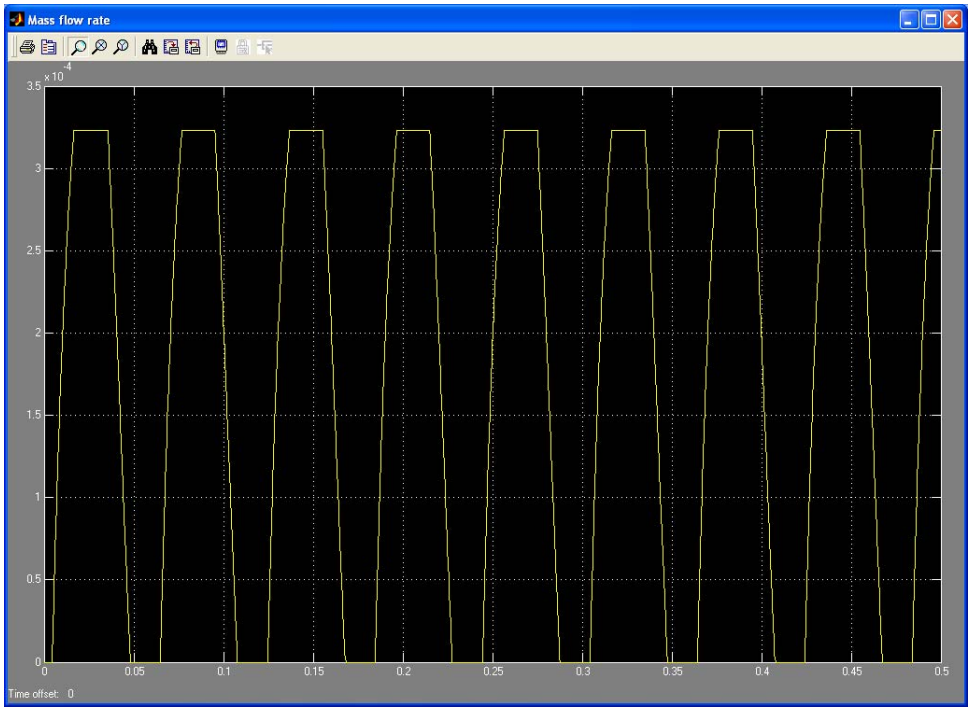

Figure 6.49: Injector mass flow rate for a duty cycle of 50%.

6.4.3 Effect of the injector actuation frequency on the dynamic response

The injector actuation frequency is an important parameter since it is intimately related with the engine operating speed. It is necessary to determine the limit of injector speed of operation and how the frequency of its actuation affects the actuator speed and the mass flow rate of hydrogen in the engine.

In this study, the actuation frequency was varied, while the remaining operating variables are kept constant.

If pulsed injection of hydrogen is to be implemented, then the injector must be capable of operating at very high frequencies.

Figures 6.50-6.59 show the effect of actuator frequency on the actuator speed and mass flow rate for a hydraulic pressure of 50 bar, H_2 pressure of 200 bar, static force of 500 N, cylinder pressure of 80 bar, actuator mass of 5 g, and a duty cycle of 50%.

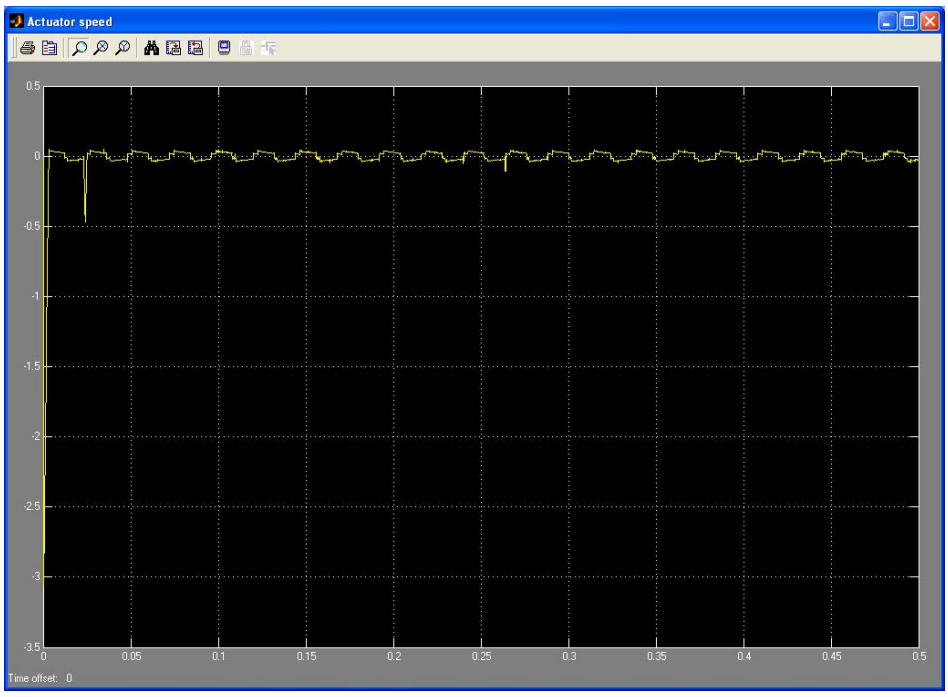

Figure 6.50: Actuator speed with period of injection 0.024 s (5000 RPM).

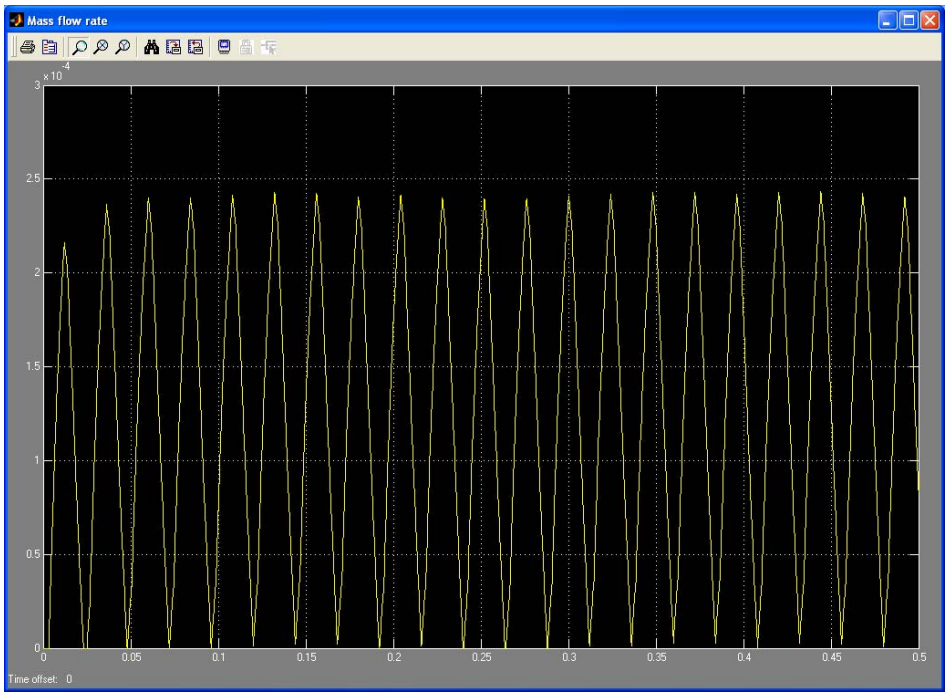

Figure 6.51: Mass flow rate with period of injection 0.024 s (5000 RPM).

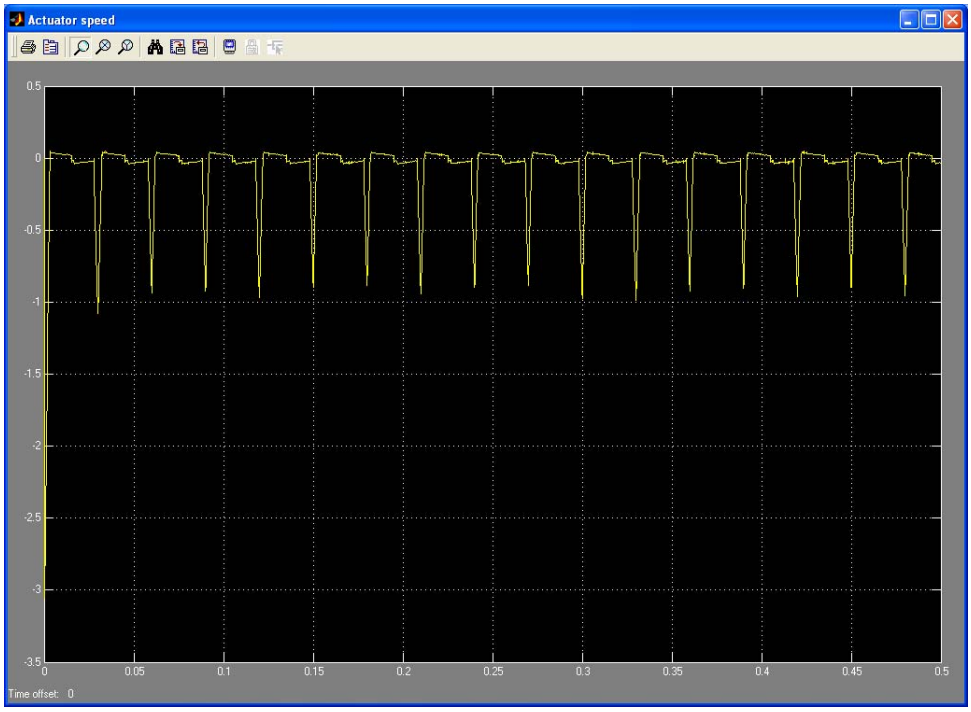

Figure 6.52: Actuator speed with period of injection 0.03 s (4000 RPM).

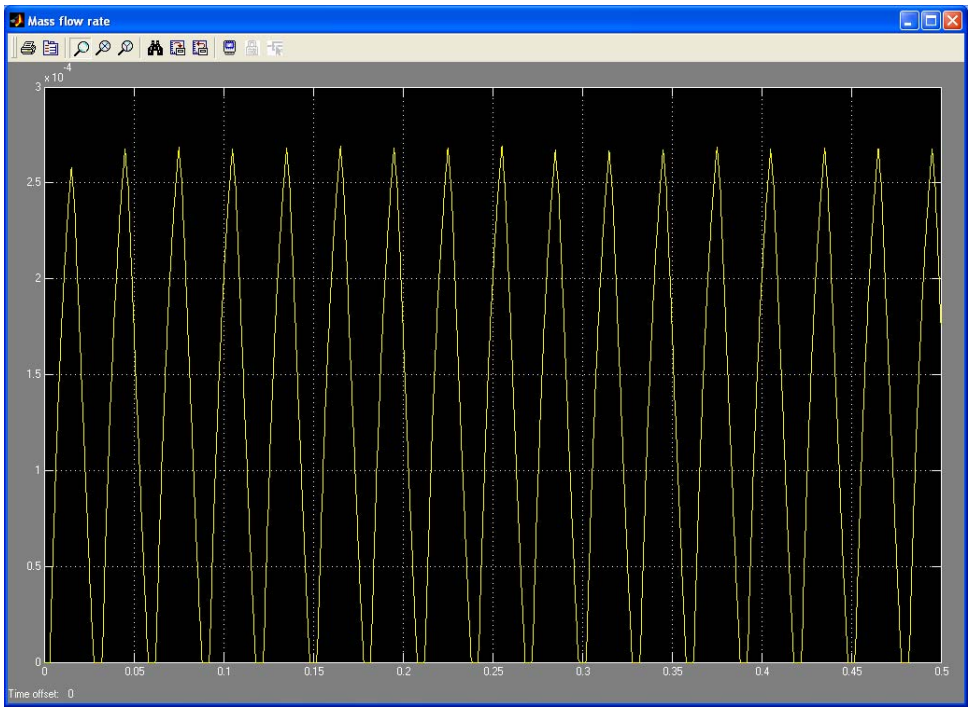

Figure 6.53: Mass flow rate with period of injection 0.03 s (4000 RPM).

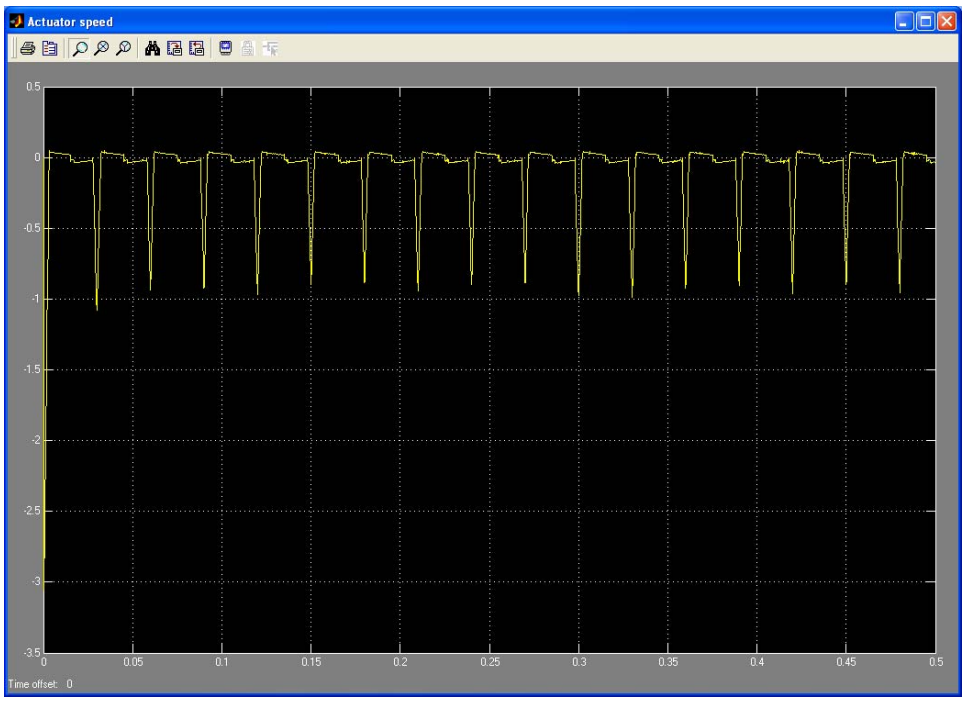

Figure 6.54: Actuator speed with period of injection 0.0333 s (3600 RPM).

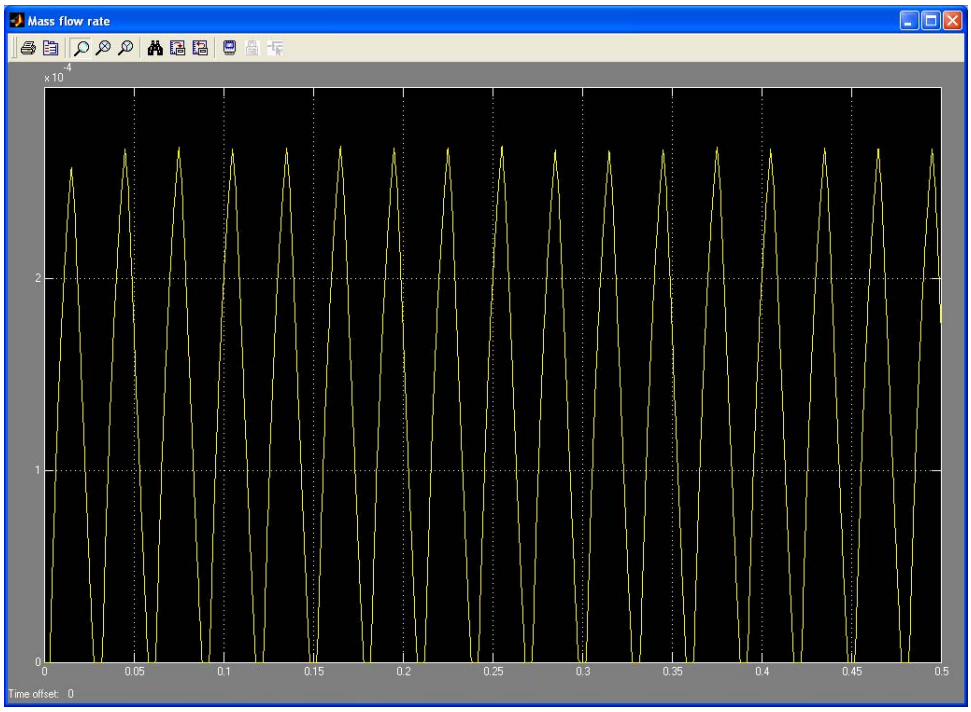

Figure 6.55: Mass flow rate with period of injection 0.0333 s (3600 RPM).

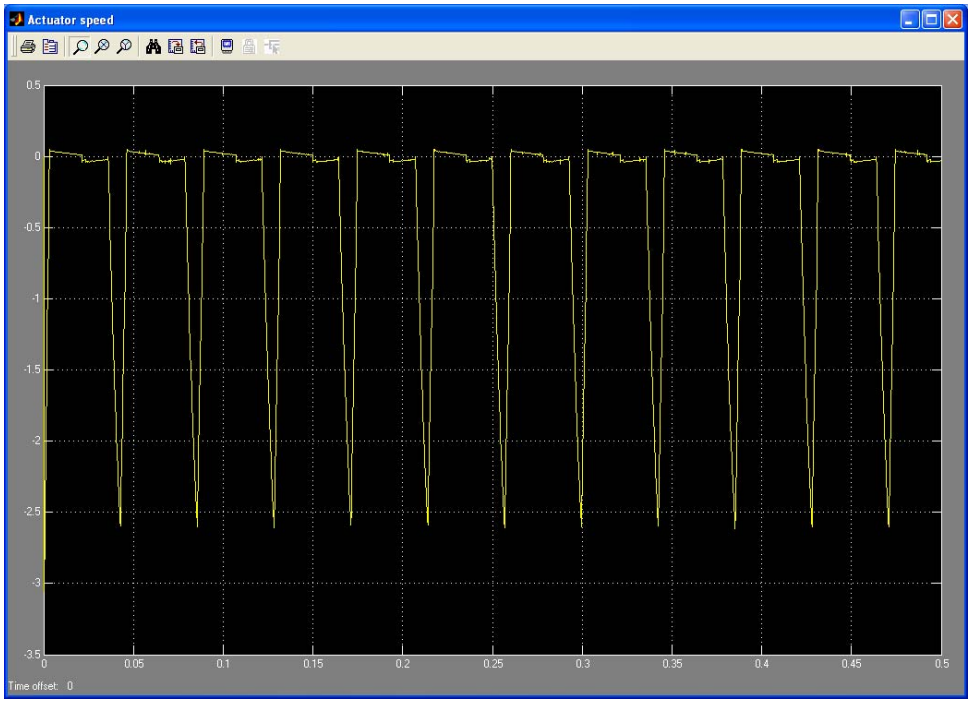

Figure 6.56: Actuator speed with period of injection 0.0428 sec (2800 RPM).

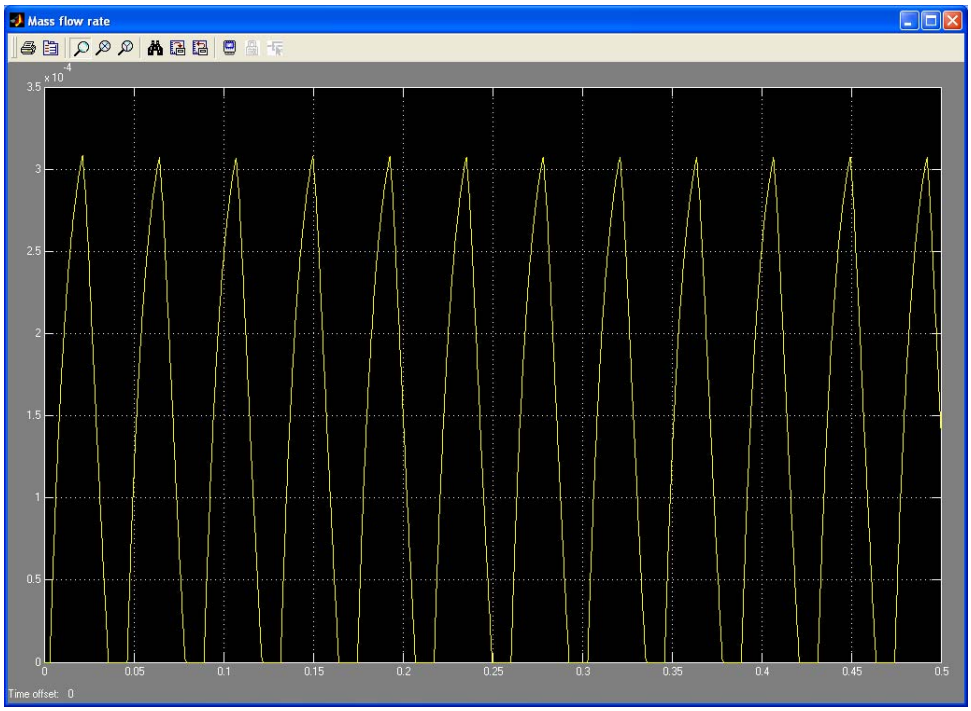

Figure 6.57: Mass flow rate with period of injection 0.0428 s (2800 RPM).

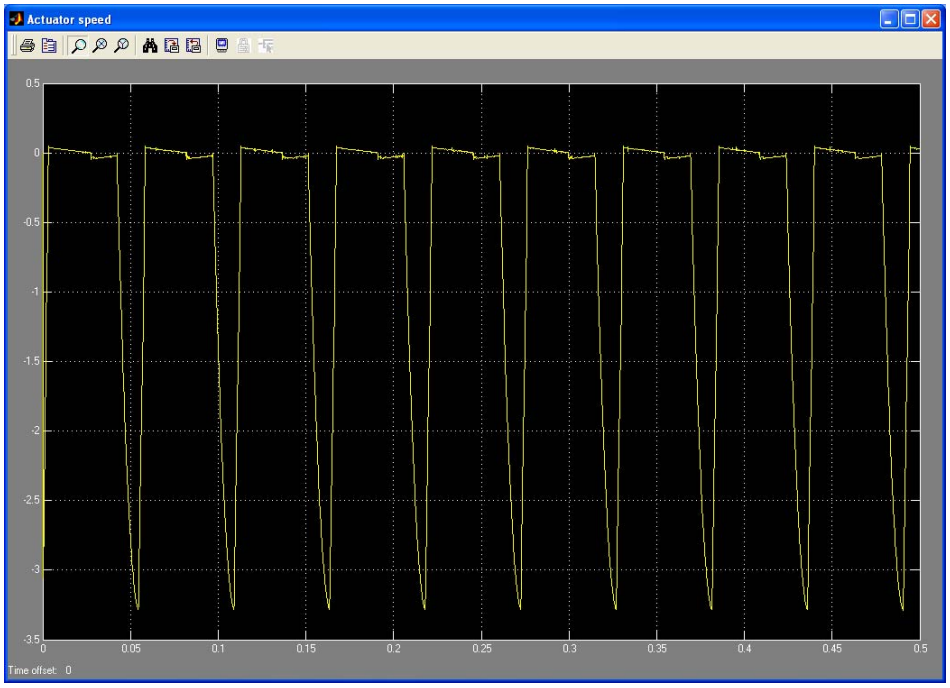

Figure 6.58: Actuator speed with period of injection 0.0545 s (2200 RPM).

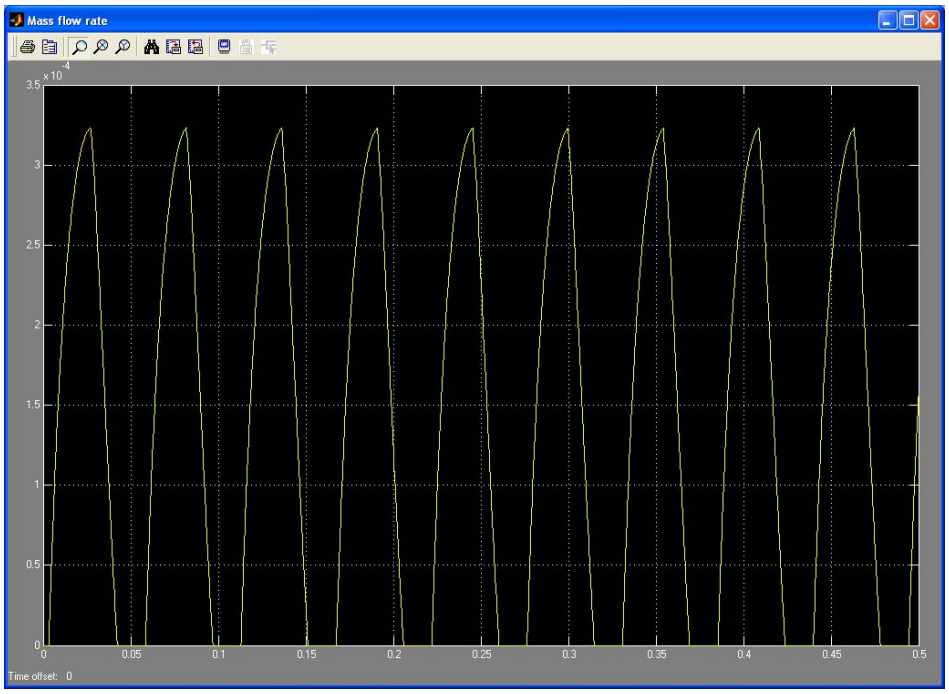

Figure 6.59: Mass flow rate with period of injection 0.0545 s (2200 RPM).

From the simulation results, it can be seen that the hydraulic injector is limited in terms of its speed of response, to a maximum operating speed of 2200 RPM. For higher speeds, the injector will be not even injecting hydrogen into the cylinder, this condition is represented in figure 6.50 that illustrates a “vibration” of the actuator around zero.

The simulated results indicate that the current injector is not capable of operating satisfactorily above a 5 kHz PWM injection.

6.4.4 Effect of the hydraulic pressure on the injector dynamic response

Another important variable to study is the hydraulic pressure to actuate the injector. To understand its influence on the operation of the injector the actuator speed and hydrogen mass flow rate were analysed for various pressures with all the other operational parameters kept constant.

Figures 6.60-6.67 show the actuator speed and mass flow rate for varying hydraulic pressure, with a H_2 pressure of 200 bar, static force of 500 N,

cylinder pressure of 80 bar, actuator mass of 5 g, a period of 0.0599 s (2000RPM), and a duty cycle of 20%.

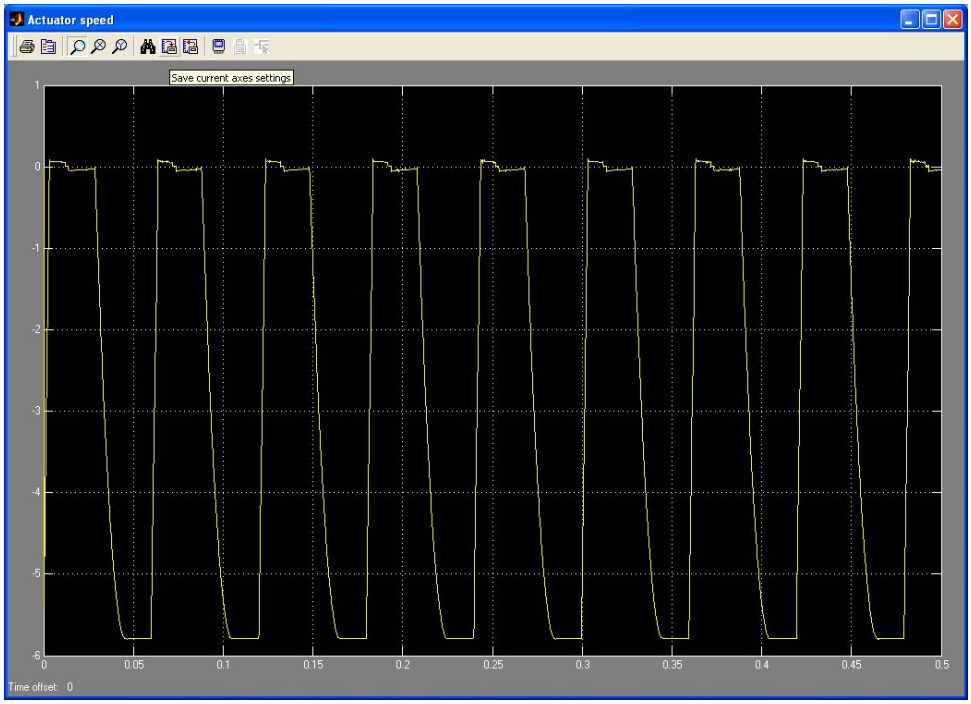

Figure 6.60: Actuator speed for 200 bar hydraulic pressure.

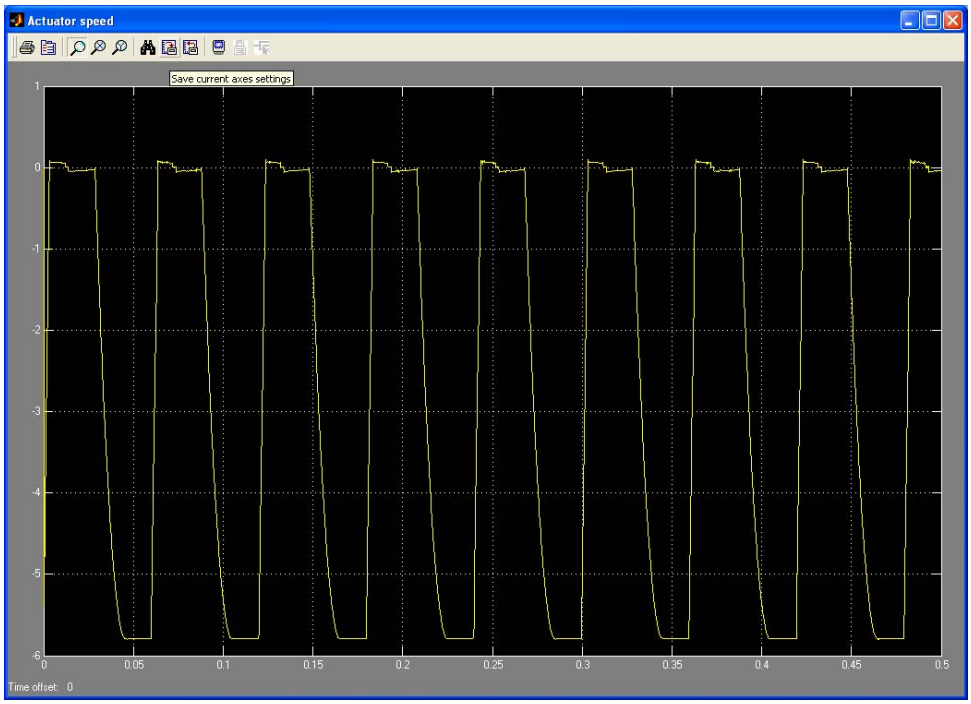

Figure 6.61: Actuator speed for 150 bar hydraulic pressure.

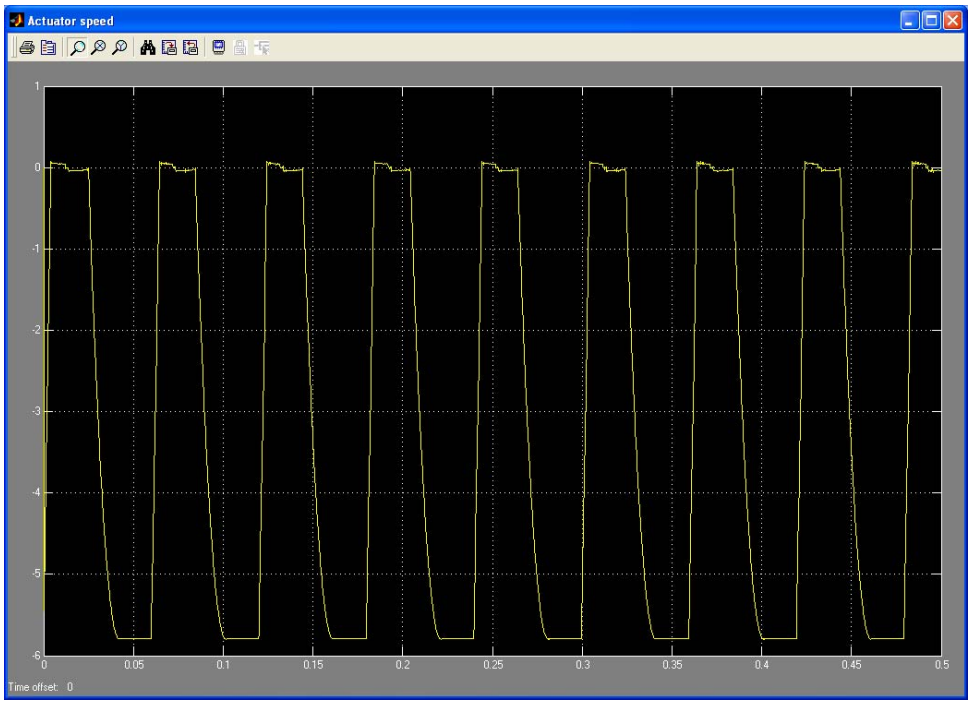

Figure 6.62: Actuator speed for 100 bar hydraulic pressure.

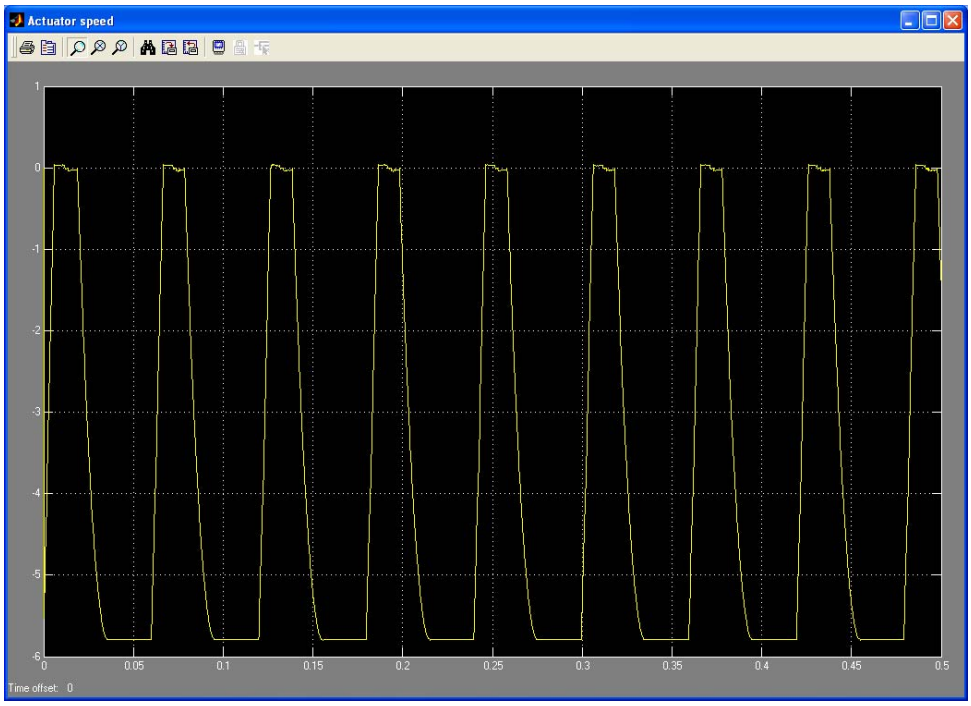

Figure 6.63: Actuator speed for 50 bar hydraulic pressure.

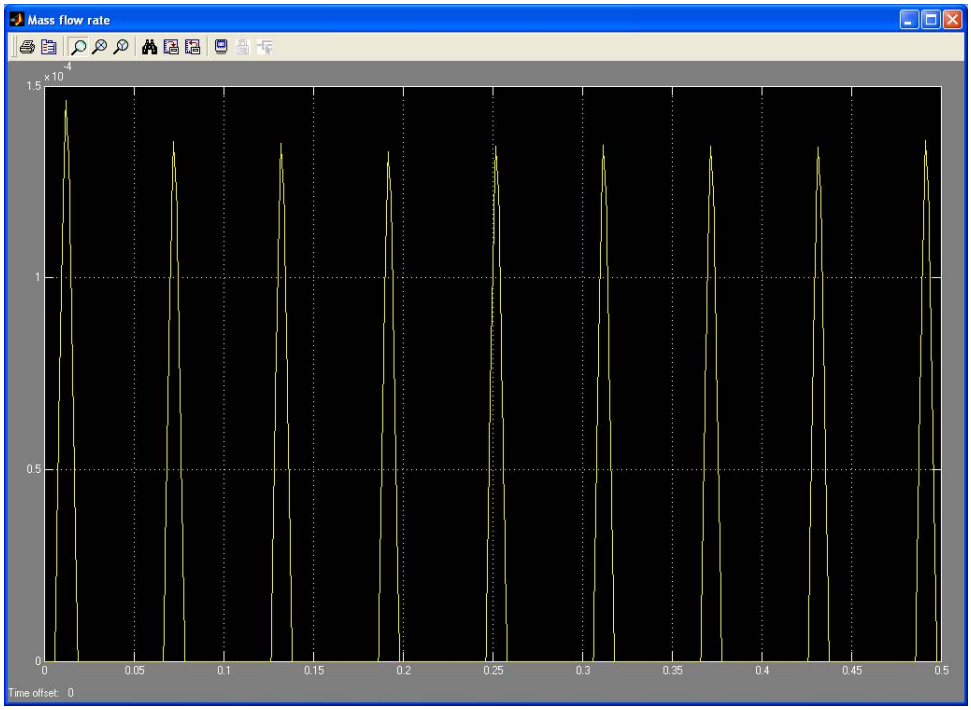

Figure 6.64: Mass flow rate for 50 bar hydraulic pressure.

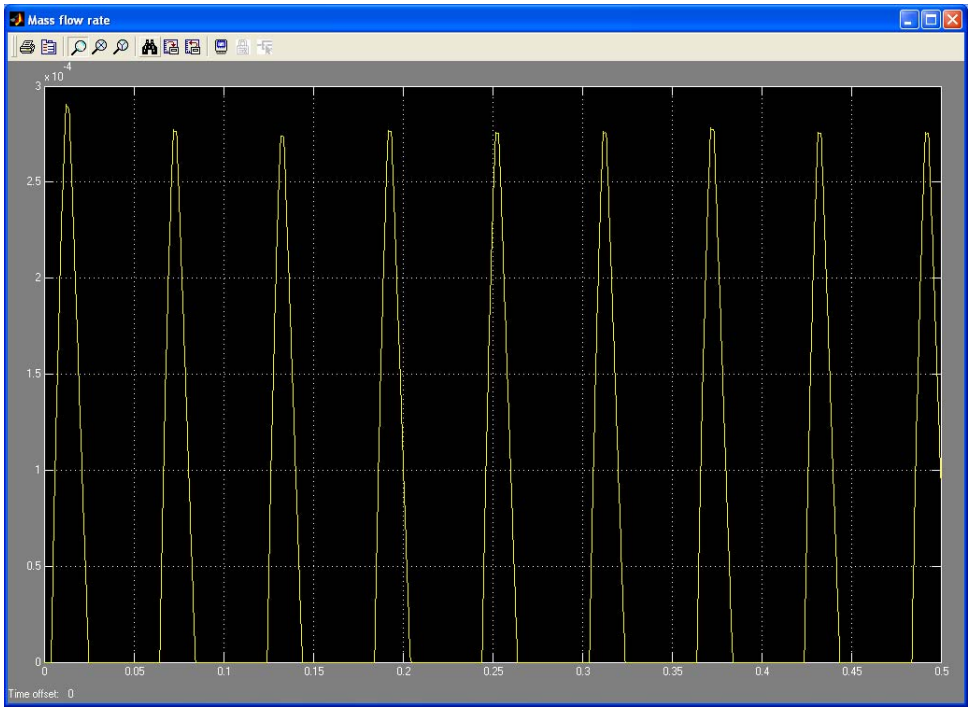

Figure 6.65: Mass flow rate for 100 bar hydraulic pressure.

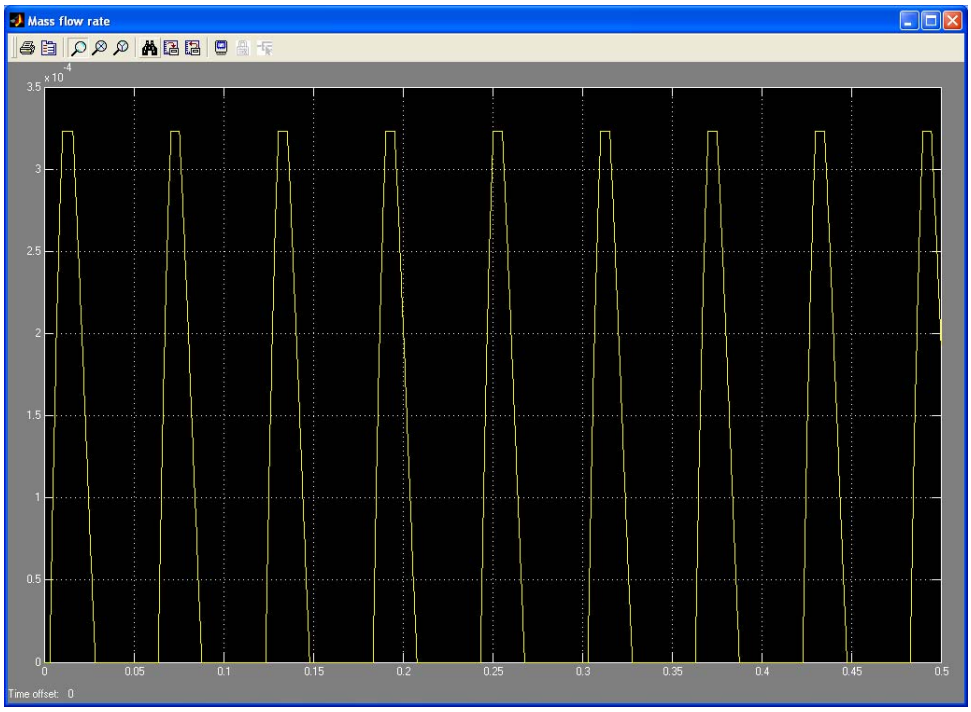

Figure 6.66: Mass flow rate for 150 bar hydraulic pressure.

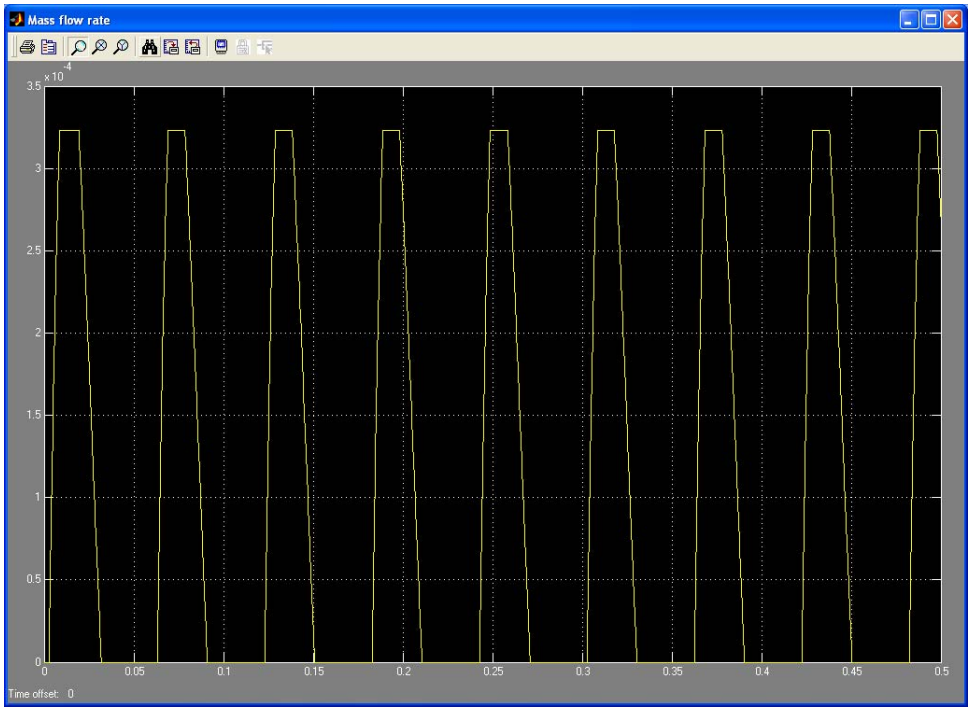

Figure 6.67: Mass flow rate for 200 bar hydraulic pressure.

Figure 6.68 summarises the influence of hydraulic pressure on the mass flow rate. It can be concluded that the increase in hydraulic pressure is beneficial regarding the mass flow rate up to a pressure of 200 bar. Higher

pressures do not produce higher flow rates as indicated in Figure 6.68, since the actuation delay is reduced to a minimum and the fluid dynamics delays then dominate.

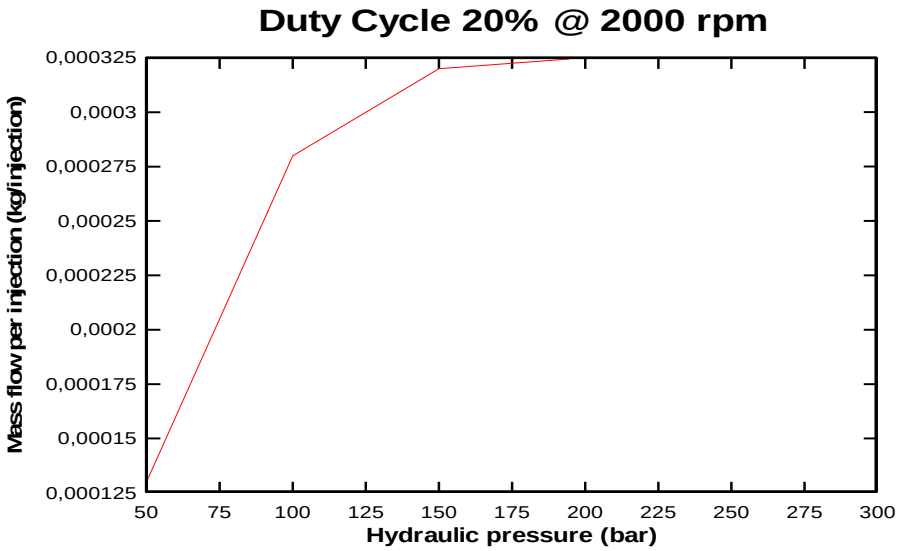

Figure 6.68: Relationship between hydrogen mass flow rate per injection and hydraulic actuation pressure.

6.4.5 Effect of the static force (pre-load) on the injector dynamic response

To understand the influence that the static force or pre load force has over the operation of the injector, this force was increased from 125 N up to 750 N while all other parameters were kept constant, as above.

Figures 6.69-6.72 show the actuator speed for varying static force, with a constant hydraulic pressure of 50 bar, H_2 pressure 200 bar, cylinder pressure 80 bar, actuator mass 5 g, period 0.0599 s (2000RPM), and duty cycle 20%.

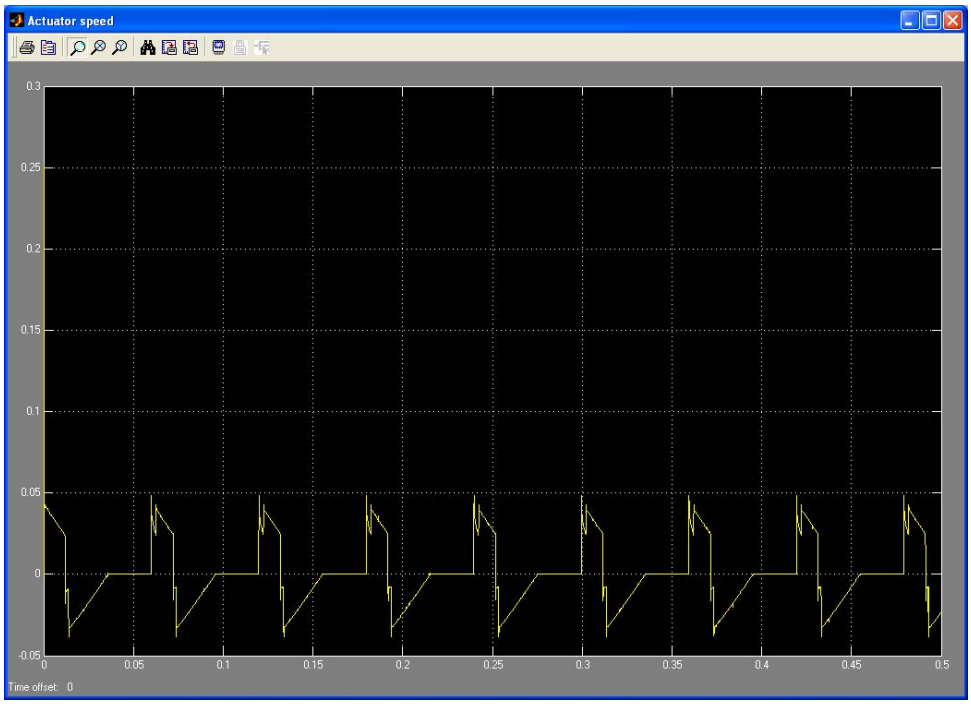

Figure 6.69: Actuator speed for a static force of 125 N.

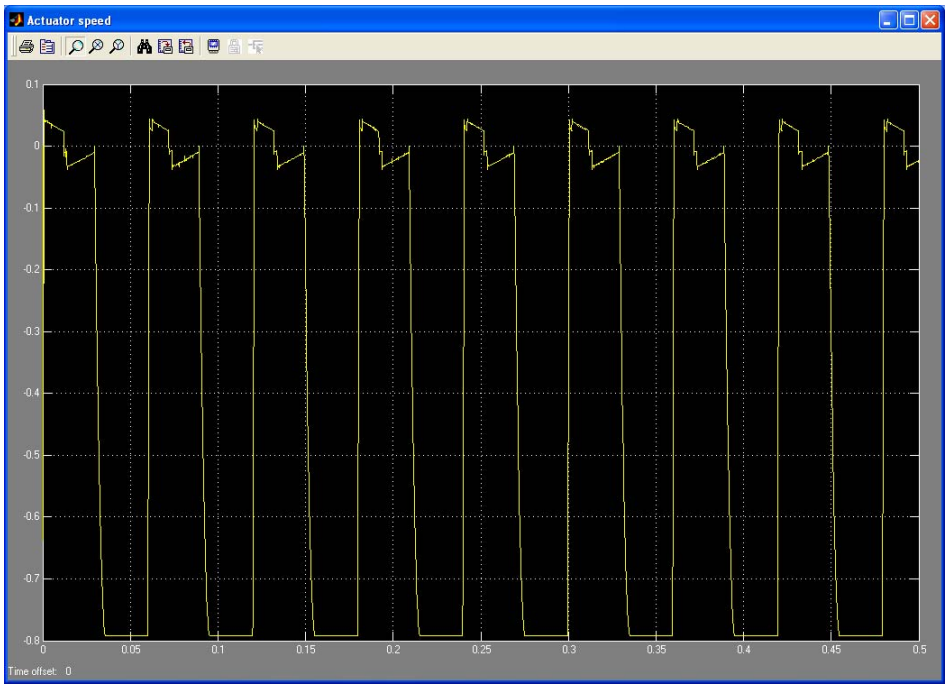

Figure 6.70: Actuator speed for a static force of 250 N.

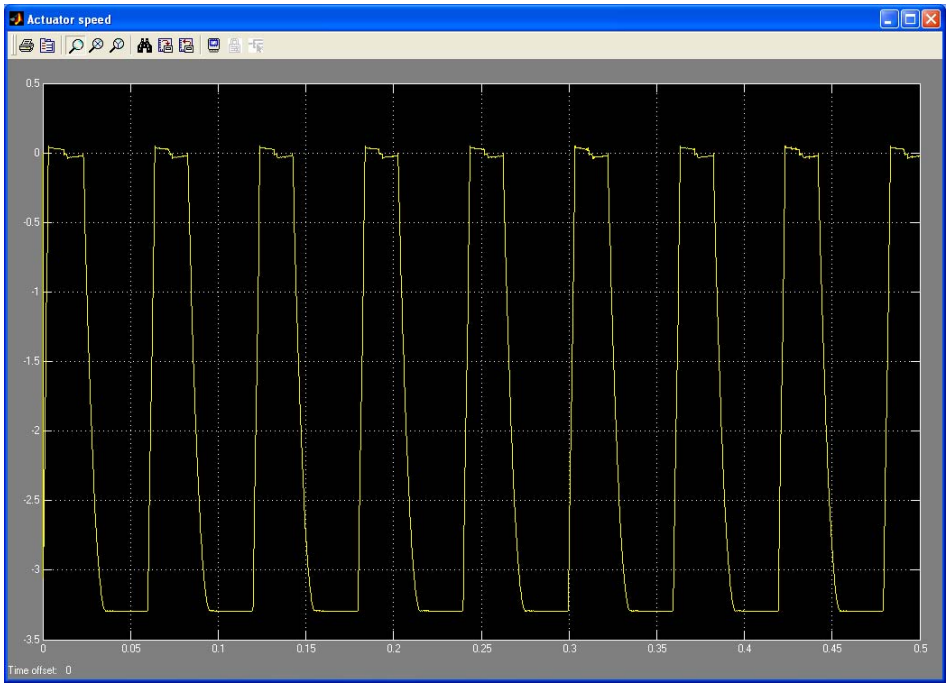

Figure 6.71: Actuator speed for a static force of 500 N.

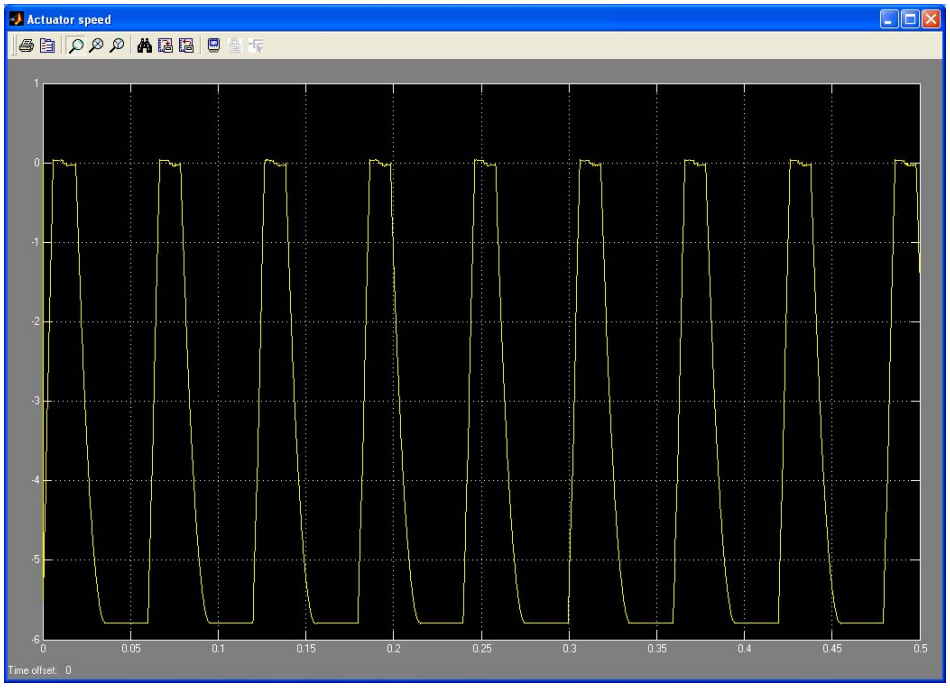

Figure 6.72: Actuator speed for a static force of 750 N.

Figure 6.73 shows the relationship between the static force and the speed of response. It can be concluded that the increase of the static force or pre-load of the actuator, through compression of the spring, increases the

speed of response of the injector. This force is, however, limited by the spring allowable compression. Therefore, in the design of the injector, an optimum trade-off between the static spring force and the hydraulic pressure with the view of achieving satisfactory dynamic performance must be made.

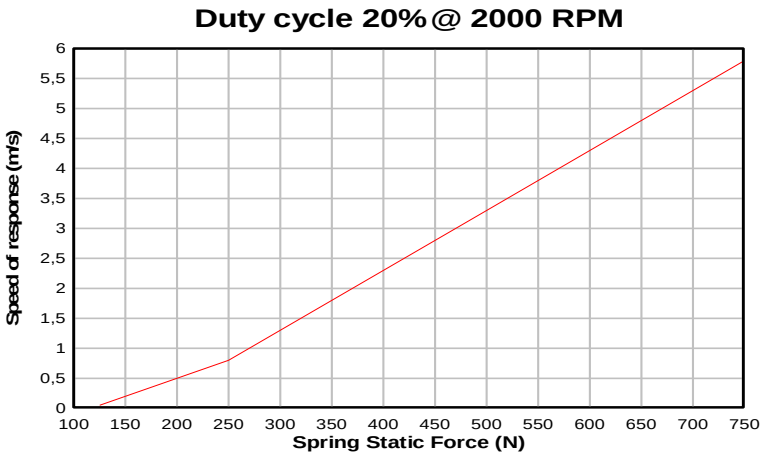

Figure 6.73: Relationship between the speed of response and the static spring load.

6.4.6 Summary of injector design analyses

The weight of the moving parts of the present design is not a limiting factor of the injector operation. The findings indicate that the operating hydraulic pressure of the injector should be between 80 bar and 100 bar, and the static spring load should be around 800N to provide adequate dynamic performance. The operating speed of the engine with this injector is limited to around 2000 RPM. This limitation is due to the mass spring system response.

It is not possible to use the present injector to deal with pulsed injection, due to the high frequencies involved and its poor frequency response. Further, due to deficient regulation of the flow, the injector can cause the engine to operate erratically for values of PWM smaller than 30%.

6.4.7 Possible injector design improvements

There are a number of possible improvements to this injector. With the objective of assuring that no seizure of the moving parts will occur, the parts were machined with clearances to allow some passage of hydraulic oil to lubricate the needle valve. Because these clearances were too generous, and the hydrogen pressure was higher than the hydraulic pressure, a substantial amount of hydrogen passed through the clearances to the hydraulic oil return pipe. Therefore better machining and tighter clearances are need for future design of such a type of injector.

Also it is obvious that the dynamic characteristics of the injector need to be improved. This can be achieved by constructing a new injector with a different approach, so that pulsed injection can be used. The use of new magnetostrictive materials, such as TERFENOL D, could provide the solution, as this material can cope with frequencies in the order of several MHz and do not need oil lubrication if graphite is used on the needle rubbing surfaces.

6.5 Summary

This chapter demonstrated the use of simulation as a tool to further complement the experimental work. In particular they allowed investigation where experiments would be too costly, difficult or even impossible to carry out.

Using the simulation programs developed during this research, it was possible to determine the range of the physical parameters to control the hydrogen injection process and therefore the engine performance.

The simulation of the rate of pressure rise demonstrated the difficulties in predicting operating parameters with such a random behaviour with the same accuracy as the other variables, such as peak cylinder pressure. This possibly is due to the limitations of the mathematical model used for the simulation studies of this research. However, improvements can be made to

better predict such variables, although the results obtained were satisfactory for the present research since the simulation model allowed the study of the parameter influence that could not be easily tested using the test engine, giving one insight on the ruling variables of the hydrogen fuelled CI engine.

It was found that to overcome the difficulties encountered in terms of control of the ignition angle, as well as in terms of the rate of pressure rise, that this cannot be solved by the optimisation of one design variable only. The optimisation of the engine compression ratio, variable valve timing, and pulsed injection can be used to provide good engine performances. However, the simulation evidenced that the use of high speed and accurate injectors is required for DIH_2 operation and this introduces a number of problems to solve. It was concluded that for HCCI engines, the injectors do not need to be so fast and accurate as there is plenty of time to inject the hydrogen into the cylinder, being the main problem of this mode of operation the control of the ignition angle, that by itself is a function of the residual gases inside the cylinder, the air temperature, speed and load.

For hydrogen direct injection it is extremely important that the temperature of the air at the beginning of compression is controlled, and it was found that the start of injection should be retarded compared to diesel operation in order to avoid excessive in-cylinder pressures.

It was found that for the hydraulically actuated injectors, the inertia of the moving parts is not critical, but the pre load force and the hydraulic pressure play a fundamental role in the performance of such injectors.

Chapter 7

Conclusions and recommendations

« **Standing still is the fastest way of moving backwards in a rapidly changing world** »

This thesis has presented a research work developed into the use of hydrogen as a fuel for CI engines.

A revision of the historical research carried around this subject was performed, identifying a path for the research and the achievements and requirements of further research. The use of hydrogen as a fuel for CI engines when this research started was a new area of research, with very few available data and reports.

To perform such research an existing Diesel engine was adapted to operate under HCCI and DIH_2 modes, requiring the design and manufacture of a considerable number of systems, components, such as hydrogen injectors, injector controllers, hydraulic load brake, hydrogen fuel system, hydraulic actuator system, inlet air temperature control system, hydrogen detection system, and a data acquisition software.

A simulation model was developed and validated against the actual engine, or physical model, for both modes of operation HCCI and DIH_2, and used at a later stage as a complementary research tool. The dynamic simulation model of the engine operating under HCCI and DIH_2 was used extensively as a tool to overcome the limitations of the physical test stand, such has variable compression ratio, variable valve timing, high speed pulsed injection and evaluation of some dynamic variables such as the rate of heat release, temperature profile in the combustion chamber, angle of maximum rate of heat release, that would be very expensive to measure if not impossible. The engine dynamic model allowed also the evaluation of the effect of environment variables such as inlet air temperature, or

atmospheric pressure, but also the study of the impact on the cycle of the change of some characteristic engine parameters such as compression ratio, injection duration, fuel mass flow rate, bore, stroke, speed and valves timing performing the Miller cycle.

An important part of this research was devoted to the design of the injection systems, in particular the injectors for HCCI mode of operation, operating at low pressures (less than 6 bar) and the injectors for DIH_2 mode of operation operating at pressures above 50 bar, therefore requiring the use of hydraulic force for their actuation. For the design of such hydraulic injectors the use of a mathematical model was also a valuable tool, helping the understanding of how the design parameters were interrelated with each other, therefore allowing the construction of a working injector.

Once the required hardware for hydrogen operation (HCCI and DIH_2 injection systems) was manufactured and characterised, it was fitted on the test engine, to operate it under HCCI and DIH_2 modes. Then, a number of test runs were performed to gather data for comparison between the various modes of operation including diesel. These comparisons were focused in particular in what concerns thermal efficiency, performances and identification of aspects that needed to be solved to achieve a safe and reliable operation with hydrogen under each mode of operation.

The existing rules and standards applicable to safety and manipulation of hydrogen applicable to engines are inexistent, therefore, during the course of the present research general rules had to be adapted, and above all a good sense and fair engineering judgement was employed to avoid unsafe circumstances.

The findings have been summarised at the end of each chapter and will be recapped and synthesised in this last chapter. In addition, design considerations for hydrogen-fuelled engines will be discussed, based on the experience accumulated during the present research, and recommendation for further work will be presented.

As a result of the present research the author, developed the sufficient knowledge to design an injection system and respective engine control to

convert two marine diesel alternators of 4.000 kW with a 320mm bore engines to operate as dual fuel engines (natural gas). Later the author converted to dual fuel operation (natural gas) also one marine diesel alternator of 11.000 kW and a smaller diesel alternator to hydrogen operation. Please refer to appendices A and B.

To achieve, an effective engine protection and control, the author developed a knocking control system called KDS (Knock Detection System), based on automatic comparison of vibration spectrums measured at the cylinder head of the experimental engine, controlling the flow rate of hydrogen and therefore the high RPR characteristic of hydrogen operation.

The present research, resulted into two papers, edited by the International Journal of Hydrogen Energy, and a two more papers presented in conferences and symposiums.

7.1 Summary of the results

Chapter 2 presented a review of the reported hydrogen technologies related to the properties, handling and applications of hydrogen fuel, as well as to its use in reciprocating engines. Particular features and challenges associated with hydrogen-fuelled engines were identified, such as the potential for high fuel efficiency, lean-burn operation and low emissions formation, as well as challenges of high pressure rise rates and ignition timing control. This chapter also presented a review of reported research, from the early stages of hydrogen use as a fuel until recent studies highlighting modern engine performance and the difficulties in storing and handling hydrogen fuel.

In Chapter 3, the design and development of the engine and injectors test rig systems used in the research were described. The purpose-developed system controllers, the high-speed frequency data acquisition system and related hardware and software, and experimental safety requirements were presented in detail.

Chapter 4 presented the experimental methodology followed during the experimental phase of the research, as well as experimental results and their interpretation. Main conclusions from the experimental work are as follows:

From the experimentation tests performed, it was found that:

- The hydrogen operated engine, in HCCI and DIH_2 modes, have better thermal efficiencies (48 % and 42.8% respectively) than the same engine operated with diesel oil (brake thermal efficiency of 27.9 %).
- From a breakdown of the engine heat balance, it was found that the bigger heat loss is through the exhaust for the hydrogen-fuelled modes of operation, rather than through the cylinder liner and cylinder head as in the diesel oil operated engine.
- The experimental tests further showed that extremely high rates of pressure rise can result from too high air inlet temperatures, and these can have a negative impact on the piston crank mechanism bearings.
- It was found that the HCCI engine is limited in power due to the gaseous hydrogen fuel displacing a significant amount of intake air.
- However, it was demonstrated that the HCCI engine can be operated successfully with extremely lean cylinder charges, albeit with higher cycle-to-cycle variations.
- The power output of the DIH_2 engine is not limited in the same way, but the maximum power may be limited by high peak pressures and high rates of pressure rise which can cause mechanical problems.
- The controllability and operational stability of the HCCI engine was found to be challenging due to difficulty in controlling the ignition angle, whereas the controllability of the DIH_2 engine is excellent as ignition takes place at the initiation of the injection as in a conventional diesel engine.

- The tests of Dual-fuel mode of operation, demonstrated that hydrogen can be used simultaneously with diesel oil as a source of ignition, improving the thermal engine efficiency, and the emissions even in small induced quantities.
- Therefore the Dual-fuel mode of operation has a large potential for the penetration of hydrogen in the industry, namely on board vessels where there is a considerable amount of wasted energy to recover and accumulate as hydrogen, that can be used to drive auxiliary engines in port, therefore complying with the ever stringent local air pollution laws.
- High flame speed within the engine cylinder over a wide range of temperature and pressure. High flame speeds were identified even for lean mixtures. The energy release is also so fast that the combustion duration is short contributing for the high power output, high efficiencies and high rates of pressure rise.
- The high rates of pressure rise, are noticeable even at low loads for both modes of operation, in particular for HCCI.
- The DIH_2 mode of operation allow the use of very lean cylinder charges, that in combination with the fast rates of heat release around TDC, results in high thermal efficiency values and simultaneously in high power output.
- The HCCI mode of operation allow the use of extremely lean cylinder charges, that in combination with the fast rates of heat release, that in the case of optimised ignition angle, results in high thermal efficiency values and simultaneously in lower power output when compared with DIH_2 and diesel operation.
- One of the most important features of HCCI and DIH_2 are the less undesirable exhaust emissions when compared with Diesel fuel. The lubricating oil is the only source of hydrocarbon emissions that in a well maintained engine tends to be negligible. Only NO_x and water

vapour were identified as being the main products of the combustion.

- For the HCCI mode of operation the hydrogen presence on the exhaust gases is negligible when timed port injection is used. If hydrogen is simply fumigated ate the cylinder inlet, the presence of hydrogen in the exhaust can be quite important as the cylinder is scavenged with a mixture of air and hydrogen.
- For DIH_2 the presence of hydrogen in the exhaust is negligible and it is a function of the combustion chamber crevices.
- The hydrogen fast burn characteristics allow its use in high speed CI engines as there is no charge preparation time required by the diesel fuel, therefore allowing an increase in power output with a reduced penalty for lean cylinder charges.
- As the self-ignition temperature of hydrogen is quite high when compared with other hydrocarbon fuels, the compression ratio of these CI engines must be higher than the ones used for diesel fuel operation, therefore contributing for higher efficiencies and higher power outputs of the HCCI and DIH_2 engines.
- Hydrogen operation therefore is associated with less heat loss than with diesel fuels.
- Due to the hydrogen high burning rates and its diffusivity, the HCCI and the DIH_2 are less sensitive to combustion chamber shapes, level of turbulence and charge swirling effects.
- The thermodynamic and heat transfer characteristics of hydrogen are accompanied by higher final compression temperatures contributing to improvements in engine efficiency and lean mixture operation.
- Less cyclic variations are encountered for hydrogen than with other fuels, even for lean operation, however for very lean operation these cyclic variations are a reason for the engine control difficulties.

- Less cyclic variations lead to the reduction of emissions, smoother operation and improved efficiency.

The development of the HCCI and DIH_2 injectors was essential to carry out the experimental studies presented, in particular for the DIH_2 engine. The design, construction and testing of the injectors were described in detail.

In Chapter 5, the development of a full cycle simulation model for the HCCI and DIH_2 was introduced and its functional organization, the sub models implemented and assumptions made were described. The modelling of the HCCI and DIH_2 injectors were also presented.

It was found that to model the combustion of hydrogen, commonly used compression ignition engine models for liquid fuels do not apply. The differences in the combustion properties between conventional liquid fuels and hydrogen include factors such as the atomisation and preparation of cylinder charge (since hydrogen is already in its gaseous form), in-cylinder gas dynamics and fuel-air mixing, and radiative heat transfer losses.

The ignition delay characteristics are different for hydrogen-fuelled engines, since for temperatures below 1000 ºK it can be very long when compared with a modern diesel oil injection system ignition delays, but for higher temperatures the ignition delay is extremely short.

Further, the use of a heat loss model calibrated against the measured temperatures on the liner and piston head and assuming that the temperature of cylinder head is the same as the temperature of the piston crown was essential to achieve thermal efficiencies similar to those registered during the tests.

In Chapter 6, the engine model was validated against the experimental data and the uncertainties calculated. Based on simulation, the influence of various operational variables, such as ambient conditions, was systematically investigated. Mitigation actions of the high rates of pressure rise were studied with the objective of reducing the dynamic bearing loads and improving the engine controllability. The optimisation of the engine

operation was studied by evaluating the valve timing, resulting in the implementation the Miller cycle. Other techniques were also evaluated, such as pulsed injection, inlet air pre-heating, and compression ratio variation. Chapter 6 also presents the dynamic simulation of the DIH_2 injector, resulting in the identification of the dominating variables for the DIH_2 operational characteristics.

- As a consequence of the short ignition delay and rapid combustion, the hydrogen combustion process for HCCI and DIH_2 approaches the constant volume cycle.
- The simulation analysis indicated that pulsed injection can partly mitigate problems associated with high peak pressures and high rates of pressure rise, but does not provide a complete solution.
- It was proved that controllability of the HCCI engine is influenced by the ignition angle variations, which are a direct function of the end-of-compression temperature, which is therefore affected by all the parameters on which this temperature depends like residual gases temperature.

The main parameters influencing the angle of ignition include the temperature of the air at the inlet of the cylinder, engine load, compression ratio and heat exchange between the cylinder walls and the cylinder charge. However, the dominant variable is the air temperature entering the cylinder, with which engine control can be improved using one of the solutions presented in the recommendations.

- It was confirmed by simulation that unlike the diesel fuelled engine, the main losses of heat in the hydrogen engine are through the exhaust gases, rather than through the liner and cylinder head.
- The reason for such exhaust losses is that the hydrogen combustion is extremely fast compared to diesel combustion and without production of radiating particulate matter as for hydrocarbon combustion.

- It was found by simulation that due to the fast combustion, hydrogen injection could be initiated closer to TDC, thereby improving engine efficiency.
- Through the simulation study, it was found that an efficient way of controlling the compression ratio and rate of pressure rise is to implement valve timing control. Adjusting the valve timings to the engine load can contribute positively to the engine controllability, as well as for the control of the emissions of NOx.
- Therefore the Miller cycle was simulated, confirming the above conclusions.
- The DIH2 injector model was found to be adequate, as it allowed the setting up of the injector for the tests, but also gave knowledge of its limitations, learning among other things that the inertia of the moving parts is a less dominant variable compared with the pre-load and the hydraulic pressure.
- Simulation studies indicated that pulsed injection can contribute to mitigate the high rates of energy release, and therefore the rate of pressure rise, but with the increase of the pulses frequency, the effect approaches the continuous injection.
- The pulsed injection frequency needs to be adapted and optimised to the engine speed of operation, to sort some effect. From the simulation studies and for an engine speed of 2200 RPM it was found that the combination of start of injection 25° BTDC, duration of injection 33°, plus pulsed injection at 5 kHz, resulted in the lowest maximum combustion temperature, lower RPR, lower MRPR, while maintaining engine power output
- Such high injection frequencies and required accuracy, cannot be met by using common mechanical injectors as the one used on this research, which whoever can be employed in low speed engines. A new technology must be developed, which is introduced on the recommendations.

7.2 Hydrogen as a fuel for CI engines, further considerations

Hydrogen has a number of unique features that potentially make it a particularly interesting CI engine fuel. Some of these features are the following:

- Hydrogen fuelled CI engines are less sensitive to hydrogen purity than other hydrogen fuelled energy conversion devices such as fuel cells.
- Heat transfer characteristics of hydrogen fuelled CI engines are significantly different from those engines operating with hydrocarbon fuels, as hydrogen combustion is characterised by lower radiation therefore taking a bigger importance the convective component of the heat transfer specially for lean cylinder charges.
- Hydrogen engines are suitable for waste heat recovery applications since the energy transfer from some water vapour can add up to the thermal load output and the corresponding energy efficiency.

Despite the above listed advantages of hydrogen as a fuel, there are a number of limitations and mechanisms associated with its used as a CI fuel that is worth to mention. There is a need to address equally this limitation and suggest means to overcome them.

The following points are a list of features associated with hydrogen as a CI engine fuel that may require some further engineering effort or remedy:

- Hydrogen as a compressed gas at 200 bar and atmospheric temperature has only approximately 5% of the energy of diesel oil for the same volume.
- Unless the energy required to produce the hydrogen is from a renewable source or from a low temperature waste heat source the energy required is bigger than the energy produced as ¾ of the energy contained in one kilogram of hydrogen may be used to liquefy

it. Therefore, the existence of a hydrogen fuelled engine must be associated to some renewable or waste heat recovery source of energy.

- Dual-fuel (hydrogen+ diesel oil) operation mode, results in a brake fuel efficiency improvement of up to 5%.
- Dual-fuel mode of operation results in drastic particulate matter emission, even in small quantities such as 10% of the energy per cycle.
- Dual-fuel mode of operation is characterised by stable engine governing for hydrogen quantities up to 50% of the heat input per cycle.
- Dual-fuel mode of operation can constitute an important way of dissemination of hydrogen as a fuel for CI engines in the industry.
- Dual-fuel mode of operation can potentiate projects where hydrogen is produced from renewable or waste heat recovery projects, as diesel-oil or bio-oil working as pilot fuels can be reduced to 5% of the energy required per cycle, being the remaining 95% of the energy supplied by the hydrogen.
- HCCI engines operated with hydrogen suffer from limited power output, mainly due to the very low heating value on volume basis. This effect is more noticeable when operating with very lean cylinder charges.
- The above effect is aggravated due to the relative high stoichiometric hydrogen to air ratio.
- There are considerable potential problems associated with backfiring and pre-ignition into the intake manifold of HCCI engines, noticed clearly during the tests carried. Hydrogen pre-ignition is mainly due to its low ignition energy.
- The high burning rates of hydrogen may produce high temperatures and pressures during combustion, in particular for less lean cylinder

charges, and may lead to higher rates of thermal NO_x emissions. Therefore an optimised engine control system is required to provide acceptable engine performance and lower emissions.

- The use of cold exhaust gas recirculation, may be a limitation as the cylinder temperature control has a major importance on the angle of ignition and therefore on engine control.
- There is always some potential for increased safety problems with hydrogen handling systems and operation.
- Materials compatibility problems need to be considered for all engine components in direct contact with hydrogen.
- There is a potential for corrosion problems and lubricating oil deterioration due to condensed water from its combustion and viscosity reduction due to hydrogen incorporation by the lubricating oil molecules.
- It was found that the cylinder charge temperature at the end of the compression stroke is the variable that has the highest influence on the ignition angle and subsequent rate of pressure rise. This variable is therefore of critical importance for engine controllability.
- Consequently, all the variables influencing the end-of-compression temperature, like inlet air temperature, temperature of the residual gases, temperature of combustion chamber, compression ration must be controlled to control the rate of pressure rise and angle of ignition. Therefore, one or more of these variables need to be controlled to achieve an acceptable engine controllability and efficiency.
- Due to the high self-ignition temperature of hydrogen, it was found that to achieve stable operation of the engine in compression ignition hydrogen fuelled mode, the intake air had to be heated above 70ºC.
- In the HCCI operation, the higher the air fuel ratio the lower is the required inlet air temperature to achieve the cylinder charge

ignition as higher temperature of the residual gases help on the required end of compression temperature. Therefore the higher the engine speed the earlier would be the ignition, contributing for lower engine controllability.

- In HCCI engines the angle of ignition is an inverse linear function of the air at the cylinder inlet temperature.
- In the HCCI, exhaust gas temperature, maximum combustion pressure and angle of ignition, increase with engine load.
- Hydrogen ignition delay is short and its combustion is extremely fast. To achieve a good thermal efficiency, the angles of injection and ignition of the cylinder charge need to be very close the TDC, therefore producing the maximum of positive work.
- For HCCI CI engines, the parameters influencing the angle of ignition need to be accurately controlled, being the most effective way of doing it through the control of the compression ratio, through the used of variable valve timing system. Despite the possible contribution to the control of the angle of ignition and rate of pressure rise, of variables like cylinder inlet air temperature they not sufficiently fast.
- The variable valve timing control system, it is an extra complication and cost to consider for a controlled HCCI engine operation.
- By comparing the heat losses between the various modes of operation at the same speed, and load, it was concluded that exhaust losses are less predominant on the HCCI engines than on diesel and DIH_2. This fact is due to a lower heat input per cycle (high equivalence ratio) characteristic of HCCI operation.
- DIH_2 operation has lower cooling losses than the HCCI and diesel mode of operation as combustion takes place closer the TDC than the other modes of operation.
- For the HCCI engine, the higher the temperature inside the cylinder the earlier is the ignition, and therefore the lower is the engine

efficiency and the higher the rate of pressure rise. Whereas for the DIH_2 the cylinder charge temperature has only effects on the ignition delay angle and rate of pressure rise, that some how can controlled if the pressure development takes place only after TDC.

- DIH_2 mode of operation can deliver more power, than HCCI and Diesel modes, this is mainly due to the absence of an air fuel ratio limit, therefore the combustion can be made so rich as required. Also there is no need for cylinder charge preparation time, as hydrogen is injected in gaseous state, which allied to its diffusivity and fast combustion development after TDC contribute for such high power capability.
- For the DIH_2 mode of operation, the production of NO_x is an exponential function of the indicated mean effective pressure for both modes of operation.
- For a constant heat input per cycle, the DIH_2 thermal efficiency is higher for higher engine speeds, and the RPR is practically constant through all the engine load range.

7.3 Recommendations for further work

Hydrogen fuelled CI engines can exhibit operational characteristics that are superior to those associated to conventional diesel fuels. The results presented in this thesis indicate that further developments of hydrogen fuelled CI engines should be oriented towards the control of the angle of ignition and rate of pressure rise, necessarily including the development of fast response control systems. For the HCCI engine, operational stability and the minimising of cycle-to-cycle variations is of critical importance, and these must be resolved before such engines can become commercially viable. This research has identified the important control variables for combustion control, including the level of pre-heating of the intake air and compression ratio control. Significant improvements in the controllability of such engines can probably be achieved in a more detailed study focussing on engine control issues related to the control of such variables.

The work presented has shown that satisfactory hydrogen injectors can be developed using standard techniques and materials, however the designs can be refined and improved using advanced materials and fast-acting actuators.

The information contained on this research work have given new insights into the areas that require further development, but complementary knowledge concerning the engine applications and integration should also be studied.

In the next paragraphs, are outlined some possible approaches contributing for the improvement of the hydrogen fuelled compression ignition engines. A number of possible design and operation features need to be addressed to make the hydrogen CI hydrogen fuelled engines serious candidates for some applications. When most of these following recommendations are implemented in the design of CI hydrogen fuelled engines, then most of the apparent limitations associated with hydrogen as a fuel for CI engines will be minimised or even disappear.

7.3.1 Feasibility of the hydrogen fuelled CI engine

As mentioned above, the feasibility of the hydrogen fuelled CI engine depends on the solving of the problems identified during this and previously reported research. If these challenges can be solved, this could make hydrogen engines (with HCCI or DIH_2 mode of operation) an interesting alternative to the fuel cell technologies. The main problems that need to be solved, not considering the fuel storage and safety aspects, are related to the control of the combustion process and associated mechanical stress, as well as the operational control of the HCCI engine, in particular the angle of ignition in order to obtain stable engine operation.

In what concerns the engine controllability, one of the main difficulties identified during the research was that the end-of-compression temperature may be below the hydrogen self-ignition temperature, leading to ignition failure. There are various methods to overcome this difficulty, such as a mechanism for compression ratio adjustment or pre-heating of the intake air. These will have varying technical difficulties in their implementation, related with the technologies to employ and their speed of response.

7.3.2 Engine mechanical loading and controllability

When considering the use of the hydrogen as a fuel to operate the engine under HCCI or DIH_2 mode, the mechanical loads applied to the engine crank mechanism and piston rings as a consequence of the combustion characteristics of hydrogen must be considered. Due to the fast combustion and rapid pressure rise, mechanical loading must be calculated to confirm that it will not exceed acceptable limits for conventional engine piston, crankshaft and bearings design.

As a practical engineering rule, the maximum load-carrying capacity of a crank bearing should be less than 410 m bar / s (Miralles et al, 1986). Figure 7.1 illustrates the bearing dimensions and Figure 7.2 illustrates the

connecting rod and crank mechanism, in particular the big end bearing shell.

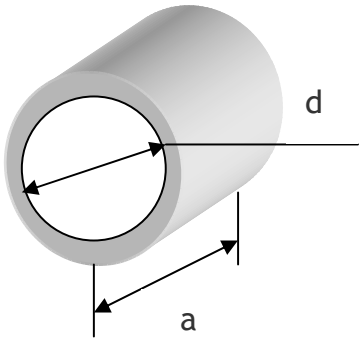

Figure 7.1: Main bearing dimensions.

The analysis required to determine the relationship between cylinder peak pressure and main engine bearing load capacity is as follows. Bearing load capacity is defined as the product of the peripheral velocity of the bearing journal and the minimum bearing surface contact pressure (Miralles, 1986). Therefore

$$C = v_p \times P_S \,, \tag{7.1}$$

C is the load carrying capacity (m bar/sec),v_p is the peripheral velocity (m/s), and P_S is the minimum surface pressure (bar).

The peripheral velocity is given by

$$v_p = \frac{n_e \pi d}{60} \,, \tag{7.2}$$

n_e is the engine velocity (rad/s) and *d* is the bearing diameter (m).

The minimum surface pressure is given by

$$P_s = \frac{p\pi\pi^2}{4ad} \,, \tag{7.3}$$

Where, *a* is the bearing width (m) and *B* is the cylinder bore (m).

Substituting Equations 7.2 and 7.3 into Equation 7.1 gives the load carrying capacity as

$$C = \frac{4.1\mathrm{B}^2 n_e p}{10^5 a}. \qquad (7.4)$$

It can be seen from Equation 7.4 that the load carrying capacity of the engine bearings for a particular engine cylinder bore and speed is directly related to the maximum cylinder pressure. Accurate control of the ignition angle and rate of pressure rise is therefore essential.

7.3.3 Compression ratio adjustment

The possibility of using a variable compression ratio mechanism will allow indirect control of the cylinder charge final compression temperature. By implementing a valve timing control system, a dynamically optimised compression ratio can be obtained as a function of the engine operating parameters. This can give direct control over the angle of ignition and actual rate of pressure rise and therefore the engine controllability will be improved. Such mechanism, if optimised, will also help in the control of the NO_x emissions. This mechanism was simulated on Chapter 6.

7.3.4 Control of the inlet air temperature

As mentioned above the control of the temperature of the air entering the cylinder is another possibility for controlling the angle of ignition and rate of pressure rise, in particular for the HCCI engine. Figure 7.2 illustrates a proposal for a system based on the circulation of exhaust gas trough a heat exchanger fitted at the inlet air manifold. In this way air is heated or cooled throughout the entire engine load range, by using a fast acting three way by-pass valve. The speed of response of this by-pass valve needs to be high, as the heat transfer via an heat exchanger is not a sufficiently fast

process to cope with sudden engine load changes. A challenge that is not solved by this proposed system is the unavailability of hot gases during the engine start up.

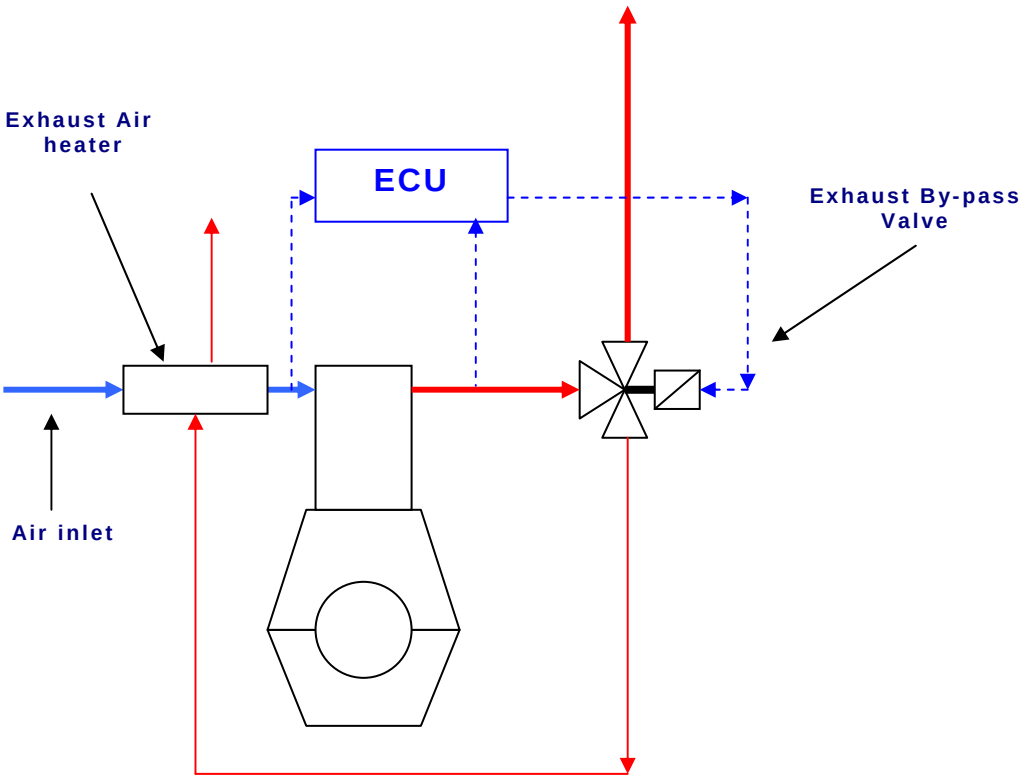

Figure 7.2: Ignition angle control through inlet air heating using an exhaust gases heat exchanger.

To start the engine, the use of auxiliary power must therefore be provided, for example through the use of an electric heater fitted on the air inlet manifold, as used on the test engine. Once the engine is started and the exhaust gas flow is controlled by the ECU through the three-way valve, the electric heater is switched off.

Figure 7.3 illustrates another system proposal based on the heating of the cylinder charge using recirculation of exhaust gas. The heating is achieved by direct contact of the hot gases with the air entering the cylinder. This solution also has some interesting “side effects”, one of them is the control of some exhaust chemical species such as NO_x. Nevertheless, this solution has limitations regarding the percentage of exhaust gas that can be

recirculated, associated with the availability of oxygen for combustion and humidity in the lubricating oil and engine components.

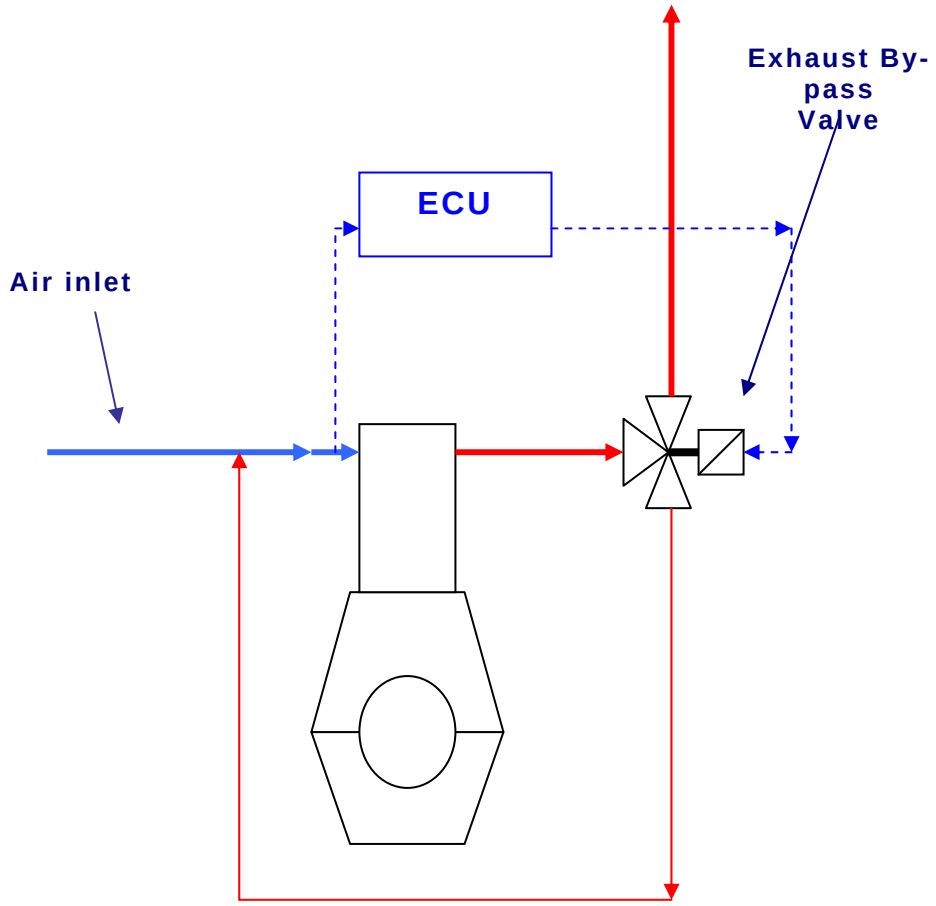

Figure 7.3: Combustion control through cylinder charge heating by recirculation of exhaust gases.

However, the system proposed in Figure 7.3 has the advantage of being much faster acting than that proposed in Figure 7.2, since the heat is transferred by direct contact of the cylinder residual gases with the cylinder incoming air.

7.3.5 Internal exhaust gas recirculation

Internal exhaust gas recirculation can be implemented using the valve timing mechanism, requiring a valve control system to let a specific volume of hot exhaust gases remain inside the cylinder.

Care must be taken to avoid increasing hydrogen slip, which results in poorer fuel efficiency and presence of unburnt hydrogen in the exhaust gases. This difficulty can be slightly improved by reducing the valve overlap timing, therefore decreasing the waste of hydrogen and making better use of it. As a consequence, the decrease of the valve overlap period increases the amount of residual gases trapped inside the cylinder, resulting in an internal exhaust gas recirculation.

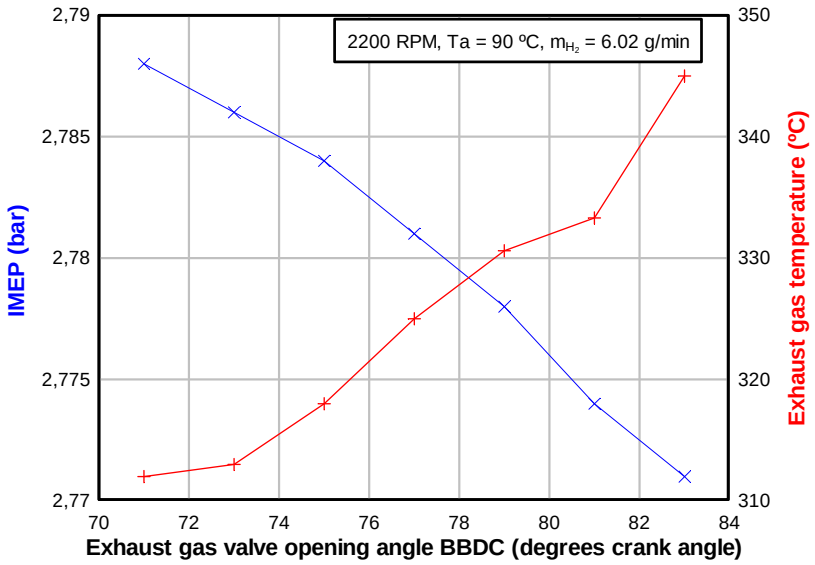

Figure 7.4: Exhaust gas internal recirculation by reduction of valve overlap period.

As can be seen in Figure 7.4, there are two obvious effects on the engine performance resulting from the reduction of the valve overlap period. One is a decrease in the indicated mean effective pressure and corresponding power, the other a substantial increase of the exhaust gas temperature resulting in a lower thermal efficiency. This was shown in more detail in Chapter 6 in the simulation of the Miller cycle.

7.3.6 Pulsed injection for DIH_2

The simulation study of the pulsed injection in Chapter 6 indicated that this technique can be beneficial for the control of the heat release and the corresponding rate of pressure rise. The release of the hydrogen in small controlled quantities will avoid the sudden heat release and uncontrolled pressure rise if the whole amount of hydrogen is burnt in one process.

If hydraulic injectors can perform well when installed in the slow to medium speed engines, the same would not be possible for high speed engines, therefore calling for high speed and highly accurate injectors. To implement such a high speed and accurate injection system, new technical solutions are required, as the present technologies are not sufficiently fast and accurate to satisfy such requirements. Pulses with frequencies above 1 kHz can be achieved by using new magneto-restrictive materials such as Terfenol-D. These materials can be used to produce fast acting and simpler hydrogen injectors.

These materials, known as *magnetostrictive* or *giant magnetostrictive materials* (GMM), are alloys that change their physical form (dimensions) as a function of the magnetic field applied. The physical phenomena that characterises the effect is illustrated in Figure 7.5. Under a magnetic field action the dipoles become oriented in such way that the original geometry of the *magnetostrictive* material rod is changed.

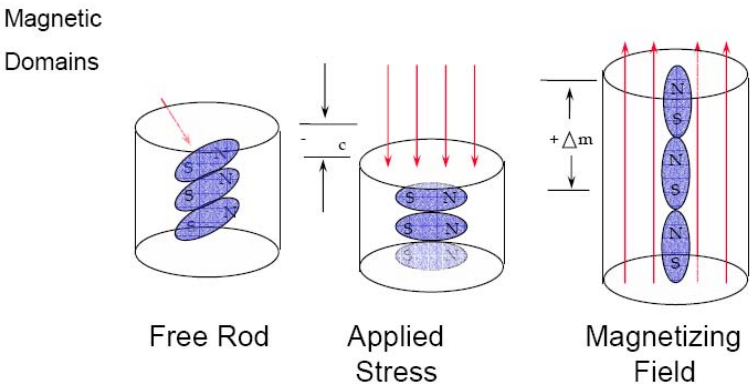

Figure 7.5: Working principle of magnetostrictive materials (*www.etrema-usa.com).*

Magnetic field induced strain materials are classically represented by GMMs such as rare earth-iron discovered by Clark (www.Wikipidia.org) These materials feature magneto strains which are two orders of magnitude larger than Nickel. Among them, bulk $\mathbf{Tb_{0.3}Dy_{0.7}Fe_{1.9}}$, called Terfenol-D, has been commercially available since 1987 and presents the best compromise between a large magneto strain and a low magnetic field at room temperature. The electric actuating circuit, illustrated in Figure 7.6, is very simple. The deformation is a direct function of the intensity of the magnetic field applied to the material. A coil wounded around the material rod induces the required magnetic field to obtain the desired rod deformation. A Zener diode serves to limit the currents induced by the coil.

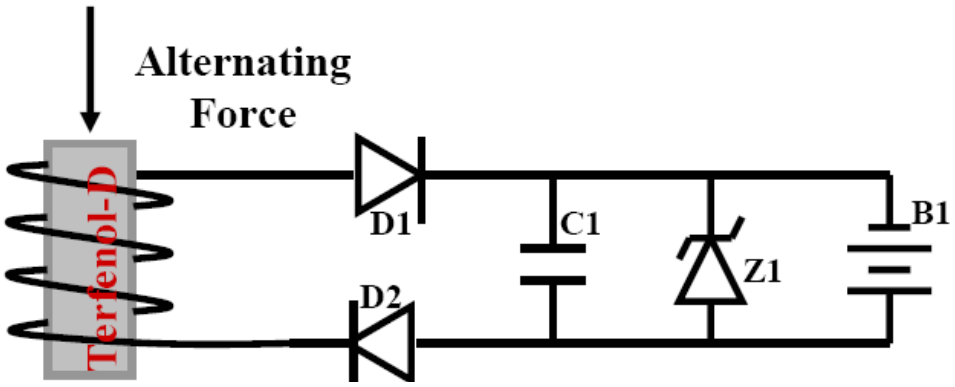

Figure 7.6: Basic electric actuating circuit.

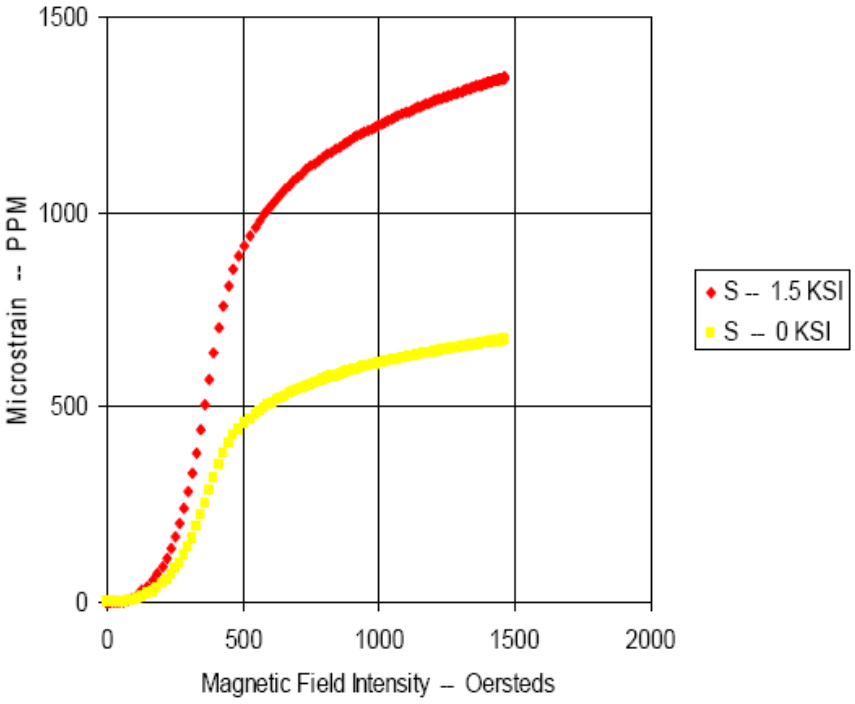

Figure 7.7: Strain magnetic field intensity of Terfenol-D (*www.etrema-usa.com).*

Figure 7.7 illustrates the characteristics of strain as a function of the magnetic field at room temperature for Terfenol D. Positive magneto strain of 1000 to 2000 ppm (0.1-0.2%) obtained with fields of 50 to 200 KA/m are reported for bulk materials, giving the possibility of building high power transducers and actuators. These characteristics have renewed the interest for magneto striction and much progress in the applications of GMMs has been made in the last 20 years.

Magnetostrictive materials for actuators

From the commercial point of view, there are three available sources of $\mathbf{Tb_{0.3}Dy_{0.7}Fe_{1.9}}$, GMM. Etrema Products Inc. (US) produces rods with dimensions varying from 2 to 68 mm in diameter and from 6 to 250 mm in length, as well as plates and powder. Figure 7.8 shows some of the material shapes available and Table 7.1 lists the main physical properties of Terfenol-D. Gangsu Tianxiang Rare Earth Functional Material Co. Ltd (China) produces rods with dimensions varying from 5 to 50mm in diameter

and up to 200mm in length. The third manufacturer is Materi Tek Co. Ltd (China). These latter two companies explore the wealthy resources of rare earth materials in China.

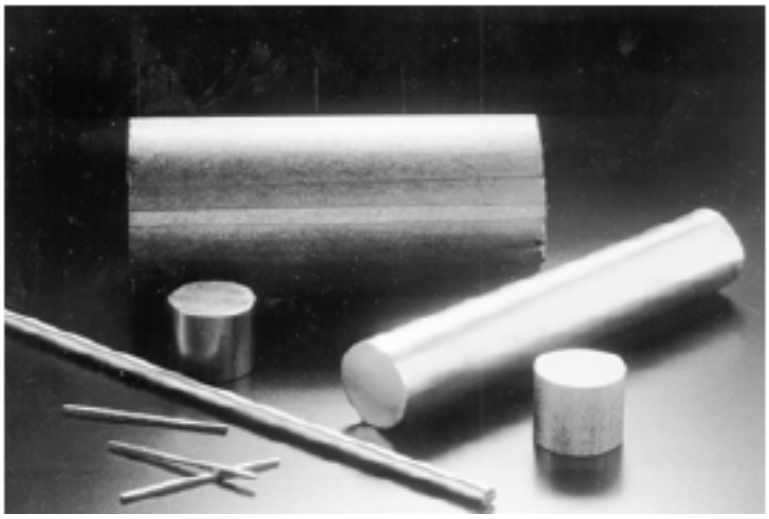

Figure 7.8: Various shapes of Terfenol-D (*www.etrema-usa.com).*

Table 7.1: Terfenol-D mechanical properties (*www.etrema-usa.com).*

Elastic Modulus	20-50 GPa	Thermal Conductivity	10.0 W/mK
Density	9210 kg/m^3	Specific Heat	350 J/kgK
Speed of Sound	1470 – 2330 m/s	Relative Permeability	1.5 – 12
Tensile Strength	28 MPa	Electrical Resistivity	60 Ω cm
Compression Stregth	700 MPa	Curie Temperature	380 ºC
Bulk Modulus	90 GPa	Energy Density	1-25 kJ/m^3
Thermal Expansion	12 ppm/ºC	Coupling Factor	0.75

Figure 7.9 shows a comparison of various materials stress strain curves.

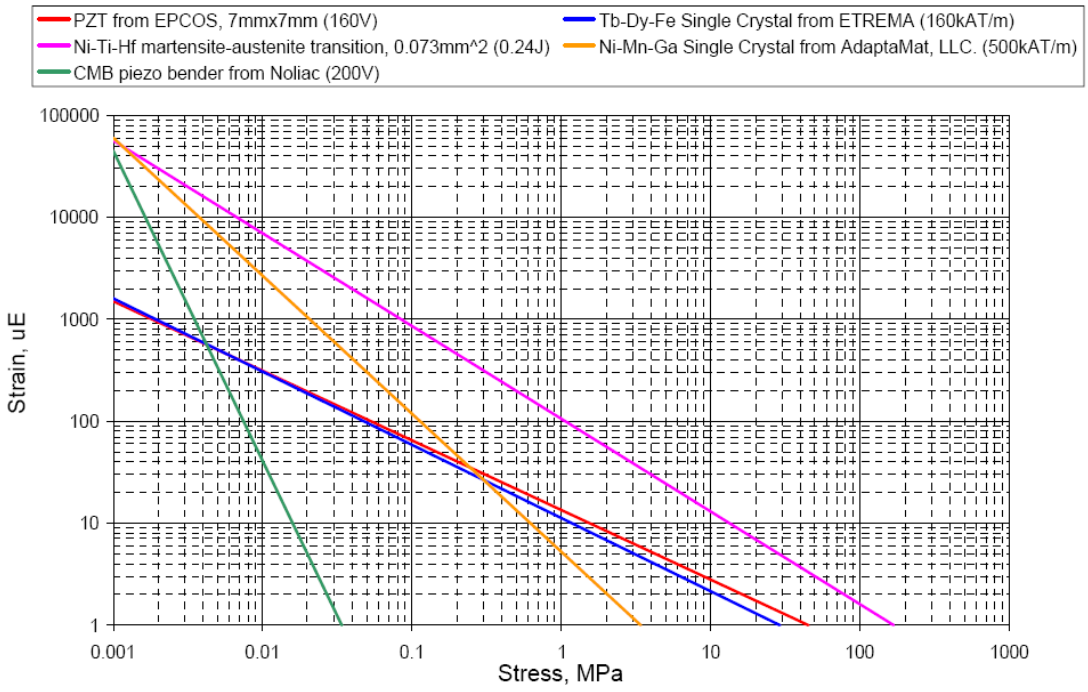

Figure 7.9: Stress-strain comparison for various selected active materials (*www.etrema-usa.com).*

Another class of materials potentially suitable for this purpose is memory shape materials, or MSMs. The MSM material is a ternary Heusler-type alloy of Nickel, Manganese and Gallium with the characteristic of "one way colossal magnetosctrictive effect" when magnetized in the active plane (www.etrema-usa.com). These materials have a maximum unloaded elongation measure of 5.8 %, which is 32 times more strain than the 0.18 % elongation of the Terfenol-D. There is, however, a trade-off as for greater strain, the elastic modulus (stiffness) is lower, measured as 0.5 GPa, or 46 times less than the 23.4 GPa of Terfenol-D. Also, the material is not suitable for high temperature operation, because it displays a full austenite transition at 48ºC.

Figure 7.10 shows the strain temperature characteristics of Terfenol-D as a function of temperature for different Telurium concentrations.

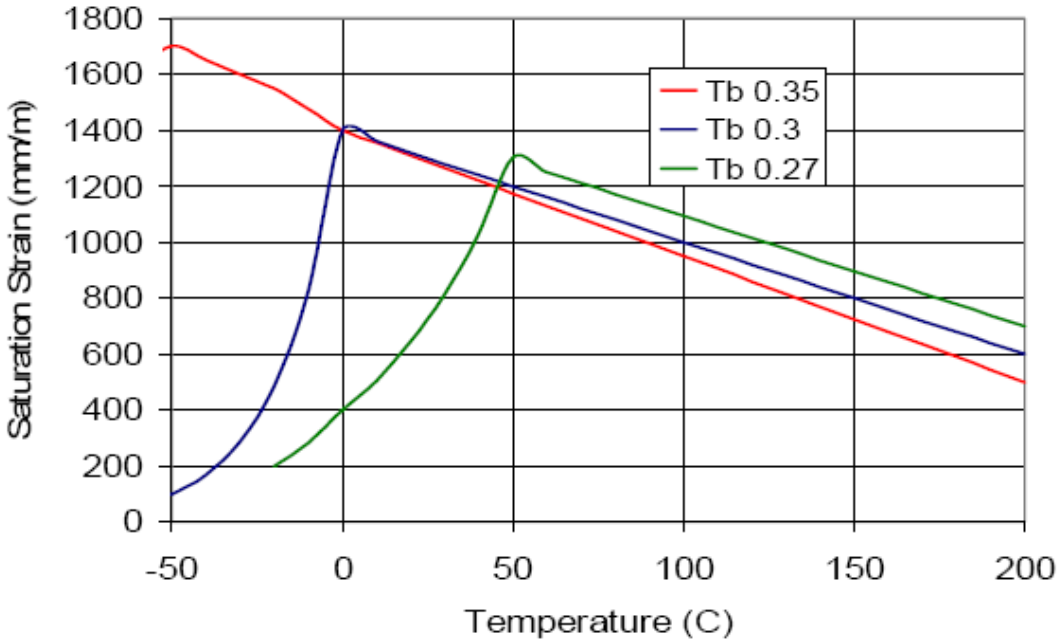

Figure 7.10: Terfenol-D temperature saturation strain.

(*www.etrema-usa.com).*

A proposed injector based on Terfenol-D is shown in Figure 7.11, and is characterised by a broad band frequency range of operation, wide temperature range, high energy density, fast response, high reliability and high energy conversion.

However, due to difficulties in buying a rod of Terfenol-D, this injector was not manufactured and tested, but it constitutes an interesting and promising area for further development and research.

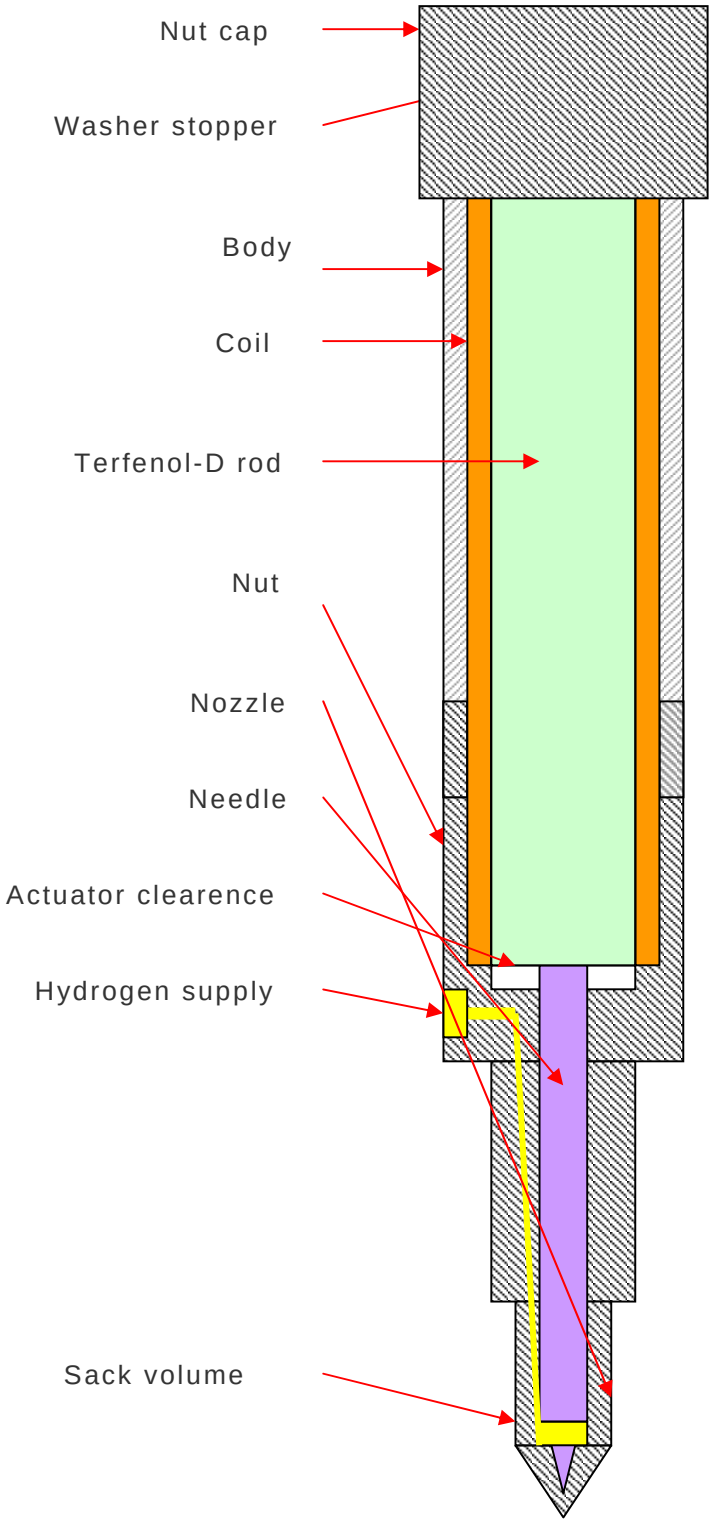

Figure 7.11: Terfenol-D based hydrogen injector.

References

Allenby S, Chang W-C., Megaritis A. and Wyszynski M. (2001). Hydrogen enrichment: a way to maintain combustion stability in a natural gas fuelled engine with exhaust gas recirculation, the potential of fuel reforming. *Proc. Inst. Mech. Eng., Part D: Journal of Automobile Engineering*, Vol. 215, pp 405-418.

Alperstein M., Swim W.B. and Schweitzer P.H. (1958). Fumigation kills smoke — improves diesel performance. *SAE Transactions*, Vol. 66, pp 574-588.

Aly H. and Voss A. (1993). Experimental investigation of gaseous hydrogen utilization in a duel-fuel engine for stationary power plants. Trans. ASME, Vol. 20, pp 67-79.

Antunes J. and Roskilly A.P. (2004). The use of H2 on compression ignition engines. In: 3rd European Congress on economics and management of energy in industry, Lisbon.

Antunes J. and Roskilly A.P. (2006). Opportunities and advantages of the use of hydrogen on board ships – new concepts. In: X International Naval engineering conference, Lisbon.

Antunes J., Roskilly A.P., Mikalsen R. (2008). **An investigation of hydrogen fuelled HCCI engine performance and operation**. *International Journal of Hydrogen Energy, Volume 33, Issue 20, October 2008, Pages 5823-5828.*

Antunes J., Roskilly A.P., Mikalsen R. (2008). **An experimental study of a direct injection compression ignition hydrogen engine**. *International Journal of Hydrogen Energy*, *Volume 34, Issue 15*, *August 2009*, *Pages 6516-6522.*

Arenas V.M. (1978). Motores de Combustion Interna. Tomo I, ed. 78-79, ETSIN, Spain.

Arnason B. and Sigfusson T. (2003). Application of geothermal energy to hydrogen production and storage. Bragastofa, Hydrogen Energy Research Institute, University of Iceland, Iceland.

Arnold W.C., Beadle R.H., Logelin R.L., and Young H.D. (1958). Bifuel approach to burning residual fuels in diesel engines. *SAE Transactions*, Vol. 66, pp 55-64.

Bade Shrestha S. and Karim G. (1999). Hydrogen as additive to methane for sparking ignition engine applications. *International Journal of Hydrogen Energy*, Vol. 24, No. 6, pp 577-586.

Baird B. and Gollahalli S.R. (2000). Emissions and efficiency of a spark ignition engine fuelled with a natural gas and propane mixture. In: Proc. 2000 International Joint Power Generation Conference, Florida, USA.

Benson R.S. (1982). The Thermodynamics and Gas Dynamics of Internal-Combustion Engines, Volumes I and II. Clarendon Press, Oxford.

Beruoun S., Martins J. (2001). The development of gas (CNG, LPG and H2) engines for buses and trucks and their emission and cycle variability characteristics. *SAE paper* 01-01444.

Bishop, R.H. (1993). Modern Control Systems Analysis and Design Using MATLAB®. Addison-Wesley Publishing Company, USA

Blair, G.P. (1999). Design and Simulation of Four-Stroke Engines. SAE International, USA.

Borman G. and Ragland K. (1998). Combustion Engineering, McGraw-Hill International editions, Mechanical engineering series, Singapore.

Bowns D.E., Cave P.R., Hargreaves M.R.O. and Wallace F.J. (1973). Transient characteristics of turbocharged Diesel engines. Proc. Inst. Mech. Eng., CP15, 1973.

Brian D.H. (2002). Essential MATLAB for Scientists and Engineers, Butterworth Heinemann, 2002.

Brian R.H., Lipsman R.L., Rosenberg J.M. (2001). A guide to MATLAB for Beginners and Experienced Users. Cambridge University Press, 2001.

Calkins F., Smith R. and Flatau A. (2000). An energy-based hysteresis model for magnetostrictive transducers. *IEEE Transactions on Magnetics*, Volume 36, pp 429-439.

Çengel, Y.A. and Boles, M.A. (2001). Termodinâmica, 3rd edition. McGraw-Hill de Portugal, Portugal.

Chang J., Güralp O., Filipi Z., Assanis D., Kuo T., Najt P. and Rask R. (2004). New Heat Transfer Correlation For an HCCI Engine Derived from Measurements of Instantaneous Surface Heat Flux. *SAE Paper* 2004-01-2996.

Chesse P., Chalet D., Tauzia X., Hetet J. and Inozu B. (2004). Real-time performance simulation of marine diesel engines for the training of navy crews. *Marine Technology Society Journal*, Vol. 41, pp 95–101.

Chryssakis C. and Assanis D. (2005). Effect of multiple injections on fuel-air mixing and soot formation in diesel combustion using direct flame visualization and CFD techniques. Proceedings of ICES2005, ASME Internal Combustion Engine Division 2005 Spring Technical Conference, Chicago, IL, USA.

Citron S., O´Higgins J., and Chen L. (1989). Cylinder by cylinder engine pressure torque waveform determination utilizing crankshaft speed fluctuations. *SAE paper* 890486.

College of the desert and SunLine Transit Agency (2001). Hydrogen use in internal combustion engines. Hydrogen Fuel Cell Engines and Related Technologies Course Manual, Module 3, Rev. 0, U.S. Department of Energy - Energy Efficiency and Renewable Energy, Hydrogen, Fuel Cells and Infrastructure Technologies Program – Technology Validation, USA.

Collier K. (2001). Hydrogen/Natural Gas Blends for Heavy-Duty Applications. Proceedings of the 2001 DOE Hydrogen Program Review.

Das L., Gulati R. and Gupta P. (2000). Comparative evaluation of the performance characteristics of a spark ignition engine using hydrogen and compressed natural gas as alternative fuels. *Journal of Hydrogen Energy* Vol. 25, pp. 783-793.

Derry L., Dodds E., Evans E. and Royle D. (1954). The effect of auxiliary fuels on the smoke-limited power output of diesel engines. *Proc. Inst. Mech. Eng*. Vol. 168.

Duane H. and Littlefield B. (2001). Mastering MATLAB® 6: A Comprehensive Tutorial and Reference. Prentice Hall, USA.

Eastop, T.D. and McConkey A. (1993). Applied Thermodynamics for Engineering Technologists. 5th Edition, Prentice Hall.

Evenson W. (2004). The potential for a hydrogen energy economy, In: IUPAP Energy Reports - Report on research and development of energy technologies, USA, pp 207-232.

Ewan, B.C.R and Moody K. (1986). Structure and Velocity Measurements in Under expanded Jets. *Combustion Science and Technology*, Vol.45, pp 275-288.

Favennec A-G., Minier P. and Lebrun M. (1999). Analysis of the Dynamic Behaviour of the Circuit of a Common Rail Direct Injection System. In: Fourth JHPS International Symposium on Fluid Power, Tokyo.

Ferguson C. and Kirkpatrick A. (2001). Internal Combustion Engines: Applied Thermosciences. Wiley.

Filipi Z., Homsey S., Morrison K., Hoffman S., Dowling D., Assanis D. (1997). Strain Gage Based Instrumentation for In-Situ Diesel Fuel Injection System Diagnostics. W.E. Lay Automotive Laboratory, University of Michigan.

Filipi Z.S. and Assanis D.N. (1997). A non-linear, transient, single-cylinder diesel engine simulation for predictions of instantaneous engine speed and torque. In: Proc. Tech. Conf. ASME ICE division, number 97-ICE-8, pages 61-70.

Fiveland S. and Assanis D. (2000). A four-stroke homogeneous charge compression ignition engine simulation for combustion and performance studies. *SAE paper* 2000-01-0332.

Fukuma T., Fujita T., Pichainarong P. and Furuhama S. (1986). Hydrogen Combustion Study in Direct Injection Hot Surface Ignition Engine. *SAE Paper* 861579.

Gao Z. and Schreiber W. (2001). The effects of EGR and split fuel injection on diesel engine emission. *International Journal of Automotive Technology*, Vol.2, pp 123-133.

Geisler O. and Rulfs H. (1993). Research investigations of the combustion of heavy fuel , natural gas and hydrogen in marine diesel engines.

Marine system design and operation Marine Management (Holdings) Ltd.

Haddad S. and Watson N. (1984). Principles and Performance in Diesel Engineering. Ellis Horwood Limited, England.

Hann B. (2002). Essential MATLAB for Scientists and Engineers. Second edition, Butterworth Heinemann, England.

Harris H. L. and Taber W. (1996). Control of industrial engine and gas turbine exhaust emissions to meet present and future clean and regulations. American Society of Mechanical Engineers; Book No. H1048B

Hawley J., Wallace F. and Khalil-Arya S. (2003). A fully analytical treatment of heat release in diesel engines, Proc. Inst. Mech. Eng., J. Automobile Engineering, Vol. 217, pp 701-717.

Heffel J. (2003). NOx emission and performance data for a hydrogen fuelled internal combustion engine at 1500 rpm using exhaust gas recirculation. *International Journal of Hydrogen Energy*, Vol. 25, pp. 901-908.

Heywood J. (1988). Internal Combustion Engine Fundamentals. McGraw-Hill, USA.

Hicks, T.G. (1985). Standard Handbook of Engineering Calculations. 2nd Edition, McGraw-Hill Book Company, USA

Hunt B., Lipsman R., Rosenberg J., Coombs K., Osborn J. and Stuck G. (2001). A guide to MATLAB for Beginners and Experienced Users. Cambridge University Press, Cambridge, UK.

Imperial, J.M. (1980). Sobrealimentação de Motores. Edições Cetop, Mira-Sintra Mem Martins.

Imperial, J.M. (1980). Turbo: Sobrealimentação de Motores Rápidos. Ediciones CEAC, Mem Martins.

International Organization for Standardization (1995). Guide to the Expression of Uncertainty in Measurement, Switzerland.

Jensen J.P., Kristensen A.F., Serenson S.C., Houbak N., and Hendricks E. (1971). Mean Value modeling of a small turbocharged diesel engine. *SAE paper* 910070.

Kabat D., Heffel J. (2002). Durability implications of neat hydrogen under sonic flow conditions on pulse-width modulated injectors. *International Journal of Hydrogen Energy*, Vol. 27, pp. 1092-1102.

Karim G. (2003). Hydrogen as a spark ignition engine fuel. *International Journal of Hydrogen Energy*, Vol. 28, pp. 569-577.

Klass D. (1998). Biomass for Renewable Energy, Fuels, and Chemicals. Academic Press, USA.

Klein M. and Erikson L. (2002). Models, methods and performance when estimating the compression ratio based on cylinder pressure. Vehicular systems, Limkopings Universitet, Sweden.

Kubesh J. (2002). Uncertainty in the determination of thermal efficiency in natural gas engines. Proceedings of ICEF2002, 2002-522 Fall Technical Conference of ASME Internal Combustion Engine Division, New Orleans, Lousiana, USA.

Lapuerta M., Hernández J. and Armas O. (2001). Kinetic Modelling of Gaseous Emissions in a Diesel Engine. *SAE Paper* 2001-01-2939.

Ledger J. and Walmsley S. (1971). Computer simulation of a turbocharger diesel engine operating under transient load conditions. *SAE paper* 710177.

Lee J., Kim Y. and Caton J. (2002). The Development of a Dual Injection Hydrogen Fueled Engine with High Power and High Efficiency. In: Fall Technical Conference of the ASME-ICED New Orleans, Louisiana, USA.

Lyn W. (1952). An Experimental investigation into the Effect of Fuel Addiction to Intake Air on the Performance of a Compression-ignition Engine.

Miedema S. and Lu Z. (2002). The dynamic behaviour of a Diesel engine. Proc. WEDA XXII Technical Conference & 34th Texas A&M Dredging Seminar, June 12-15, Denver, Colorado, USA.

Moore N. and Mitchell R. (1955). Combustion in Dual-fuel Engines.

Naber J. and Siebers D. (1997). Hydrogen combustion under diesel engine conditions. Pergamon PII:SO360-3199(97)00083-9

Naber J. and Siebers D. (1996). Effects of Gas Density and Vaporisation on Penetration and Dispersion of Diesel Sprays. *SAE Paper* 960034.

Nagaki H., Hitohidde F. and Takahashi S. (1999). Acceptability of Premixed Hydrogen in Hydrogen Diesel Engine. SAE Paper 1999-01-2521.

Norbeck J., Barth M., Farrel J. and Heffel J. (1997). Development and Evaluation of a Hydrogen Fuel Power Plant for a Hybrid Electric Vehicle - Phase II. Report submitted to the South Coast Air Quality Management District, contract 95073, project 7, University of California, College of engineering, Center for Environmental Research and Technology, USA.

Numata A., Kumagai T., Nagae Y. and Osafune S. (2001). Increase of Thermal Efficiency and Reduction of NOx Emissions in DI Diesel Engines. Mitsubishi Heavy Industries, Ltd; Technical Review Vol. 38 No.3.

Nwafor O. (2002). Knock characteristics of dual-fuel combustion in diesel engines using natural gas as primary fuel. Sādhanā - Academy Proceedings in Engineering Sciences, Vol. 27, part 3, pp 375-382.

Ohta T. (1979). Solar-Hydrogen Energy Systems. Pergamon Press, England.

Olsson J-O., Tunestal P. and Haraldsson G. (2001). A turbo charged dual fuel HCCI engine. SAE Paper 11896, SAE Fuels & Lubricants Meeting and Exposition, Orlando FL, USA.

Olsson J-O., Erlandsson O. and Johansson B. (2000). Experiments and simulation of a six-cylinder homogeneous charge compression ignition (HCCI) engine. SAE transactions, Vol. 109, 3, pp 2046-2056.

Paramo M. and Santavicca, (2002). Gasoline Direct Injection Engine Cold Start Improvement by Injection of Hydrogen, Available at: http://forms.gradsch.psu.edu/equity/sroppapers/2002/ParamoMelvin.pdf

Passarini L.; Nakajima P. (2003). Development of a high-speed solenoid valve: an investigation of the importance of the armature mass on the dynamic response. *Journal of the Brazilian Society of Mechanical Sciences and Engineering*, Vol. 25, pp. 329-335.

Peschka W. (1998). Hydrogen: the future cryofuel in internal combustion engine. *International Journal of Hydrogen Energy*, Vol. 23, pp. 27-43.

Petrovsky N. (1960). Marine Internal Combustion Engines. MIR Publishers, Moscow.

Pratap R. (2002). Getting Started with MATLAB – A Quick Introduction for Scientists and Engineers. Oxford University Press, New York.

Pratt J., Flatau A. (1993). Development and analysis of a self-sensing magnetostrictive actuator design. Proc. SPIE, Smart Structures and Materials 1993, Vol. 1917, pp 952-961.

Rai G. (1983). Practical Thermodynamics with Questions and Answers. Khanna Publishers, Delhi.

Reed R. (2004). Study of the feasibility and energy savings of producing and pre-cooling hydrogen with a 5-kW ammonia based combined power/cooling cycle. MSc thesis, University of Florida, USA.

Rizzoni G. (1989). Estimate of indicated torque from crankshaft speed fluctuations: a model for the dynamic of the IC engine. *IEEE Trans. Vehicular Technology*, Vol. 38, 168-179.

Rogers G. and Mayhew Y. (1980). Engineering Thermodynamics Work & Heat Transfer. Third Edition, Longman Group Limited, USA.

Rottengruber H., Berckmüller M., Elsässer G., Brehm N. and Schwarz C. (2004). Direct-injection hydrogen SI-engine – operation strategy and power density potentials, SAE Paper 2001-01-2927.

Rottengruber H., Wiebicke U., Woschini G. and Zeilinger K. (2000). Hydrogen diesel engine with direct injection, high power density and low exhaust gas emissions. Part 3: engine testing and calculation. *MTZ Worldwide*.

Rottengruber H., Wiebicke U., Woschini G., Zeilinger K. (1998). Investigation of a direct injecting hydrogen diesel-engine. Chair for Combustion Engines and Road Vehicles (LVK) Technische Universität München, Germany.

Ryan T. (2003). Diesel engine alternatives, In: 2003 Diesel Engine Emissions Reduction (DEER) Conference Presentations, Session 7: Combustion and HCCI Regimes; Newport, Rhode Island, USA.

Shao, J., Yan Y., Greebes G. and Smith S. Quantitative characterization of Diesel sprays using digital imaging techniques. Institute of Physics Publishing Measurement Science and Technology PII:so957-0233(03)55986, 2003.

Shengchang Z., Yangzeng X., Guanglin S. and Tingxiu Z. (2001). Study on extra-high speed digital valve. In: Proc. Fifth International Conference On Fluid Power Transmission And Control (ICFP2001), Hangzhou, China.

Sher E. (1998). Handbook of Air Pollution from Internal Combustion Engines: Pollutant Formation and Control. Academic Press Limited, UK.

Shudo T, and Suki H. (2002). Applicability of heat transfer equations to hydrogen combustion. JSAE Review, 23, pp. 303-308.

Shudo T., Nakajima Y. and Futakuchi T. (2000). Thermal efficiency analysis in a hydrogen premixed combustion engine. JSAE Review, 21, pp. 177-182.

Shudo T., Shimamura K. and Nakajima Y. (2000). Combustion and emissions in a methane DI stratified charge engine with hydrogen pre-mixing. JSAE Review, 21-1, pp. 3-7.

Shudo T., Suzuki H. (2002). New heat transfer equation applicable to hydrogen-fuelled engines. Proc. of ICEF2002, New Orleans, Louisiana, USA.

Sorensen H. (1983). Energy Conversion Systems. John Wiley and Sons Inc, USA.

Stan C., Lefebvre J.-L., Lebrun M. and Martorano L. (1999). Direct gasoline injection for two-stroke-scooter engines: concept, modelling and performance, Proceedings 4th International Conference on Internal Combustion Engines: Experiments and Modeling, ICE 99, Capri 1999.

Stenlåås O., Christensen M., Egnell R., Johansson B. and Mauss F. (2004). Hydrogen as homogeneous charge compression ignition engine fuel. In: SAE Fuels & Lubricants Meeting & Exhibition, Toulouse, France.

Stone, R. (1999). Introduction to Internal Combustion Engines. 3rd Edition, Palgrave MacMillan Press.

Taylor C. (1985). The Internal-Combustion Engine in Theory and Practice - Volume 1: Thermodynamics, Fluid Flow, Performance. Second Edition, MIT Press, USA.

Tazerout M., Le Corre O. and Rousseau S. (1999). TDC determination in IC engines based on the thermodynamic analysis of the temperature-entropy diagram. *SAE paper* 1999-01-1489.

Tazerout M., Le Corre O. and Rousseau S. (1999). TDC determination in IC engines based on the thermodynamic analysis of the temperature-entropy diagram. *SAE Paper* 1999-01-1489.

The MathWorks, Inc. (2003) MATLAB: Reference guide, MA, USA.

Tsujimura T., Mikami S., Achiha N., Tokunaga Y., Senda J. and Fujimoto H. (2003). A study of direct injection diesel engine fueled with hydrogen, Proc. 2003 SAE World Congress, Detroit, Michigan, USA.

Tsujimura T., Nakatani K., Mikami S. and Okui N. (2001). Construction of optimum injection and combustion for gaseous fuel engine. *Nihon Kikai Gakkai Nenji Taikai Koen Ronbunshu*, Vol.2, pp. 557-558.

TÜV Süddeutschland (2004). Hydrogen - a world of energy. Munich.

US Department of Energy (2002). National Hydrogen Energy Roadmap. Proc. National Hydrogen Energy Roadmap Workshop, Washington, DC, USA.

Van Blarigan P. and Keller J. (1998). A hydrogen fuelled internal combustion engine designed for single speed/power operation. *Int. J. of Hydrogen Energy*, Vol. 23, pp. 603-609.

Van Blarigan P. (2000). Advanced internal combustion engine research, Proc. of 2000 DOE Hydrogen Program Review, San Ramon, California, USA.

Van Der Drift A., Tjeng S., Beckers G. and Beesteheerde J. (1996). Low-NOx hydrogen burner. *International Journal of Hydrogen Energy*, Vol. 21, pp. 445-449.

Verhelst S. and Sierens R. (2001). Hydrogen engine-specific properties, *International Journal of Hydrogen Energy*, Vol. 26, pp. 987-990.

Wakuri Y., Fugii M., Amitani T. and Tsuneya R. (1960). Studies of the penetration of fuel spray in a diesel engine. *Bulletin of JSME*, Vol.3, pp. 123-130.

Wang Y., Zeng S., Huang J., He Y., Huang X., Lin L. and Li S. (2005). Experimental investigation of applying Miller cycle to reduce NOX emission from diesel engine. *Proc. Inst. Mech Eng., Part A - Journal of Power and Energy*, Vol.219, pp. 631-638.

Watson J. (2004). The Development of Large Technical Systems: Implications for Hydrogen. Tyndall Centre for Climate Change Research, Working Paper nº 18.

Watson N. (1984). Dynamic turbocharged diesel engine simulator for electronic control system development. *ASME Journal of Dynamic Systems, Measurement, and Control*, Vol. 106, pp. 27-45.

Welch A. and Wallace J. (1990). Performance characteristics of a hydrogen-fueled diesel engine with ignition assist. Proc. SAE Int. Fuels and Lubricants Meeting, Tulsa, Oklahoma, USA.

Wheeler A. and Ganjianji A. (1996). Introduction to Engineering Experimentation. Prentice Hall, New Jersey, USA.

Winterbone D., Thiruarooran C. and Welltead P. (1977). A wholly dynamic model of turbocharged diesel engine for transfer function evaluation. *SAE paper* 770124.

Woud H. and Stapersma D. (2003). Design of Propulsion and Electric Power Generation Systems. IMarEST, England.

Xu Y., Nishida K. and Hiroyasu H. (1992). A practical Calculation Method for Injection Pressure and Spray Penetration in Diesel Engines, *SAE paper* 920624.

Yamin J. and Badran O. (2002). Analytical study to minimise the heat losses from propane powered 4-stroke spark ignition engine. *Renewable Energy*, Vol. 27, pp. 453-478.

Yamin J., Gupta H., Bansal B. and Srivastava O. (2000). Effect of combustion duration on the performance and emission characteristics of a spark ignition engine using hydrogen as a fuel. *International Journal of Hydrogen Energy*, Vol. 25, pp. 581-589.

Yi H., Min K. and Kim E. (2000). The optimised mixture formation for hydrogen fuelled engines. *International Journal of Hydrogen Energy*, Vol. 25, pp 685-690.

Zevenhoven R. (2001). Non-ideal gases in diesel engine processes. In: First biannual Meeting and General Section Meeting of The Scandinavian-Nordic Section of the Combustion Institute, Gothenburg, Sweden, pp. 103-108.

Zhang Y. and Rizzoni G. (1993). An on-line indicated torque estimator for IC engine diagnosis and control. *ASME J. Advanced Automotive Tech.*, Vol. 52, pp. 147-162.

Zhenzhong Y., Jianquin W., Zhuoyi F. and Jinding L. (2002). An investigation of optimum control of ignition timing and injection system in a in cylinder injection type hydrogen fuelled engine. *Int. J. of Hydrogen Energy*, pp. 213-217.

Züttel A. (2003). Hydrogen Storage Methods and Materials, Physics Department, University of Fribourg, Switzerland.

Zweiri Y., Whidborne J. and Seneviratne L. (1999). Complete analytical model of a single-cylinder Diesel engine for non-linear control and estimation, Report EM/99/10, Department of Mechanical Engineering, King's College London, Strand, London, UK.

Appendix A:

Commercial dual fuel engine developments

In this appendix, a commercial task to convert two large-scale industrial engines for dual fuel operation will be described. The work was based around the technology for port injection of gaseous fuels in compression ignition engines, described earlier in this thesis.

The author, through his company TecnoVeritas, was commissioned in 2007 to convert two 4.5MW diesel engines running on heavy fuel oil (HFO) to dual fuel operation with natural gas. This included development of engine monitoring and management systems, as well as the use of knock identification to control the amount of natural gas used. During testing, it was possible to obtain some experimental results which are presented below, showing the performance of the engines under different modes of operation.

A.1. Introduction

Increasing fuel costs and tightening environmental legislation drive an interest among users of existing diesel engines to look at options to improve fuel efficiency and reduce exhaust gas emissions formation. In most places of the world, natural gas is continuously available at a reasonable price, and its properties make it an interesting alternative fuel for use in internal combustion engines. The option of converting existing diesel engines to dual fuel capability gives more flexibility in the fuel supply, but also potential reductions in operational costs and exhaust gas emissions. However, the conversion of existing diesel engines to dual fuel operation implies possible combustion problems that need to be addressed.

Natural gas as a fuel exhibits a number of interesting advantages such as a reasonable net calorific value (approximately 38,500 kJ/Nm^3), low emissions of CO_2, NO_x and particulate matter, and generally a good knock

resistance (which is necessary to use it in diesel engines without engine modifications). Where available, its supply is continuous and its price is commercially appealing. When converting a standard diesel engine to dual fuel operation, engine operational characteristics can remain largely unchanged, with the liquid fuel acting as a pilot fuel to ignite the cylinder charge. Therefore the quantity of pilot fuel must be set to release at least the minimum ignition energy required to ignite the gaseous fuel, which can constitute the main energy source of the working cycle. Due to the pre-mixed charge, problems of pre-ignition and detonating combustion (knock) may, however, occur, and the use of an appropriate engine control system is therefore essential.

Numerous researchers have studied the use of natural gas as a second fuel in diesel engines [1-9]. Generally, fuel efficiencies similar to those under pure diesel engine operation are achieved at high engine loads. At low loads dual fuel operation gives poorer fuel efficiency. Papagiannakis and Hountalas [1,2] attribute this to the poor combustion of the gaseous fuel at part load operation. With a reduction in the use of liquid diesel fuel, the particulate matter (PM) emissions are significantly reduced; reductions of above 50% are frequently reported. Also nitrogen oxides (NO_x) can be reduced in dual fuel mode, however increases are usually seen in the emissions of carbon monoxide (CO) and unburned hydrocarbons (HC).

A.2. Dual fuel operation

The cylinder charge of dual fuel engines (converted existing diesel engines or simply diesel derived engines) is usually made up of two fuels with distinct ignition temperatures and different physical states, typically one liquid and one gaseous. This gives a combustion process different from those of conventional diesel or spark ignition engines, and gives the dual fuel engine some particular operating characteristics which need to be taken into account when working with such engines.

A.2.1 The dual fuel combustion process

The combustion process in dual fuel engines is more complicated than that of conventional engines since a combination of premixed and diffusion combustion occur in this mode of engine operation. The contribution and characteristics of each type of combustion depends on several parameters, including fuel properties, injector characteristics, and combustion chamber design, as well as operational variables such as the engine load, speed, manifold air pressure and temperature, and the amount of each fuel present in the combustion chamber.

The combustion process in a dual fuel engine can be divided into three distinct sub-processes:

- ignition of the pilot fuel;
- combustion of the gaseous fuel which is in the vicinity of the pilot fuel cores; and
- combustion of the gaseous fuel due to flame propagation into the premixed lean charge.

The equivalence ratio of the cylinder charge varies spatially from point to point within the combustion chamber, since a fast homogenisation of the mixture of natural gas and liquid fuel in most cases is not possible. At low loads, the air-gas mixtures may be so lean that it causes flame propagation interruptions, resulting in incomplete combustion. This will lead to loss of fuel through the exhaust, contributing to a reduction in fuel efficiency and high levels of unburned hydrocarbons in the exhaust.

A.2.2 Detonation

Detonation occurs during the combustion process when the burnt gas zone, which is pressurising and heating the unburned part of the cylinder charge ahead of the flame front, does so at such a rate that the unburned fuel achieves its auto-ignition temperature before the arrival of the actual

flame front. The result is that the unburned charge volume ignites spontaneously over the entire zone where the auto-ignition conditions have been achieved. The apparent flame speed in this zone is many orders of magnitude faster than that of conventional combustion initiated by the normal flame front, resulting in higher rates of pressure and temperature rise. Knocking is usually associated to small portions of volume of the combustion chamber, whereas detonation is associated to the entire compressed cylinder charge.

Engine knock is directly related to the compression ratio, because the higher the compression, the closer the charge will be to its autoignition conditions. Moreover, the knock intensity will depend on the intake air conditions, combustion chamber design and turbulence levels within the cylinder, as well as the flame speed of the fuel-air mixture. Therefore, for turbocharged dual fuel engines the temperature of the air entering the cylinder and its pressure are factors that influence detonation sensitivity. Detonation is accompanied by a drastic increase in temperature and pressure within the cylinder, resulting in some cases in serious engine damage.

In converted diesel engines, the quality of the fuel oil used is of utmost importance to attain good control of the combustion process as well as a smooth and clean combustion. Heavy fuel oils with bad ignition quality may have long, and varying, ignition delays, leading to reduced combustion efficiency and poorer utilisation of the gaseous fuel. The temperature of the heavy fuel oil is also an important factor to consider, as viscosity and therefore atomisation of the fuel play an fundamental role in the homogenisation of the cylinder charge. If fuels of very low quality are used, viscosity control may be necessary in order to maintain satisfactory engine performance.

A.2.3 Pre-ignition

Another dangerous and damaging phenomenon of pre-mixed engine operation is the pre-ignition of the cylinder charge. This phenomenon

results from the igniting of the cylinder charge through contact with a high temperature surface prior to the desired ignition timing (i.e. the time of pilot fuel injection, or spark discharge in a spark ignited engine). Pre-ignition is particularly dangerous since ignition can occur during the compression stroke, leading to excessive mechanical stress and damages in the crank system, piston rings, bearings, etc., as well as increased thermal stress and detrimental effects on cylinder lubrication due to very high in-cylinder gas temperatures.

The main cause of such a phenomenon is the presence of carbonaceous residues on the combustion chamber surface. With the use of low-quality fuels such as heavy fuel oils, the amount of residues on the combustion chamber components are likely to increase, and this must be taken into consideration when converting an engine to dual fuel operation. The ignition temperature of a natural gas-air mixture will depend on the fuel-air ratio, and the fuel substitution ratio and natural gas concentration may therefore be limited by pre-ignition tendencies of the cylinder charge.

Pre-ignition in a cylinder will also have a self-enhancing effect in that the increased in-cylinder gas temperatures and pressures resulting from such an occurrence will increase the temperatures of the combustion chamber walls and thereby increase the probability of pre-ignition in the next cycle. With the use of low-quality fuels in a dual fuel engine, continuous monitoring and control of the combustion process to avoid pre-ignition is therefore essential in order to maintain engine integrity and operational stability.

A.3. Engine conversion

TecnoVeritas has performed engine conversions worldwide since 1999 for a range of engine makes, sizes, and different fuels including dual fuel and multi fuel using diesel oil, heavy fuel oil, natural gas, producer gas, and hydrogen. A range of in-house developed technology solutions for engine monitoring, control, and operational optimisation have been developed. The following sections present the conversion of two Wärtsilä 9L32 diesel

engines to dual fuel operation on heavy fuel oil and natural gas, and describe technological solutions chosen as well as operational data from the engines.

In December 2008, TecnoVeritas finished the commissioning of two nine-cylinder Wärtsilä type 9L32 diesel engines, each with approximately 96,000 hours of operation on heavy fuel oil (HFO). The objective was to convert these two HFO engines to use as much natural gas as possible, without creating mechanical stress higher than that created under normal HFO operation. Simultaneously, the development of operation software with an appropriate human interface was required. Figure 1 shows a photograph of the two engines, and main engine design data are listed in Table 1.

Engine model	**Wärtsilä 9L32**
Number of cylinders	**9**
Cylinder bore	**320 mm**
Stroke length	**350 mm**
Speed	**750 rpm (12.5 s^-1)**
Mean effective pressure	**21.3 bar (2130 kPa)**
Mean piston speed	**8.75 m/s**
Rated power	**4,450 kW**
Boost pressure	**2.4 bar (240 kPa)**
Compression ratio	**12**

Table 1: Engine data

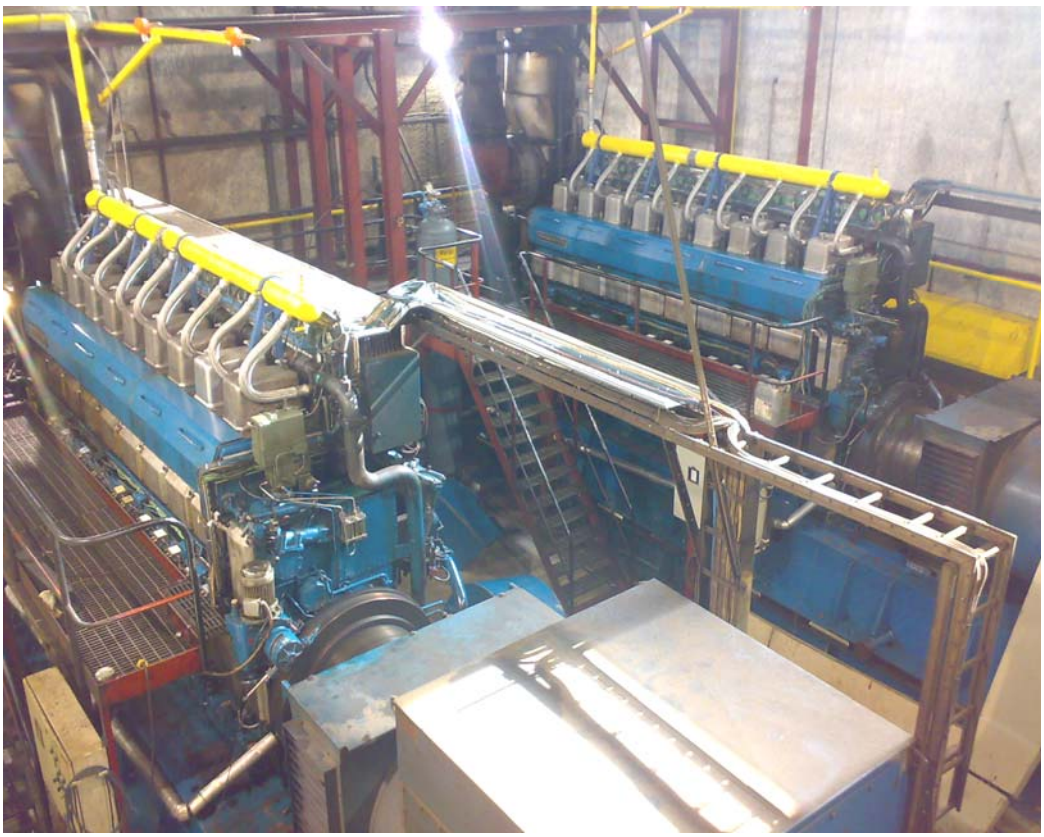

Figure 1: The two Wärtsilä 9L32 diesel engines converted at ECE, Portugal.

A.3.1 Fuel injection system

In order to allow dual fuel operation, modifications were made to the intake and injection systems. Gas fuel injectors were fitted to the intake manifold, with one injector per engine cylinder. The gas injection valves are controlled by an injection controller receiving information from various sensors and systems installed on the engine, from the gas regulating unit and from the process controller. The original mechanical controller was replaced by a hydraulic actuator, controlled by the main injection controller, allowing seamless transfer from conventional to dual fuel mode and vice versa. The injection of the correct quantity of gas during the induction stroke, i.e. after the closing of the exhaust valve and before the closing of the inlet valve, is continuously adjusted through the injection angle and gas pressure, thereby allowing a fine adjustment of the gas

energy supplied per cycle. The system allows for the control of the gas injection rate individually for each cylinder, therefore offering a high flexibility in the operation of the engine. The gas fuel injection is continually controlled using the data from the KDS knock detection system (described below) to allow immediate adjustments of the injection rate to a given cylinder in the case of knock or misfiring.

A.3.2 Performance monitoring and control

Performance monitoring and engine control equipment for dual fuel conversions has been developed by TecnoVeritas, including dedicated hardware and software such as the VTec multi-point port injection system for the conversion of existing diesel engines into true dual fuel engines, the KDS knock detection system, and the EDS engine diagnosis system.

Prior to conversion, the Wärtsilä engines were surveyed and operating variables such as pressures, temperatures, and specific fuel consumptions were logged to be used as a reference. Based on the operational values, the engineering team proceeded with the customised design of the system.

As a consequence of such a demanding contract, a comprehensive cylinder pressure monitoring system was fitted to monitor the combustion cycles during system tuning and normal operation. The VTec system is based on individual cylinder gas port injection, therefore allowing the correction of cylinder parameters such as temperature, maximum combustion pressure and knocking, by controlling the quantity of gas being injected in each cylinder per cycle.

The KDS knock detection system, connected via a CAN-bus network, includes one accelerometer per cylinder, identifying in each cycle any knock or the absence of combustion (misfiring). The KDS acceleration sensors are incorporated into the cylinder head, and give information on the vibration levels in the proximity of each cylinder. In addition, the KDS system has two position transducers, one on the flywheel and a second on the camshaft; both signal are acquired to exactly determine the position and phase of the TDC of each cylinder. The KDS system uses an algorithm to

perform a Fast Fourier Analysis at each cycle, therefore allowing the identification of knocking frequencies an their maximum amplitude before raising an alarm and output an demand to the injection controller for the reduction of gas to a given cylinder, or even the switching of operation from dual-fuel mode to conventional HFO or diesel-fuelled operation.

By using the information on the knock or pre-ignition intensity, the injection timing and/or gas injection pressure can be adjusted for optimal engine operation. Another function of the KDS system is to determine if any misfiring occurs, for example in the case of a gas injector malfunctioning. In such case, an alarm with indication of the defective cylinder is raised and the engine immediately transferred from dual fuel to standard HFO operation.

As the objective is to maximise the use of natural gas, the engine management system will seek the highest possible substitution ratio of natural gas to HFO. If the knocking or pre-ignition intensity increases, the gas flow is reduced after a number of cycles (typically 5). Should the knocking or pre-ignition continue beyond pre-set limits, the gas will be switched off and the engine operation is transferred seamlessly to HFO or diesel. Hence, the use of natural gas is maximised, while taking into account the varying conditions in the engine, in particular in relation to carbon deposits which promote pre-ignition of the cylinder charge.

The use of a dual fuel system operated with HFO and natural gas requires particular attention on the injection equipment condition. For this reason, both engines were equipped with the EDS engine diagnosis system, which allows the monitoring of the combustion process in each individual cylinder. In addition to detecting any injection valve malfunction, the injection controller is capable of making corrections and optimising engine operation based on operational variables such as the engine manifold pressure, exhaust gas temperatures, etc.

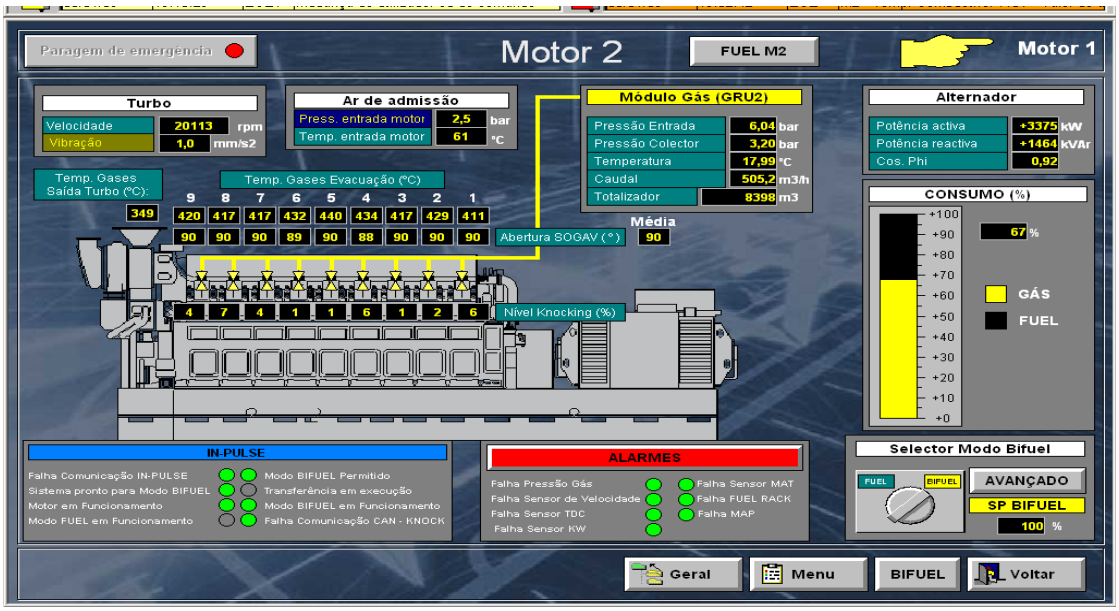

Figure 2: Graphical user interface of the engine diagnostics and performance monitoring system.

Figure 2 shows the graphical user interface of the engine management system. It provides the operator with vital engine performance variables, including boost air pressure and temperature, natural gas properties, exhaust gas temperatures, knock intensity, and electric output, as well as fuel consumption and fuel substitution ratio. The operator can decide the substitution ratio set-point, as well as switching the engine back to conventional diesel or HFO operation.

A.4. Experimental results and engine performance

After successful conversion, some performance tests were done to study engine fuel consumption and exhaust gas emissions under different modes of operation. As described above, the engines were run with the highest possible substitution ratio of natural gas to heavy fuel oil, limited by the knocking intensity in the cylinders.

A.4.1 The combustion process

Figure 3 shows in-cylinder pressure traces obtained during the tests. The graphs show pressure plots for operation on heavy fuel oil only, normal dual fuel operation, and for dual fuel operation with knocking due to too high natural gas substitution ratio. At normal dual fuel operation, the fuel composition is approximately 70% natural gas and 30% HFO (on an energy basis), and it can be seen that the performance closely resembles that of normal, HFO-fuelled operation. For higher substitution ratios, a significantly faster pressure rise and higher peak pressure can be seen, illustrating the need for the knock detection system and appropriate gas injection control.

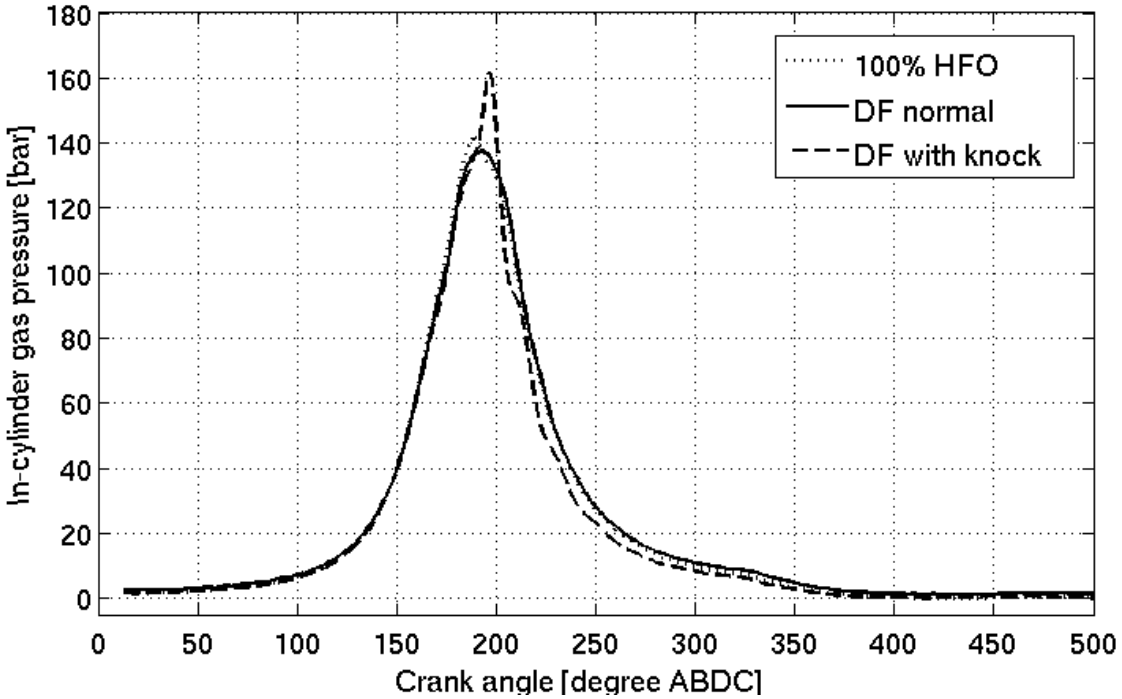

Figure 3: In-cylinder pressure plots for different engine operating modes.

Figures 4 and 5 further illustrate this, showing the calculated net heat release rates from combustion, derived from the pressure plots. Again, with an appropriate substitution ratio, the operation in dual fuel mode differs only very little from that on heavy fuel oil. However, with too high

levels of natural gas, characteristic knocking behaviour is observed, with detonating combustion at a crank angle of around 190. The knock behaviour leads to pressure waves in the combustion chamber, compromising the measurements. Since the heat release rate is calculated from the pressure data, one gets oscillations as can be seen in the graph.

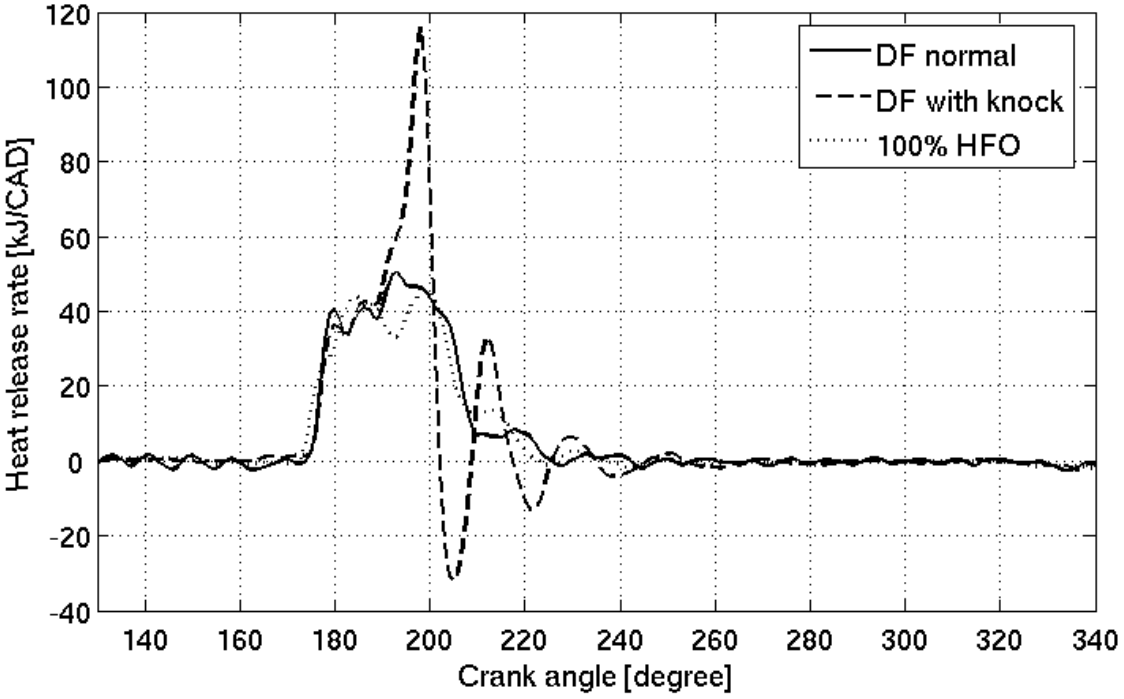

Figure 4: Net heat release rates.

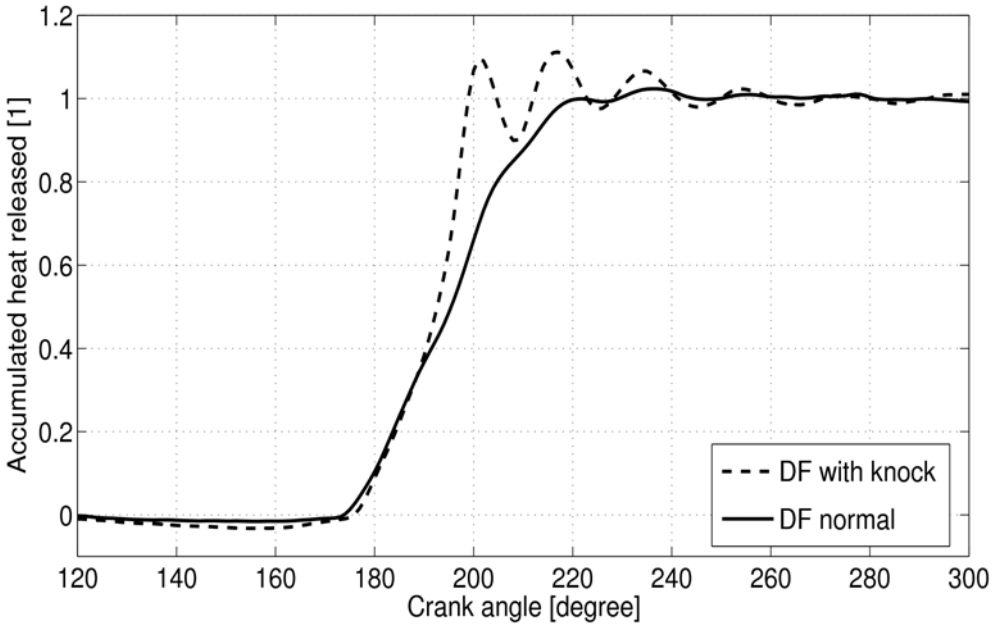

Figure 5: Accumulated heat release in dual fuel mode with and without knock.

A.4.2 Exhaust gas emissions formation

Regarding emissions formation, natural gas has a number of advantageous features compared with diesel oil or heavy fuel oil. First, the amount of CO_2 produced per unit energy delivered is lower than that of more complex hydrocarbons (with a higher carbon to hydrogen ratio). In the tests, a reduction in CO_2 emissions of approximately 16% was obtained in dual fuel mode compared to that of HFO operation. Second, particulate matter emissions (PM), an issue of great concern in diesel engines, dropped by 50% compared to the exhaust emissions at the same load on HFO, due to the replacing of a large fraction of HFO with natural gas, which produces negligible PM emissions. Finally, NO_x emissions dropped by 10%, which is somewhat lower than the NO_x reductions reported by other authors, such as Mustafi and Raine [9]. This is probably due to the fact that the engines considered here are significantly larger, and therefore have a lower operating speed, than most systems described in the literature.

A.4.3 Fuel cost and financial viability

The pay-back period of the present conversion project, based on the achieved substitution ratio and the price of natural gas and HFO at the time of commissioning (Oct. 2008), was estimated to be less than one year. For diesel oil operated engines, the payback period can be even shorter; diesel oil is more expensive than HFO and higher substitution ratios can be achieved (above 90% has been demonstrated), while maintaining the same power and slightly reducing the exhaust gas temperatures.

A.5 Summary

A commercial job to convert two industrial, large-bore diesel engines for operation on heavy fuel oil and natural gas was described. The technical solutions for engine conversion were outlined, including the fuel injection system, performance monitoring system, and knock detection system. Experimental results were presented showing the performance under standard heavy fuel oil operation and dual fuel operation.

Testing showed that a high substitution ratio could be achieved with natural gas supplying 70% of the fuel energy under dual fuel operation. Knocking behaviour was observed for too high substitution ratios, demonstrating the need for a knock detection system to allow optimised engine operation and maximised substitution ratio. Significant reduction in exhaust gas emissions, including NO_x, particulates, and CO_2 were found under dual fuel mode compared with conventional heavy fuel oil based operation.

A.6. References

[1] R. G. Papagiannakis, D. T. Hountalas. Experimental investigation concerning the effect of natural gas percentage on performance and

emissions of a DI dual fuel diesel engine. *Applied Thermal Engineering*, Volume 23, Issue 3, February 2003, Pages 353-365.

[2] R. G. Papagiannakis, D. T. Hountalas. Combustion and exhaust emission characteristics of a dual fuel compression ignition engine operated with pilot Diesel fuel and natural gas. *Energy Conversion and Management*, Volume 45, Issues 18-19, November 2004, Pages 2971-2987.

[3] R. G. Papagiannakis, D. T. Hountalas, P. N. Kotsiopoulos. Experimental and Theoretical Analysis of the Combustion and Pollutants Formation Mechanisms in Dual Fuel DI Diesel Engines. *SAE Paper 2005-01-1726*, 2005.

[4] A.P. Carlucci, A. de Risi, D. Laforgia, F. Naccarato. Experimental investigation and combustion analysis of a direct injection dual-fuel diesel natural gas engine. *Energy*, Volume 33, Issue 2, February 2008, Pages 256-263.

[5] M. Y. E. Selim. Pressure–time characteristics in diesel engine fueled with natural gas. *Renewable Energy*, Volume 22, Issue 4, April 2001, Pages 473-489.

[6] M. Mbarawa, Brain Edward Milton, Robert Thomas Casey. Experiments and modelling of natural gas combustion ignited by a pilot diesel fuel spray. *International Journal of Thermal Sciences*, Volume 40, Issue 10, 2001, Pages 927-936.

[7] V. Balasubramanian, K. Sridhara, V. Ganesan. Performance Evaluation of a Small Agricultural Engine Operated on Dual Fuel (Diesel + Natural Gas) System. *SAE Paper 951777*, 1995.

[8] R. Papagiannakis, D. Hountalas, C. Rakopoulos. Combustion and Performance Characteristics of a HSDI Diesel Engine Operating from Low to High Natural Gas Supplement Ratios at Various Operating Conditions. *SAE Paper 2008-01-1392*, 2008.

[9] N. N. Mustafi, R. R. Raine. A Study of the Emissions of a Dual Fuel Engine Operating with Alternative Gaseous Fuels. *SAE Paper 2008-01-1394*, 2008.

Appendix B:

Development of a dual fuel combined heat and power research facility

This appendix describes a project to develop a dual fuelled hydrogen and bio-oil combined heat and power (CHP) system for as a research tool. The project was carried out as a cooperation between Newcastle University and TecnoVeritas, and funded by Carbon Connections. TecnoVeritas contributed the technology for use of gaseous fuels in CI engines, including engine monitoring and management systems, developed during the course of the PhD work described in this thesis.

B.1 Introduction

The use of unprocessed bio-oil with hydrogen from renewable sources in a dual fuel CHP system potentially allows power and heat generation with near-zero carbon emissions. The known challenges associated with the use of unprocessed bio-oils in diesel engines, such as their poor ignition and combustion properties, may be eased by the use of hydrogen in a dual fuel system, in which the hydrogen will act as a combustion improver.

The objectives of the project were to develop a research tool to allow wide ranging investigations of the potential of such a system. This included the construction of an engine system with heat recovery from the exhaust and engine cooling circuit, development of a bio-oil viscosity control and supply system, implementation of a timed hydrogen injection system, and the design of a flexible engine management, performance monitoring and data acquisition system.

The CHP plant construction and commissioning was completed in March 2009. Preliminary system testing was undertaken in April 2009. These tests

were carried out using sunflower oil and rapeseed oil as liquid fuels, as well as conventional diesel in order to provide a baseline for comparison. Hydrogen was used as gaseous fuel, but operation of the system with butane gas was also demonstrated to show the flexibility of the system. The choice in liquid and gaseous fuels allows studies of CHP system feasibility in a range of applications, including, for example, the use of low-calorific gaseous fuels (pyrolysis gas, landfill gas etc.) or different blends of bio-oils, as well as blends with fossil diesel.

B.2 System description

The system is built in a standard 40-foot freight container, which is divided into three sections: a fuel storage room, a control room, and an engine room. Figure 1 shows the outside view of the container.

Figure 1: Outside view of Dual Fuelled CHP system container.

B.2.1 Engine and control system

The Dual fuelled CHP system is based around a Deutz turbocharged industrial diesel engine with a maximum power output of 45kW. The engine is coupled to an electric generator to produce electric power, and heat exchangers allow utilisation of the excess heat normally lost to the exhaust gases and cooling system.

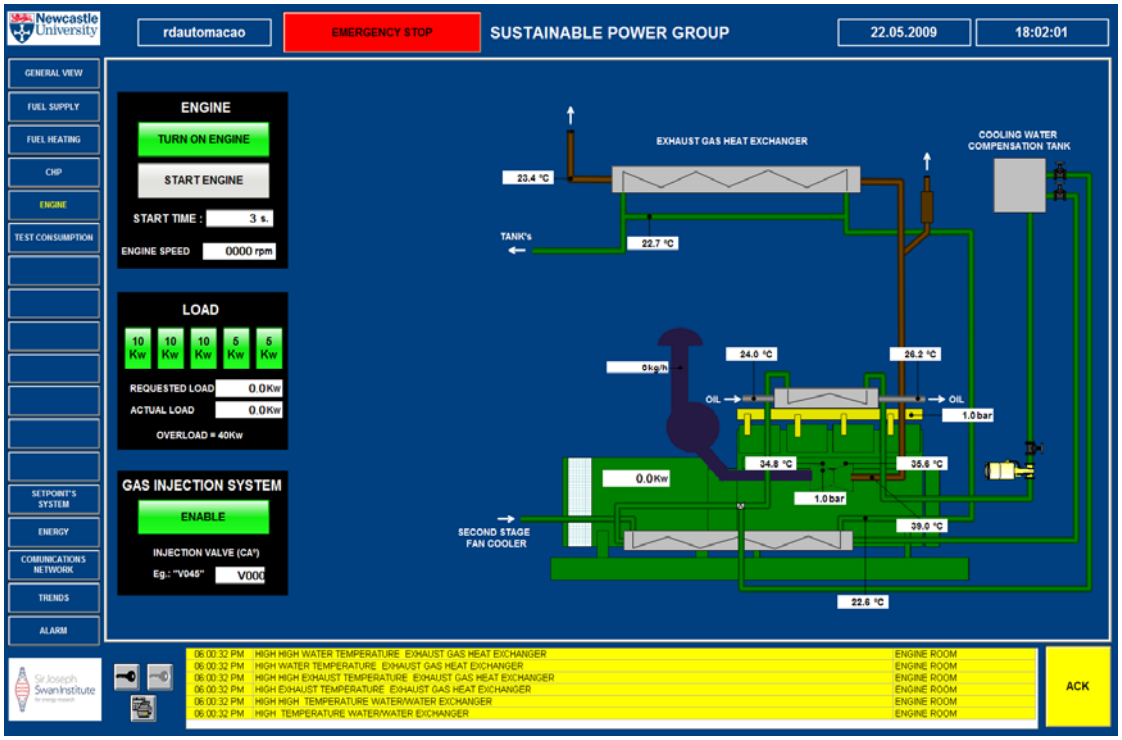

Figure 2: SCADA display of engine system.

Figure 2 shows the SCADA (user interface and control system) display of the engine system and shows how it is controlled. The system is fully instrumented with temperature and pressure sensors to allow online readings of the performance during operation. All operational variables of the engine are controlled from the control software, such as starts/stop, load level, and fuel substitution ratio (i.e. percentage of liquid fuel to percentage gaseous fuel). Figure 3 shows a photograph of the engine room. In the front of the engine is the electric generator. Above the engine, the exhaust line can be seen, leading to the exhaust gas heat exchanger, which

can be seen in the top of the photograph. On the right hand side, the engine cooling circuit heat exchanger is seen. The temperature sensors are visible, which, together with a flow sensor, allow calculation of the heat flow rejected to this cooler.

Figure 3: View of the CHP system engine room.

B.2.2 Fuel supply system

A fuel supply system allowing the use of three different liquid fuels as well as gaseous fuel has been implemented. The liquid fuel supply system is illustrated in Figure 4. It allows for the use of a single fuel from one of the three tanks or the use of a mixture of two fuels at any composition. In mixed fuel mode, the operator sets the relative fuel flow from each of the two selected tanks (e.g. 20% fuel A and 80% fuel B), as shown in Figure 4. Prior to being supplied to the engine, the fuel is passed through a blending tank to ensure proper mixing. The blending tank includes a recirculation pump which passes the fuel through a homogenising unit and returns it to the tank. This allows testing of combination of fuels in which separation can be a problem.

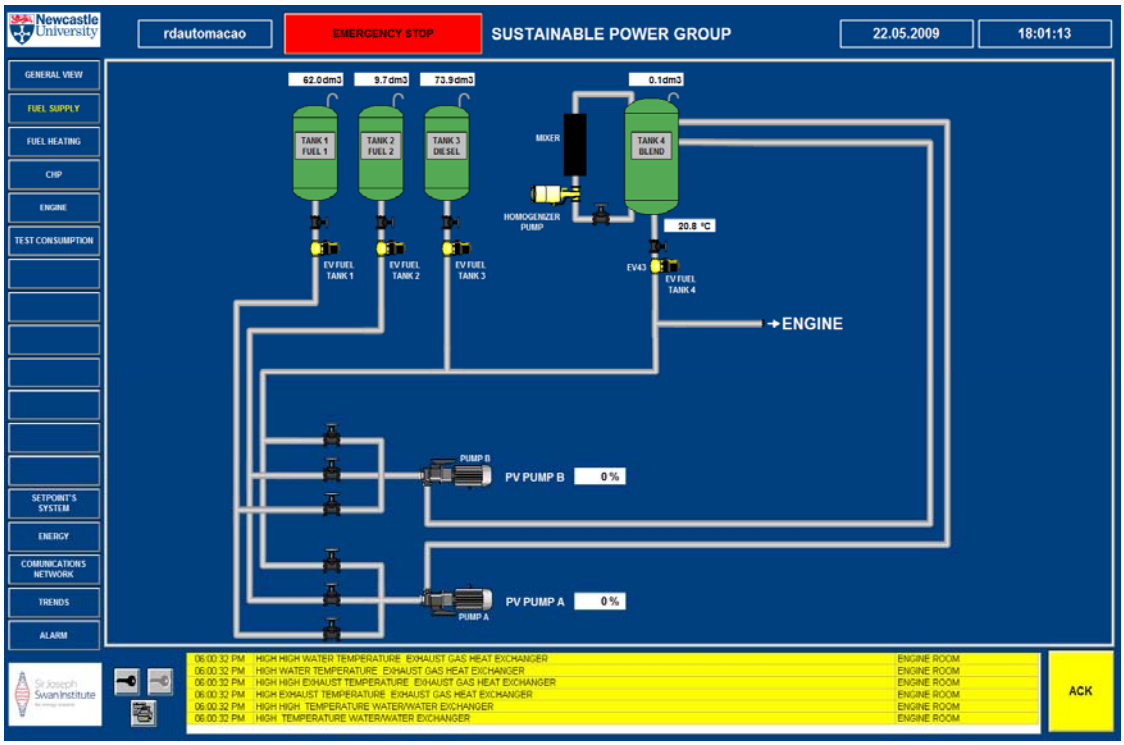

Figure 4: SCADA display of liquid fuel supply system.

Photographs of the fuel storage room are shown in Figures 5 and 6. In Figure 5, the three fuel tanks are shown, one of which is used for conventional diesel fuel (to provide a baseline for comparison during

testing and to purge the fuel lines if necessary) whereas two are used for different bio-oils. The fuel storage room also contains a water tank for the heat recovery system. On the floor, the fuel pumps controlling the fuel flow, and thereby the mixing of fuel from the different tanks, can be seen. Figure 6 shows the blending tank, with the homogenising unit (in the front) which ensures that any fuel mixture is properly blended before being supplied to the engine.

Figure 5: View of fuel storage room.

Figure 6: View of fuel mixing tank.

The gaseous fuel injection system receives supply gas, for example hydrogen, from a storage system outside the container for safety reasons. (Other types of gaseous fuels can also be used, such as natural gas or butane.) Fuel injectors (one for each cylinder) are fitted to the inlet manifold and the injection of gaseous fuel is electronically controlled. Based on the crank angle position reading, the system allows for timed injection of gas into the pipe between the inlet manifold and each cylinder during the intake stroke, to avoid build-up of hydrogen gas in the inlet manifold. Figure 7 shows the gas injection system on the inlet manifold

with the lines supplying the four individual cylinders. The gas supply (from the outside storage system) is the pipe seen on the right hand side of the unit, while in the front the four gas valves are seen with their individual power and control signal cables.

Figure 7: Engine gas injection system.

The SCADA user interface and control system allows the operator to determine the substitution ratio of gaseous to liquid fuel, e.g. operation on 70% bio-oil and 30% hydrogen (all ratios are calculated on an energy basis), in which the bio-oil can be any mixture from the fuel oil tanks as described above. This gives very powerful control in the operational optimisation of the system, in that the fuel composition can be suited for any operating conditions (e.g. load level) and performance targets (e.g. emissions and efficiency targets). In order to avoid engine damage due to knock or pre-ignition at high gas substitution ratios, a knock detection system, as described in Appendix A, is implemented. Knock is detected using acceleration sensors fitted on the cylinder head of each cylinder. The

sensors measure any vibrations due to detonation during combustion, and the signal is processed using Fast Fourier Transform to obtain a knock intensity variable in the engine control system. If the knock intensity exceeds a pre-set limit, the substitution ratio of gaseous to liquid fuel is reduced. This safety feature ensures that no engine damage (e.g. breakage of piston rings) occurs if too high gas substitution is demanded by the operator.

Figure 8 shows the view from the engine control room into the engine room.

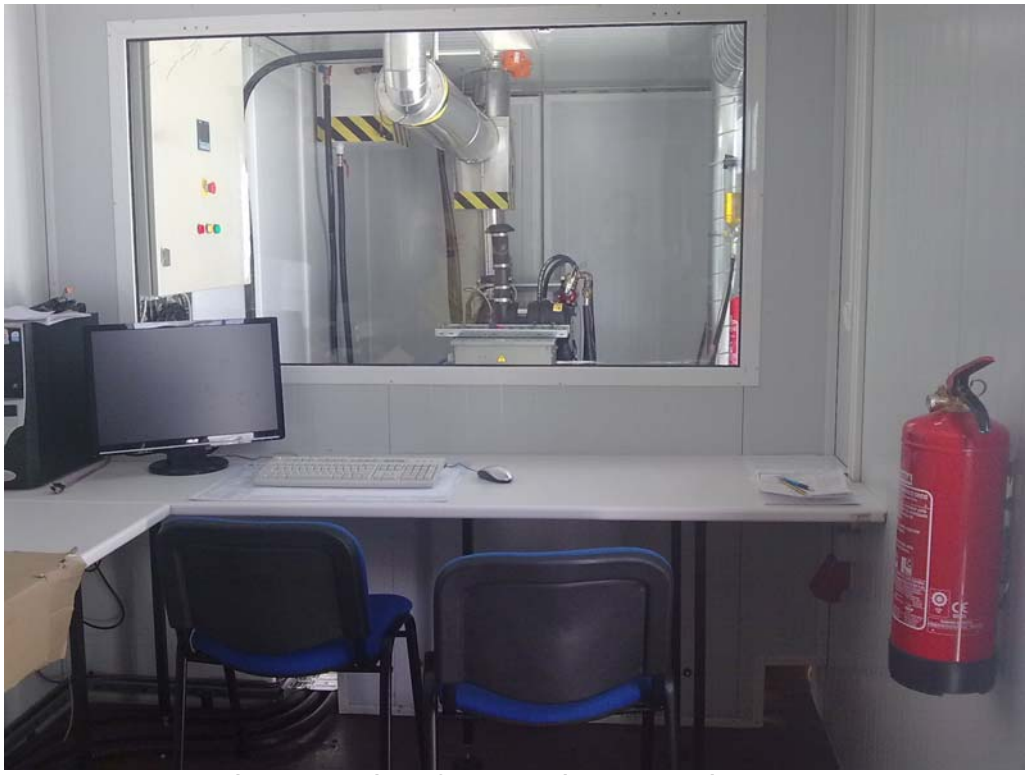

Figure 8: View from engine control room.

B.2.3 Heat recovery

The heat recovery system allows recovery of the exhaust gas heat and the heat lost to the engine cooling system, to achieve a total system efficiency of above 80% at full load. Heat is recovered in an exhaust gas heat

exchanger located in the exhaust line and in an oil heat exchanger recovering heat lost to the engine cooling system. Figure 9 shows the layout of the heat recovery system. The system is fully instrumented with temperature and flow sensors to allow calculation and logging of the heat flow and recovery rates. Cooling water for the circuit is supplied from a storage tank (left hand side of the figure), and the recovered heat is currently dumped using fan coolers located on the container roof.

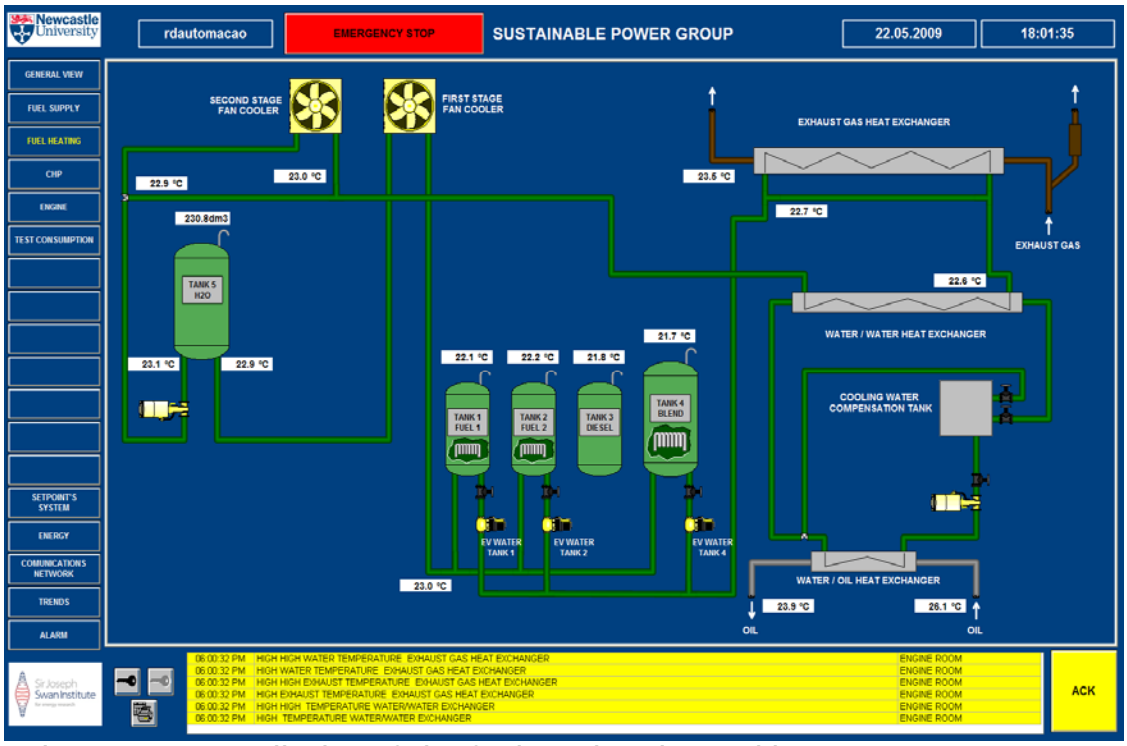

Figure 9: SCADA display of the fuel pre-heating and heat recovery system.

B.2.4 Viscosity control system

A viscosity control system for the liquid fuel tanks is implemented, using heat from the heat recovery circuit to control the temperature and viscosity in the fuel storage tanks and in the blending tank. This is necessary to maintain satisfactory combustion properties of highly viscous fuels. The viscosity control system is automatically controlled, with the set points provided by the operator in the control software. Viscosity

measurement equipment (viscometer) is provided in the fuel storage room to allow manual tests of the properties of the different fuels.

B.2.5 Hydrogen-related safety measures

As the project is based on the use of hydrogen, compliance with ATEX / DSEAR safety standards is required. Therefore the use of extra safety equipment, such as Zener barriers (galvanic isolators), hydrogen leak detectors, and ATEX hydrogen valves in the demonstration CHP system was required.

B.3 Preliminary test results

The hydrogen/bio-oil CHP plant has a maximum continuous electric power output of 45 kW, and a total efficiency above 80%. (This excludes the waste heat recovered and used for the controlled heating of the bio-oil storage tanks.) The inline blending system and homogenisation system allows a blend of various bio-oils to be used and its quality optimised. With the construction of the test CHP system, it is possible to study the influence of the hydrogen as a combustion improver, aiding the combustion of bio-oils and contributing to engine overall efficiency improvements and emissions reductions.

B.3.1 Combustion and emissions formation

Preliminary results demonstrated that hydrogen is an excellent combustion improver, and that only a small quantity of this gas significantly reduces the ignition delay of the bio-oil combustion. The effect of hydrogen on the combustion includes an engine performance improvement as well as a lowering of the thermal NO_x formation and particulates emissions as the fuel is combusted with a higher efficiency and the time at which the cylinder charge is exposed to high temperatures is reduced. It was further identified that the hydrogen percentage influences the heat loss characteristics, with a high hydrogen percentage giving higher heat losses

through the exhaust and lower heat losses through the combustion chamber walls. This benefits overall system performance, as the use of an appropriate exhaust gas economiser allows more efficient heat recovery when compared with recovery of heat lost to the cooling system, since the exhaust gases will have a higher temperature.

Tests have been run under a range of operating conditions with encouraging results. Comparing operation on liquid fuel only with a substitution of 50% hydrogen (on an energy basis), the following effects were observed:

– The formation of nitrogen oxides (NO_x) decreased by approximately 60%, which is due to the lower peak gas temperatures in the cylinder. A more homogeneous fuel-air mixture reduces the high-temperature zones in the burning fuel spray, in which NO_x is predominantly formed.

– Formation of particulate matter decreases by approximately 20% with the introduction of hydrogen, indicating that hydrogen enhances the combustion of the liquid fuel and the oxidation of carbonaceous material.

B.3.2 Heat recovery

While the engine is operating at full load (45kW electric power), the waste heat recovered from the engine block and lubricating oil cooling system amounts to 21.6 kW, and from the exhaust gas the heat recovery reached 32.8 kW. In terms of overall energy efficiency, the value reached during the first tests was 79.6%.